Geostatistics and petroleum geology

Geostatistics and petroleum geology

Second edition

Michael Edward Hohn

West Virginia Geological Survey

SPRINGER SCIENCE+BUSINESS MEDIA, B.V.

Library of Congress Cataloging-in-Publication Data is available.

ISBN 978-94-010-5901-5 ISBN 978-94-011-4425-4 (eBook)
DOI 10.1007/978-94-011-4425-4

Printed on acid-free paper

Typeset by Photoprint, Torquay, Devon.

To my wife, Kay,
and my children, Geoffrey and Abigail

Contents

Preface

This is an extensive revision of a book that I wrote over ten years ago. My purpose then has remained unchanged: to introduce the concepts and methods of spatial statistics to geologists and engineers working with oil and gas data. I believe I have accomplished more than that; just as I learned the basics of variography and kriging from books for mining engineers, this book could be used by scientists from many fields to learn the basics of the subject.

I have tried to adopt an introductory and practical approach to the subject, knowing that books that detail the theory are available. What I say and write comes from my own experience. As a geologist working in the public sector, I have had the privilege of using geostatistics in funded research, in answering service requests from industry, and in short courses. I have taught geostatistics in the university classroom, and advised graduate students in theses and dissertations. I have attempted to anticipate the needs and questions of the enquiring scientist because I was there myself, and know the kind of questions and concerns I had at the time I was trying to learn the subject.

Geostatistics has become a toolbox of methods useful for attacking a range of problems. The number of methods is now broad enough – even for such an established method as kriging – that determining the best one for all situations has been largely abandoned. One still finds comparative studies, but most leave the impression that the efficacy of a particular method varies with the data. Hence, I have avoided direct comparison of techniques, preferring instead to illustrate features of each. In general, the geostatistician should learn a range of methods, and pick the one that works best for a given situation, given available software or a willingness to write computer programs.

Necessary items in the geostatistical toolbox of today are the ability to calculate and model semivariograms, linear methods of kriging, cokriging and variants of cokriging, nonlinear methods such as indicator kriging or disjunctive kriging, and conditional simulation. All geostatistics depends on a model of spatial dependence, hence variography. Even nonlinear geostatistical estimation methods, and most methods of simulation require setting up and solving the systems of equations used

in linear kriging. Indicator approaches to estimation and simulation are used widely. Although disjunctive kriging is encountered less often, it uses that important technique, the computation of normal scores. There has been a virtual explosion in methods and application papers on conditional simulation (or stochastic simulation) in the ten years since my original book came out. Conditional simulation has become important in the area of reservoir characterization, an area where the geologist and engineer can cooperate effectively.

To learn any method, one needs to know the motivation for the method, how it works, the steps the user must go through, and problems the user might encounter. The best way to do all this is through real examples. I have placed a strong emphasis on the examples; most of the time spent on this revision was on developing new examples to reflect where geostatistics has gone in the past ten years. I have elected to use real data sets, with all the ensuing problems, and I have 'let the warts show'. Some of the examples did not turn out as well as I expected, but they had the advantage of being data that I was familiar with because in most cases they came out of projects that I worked on.

Geostatistics is by nature mathematical and statistical. I have not tried to avoid mathematics when it seemed necessary; the educated user should be exposed to the mathematical underpinnings of any method. No advanced mathematical knowledge is required, and in places I have tended to simplify where possible. The emphasis throughout is on what the practitioner needs to know, and the results one can expect to get.

I wish to thank Ronald R. McDowell, Senior Research Geologist at the West Virginia Geological Survey, for help in programming and for reading the manuscript. Raymond Strawser drafted some of the figures. Richard Chambers provided data used in Chapter 4. Frank Curriero fielded some of my statistical questions. This work would not have been possible without the support and encouragement of Larry D. Woodfork, Director and State Geologist, and Carl J. Smith, Deputy Director, of the West Virginia Geological and Economic Survey.

Michael Edward Hohn
1998

CHAPTER 1

Overview of geostatistics

Geostatistics is the statistics of observations located in space or time. Such data can be correlated spatially or temporally. Thickness of a stratigraphic unit is spatially correlated; at a particular locale, the thickness is constant, but the similarity in thickness varies with distance. In the subsurface, thickness can be estimated from nearby wells. The assumption that a variable such as thickness is correlated with itself in space – i.e. autocorrelated – lies at the heart of contour mapping.

Several features set geostatistics apart from *ad hoc* and manual approaches to local estimation. First of all, methods for estimation such as kriging use an explicit criterion of optimality requiring a model of spatial dependence. Second, parameters of this model are unique to each set of data. Third, geostatistical methods such as kriging provide a measure of uncertainty in the estimate.

The criterion most often optimized in geostatistical estimation is estimation variance, also called kriging variance. In essence, one tries to minimize a sum of squared deviations. Other criteria may be used, such as mean absolute deviation or some type of asymmetric loss function. Whatever the criterion optimized, it is chosen to fit the problem at hand and is reported explicitly by the author.

Estimation involves solving a set of equations that describe the expected autocorrelation between values of a variable observed at control wells and the value to be estimated. Therefore, estimation needs some model of autocorrelation. Constructing such a model is analogous to the geologist looking at a map of control points annotated with observed values of the variable to be mapped and remarking, 'The data are very noisy, so some smoothing is necessary' or 'My data are very good, so each datum should be honored exactly'. Through use of the semivariogram, the geostatistician attempts to quantify such remarks for objective and consistent use in mapping.

Whatever criterion is optimized in computing expected values, this criterion forms not only part of the algorithm, but a measure of success in estimation. Given a particular autocorrelation model, the kriging variance, for instance, generally decreases with increasing well control. Because a calculated variance accompanies each local estimate, contour

M. E. Hohn, *Geostatistics and Petroleum Geology*

maps of kriging variance may be used to spot areas needing more sampling, if possible, or to limit the area contoured for the mapped variable. Thus, geostatistics provides a measure of uncertainty.

One can take estimation one step further, and estimate local frequency distributions in addition to averages or medians. This allows one to place confidence intervals around expectations. In addition, the petroleum geologist can begin to make statements about the probability of exceeding some value of initial potential or cumulative production. Kriging variance has rather strong distributional requirements in order to be used as a measure of uncertainty, and has been supplanted by other measures, such as the variance obtained by stochastic methods.

The geostatistician finishes with two products: a map of estimates (or predictions), and local frequency distributions. The first item can come into play for ranking areas by favorability if one is interested in drilling new wells. Local frequency distributions may be used to evaluate risk and setting values in economic models.

1.1 A FEW DEFINITIONS

A reader of the geostatistical literature must know a few key words and phrases. Some terms appear strange in the context of petroleum geology, but for the sake of consistency with the rest of the literature, they are retained here. For example, **nugget effect** relates to small-scale variability, and is defined in a later chapter.

A variable distributed through space is a **regionalized variable**. Examples are formation thickness, geothermal gradient, success rate, cumulative production, porosity and permeability. The space may have one or more dimensions and can include time. For instance, inferred sea-level temperature through time at a given locality is a regionalized variable.

A **random variable** takes on values that follow a probability distribution, such as normal or uniform distribution. Take for example, permeability, $z(x_1)$, measured at a given horizon in a well at location x_1. Then $z(x_1)$ is a particular **realization** of a single random variable $Z(x_1)$. Each value of $z(x)$ observed in a gas field represents a different random variable, but the set of the random variables observed constitute a **random function**. To estimate a value at some new location, we want to use observed values in conjunction with what we can figure out with regard to the random function of cumulative production. One piece of information is how smoothly permeability varies from well to well at a particular horizon.

This random function has two components:

1. a regional component manifesting some degree of spatial autocorrelation and lack of independence in proximal values of $z(x)$, and

2. a local, random component.

The geologist usually assumes the presence of the first component and ignores the second. Geostatisticians attempt to quantify the relative contribution of each component.

1.2 A SIMPLE GEOSTATISTICAL CASE STUDY

A straightforward mapping problem includes five steps: data gathering and cleanup, univariate analysis, semivariogram calculation and modeling, estimation and mapping. In addition, the practitioner might want some measure of uncertainty, and the petroleum geologist or engineer perhaps requires multiple realizations for input to a flow simulator. This section presents a simple example that utilizes standard geostatistical techniques, along with indications of alternative strategies. Data for this example are for final open flows of gas from Upper Devonian rocks in one field in West Virginia. The values of initial potential are in thousand cubic feet per day (Mcfpd).

This example was not intended to be typical in the type of data – initial open flows – but is typical of many geological datasets with regard to the problems that the practitioner often faces in drawing a map of natural resources, or petrophysical data. These problems include poor well control in some areas, clustered wells in others, skewed data distribution with possible outliers, and poor spatial correlation caused by measurement error or poor sampling.

We assume that spurious values have been purged (Appendix A) and are ready for univariate analysis through histograms. The histogram of raw data (Fig. 1.1) shows a large positive tail. It is sometimes advisable to transform data, or use methods that are resistant to skewed distributions or outliers.

The **semivariogram** is a graphical device for modeling spatial continuity. Defining $z(x)$ as the value of initial potential at a site x, and $z(x + h)$ as the value of initial potential at a well site h km from x, we calculate the quantity

$$\gamma^*(h) = \sum_{i=1}^{n} [z(x_i) - z(x_i + h)]^2/2n$$

using all n pairs of wells separated by a distance h. If wells are drilled on a regular grid, the calculation is straightforward for each value of h, which would be integral multiples of well spacing. Where wells are situated irregularly, h must be assigned a tolerance, such as $\frac{1}{2}h$. Plotting distance h on the horizontal axis, and $\gamma^*(h)$ on the vertical, gives the semivariogram (Fig. 1.2). For small values of h, initial potentials are

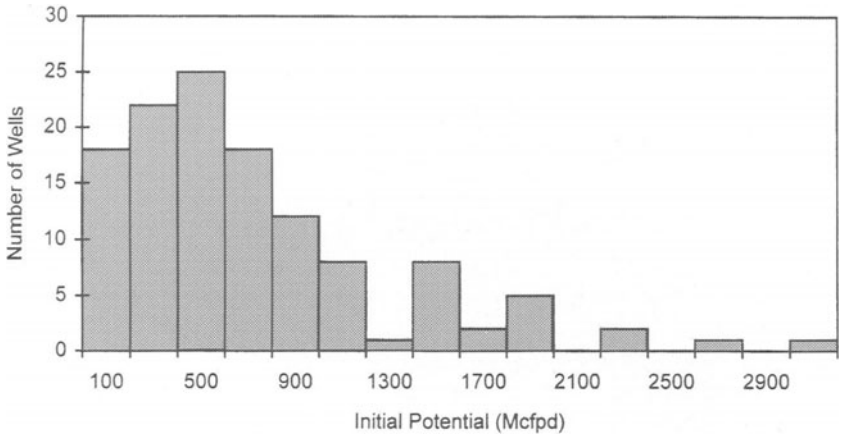

Figure 1.1 Histogram of initial potentials of gas observed in gas wells producing from Upper Devonian rocks in a field situated in West Virginia.

nearly equal, and the observed values of $\gamma^*(h)$ approach zero; as h increases, values of initial potential become more independent, $\gamma^*(h)$ increases.

Rather than using the formula given above, the geostatistician may choose to compute a so-called robust semivariogram (Chapter 2) to mitigate the effects of outliers or a skewed distribution. The h-scattergram is useful for observing outliers or spurious values and can form part of the clean-up process (Chapter 2). Again, appropriate transforms

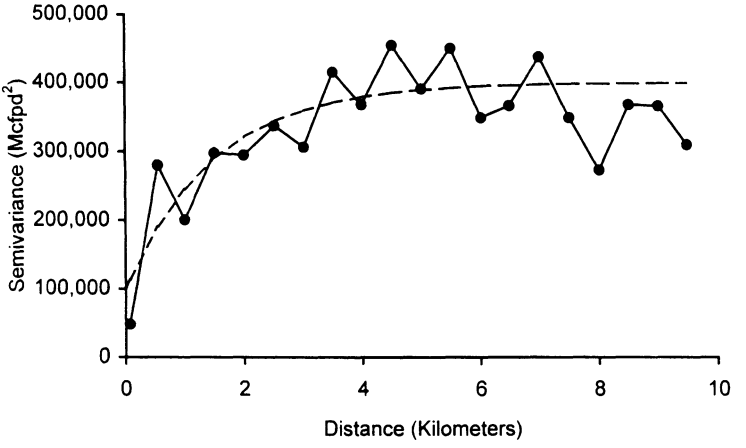

Figure 1.2 Semivariogram of initial potential (line with symbols) and model (dashed curve).

of the data can improve the appearance of the semivariogram, and make them easier to fit.

The observed semivariogram is shown in Fig. 1.2 with an exponential model:

$$\gamma(h) = C_0 + C[1 - \exp(-h/a)]$$

where C_0 is the **nugget effect**, C is a constant called the **sill**, 300 000 Mcfpd^2, and a is another constant called the **range**, 1.5 km. Although some a priori justification for a particular model for the semivariogram can exist, model fitting is usually a strictly empirical process involving an iterative technique with the help of software (Chapter 2). It is still usually the practice to fit semivariograms by eye, but Chapter 2 also describes one method for automated fitting using a least squares criterion.

Choosing a semivariogram model determines the degree of smoothing in the next stage, estimating initial potential at each node of a regular grid through **linear kriging**. For each node the estimate is a linear combination of initial potentials observed at k surrounding wells:

$$z^*(x) = \sum_{i=1}^{k} \lambda_i z(x_i)$$

where the λ_i are weights determined by solving a system of equations that minimize an **estimation variance**. Factors that influence the magnitude and sign of each weight are the proximity of each well to the grid node and to the other $k-1$ wells (Chapter 3). From the grid of local estimates a contouring program creates the final map (Fig. 1.3).

In the past, estimation variance has been used as a measure of uncertainty. Although this practice has been discouraged in recent years, estimation variance may be used to mask areas on the map with poor well control, in addition to generating distribution functions and risk qualification under special conditions.

Because uncertainty in an estimate is inversely proportional to well spacing, one would like to decrease this variance short of drilling more wells. One way to attempt this is to measure a variable that correlates highly with the variable of interest, and compute linear estimates through **cokriging** (Chapter 4). A standard cokriging approach is used when two or more variables are observed at discrete locations in a reservoir. However, a regionalized variable such as that obtained from seismic data is measured almost everywhere, in which case so-called kriging with an external drift is used, for instance, to use acoustic impedance to supplement porosities measured in wells.

In addition to estimation of regionalized variables, geostatistical methods attempts to ask questions such as: 'what is the likelihood that a well

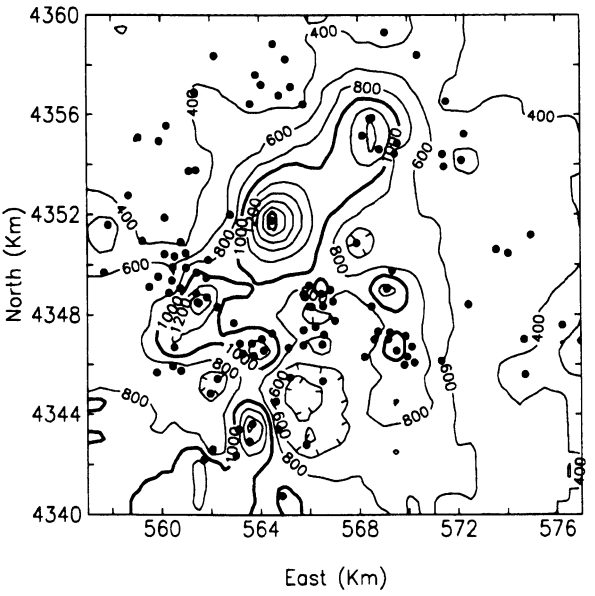

Figure 1.3 Contour map of kriged estimates of initial potentials. Wells are shown as filled circles.

will produce more than a specified number of barrels necessary for the well to be economic?' Similarly one might want to compute the probability that formation thickness, porosity or permeability exceeds some critical value. The nonlinear method of **disjunctive kriging** (Chapter 5) attempts to answer questions such as these. Because it involves a transform to normality, disjunctive kriging is appropriate for skewed data. This transform – yielding normal scores – is used in other geostatistical methods, and has become an important tool in geostatistics.

As mentioned above, estimation variance may be a useful criterion for estimating a regionalized variable at a location, but it has limited usefulness in computing confidence intervals. Many geostatisticians object to the fact that estimation variance depends solely upon the semivariogram and the local configuration of points, not on observed values. **Indicator kriging** (Chapter 6) provides both an estimate and a probability distribution. One can estimate directly the probability that a regionalized variable exceeds or does not exceed given cut-off values. In addition, indicator kriging is relatively robust to extreme values and non-normality.

The first step in indicator kriging is to create one or more indicator variables, each corresponding to a specified cutoff. A particular indicator variable is assigned a value of 1 for observations below the cutoff, and 0

for observations equal to or above the cutoff. For each indicator variable, one computes a semivariogram, fits a model, and performs a conventional kriging. Figure 1.4 shows three semivariograms for the indicator variables formed by applying cutoffs of 270, 581, and 919 Mcfpd to the initial potential data. These values are the 25th, 50th, and 75th percentiles.

Indicator kriging was performed using nine cutoffs (250; 500; 750; 1000; 1250; 1500; 1750; 2000; and 2500 Mcfpd). An immediate product of indicator kriging is a map of estimated probability of initial potential exceeding each cutoff; Fig. 1.5 is the map for a Mcfpd cutoff at 1000 Mcfpd. At a given location, one can compute probabilities of exceeding each of a number of cutoffs, yielding a cumulative distribution function, such as that in Fig. 1.6, or a histogram (Fig. 1.7).

It is straightforward to compute the mean and median of each distribution function and map this statistic over the study area (Fig. 1.8). This map is similar to the one obtained by ordinary kriging, but is relatively robust to outliers and skewed distributions. In addition, measures of uncertainty can be computed from the local distribution functions, and used in place of estimation variance. 'Estimation variance' computed through indicator kriging is highest where well density is low, and variability among neighboring observations is large. Uncertainty is lowest where well control is good, and variability is low.

When data are subject to large errors, or spatial variability is finer than sample spacing, estimates are smoothed and do not reflect the well-to-well variability found in the field. For example, kriged estimates of permeability are not appropriate inputs to flow simulators because the very low or high permeability zones will have been smoothed away.

Conditional simulation (Chapter 7) provides multiple values of a regionalized variable for any given location. The map representing one such set of values has the same mean, variance and semivariogram as known values, and passes through these known values, i.e. is conditioned to the observations. For variables such as permeability, each realization generated by conditional simulation can be used as input to a flow simulator in order to show a range of possible outcomes. Conditional simulation can also be used to quantify uncertainty, another alternative to estimation variance.

Sequential indicator simulation was used to generate the two realizations in Fig. 1.9, which resemble maps of kriged estimates, but differ in the degree of small-scale variability, and with each other. The increased variability would be more apparent if a contour map was drawn, but such maps are difficult to read because of the large number of contours within small areas. The largest variability is in areas with poor well control, where the surface is least constrained. The least variability is near well locations, and if the grid were fine enough, we would see that

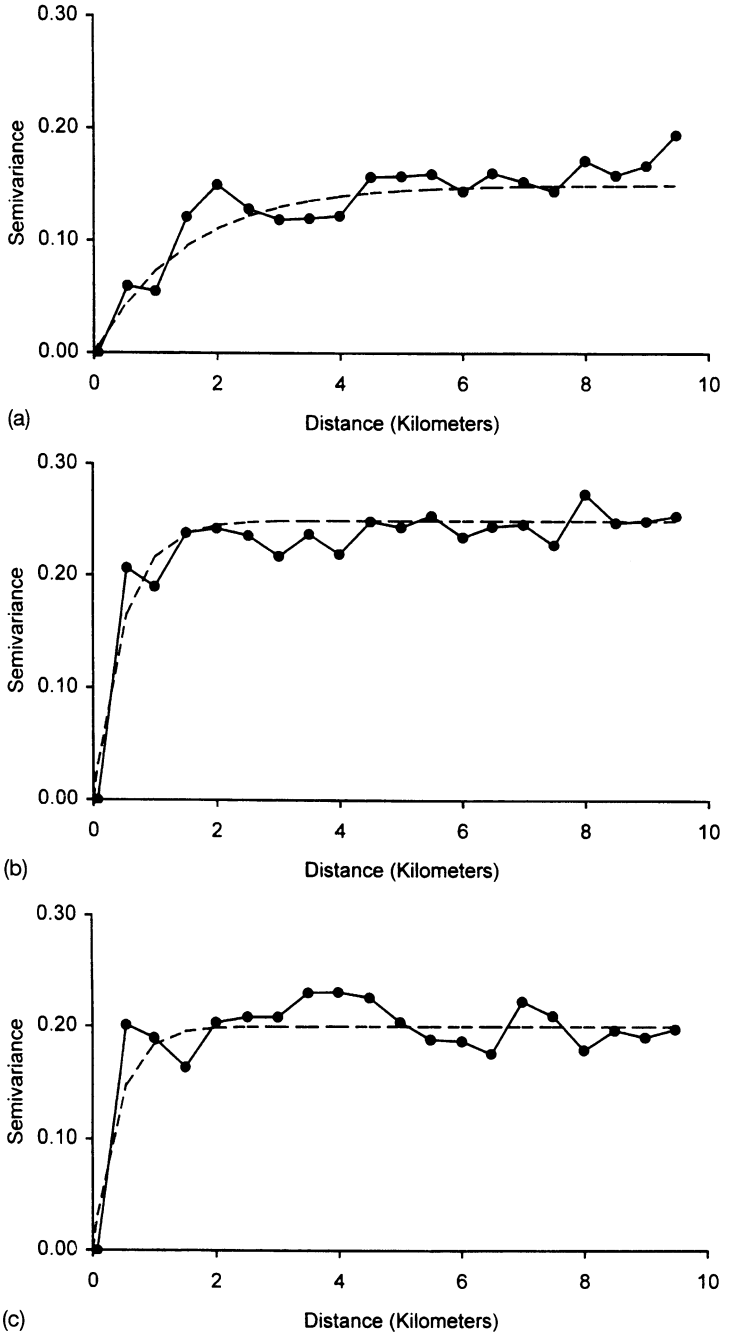

Figure 1.4 Semivariograms of indicator variables computed from gas initial potentials for three cutoff values: (a) 270 Mcfpd, (b) 581 Mcfpd, and (c) 919 Mcfpd.

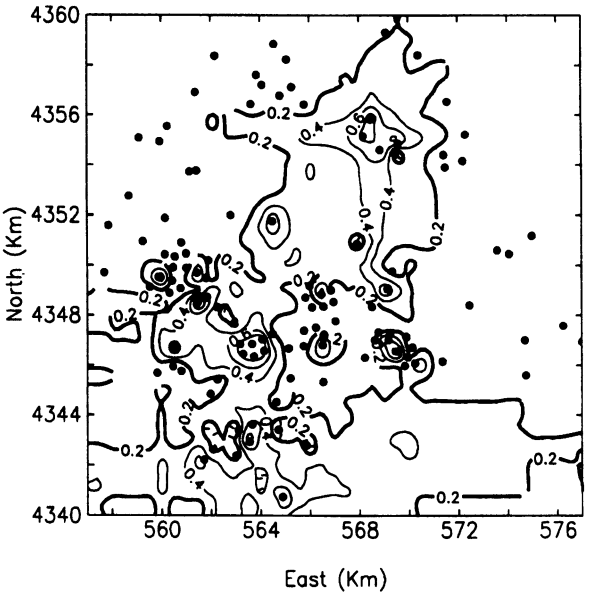

Figure 1.5 Contoured probability that gas initial potential exceeds 1000 Mcfpd, as computed through indicator kriging.

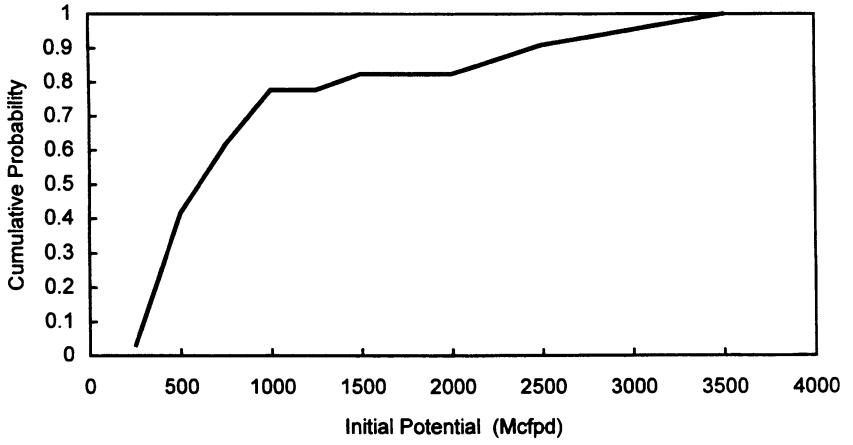

Figure 1.6 Cumulative probability distribution for initial potential at a location situated 563 East, 4350 North on Fig. 1.5.

the simulated values are the same as observed values where well locations and grid nodes coincide.

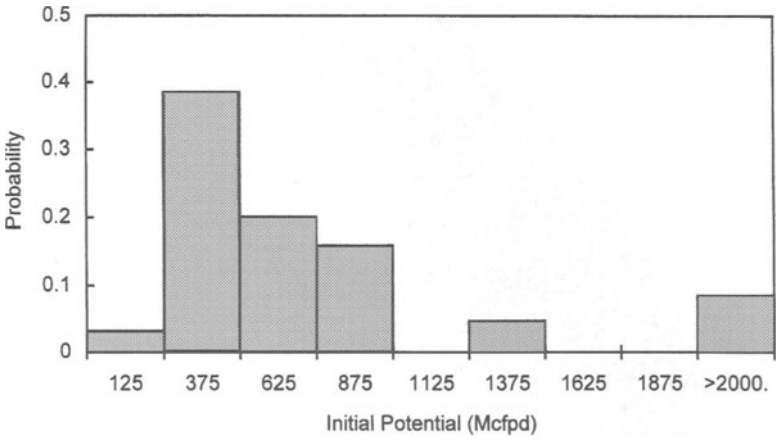

Figure 1.7 Probability distribution of Fig. 1.6 drawn as a histogram.

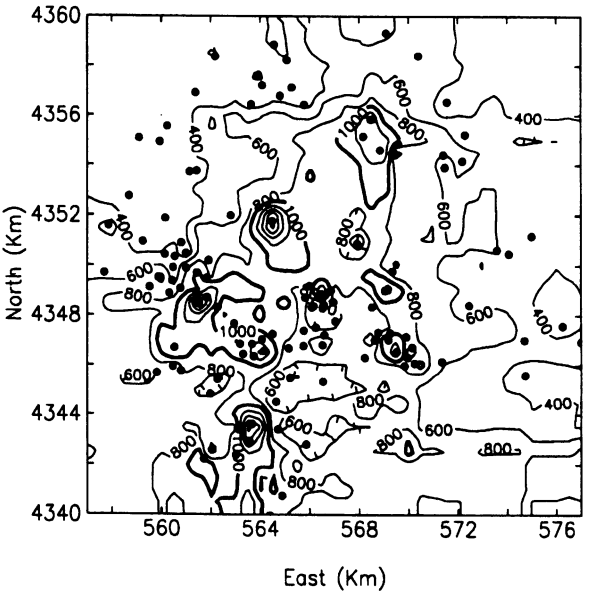

Figure 1.8 Contoured map of initial potential from indicator kriging.

1.3 GEOSTATISTICS ON THE COMPUTER

This book assumes that even the simplest calculations are performed by computer, largely because these calculations become tedious and unwieldy for large data sets. Perhaps the most effective way to test

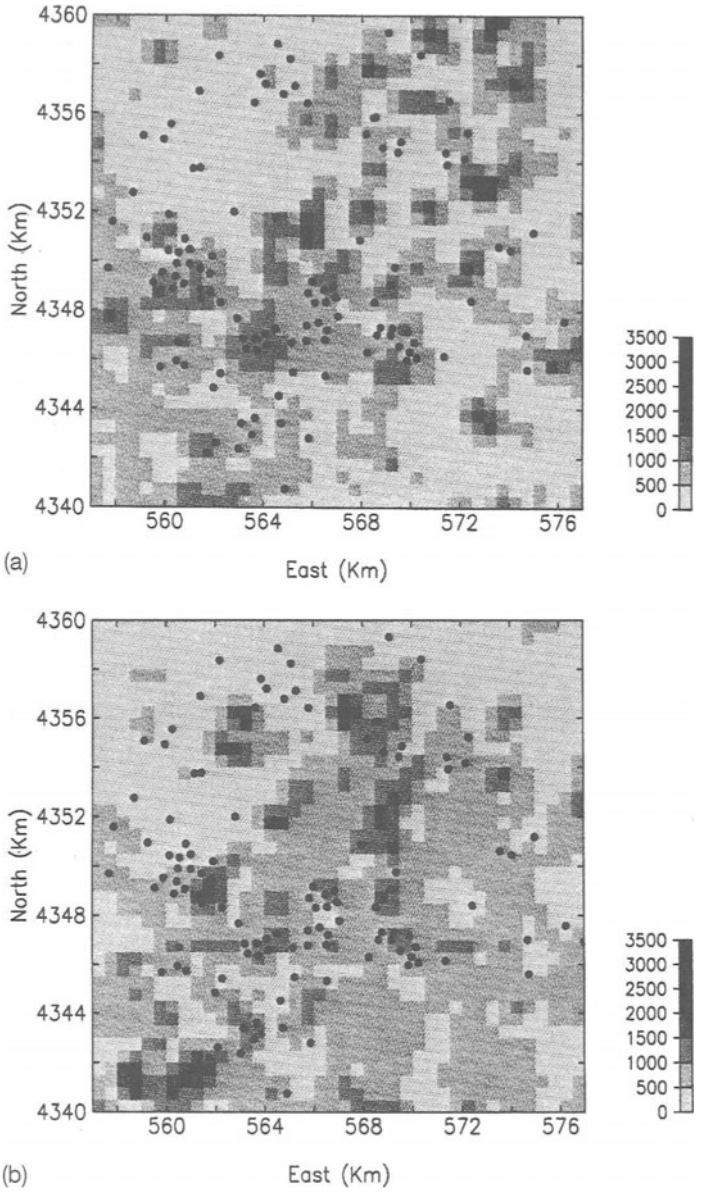

Figure 1.9 Two realizations of gas initial potential (in Mcfpd) generated by sequential indicator simulation.

understanding of a method is to program it for the computer, but a second assumption is made here that the geostatistician prefers to find programs in the literature or commercially. Because each year brings new

geostatistical software on the market, any list is soon obsolete. This section lists some programs that should belong in the geostatistician's standard repertoire, and some sources for public domain or inexpensive software.

What programs does the geostatistician need? The following tasks are routine in geostatistics.

1. Computing univariate statistics, including means, variances and histograms
2. Drawing scattergrams
3. Semivariogram calculation
4. Interactive curve fitting
5. Grid searching
6. Equation solving
7. Drawing contour or shaded maps.

Univariate and perhaps bivariate analysis and display are used for initial looks at data, when incorrect data must be eliminated, outliers detected, and distributions examined. Items 3 and 4 relate to modeling spatial continuity of a variable. Spreadsheets with interactive graphics are very useful for curve fitting, and they are readily available. Actual estimation requires searching for wells proximate to nodes on a grid, solving a system of equations for determining weighting factors, and drawing a contour map. Each function can be implemented separately, and possesses different requirements for efficiency. Bivariate plots enter the picture once again in so-called validation of a geostatistical analysis.

Application of geostatistics in the area of oil and gas differs from many other fields in the importance of conditional simulation, particularly in building reservoir models of porosity and permeability. This method requires all of the software components listed above, plus implementation of one or more simulation algorithms. Results from conditional simulation often become input for reservoir flow simulators. Conditional simulation represents an important link between the work of the geologist and the petroleum engineer.

1.4 COMPUTER SOFTWARE

An important source of programs is journals, particularly *Computers and Geosciences*. The journal *Mathematical Geology* does not publish programs, but includes many original accounts of new methods, for which code is available elsewhere. Major repositories of computer programs are the many theses and dissertations coming out of graduate departments that teach and do basic research in geostatistics.

Few programs obtained from the literature for use in writing this book escaped modification. Aside from the usual modifications related to input and output file specifications, changes included addition of more

detail in output, particularly intermediate results, clearer table formats and headings. Some algorithms were altered for greater efficiency. Many programs as published handle relatively small data sets; some authors are very conscientious about writing code in which array sizes may be easily increased and then documenting where changes need to be made. In some cases, simply increasing array sizes is not practical because the resultant code becomes too inefficient or the algorithm simply fails. Some programs gave incorrect answers.

Programs have entered the public domain through work by government agencies such as the US Geological Survey and reports of government-sponsored research (Clayton, 1994). An important example of such a program is Geo-EAS (Englund and Sparks, 1991), a personal computer-based package for semivariogram calculation and modeling, and kriging, suitable for small sets of data.

At least two sets of programs appear on diskettes with published manuals. VARIOWIN (Pannatier, 1996) provides interactive modeling of semivariograms in two dimensions. The user can create nested anisotropic models in several directions simultaneously, and very quickly. GSLIB (Deutsch and Journel, 1998) includes the whole gamut of programs for geostatistics, including summary statistics, semivariogram calculation, kriging, cokriging, and conditional simulation. As published, the programs are not interactive, and the user must find a way to interactively model semivariograms. Nevertheless, GSLIB was used extensively throughout this book for estimation and simulation.

Most, if not all methods described in this book exist in commercial software. In addition to the drawback of cost, implementation of new methods can take time to appear on the marketplace.

1.5 DATA SOURCES

Most of the examples used in this book are taken from a data base developed at the West Virginia Geological and Economic Survey, and in many instances, were the results of research that involved the author. Some data were taken from the literature in order to provide diversity.

Richard Chambers of Amoco Production Research kindly provided the seismic and porosity data used in Chapter 4 (Chambers, Zinger, and Kelly, 1994).

Some of the data sets used in this book can be obtained electronically at *http://www.wvgs.wvnet.edu/www/geostat/geostat.htm*.

FURTHER READING

The two most general books available to the interested reader are by Cressie (1993) and Isaaks and Srivastava (1989). The first is by a statistician

and includes much theory as well as examples. The book by Isaaks and Srivastava includes some of the theoretical underpinnings, but its strength lies in the authors' ability to explain and give examples of variography and estimation. They do not include simulation.

A recent book by Goovaerts (1997) is a broad survey of geostatistical methods, including simulation, in the context of environmental applications. Classic texts on geostatistics are those by David (1977), Journel and Huijbregts (1978), and Clark (1979).

REFERENCES

Chambers, R.L., Zinger, M.A. and Kelly, M.C. (1994) Constraining geostatistical reservoir descriptions with 3-D seismic data to reduce uncertainty, in J.M. Yarus and R.L. Chambers (eds), *Stochastic Modeling and Geostatistics*. Am. Assoc. Petroleum Geologists, Tulsa, OK, pp. 143–57.

Clayton, C.M. (1994) Public Domain Geostatistics Programs: STATPAC, Geo-EAS, GEOPACK, Geostatistical Toolbox, and GSLIB, in J.M. Yarus and R.L. Chambers (eds), *Stochastic Modeling and Geostatistics*. Am. Assoc. Petroleum Geologists, Tulsa, OK, pp. 349–67.

Clark, I. (1979) *Practical Geostatistics*. Applied Science Publishers, London, 129 pp.

Cressie, N.A.C. (1993) *Statistics for Spatial Data*, revised edition. John Wiley & Sons, New York, 900 pp.

David, M. (1977) *Geostatistical Ore Reserve Estimation, Developments in Geomathematics* 2. Elsevier Scientific Publishing, Amsterdam, 364 pp.

Deutsch, C.V. and Journel, A.G. (1998) *GSLIB: Geostatistical Software Library and User's Guide*. Oxford University Press, New York, 369 pp.

Englund, E. and Sparks, A. (1991) Geo-EAS 1.2.1 (Geostatistical Environmental Assessment Software) User's Guide, U.S. EPA Document EPA/600/B-91/008, 128 pp.

Goovaerts, P. (1997) *Geostatistics for Natural Resources Evaluation*. Oxford University Press, New York, 487 pp.

Isaaks, E.H. and Srivastava, R.M. (1989) *An Introduction to Applied Geostatistics*. Oxford University Press, New York, 561 pp.

Journel, A.G. and Huijbregts, C.J. (1978) *Mining Geostatistics*. Academic Press, London, 600 pp.

Pannatier, Y. (1996) VARIOWIN Software for Spatial Data Analysis in 2D. Springer-Verlag, New York, 91 pp.

CHAPTER 2

The semivariogram

2.1 BASIC CALCULATION AND PRINCIPLES

The first step in a geostatistical analysis is variography: computing and modeling a semivariogram. The semivariogram is the basic geostatistical tool for measuring spatial autocorrelation of a regionalized variable. As the name implies, a semivariogram is a measure of variance. Although procedures exist for modeling the semivariogram through iterative or least-squares methods, practitioners recommend actual inspection of the observed semivariogram and the fitted model. A properly fitted model then allows the computer program to calculate linear estimates that reflect the spatial extent and orientation of autocorrelation in the variable to be mapped.

A straightforward way of measuring how a variable z changes in value between site x and another site h units distant, say $x + h$, is to compute the difference $z(x) - z(x + h)$, as in Fig. 2.1. If the surface represented by the two points is continuous and h is a small distance, one expects the difference to be small. With increasing h, the difference increases. Translating this intuitive notion into a formula, one would like to observe the behavior of

$$2\gamma^*(h) = \frac{\Sigma\,[z(x) - z(x + h)]^2}{n}$$

or

$$\gamma^*(h) = \frac{\Sigma\,[z(x) - z(x + h)]^2}{2n}$$

The quantity $\gamma^*(h)$ is the semivariogram. Like the familiar variance of basic statistics, it is a sum of squares divided by the number n of sampled differences. Unlike simple variance about a mean, the semivariogram measures difference between two samples. However, simple variance can equal the semivariogram if one considers large values of h relative to

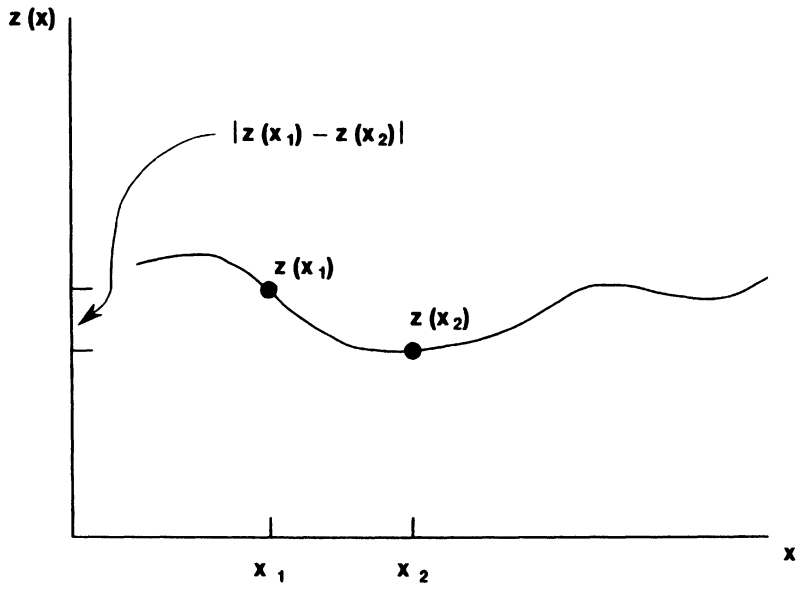

Figure 2.1 A hypothetical regionalized variable, z, in a single dimension, x.

the spatial variability of the area sampled and there exists no regional trend, called 'drift'.

The 'semi' in semivariogram comes from the fact it is a variance divided by 2. For reasons of convenience and brevity, the word is shortened to variogram by many authors, who consider the insistence on 'semivariogram' to be pedantic. I find variogram easier to say repeatedly. Above all, the writer should be consistent in a given paper or talk.

The semivariogram shows the values that $\gamma(h)$ takes on with h. The best way to understand the meaning of the semivariogram is to actually compute it from an example. At this point one wants to distinguish the true or theoretical value of $\gamma(h)$ from one estimated from samples, $\gamma^*(h)$. When a variable is measured at regular intervals along a transect, one can compute the semivariogram for integer values of h. In petroleum geology, irregularly spaced samples in a two-dimensional or three-dimensional space is the norm. Therefore, a value of $\gamma^*(h_1)$ is calculated from all sample pairs separated a distance between $h_1 - h/2$ and $h_1 + h/2$. Semivariance may be influenced by the direction of the vector between x and $x + h$, requiring the use of directional envelopes in addition to distance envelopes.

For an example, data were obtained from Fig. 10 of a paper by Gumati and Kanes (1985), describing Paleocene sedimentary rocks in Libya. Distances north and east in Appendix B are in arbitrary units equal to

about 0.3 mile per unit, and the regionalized variable is the thickness of the Paleocene rocks. In the original paper, these data were used to construct a hand-contoured isopach map. As the first step in making the semivariogram, one selects increments of distance and the size of the distance tolerance. The smaller the increment, the more points available to plot on the semivariogram, but also the fewer the number of pairs used to compute each value. The number of increments is limited by the extent of the area under study. Although a constant distance tolerance is usually assumed in running available computer programs, an alternative approach might be to use a smaller tolerance for a small distance, a larger one at large distances. Such a procedure is reasonable if sample locations are clustered such that small distance tolerances are overly represented relative to larger distances. As a further option, one can compute all possible intersample distances less than a certain value, calculate the squared differences, sort the results by distances, then calculate a mean semivariogram value for all pairs in the first tenth percentile, say, and similarly for all ten increments, to yield a constant sample size for each point on the semivariogram. Unfortunately, this procedure could yield few values of the semivariogram function at small distances.

Myers *et al.* (1982) studied variogram models for 13 elements and other geochemical variables measured in groundwater in Texas. Although not occurring on a regular grid, observations were not clustered, and the sample size for $\gamma^*(h)$ at small values of h would have been small. Therefore, values of h were sorted and grouped into irregular intervals of equal sample size n. The calculated value of $\gamma^*(h)$ was graphed against the mean h for each interval. They followed this procedure for several values of n to determine an optimal sample size.

In practice, drawing the semivariogram is an iterative job in which one attempts to strike a balance between the smooth curve afforded by large sample sizes and a sufficient number of points to fit a semivariogram model. Journel and Huijbregts (1978) offer two rules of thumb: for each computed value of the semivariogram function, the number of pairs should be greater than 30; the section of interest of the semivariogram, usually the increase at relatively small distances, should be represented by three or four values. Webster and Oliver (1993) maintain that this number of pairs is far too low, and that 150 to 200 samples are necessary to obtain the minimum number of pairs for reasonably precise measurement of the semivariogram. With the small number of samples available in the Paleocene thickness data, either rule of thumb is hard to follow.

Returning to the example, assume a distance increment of 2 units and a tolerance of +1 unit. Seven pairs of samples fall in the range: $1 \leqslant h < 3$; these are shown in Fig. 2.2 as the solid lines connecting sample locations. Therefore, $\gamma^*(2)$ is calculated as follows:

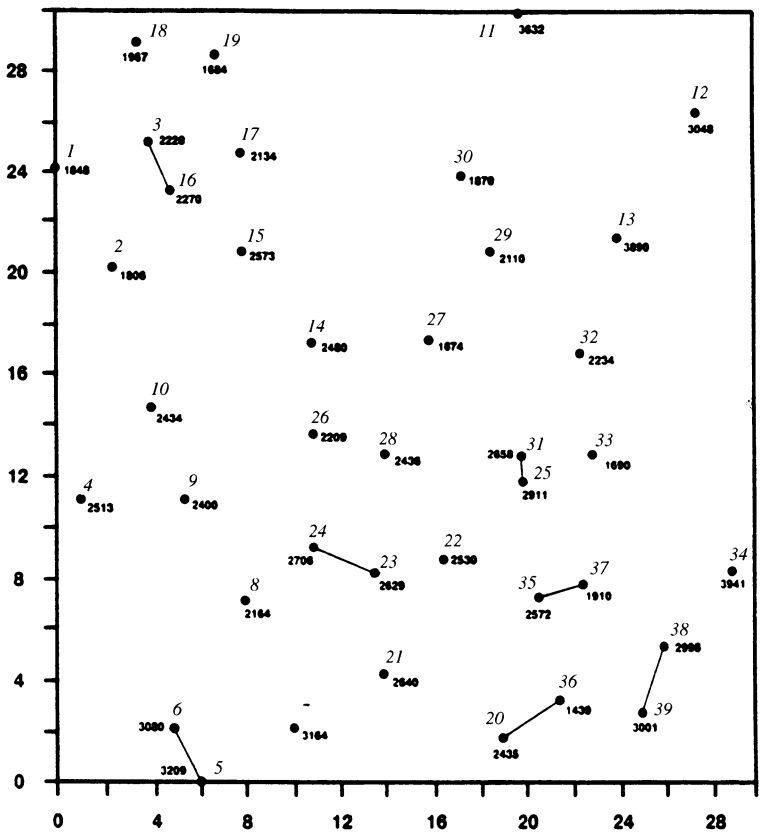

Figure 2.2 Sample location map of Paleocene clastic thicknesses taken from Gumati and Kanes (1985). Solid lines connect points separated by distances between one and three units.

$$\begin{aligned}\gamma^*(h) &= 1/2n[(2911-2658)^2+(2572-1910)^2\\ &\quad +(3209-3080)^2+(2220-2270)^2\\ &\quad +(2995-3001)^2+(2629-2706)^2\\ &\quad +(2435-1439)^2]\\ &= 108\,500\end{aligned}$$

Table 2.1 shows the calculated values of the experimental semivariogram for seven values of h, and Fig. 2.3 the semivariogram. Note that distances beyond about half the dimensions of the study area were not considered for several reasons: at greater distances the number of pairs decreases; beyond this distance the semivariogram contrasts values of the variable along the edges of the study area; finally, most mapping applications do not require knowledge of $\gamma^*(h)$ beyond a relatively small distance. One does not consider measured values at one edge of a study area when contouring the opposite edge.

Table 2.1 Calculated values for semivariogram of Paleocene clastics data

Distance	*Semivariogram*	*Number of pairs*
2.26	108 500	7
4.16	207 000	45
5.93	289 000	51
8.06	299 200	52
9.85	251 800	81
11.99	213 600	61
13.94	306 600	73
15.87	418 100	65
17.96	360 100	72

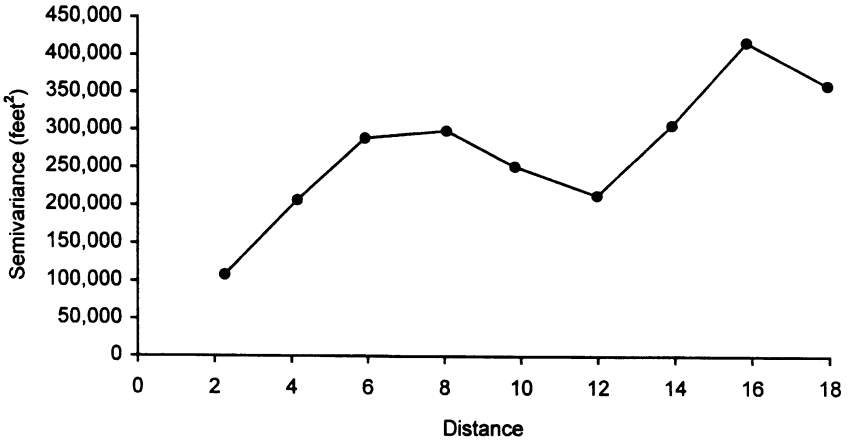

Figure 2.3 Experimental semivariogram for Paleocene clastic thickness.

2.1.1 Anisotropy

The semivariogram in the previous section was constructed under the assumption that the statistic: $[z(x) - z(x + h)]^2$ was dependent upon the value of h, and independent of x and the orientation of the vector between x and $x + h$. However, many geologic phenomena display spatial anisotropy in variance. For instance, a structure contour map of a stratigraphic horizon in the folded Appalachians shows a marked directionality in variation. Variability along the northeast–southwest axes of synclines and anticlines is much smaller for a given distance than that in a northwest–southeast direction.

Constructing the semivariogram in order to reveal anisotropy involves the same calculations used in the previous section, but now vectors

between pairs of samples are grouped into both distance and direction classes. Selecting an appropriate number of directions usually requires some experimentation and invokes the tradeoffs between sample size and detail discussed above. In addition to a distance tolerance, the computer program must also use a tolerance in orientation (Fig. 2.4). A reasonable tolerance is one-half the angle between the directions selected, analogous to the distance tolerance.

Structural data often show anisotropy in the semivariogram. The base of a Mississippian-age reservoir sandstone in Ritchie County, West Virginia is no exception. This unit includes light gray, fine- to medium-grained, poorly sorted and interbedded shales in the Pocono Group and highly calcareous or dolomitic sandstones in the overlying Greenbrier Group. The Pocono and Greenbrier portions cannot be distinguished without geophysical logs or samples and are treated as a single unit.

Subsea depths of the reservoir base were available for 348 locations, distributed across most of the county (Fig. 2.5). Experimental semivariograms were constructed for the four directions shown in Fig. 2.6. Semivariograms for north–south and northeast–southwest directions rise up to a separation distance of about 2 km, and then level off. In contrast, semivariograms for the other two directions continue to rise, and look quite different from the first two semivariograms beyond 5 km. The appearance of the semivariogram thus agrees with the well-known fact that prevailing structural grain in the Appalachians is along a roughly northeast to southwest axis, with local exceptions. In this area, structural grain appears to be north-northeast to south-southwest.

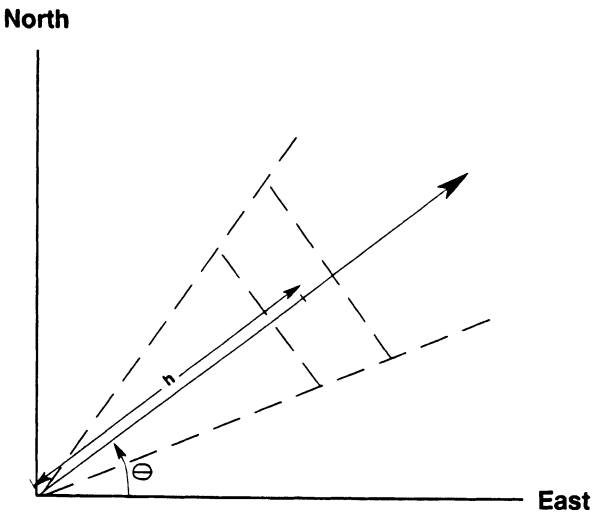

Figure 2.4 Method of setting distance and direction tolerances.

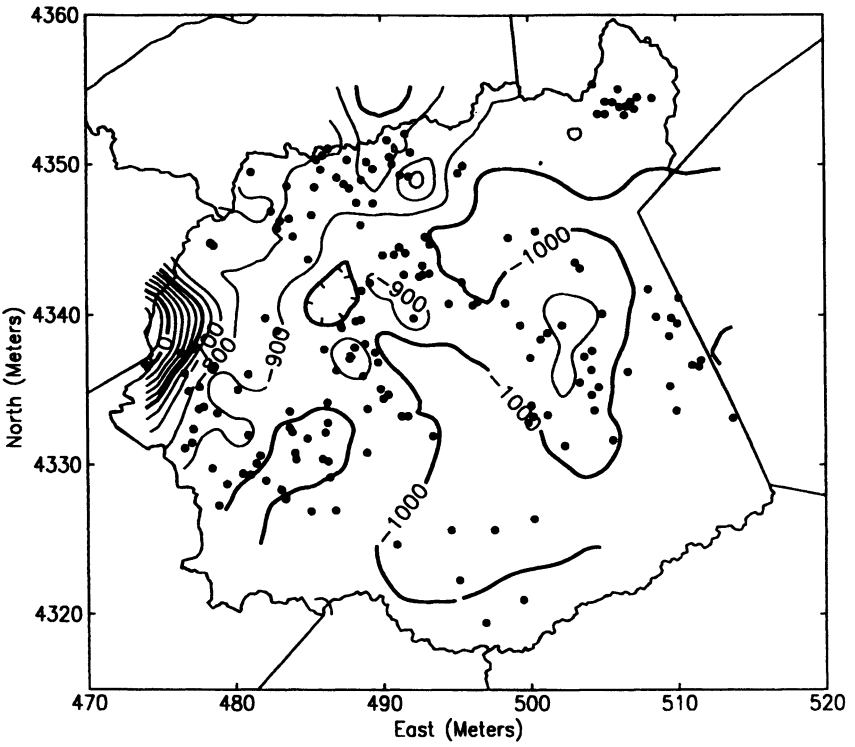

Figure 2.5 Location of wells in Ritchie County, West Virginia, with reported values of subsea depths for the base of a Mississippian reservoir sandstone. Map coordinates are in kilometers.

A useful plot for showing the principal direction of anisotropy is a contour map of the semivariogram surface. Such a plot can be generated directly from the output of most computer programs for calculating semivariograms by plotting calculated values on polar coordinates. A better display results when tolerances in h are defined on rectangular coordinates; this yields a grid of semivariogram values that can be contoured. Fig. 2.7 shows results obtained through the VARIOWIN program of Pannatier (1996). Note that the semivariogram is symmetric about the origin and therefore only an arbitrary half of Fig. 2.7 needs to be drawn, but showing a full 360° is more effective in showing the principal directions of anisotropy.

2.1.2 Effect of distance classes on the semivariogram

Data used in the previous example also show the effect of distance interval on the appearance of the experimental semivariogram. Selecting an interval of 2 km yields a very smooth curve for the northeast–

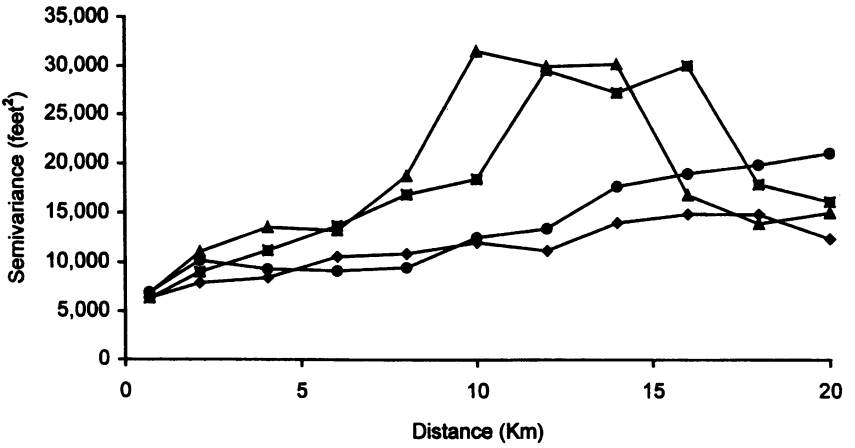

Figure 2.6 Experimental semivariograms of the subsea depth of the base of the Mississippian reservoir sandstone in Ritchie County, West Virginia. Directions are: north (diamond), northeast (circle), east (square), and southeast (triangle).

southwest direction, but only one value shows the behavior of the curve near the origin (Fig. 2.8). This lack of values can become a liability when one attempts to fit a model. On the other hand, a value of 0.5 km appears too small; the observed values of $\gamma(h)$ jump about and depend upon small numbers of pairs at 0.5 km (62 pairs) and 1 km (86 pairs). A distance interval of 1 km yields a smoother curve that preserves some detail. Unfortunately, the only value that helps to define the semivariogram near the origin is based on only 21 sample points.

One observation that can be made from this analysis is that the semivariogram increases rapidly from 0 to 1 km, where it flattens out. Beyond about 9 km, it rises again.

2.1.3 Stationarity

The first chapter stated that a group of spatially distributed samples can be treated as a particular realization of a random function. If a phenomenon is homogeneous over a study area, observed values $z(x_1)$ and $z(x_1 + h)$ can be considered realizations of the same random variable with a particular distribution function.

Only one realization of a random function such as the base of a reservoir sandstone is available for a given value of x. Knowledge that this datum occurs within certain limits allows one to use all the data to study the probability distribution of the random function. The independence of statistics such as mean, variance, or covariance with respect to location is called **stationarity**.

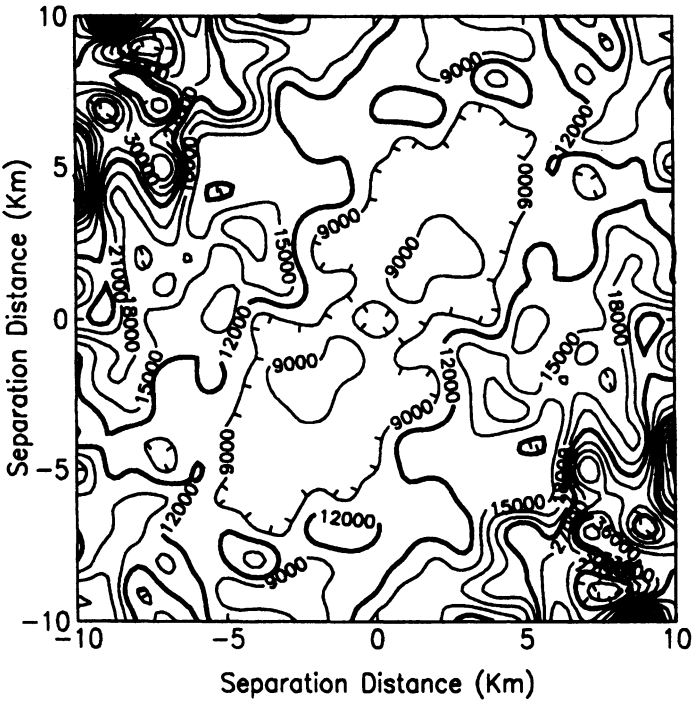

Figure 2.7 Semivariograms for depth of sandstone reservoir, displayed as a contour map.

Stationarity is defined through first- and second-order moments of the observed random function, and degrees of stationarity correspond to the particular moments that remain invariant across a study area. For a random variable $Z(x)$ observed at point x, the distribution function of $Z(x)$ has an expectation

$$E\{Z(x)\} = m(x)$$

which can depend upon x. This is the first-order moment. Three second-order moments are useful in geostatistics:

1. The variance of the random variable $Z(X)$:
   $\text{VAR}\ \{Z(x)\} = E[Z(x) - m(x)]^2\}$
2. The covariance:
   $C(x_1, x_2) = E\{[Z(X_1) - m(x_1)]\ [Z(X_2) - m(X_2)]\}$
   where $Z(x_1)$ and $Z(x_2)$ are two random variables observed at x_1 and x_2. The covariance can be a function of x_1 and x_2.
3. The semivariogram function:
   $g(x_1, x_2) = \text{VAR}\ \{Z(x_1) - Z(x_2)\}/2$

The four degrees of stationarity considered important in geostatistics are strict stationarity, second-order stationarity, the intrinsic hypothesis,

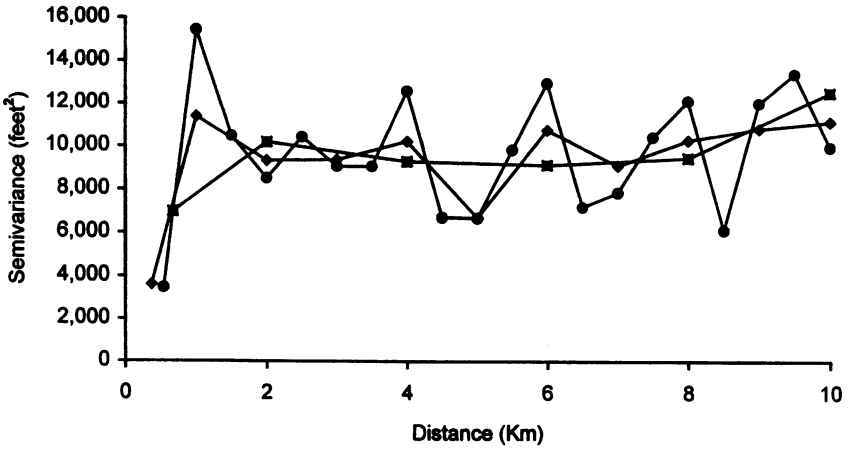

Figure 2.8 Semivariograms for depth of sandstone reservoir in the northeast–southwest direction, showing the effect of the size of the distance classes. Filled circles = 0.5 km; diamonds = 1 km; squares = 2 km.

and quasi-stationarity. Define the **spatial law** of a random function as all distribution functions observed for all possible points in a study area. Strict stationarity requires an invariant spatial law between any two random variables $\{Z(x_1), Z(x_2) \ldots Z(x_k)\}$ and $\{Z(x_l + h), Z(x_2 + h) \ldots Z(x_k + h)\}$.

In other words, the distribution function remains unchanged with respect to h. Because most geostatistical applications only need the first two moments, the assumption of strict stationarity is unnecessary.

Second-order stationarity of a random function requires the following:

1. The expectation $E\{Z(x)\} = m(x)$ does not depend upon x, i.e. the expectation is invariant across the study area.
2. The covariance depends only on separation distance h, i.e.
   $C(h) = S\ \{Z(x) \bullet Z(x + h)\} - m^2$ for all x.
   The vector h can be one dimension or more.

If the covariance $C(h)$ is stationary, the variance and the semivariogram are also stationary:

$$C(0) = E\{[Z(x) - m]^2\} = \text{VAR}\ \{Z(x)\}$$
$$g(h) = E\{[Z(x + h) - Z(x)]^2\}/2 = C(0) - C(h).$$

The **correlogram** is defined as

$$r\ (h) = C(h)/C(0) = 1 - \gamma(h)/C(0).$$

Under conditions of second-order stationarity, the semivariogram and the covariance are alternative measures of spatial autocorrelation.

The intrinsic hypothesis requires that expected values of the first moment and the semivariogram are invariant with respect to location. By not requiring stationarity of the covariance and therefore the existence of a finite variance C(0) of the random function, the intrinsic hypothesis is a reduced form of second-order stationarity. The intrinsic hypothesis is sufficient for most geostatistical problems.

The concept of stationarity is used tacitly by geologists in everyday work and is not merely a set of rules and definitions that make possible the geostatistical methods to come. Stationarity of the first moment is assumed in a statement like 'The base of the Greenbrier Group occurs about 900 feet below sea level in Ritchie County, West Virginia'. This statement does not preclude the assumption that the base of the Greenbrier Group varies in depth from well to well as a result of geologic structure. Stationarity in the semivariogram is invoked by the logic, 'My well is half a kilometer from a well where the base of the Greenbrier Group is 925 feet below sea level, so I expect the Greenbrier Group to be about 925 feet below sea level in my well'.

A variable under study may actually have a trend across the area of interest, i.e. show a 'drift'; such a variable is not stationary in the ways defined above. However, one can define quasi-stationarity as a local stationarity when the maximum distance h used in computing the semivariogram or the covariance is much smaller than the scale of the trend. For instance, elevation of a stratigraphic horizon would not be stationary across a 5-km-wide anticline, but could appear stationary within distances of 0.25 km. The impact of nonstationarity depends in part on the scale of sampling in relation to the scale of a systematic trend. With sufficient sampling, stationarity can be achieved, but the petroleum geologist seldom has control over the sample distribution. Note that if the anticline is one of dozens in a large study area, it represents local variability in the regional elevation of the stratigraphic horizon.

2.2 MODELING AN OBSERVED SEMIVARIOGRAM

2.2.1 Theoretical models

Fitting a standard model to an observed semivariogram must precede estimation and mapping by geostatistical methods. The process of fitting a model to an observed semivariogram is called a 'structural analysis' in most books on mining geostatistics. The model chosen for a given set of data depends upon both practical and theoretical considerations. Most experimental semivariograms can be described by a very few models, and thus the option of fitting more esoteric models can be ignored. As described in subsequent chapters the semivariogram model is used for

computing parameters necessary to kriging, which in turn places constraints on the properties of the theoretical semivariogram. The semivariogram must satisfy a certain criterion to be admissible. Admissible functions are discussed after a survey of semivariogram models most often encountered.

The two features of the observed semivariogram that guide practitioners in fitting a theoretical model are: (1) presence or absence of a **sill**, and (2) behavior at the origin. Most of the semivariograms illustrated in this chapter show evidence of a sill: a leveling off of $\gamma(h)$ once h increases beyond some distance a. Behavior at the origin falls into two types, linear and parabolic.

Another feature of the semivariogram that one can observe from illustrations in this chapter is the tendency of the observed curve not to approach the origin at small values of h. If one was to fit a straight line to the first two or three points in any of the figures, the y intercept would be greater than zero. This so-called **nugget effect** must be taken into account by a model.

Three models occurring most often in the literature are the spherical, the exponential, and the Gaussian. The spherical model is by far the one most often used in recent years. The equation of a spherical model is as follows:

$$\gamma(h) = C\left[\left(\frac{3h}{2a}\right) - \left(\frac{h^3}{2a^3}\right)\right] \qquad \text{for } h \leq a$$

$$\gamma(h) = C \qquad \text{for } h > a$$

where c = sill and a = range.

In the example shown in Fig. 2.9, the range a equals 9, and the sill equals 500 units. Near the origin the curve behaves linearly. This fact has been exploited when fitting the spherical model to real data; a straight line fitted to the two observed semivariogram values at lowest h intersects the sill at $\frac{2}{3}$ of the range. In Fig. 2.9 the tangent reaches the sill at $h = 6$ units.

The exponential model has the following equation:

$$\gamma(h) = C\left[1 - \exp\left(-\frac{h}{a}\right)\right]$$

Like the spherical model, this one shows linear behavior at the origin (Fig. 2.10), but unlike the previous model, a tangent drawn at the origin

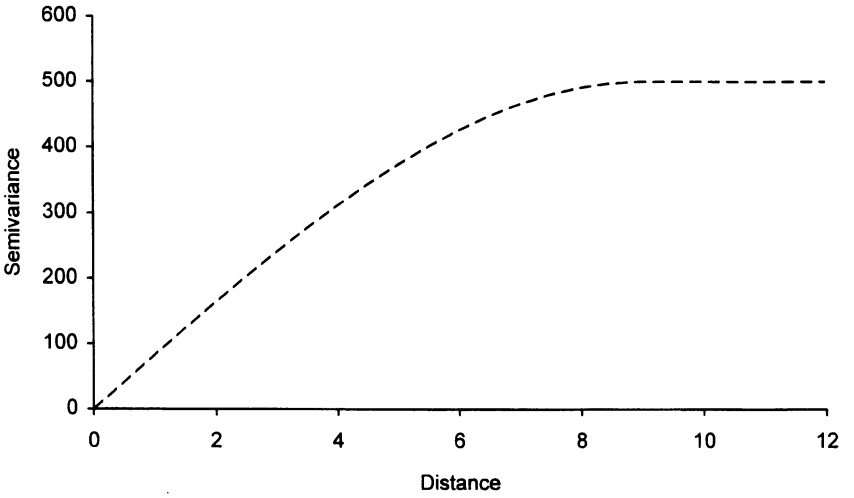

Figure 2.9 A spherical semivariogram model.

reaches a value equal to the sill at a distance one-third of the practical range, which equals 3a. Figure 2.10 shows an exponential model with a sill of 500 units and a range of 3. Beyond the practical range of 9, the exponential model approaches the sill asymptotically.

Some care must be exercised in using the exponential model with computer software for geostatistics. Some programs use the following equation:

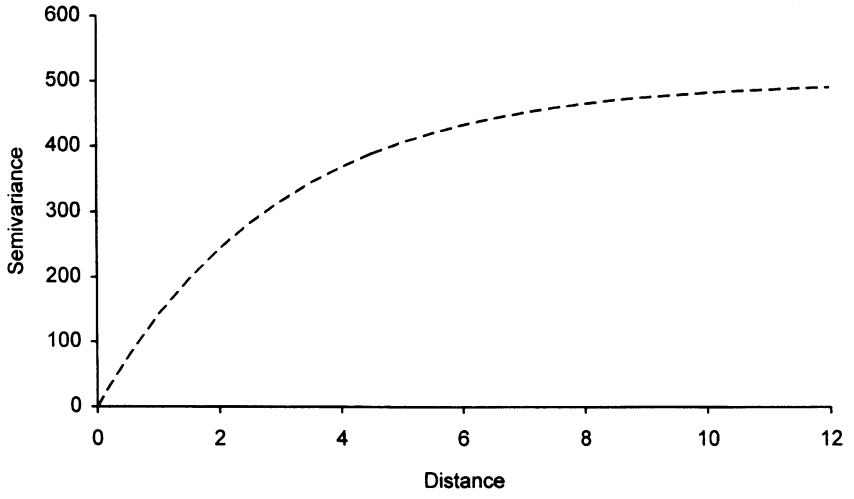

Figure 2.10 An exponential model.

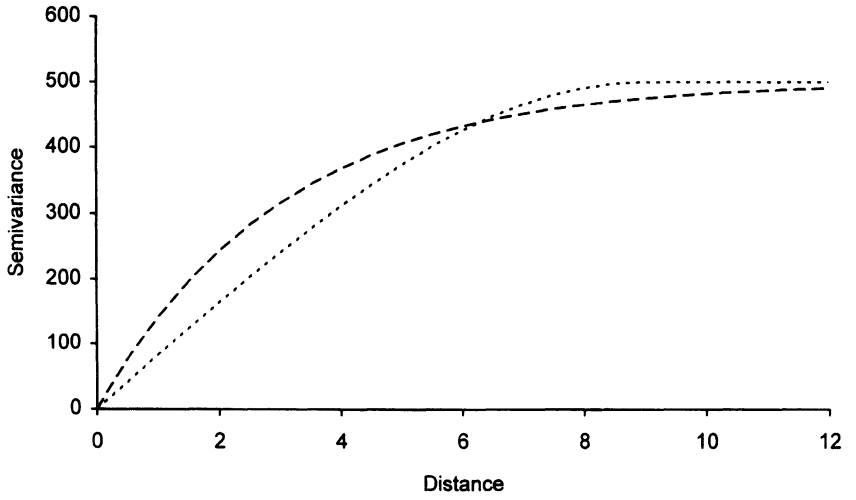

Figure 2.11 Graphical comparison of spherical (dotted line) and exponential (dashed line) models for the semivariogram.

$$\gamma(h) = C\left[1 - \exp\left(-\frac{3h}{a}\right)\right]$$

so that the range a equals the practical range. If using software from different sources for semivariogram modeling and kriging, the user can unintentionally specify a range that is wrong by a factor of three.

Figure 2.11 shows both models discussed to this point in order that the reader can compare the shapes. The exponential model rises more rapidly at the origin but levels off more gradually than the spherical model. The latter shows an abrupt change in behavior near the sill. These observations become helpful when one goes to fit a model to actual data.

The Gaussian model possesses a sill, but behaves parabolically at the origin:

$$\gamma(h) = C\left[1 - \exp\left(-\frac{h^2}{a^2}\right)\right]$$

The Gaussian model (Fig. 2.12) resembles the characteristic parabolic behavior of the experimental semivariogram in the presence of regional trend and may be used in lieu of a drift effect at small distances of h. In petroleum geostatistics, the Gaussian model is used with structural data in which there is a pronounced trend, or with seismic data in which the 'sample' spacing is very close and the degree of continuity is high.

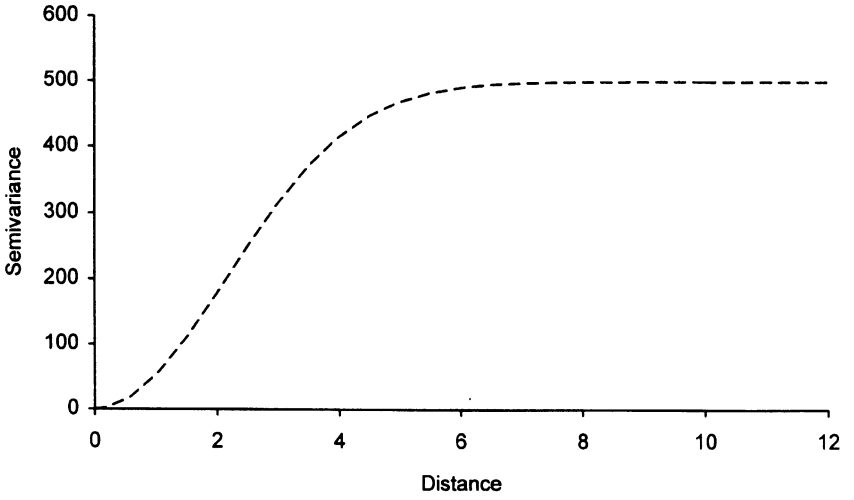

Figure 2.12 A Gaussian semivariogram model.

The simplest of models without a sill is the linear model:

$$\gamma(h) = ph$$

where p is the slope of the line. At small distances of h the linear model can be used in place of other models showing linear behavior at the origin, i.e. the spherical and exponential models, but such a procedure has little practical value.

Finally, a general linear model is possible:

$$\gamma(h) = ph^r$$

where p is a constant and $0 < r < 2$. Models with values of $r < 1$ resemble a spherical or exponential model at the origin, and those with values of $r > 1$ are parabolic at the origin. The simple linear model is a member of this class of models and is about the only one encountered in the literature.

The logarithmic or De Wijsian model also lacks a sill:

$$\gamma(h) = r \ln (h)$$

The semivariogram of the De Wijsian model is linear if plotted against the logarithm of distance.

2.2.2 Nugget effect

Many observed variograms do not approach zero with decreasing separation distance. Instead, projecting a straight line fitted to the first few

points of the experimental semivariogram gives a nonzero y-intercept, C_0. This observation has become known as the nugget effect from the characteristic appearance of the semivariogram for gold deposits.

The nugget effect implies abrupt changes in the regionalized variable over small distances, variability at a spatial scales finer than sample spacing, or low precision in the measurement.

Presence or absence of a nugget effect can depend upon the scale of sampling relative to the geographic scale of variation in the phenomenon. Taking the example of a fractured reservoir, adjacent wells can exhibit very different behavior depending upon their relative proximity to natural fractures. The need to intersect natural fractures presents nearly an all-or-nothing situation to the geologist. The range of influence of a fracture depends upon the probability that a vertical well intersects the fracture, which depends in turn upon the thickness of the target formation, whether the fracture is limited to the formation, and the degree to which the fracture is vertical. Creation of fractures through completion technology increases the chances of a well communicating with a natural fracture. Thus, the range of influence of a natural fracture is effectively increased. If a reservoir rock is very much fractured relative to normal well spacings, the variability due to fracturing no longer appears as a component of the nugget effect. Similarly, if wells were allowed to be spaced as close as physically possible, the probability of intersecting a fracture would present a continuous surface, and the contribution of fracture patterns to the nugget effect would disappear.

The sources of measurement error in petroleum geology are many. For instance, obtaining a good formation thickness from an electric log can depend upon quality of the log, the ability of the geologist to recognize formation signatures across a field or basin, and the ratio of the thickness of the unit to the scale of the log. The petroleum geologist often has little or no control over the source and quality of data. Information such as initial potential and cumulative production, can be obtained from public records, with the result that the geologist relies upon the ability and integrity of others. Initial potential can depend upon the time and duration of the measurement. A figure can be transcribed to a driller's log incorrectly and misinterpreted by the geologist assuming the figure represents final open flow from one formation when in fact flows have been commingled. Company practice in completing wells has an effect. One company completes the full thickness of the given formation; another completes an individual sand, believing it to be the principal reservoir rock. Finally, the order in which wells are drilled and completed relative to the depletion of a field can affect measured initial potential.

The preceding discussion suggests that a nugget effect is no more than one of the standard semivariogram models with a very small range,

e.g.

$$\gamma(0) = 0$$

$$\gamma(h) = C_0 \left[1 - \exp\left(-\frac{h}{a}\right)\right] \qquad \text{for } h > 0$$

where a is a very small distance relative to well or sample spacing. Thus, the observed nugget effect is the sill, C_0 of this model. In all practicality, one does not attempt to fit a specific model because it cannot be observed except through additional sampling, which is probably not possible.

Journel and Huijbregts (1978) provide a general definition of a nugget effect as the sum of all sources of variation with ranges much smaller than the distances between samples. When a semivariogram appears completely flat – or at least varies randomly about a flat line – it is said to show a pure nugget effect and represents an absence of any spatial autocorrelation. One can conclude that the samples are spatially independent. Writing the nugget effect model as follows:

$$\gamma(0) = 0 \qquad \text{for } h \leq a$$
$$\gamma(h) = C_0 \qquad \text{for } h > a$$

covariance is written:

$$C(h) = C(0) - \gamma(h)$$

so that:

$$C(h) = C(0) = C_0 \qquad \text{for } h = 0$$

$$C(h) = C_0 - \gamma(h) = 0 \qquad \text{for } h > a$$

Because a is close to 0, the covariance is zero for all observable separation distances.

Thus, the nugget effect represents a random component in a regionalized variable. It can be called noise and is modeled with a single number, C_0, which represents the sill of a model with very small range. If the petroleum geologist could be sure of the source of variation in a given context, the term nugget effect could be dropped for a more appropriate one like fracture effect or stratigraphic effect. Rarely would such an assignment be possible. In general, one would like to reduce the nugget effect in order to improve the precision of estimates. Ways one can reduce the nugget effect include obtaining better well control, re-examining the data for sources of error, and applying adjustments and correction factors.

2.2.3 Nested models

Few experimental semivariograms resemble the simple models described above; usually at least a nugget effect is present in addition to a spherical or exponential model. A model written as the sum of two or

more simple models is said to be nested. One of the simple models with nugget effect is strictly speaking a nested model, but not usually called one. For an example:

$$\gamma(h) = \gamma_1(h) + \gamma_2(h)$$

where

$$\gamma_1(h) = C\left[\left(\frac{3h}{2a}\right) - \left(\frac{h^3}{2a^3}\right)\right] \qquad \text{for } h \leq a$$

$$= C \qquad \text{for } h > a$$

and

$$\gamma_2(h) = C_0$$

for all a.

More typically, a model of the following form is called a nested model:

$$\gamma(h) = \gamma_1(h) + \gamma_2(h) + \gamma_3(h)$$

where $\gamma_1(h)$ is a nugget effect, and $\gamma_2(h)$ and $\gamma_3(h)$ are two exponential models. In general, a nested model is the sum of two or more semivariograms having different ranges and sills, and possibly directions of anisotropy:

$$\gamma(h) = \gamma_1(h) + \gamma_2(h) + \ \ldots\ \gamma_1(h)$$

Each semivariogram expresses variability at a particular spatial scale.

For an example of a nested model, a fractured reservoir such as the Devonian shales in the Appalachians can possess several sources of variation in porosity, permeability, initial potential of oil or gas, or cumulative production.

1. At the level of the well, variability attributable to completion method and measurement error.
2. At a scale of, say, 0.5 km, presence of vertical natural fractures such that the production potential of a well depends upon the probability of intersecting the fracture in or near a siltstone bed.
3. At a scale of 10 km, the thickness of the siltstone bundles that serve as a principal reservoir facies within the shales in some areas.

Each of these sources of variation can be modeled given sufficient well density, except that variation at the level of the single well would be modeled as a nugget effect. The hypothetical model in Fig. 2.13 includes three terms: $\gamma_1(h)$ for measurement error, $\gamma_2(h)$ for fracture intersection, and $\gamma_3(h)$ for thickness of siltstone. Note that all sources of variation

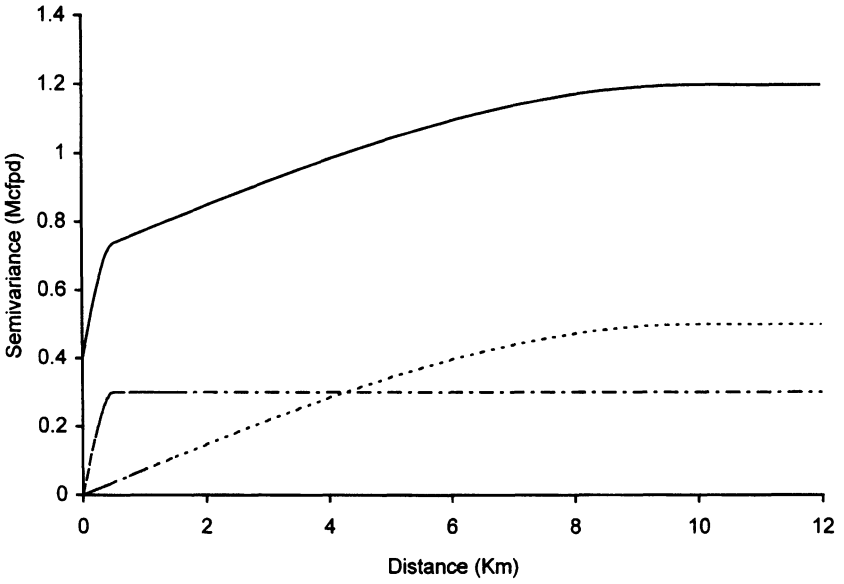

Figure 2.13 Hypothetical nested semivariogram model of initial potential. Shown are component models and the sum.

come into play at all separation distances, although the principal variability at small distances arises from sources with small ranges.

2.2.4 Admissibility

Semivariogram models described in the previous section show one property that becomes important at the estimation stage, namely, they are conditionally positive definite. Given a stationary random function $Z(x)$ with covariance $C(h)$, let Y be a linear combination with weights λ_i:

$$Y = \sum_{i=1}^{n} \lambda_i Z(x_i)$$

which is a random variable with variance

$$\text{VAR}\{Y\} = \sum_{i=1}^{n} \sum_{j=1}^{n} \lambda_i \lambda_j C(x_i - x_j)$$

which must be greater than or equal to zero. $C(h)$ is said to be positive definite. Any covariance model fitted to observed values of covariance must have the property that VAR $\{Y\} \geq 0$ because estimations such as kriging use linear combinations of known values. In terms of the semivariogram, admissible functions must satisfy the relationship:

$$\text{VAR}\{Y\} = \sum_{i=1}^{n} \sum_{j=1}^{n} \lambda_i \lambda_j \gamma(x_i - x_j)$$

for any n locations $x_1, x_2 \ldots x_n$ of a random variable, and any weights λ_1, $\lambda_2 \ldots \lambda_n$ such that:

$$\sum_{i=1}^{n} \lambda_i = 0$$

Thus, a model for $\gamma(h)$ must be checked for admissibility, or one of the standard models used. Fortunately, models such as the spherical and exponential have been shown to be positive definite: the spherical for up to three dimensions, and the exponential for more.

Nested models pose no difficulties because any linear combination of admissible functions has positive definite covariances. Thus, we generally do not have to consider the question of admissibility. One must guard against the temptation to use arbitrary polynomials for fitting semivariograms automatically with a computer program.

2.2.5 Covariance

Under conditions of second-order stationarity, graphs of covariance and the semivariogram are alternative representations of spatial dependance. The relationship:

$$\gamma(h) = C(0) - C(h)$$

means that the covariance behaves inversely with the semivariogram. Just as the semivariogram increases with separation distance, the covariance decreases (Fig. 2.14). The semivariogram of a regionalized variable possessing second-order stationarity exhibits a sill $C(0)$, which equals the sample variance of the variable. Two values observed at separation distances greater than a are independent.

2.2.6 A simple example

Data in Table 2.2 are values of the experimental semivariogram for initial potential of gas recorded from 1216 wells producing from Upper Devonian sandstones and siltstones in Barbour County, West Virginia (Fig. 2.15). Production can come from one or more sands in the Upper Devonian section (Fig. 2.16). Size and stratigraphic level of the completion zone obviously varies from well to well, and ideally one wants to study initial potential of each pay zone in isolation. In reality, most wells have more than one pay zone, and volumes are commingled on the records available. Therefore, geostatistical analysis at best treats the expected behavior of the typical Upper Devonian well in the study area.

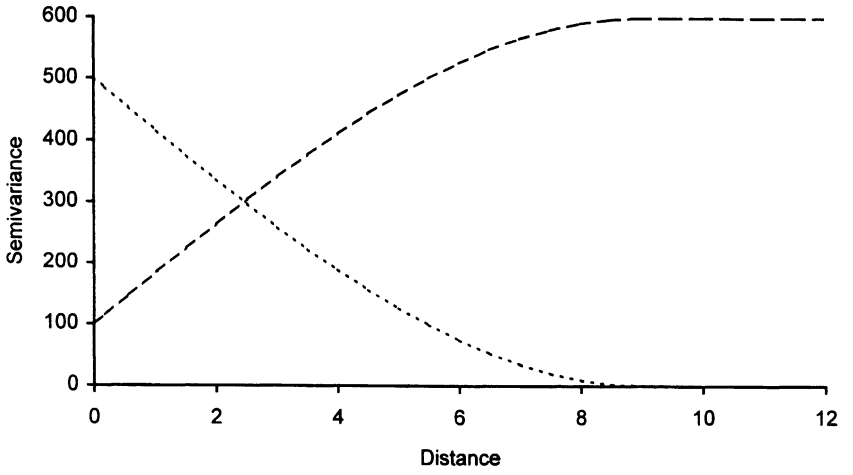

Figure 2.14 Comparison of covariance with the equivalent semivariogram.

The graph of the semivariogram (Fig. 2.17) shows the general shape of a spherical or exponential model with possibly a nugget effect. A first attempt uses a spherical model (Fig. 2.18); equation for the model is:

Table 2.2 Semivariogram of gas initial potential from wells in Barbour County, West Virginia

Distance (km)	*Semivariogram (Mcfpd²)*	*Number of pairs*
0.18	630 073	64
0.56	1 414 794	1 791
1.02	1 600 760	3 456
1.51	1 763 792	4 863
2.01	1 785 528	6 220
2.51	1 752 289	7 448
3.01	1 939 881	8 685
3.50	1 750 987	9 733
4.01	1 791 542	10 730
4.50	1 831 248	11 510
5.00	1 860 682	12 329
5.50	1 922 626	13 044
6.00	1 859 647	13 869
6.50	1 733 616	14 481
7.00	1 828 121	15 147
7.50	1 832 027	15 523
8.00	1 834 715	16 160
8.50	1 801 883	16 928
9.00	1 863 105	17 288
9.50	1 743 702	17 648
10.00	1 760 844	17 957

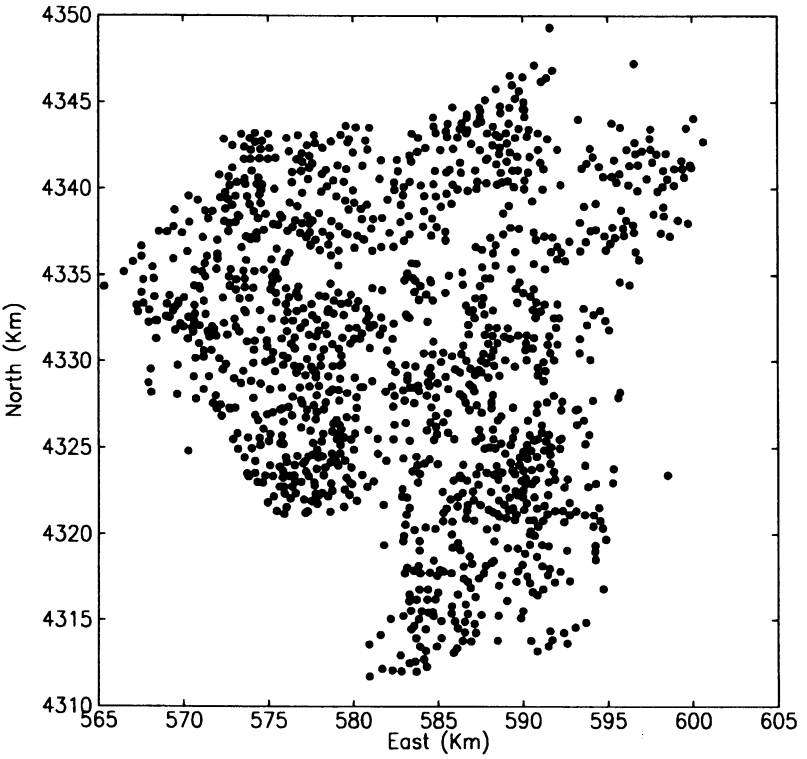

Figure 2.15 Locations of wells producing gas from Upper Devonian rocks in Barbour County, West Virginia. Map coordinates are in kilometers.

$$\gamma(h) = 1.8 \times 10^6 \left[\frac{3h}{2{\cdot}0.9} - \frac{h^3}{2{\cdot}0.9^3} \right]$$

In general, parameters used on this first pass appear good, but the model rises too quickly for small values of h. A larger range provides a better fit in this region but reaches the sill at too short a distance. The whole appearance of the spherical model appears wrong, suggesting use of an exponential model.

Figure 2.19 shows the fit of an exponential model to the observed data. Results are much better. The exponential model has a sill of 1 800 000 Mcfpd^2 and a range of 0.4 km, giving the equation:

$$\gamma(h) = 1.8 \times 10^6 \left[1 - \exp\left(-\frac{h}{0.4} \right) \right]$$

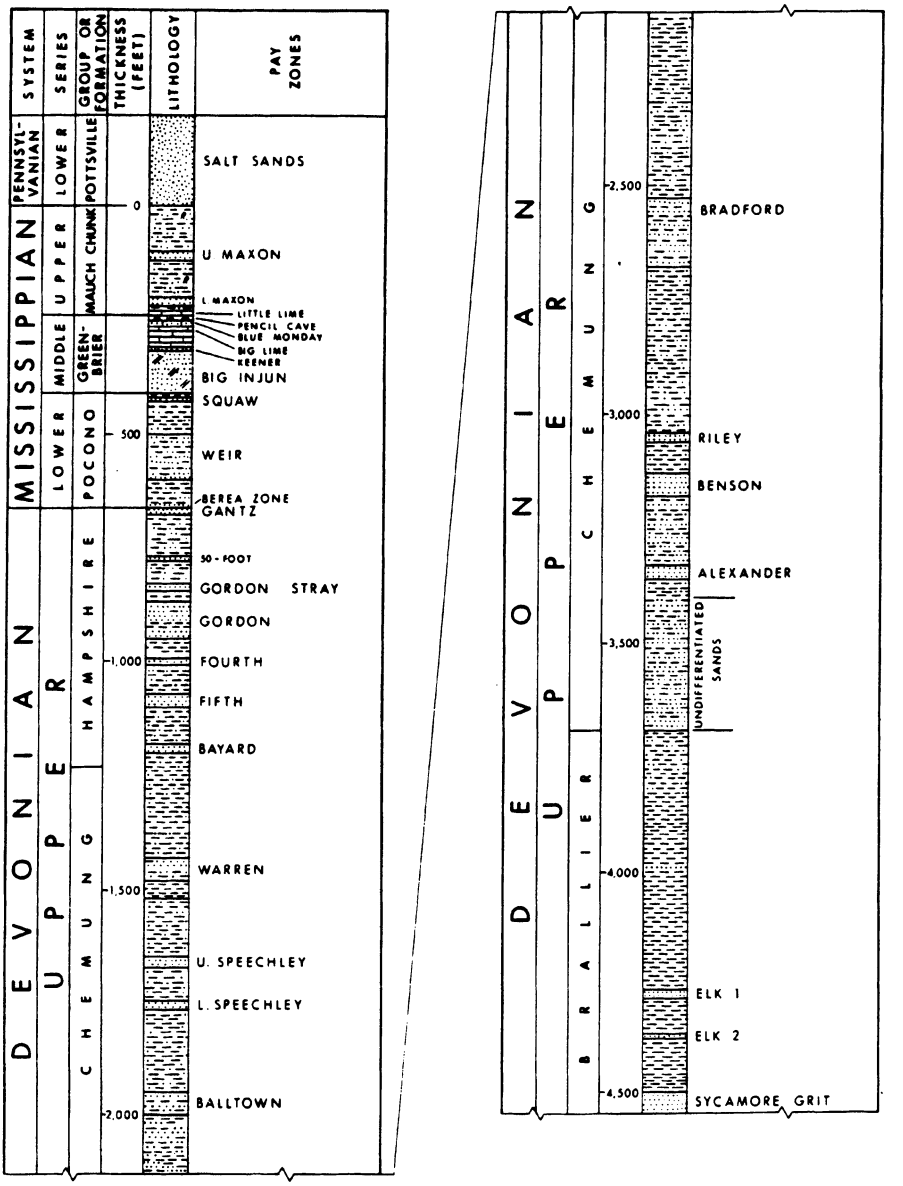

Figure 2.16 Partial stratigraphic section of subsurface rocks in Barbour County, West Virginia, including Brallier and Chemung clastics used in example.

The fit is so good that one could suspect that the data set was constructed for the occasion. However, real data were used, and the impressive appearance of the semivariogram probably follows from the large number of wells with data available, the homogeneity of initial

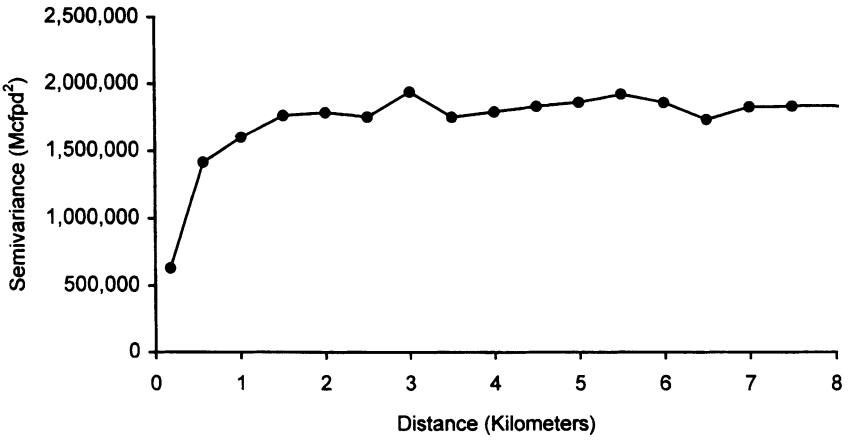

Figure 2.17 Semivariogram of initial potentials of gas from Upper Devonian clastics.

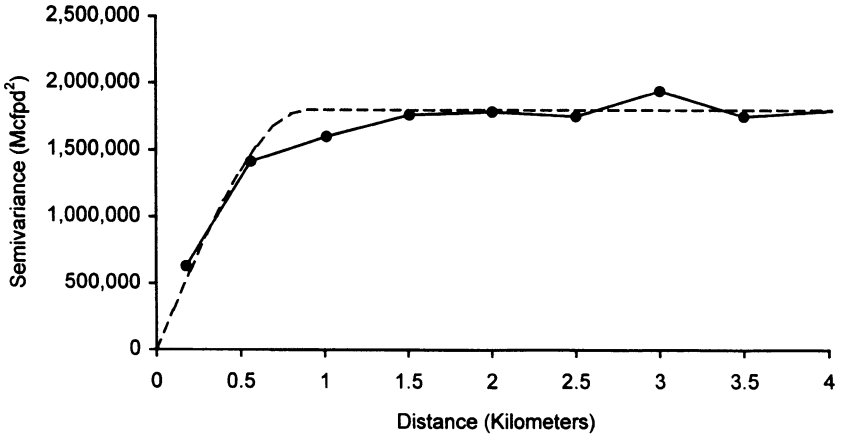

Figure 2.18 Spherical model fitted to gas initial potentials.

potential across the study area, and a sufficient number of closely spaced wells. The number of pairs per calculated value of the semivariogram function is certainly high (Table 2.2), even for small separation distances.

The geological meaning of the semivariogram of initial potential is less impressive. The semivariogram rises very quickly and has nearly reached the sill at a 2 km separation distance. The practical side of this observation is that one might not want to draw contours on a map more than 2 km away from the nearest control point.

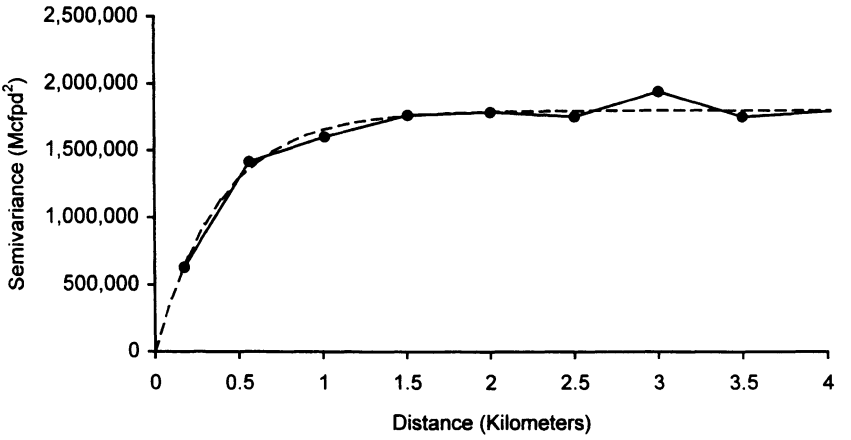

Figure 2.19 Exponential model fitted to gas initial potentials.

2.2.7 Example of a nested model

Fitting a more complex, nested model to a semivariogram follows the same iterative process of selecting parameters, comparing the resulting curve with the real data, and adjusting the parameters. This job is best done with an interactive program that allows the user to change ranges, nugget effect and sills, and display observed and semivariogram models. Although none of the computations are difficult or involved, iterations to an acceptable fit are repetitive enough to discourage the geostatistician having to do them on a calculator.

The semivariogram in Table 2.3 and Fig. 2.20 does not appear to conform to simple models. Therefore, an attempt will be made to model three main features:

1. A nugget effect
2. A rapid rise of the semivariogram at distances less than 2 km
3. A gradual, straight-line rise to a sill, around which the semivariogram meanders.

With further modeling, the meandering around the sill could be taken into account. The need to model accurately beyond a separation distance greater than 10 km depends upon the ultimate purpose of the model. In this case data are subsea depths to the base of the reservoir sandstone in Ritchie County, West Virginia, and are to be used for estimation of structure. Because of excellent well control, it is unlikely that estimates would need to be made farther than 4 or 5 km from a control well.

A preliminary model included three simple models:

1. A nugget effect of 4000 ft^2.
2. A spherical model with a sill of 6000 ft^2 and range of 1 km.

3. A spherical model with a sill of 8000 ft^2 and a range of 10 km.

Shown in Fig. 2.21, the model appears to capture the general shape of the observed semivariogram, but the model is too high at small values of h.

Table 2.3 Semivariogram of the top of a Lower Mississippian reservoir sandstone in West Virginia

Distance (km)	*Semivariogram (ft^2)*	*Number of pairs*
0.39	6140	86
1.04	8318	705
2.03	9411	1035
3.02	9205	1280
4.02	10 760	1518
5.02	10 870	1767
6.00	12 160	1987
7.00	11 890	1984
8.00	14 320	2161
9.00	17 570	2073
10.01	17 110	2395
10.99	19 750	2466
12.00	20 080	2373
13.00	23 220	2543
14.00	20 100	2483
14.99	22 000	2606
16.01	20 560	2604
17.02	17 620	2689
18.00	17 110	2651
19.01	15 790	2574
19.99	16 660	2438
20.99	15 070	2305
22.00	15 120	2083
22.99	17 730	1998
23.98	18 450	1769
25.00	22 580	1428
25.99	20 420	1291
27.00	25 040	1103
27.98	28 720	904
28.98	26 760	761
29.97	35 450	728
30.98	30 120	616
31.99	32 260	544
33.00	38 570	538
34.00	44 810	439
34.98	40 460	391
35.98	57 310	279
36.95	65 560	211
37.96	76 140	126
38.93	51 650	63
39.99	121 400	25
40.94	29 980	8
41.71	76 100	3

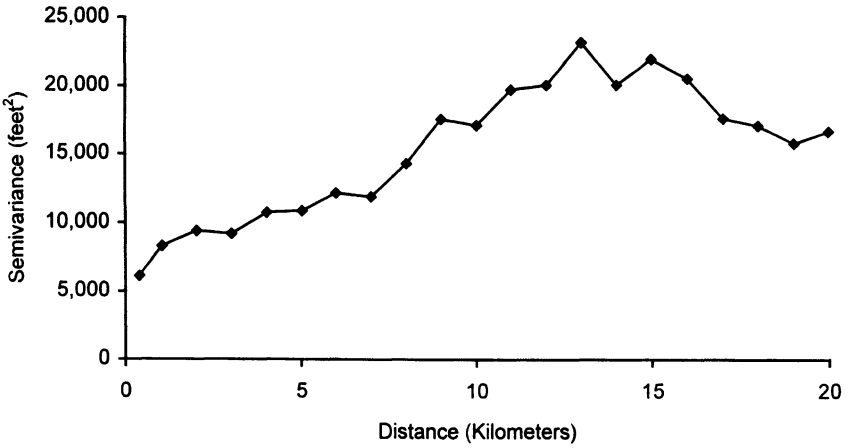

Figure 2.20 Semivariogram of subsea tops of a Mississippian reservoir sandstone in Ritchie County, West Virginia, exhibiting possible nested behavior.

Subsequent adjustments to the parameters and replotting gave better results (Fig. 2.22), which captures the essential characteristics of the data. The model is:

$$\gamma(h) = \gamma_1(h) + \gamma_2(h) + \gamma_3(h)$$

where $\gamma_1(h)$ is a nugget effect model equal to 4000 ft^2, $\gamma_2(h)$ is a spherical model with a sill of 2000 ft^2 and range of 1 km and $\gamma_3(h)$ is a spherical model with a sill of 10 000 ft^2 and a range of 12 km.

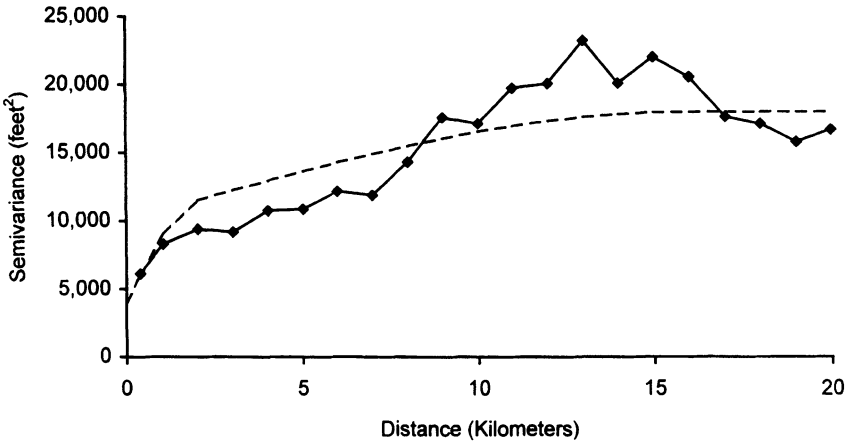

Figure 2.21 First nested model fitted to semivariogram in Fig. 2.20.

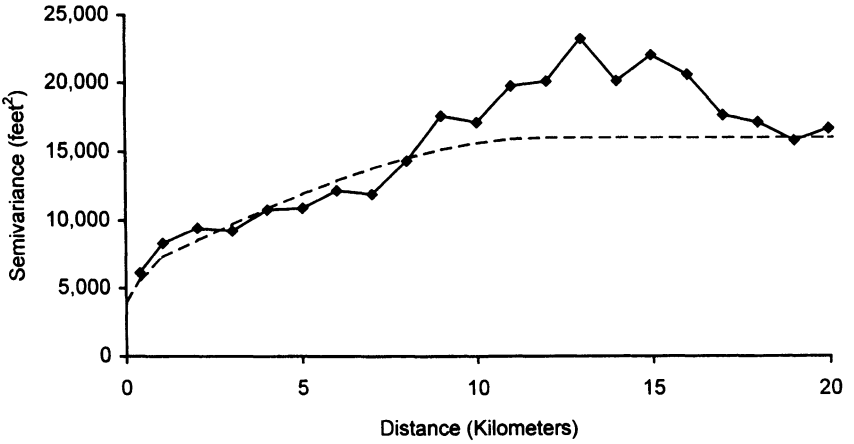

Figure 2.22 Second model fitted to semivariogram in Fig. 2.20.

This model can be further improved by giving more attention to small distances, and ignoring the hump in the semivariogram beyond 7 km. The result (Fig. 2.23) uses the following models and parameters:

$$\gamma(h) = \gamma_1(h) + \gamma_2(h) + \gamma_3(h)$$

where $\gamma_1(h)$ is a nugget effect model equal to 4500 ft^2, $\gamma_2(h)$ is a spherical model with a sill of 4000 ft^2 and range of 1.9 km and $\gamma_3(h)$ is a spherical model with a sill of 6500 ft^2 and a range of 20 km.
From consideration of the observed semivariogram and the model, one might conclude that the observed elevation of the Big Injun depends

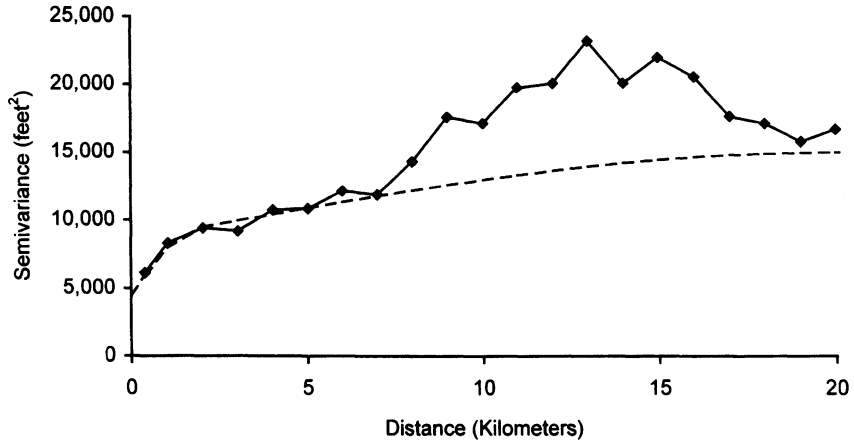

Figure 2.23 Final model fitted to semivariogram in Fig. 2.20.

upon regional structural features, a small-scale variability that could be minor structural features, and a very fine-scale variability. The small nugget effect means that well control is adequate to very good for mapping small-scale features in addition to regional structure. Note that directional effects have been ignored in this example; a better fit might be obtained if a nested, anisotropic model were considered.

2.3 HOLE EFFECTS

Some phenomena encountered by the petroleum geologist display marked pseudoperiodicity, e.g. elevation of a formational horizon in a folded belt. Whereas a semivariogram along the structural trend resembles one of the simple models described above, a semivariogram across structural highs and lows displays a so-called hole effect, named from the oscillation of the semivariogram that reflects the pseudoperiodicity of the phenomenon under study.

A hole effect may be one-dimensional or multi-dimensional; one must take care to distinguish between the dimensionality of a hole effect and that of the regionalized variable. The elevation of a formational top is a regionalized variable in two dimensions, but the hole effect described is only one-dimensional.

Two models have been used to describe a hole effect:

1. $C(h) = C\ (\sin\ ah)/ah$
   $\gamma(h) = C[1 - (\sin\ ah)/ah]$
2. $C(h) = C[\cos\ h/a]$
   $\gamma(h) = C[1 - \cos\ h/a]$

where h is expressed in radians.

The amplitude of a hole effect is the minimum value of the covariance divided by the sill value

$$\text{amplitude} = [\text{minimum value of } C(h)]/C(0)$$

For the first model above (Fig. 2.24), the maximum amplitude of an isotropic hole effect in a three-dimensional space is 0.212. An observed amplitude greater than 0.212 means that the assumed hole effect is illusory, or that a one-dimensional model must be chosen, such as the second model above, which has a maximum amplitude of 1. Thus, use of a model such as $\gamma(h) = C[1 - \cos\ h/a]$ allows one to fit large hole effects (Fig. 2.25). On the other hand, the cosine model is not admissible for more than one direction. The cosine model can be used to model regionalized variables in two or more dimensions, but the hole effect is only fully manifested in one direction, is weak in directions oblique to this one, and disappears in directions orthogonal to it.

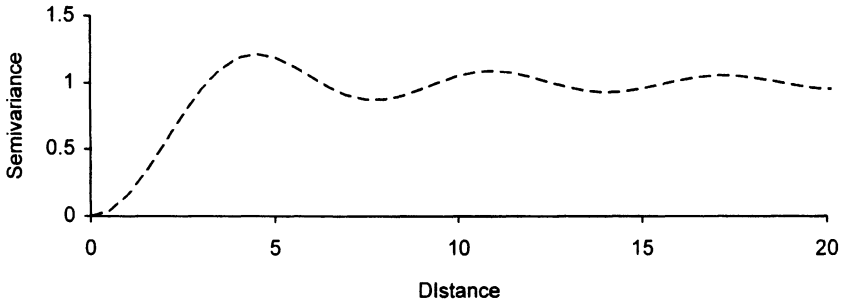

Figure 2.24 Semivariogram model of the form $[1 - \sin(1h)/(1h)]$.

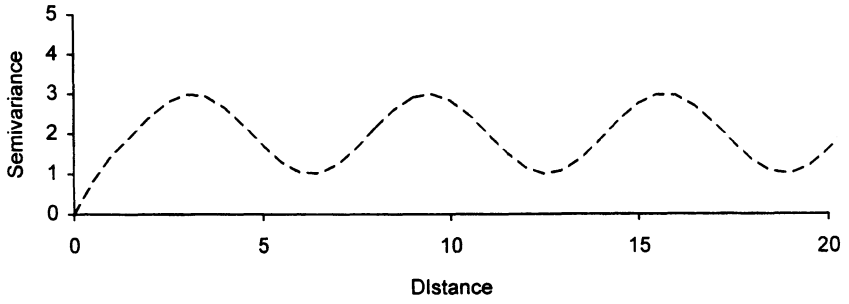

Figure 2.25 Semivariogram model of the form $(1 - \cos(h/1) = C*$ $(3h/2 - h^3/2)$.

A hole effect may be undamped or damped in its oscillations. The simple cosine model is obviously undamped, but can be damped through use of a nested model, e.g.

$$\gamma(h) = C[1 - \exp(-h/a_1) \cos h/a_2]$$

in which the exponential term serves to damp the cosine term. Figure 2.26a shows the model:

$$\gamma(h) = (1 - \exp(-h/10) \cos/(h/1) + C * (3h/2 - h^3/2)$$

and Fig. 2.26b shows:

$$\gamma(h) = (1 - \exp(-h/3) \cos/(h/1) + C * (3h/2 - h^3/2)$$

2.4 ANISOTROPIC MODELS

Models considered in previous sections depended only upon the magnitude of the separation distance h. If (x_u, x_v) represents the coordinates of a point in two-dimensional space, then a vector **h** has coordinates (h_u, h_v) and modulus h equal to

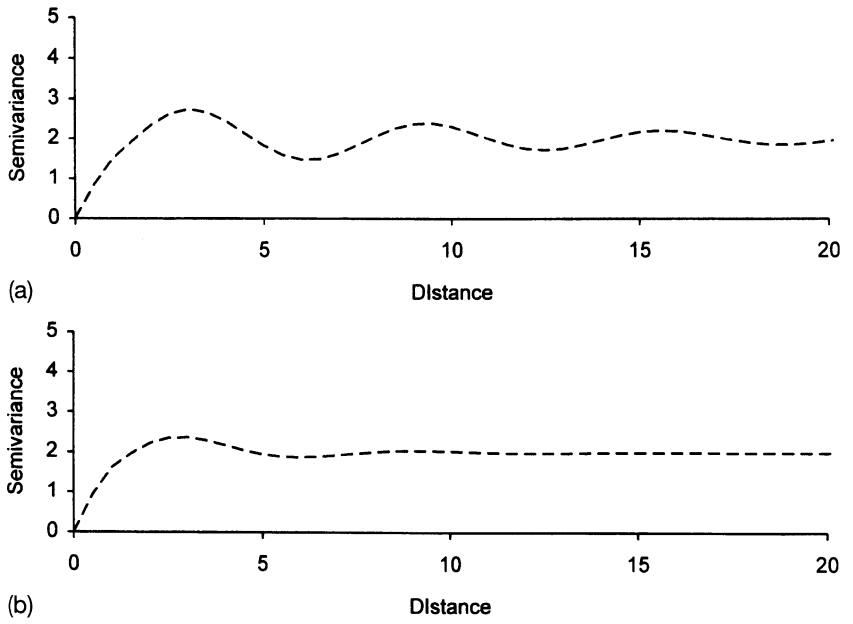

Figure 2.26 Two hole-effect models differing in degree of damping. The cosine term in (a) is damped less than that in (b).

$$|\boldsymbol{h}| = \sqrt{(h_u^2 + h_v^2)}$$

An isotropic phenomenon has the same variability in every direction, and so the semivariogram is straightforward:

$$\gamma(h_u,h_v) = \gamma\sqrt{(h_u^2 + h_v^2)}$$

In contrast, an anisotropic phenomenon has a semivariogram that is a function of the direction represented by the vector: (h_u, h_v) in two dimensions.

The most commonly recognized anisotropic models are **geometric**, in which a linear transformation of a single model describes the variability in each direction, and **zonal** anisotropy, in which each direction is modeled separately. A nested semivariogram model can include both isotropic and anisotropic models, reflecting the fact that a regionalized variable can have many sources of variation. For instance, if a given small-scale spatial variability results from measurement error, this error might be modeled by an isotropic nugget effect. The thickness of a sand unit may be less variable at a distance h in direction f_1 than at the same distance in direction f_2. Direction f_1 may be parallel to the stream channels that deposited the sand, and f_2 perpendicular to the primary direction of deposition. The semivariogram corresponding to this hypothetical situation would look like this:

$$\gamma(\mathbf{h}) = \gamma_1(\mathbf{h}) + \gamma_2(\mathbf{h})$$

where $\gamma_1(\mathbf{h}) = \gamma_1(|\mathbf{h}|) = C_0$ is a nugget effect and $\gamma_2(\mathbf{h})$ is a function of the vector $\mathbf{h}$.

Therefore, the consideration of directional effects adds an additional level of complexity to the job of fitting semivariogram models. However, the results can be very satisfying. If data are collected and semivariograms are calculated in order to detect patterns of spatial autocorrelation, then meeting the research goal requires as close a fit of the model to the data as possible, within the limits of the data. On the other hand, sources of spatial variation may be known a priori, and the semivariogram serves as a tool in the accurate mapping of a regionalized variable. The ability to recognize and model these known sources of variation indicates adequate sampling in number and spatial distribution. Failure to observe an expected effect in an experimental semivariogram should set off an alarm bell: either the sampling was inadequate for modeling the expected effect, or the effect does not exist in reality. One may be justified in including the effect if ancillary knowledge shows that the effect is present. For instance, the geologist may decide to fit an anisotropic hole effect to the elevation of a formation if it is known that a hole effect was observed in an overlying formation. Knowledge of the geological milieu of a regionalized variable should always guide fitting a model.

2.4.1 Geometric anisotropy

A geometric anisotropy is recognized by the fact that the sill remains unchanged with direction, whereas the range changes. It is represented by a single model that changes with direction as a function of a linear transformation, i.e. it can be reduced to an isotropic model by a linear transformation of the coordinates of the vector $\mathbf{h}$.

Before examining this transformation, consider the simple example of geometric anisotropy shown in Fig. 2.27. In the direction of maximum range, a spherical semivariogram with a sill of 1 has range $\mathbf{r}_1$. At a right angle to the first direction, the spherical model has the range $\mathbf{r}_2$. Models for the two directions are as follows.

$$\gamma_1(\mathbf{h}) = \frac{3\mathbf{h}}{2\mathbf{r}_1} - \frac{\mathbf{h}^3}{2\mathbf{r}_1^3}$$

$$\gamma_1(\mathbf{h}) = \frac{3\mathbf{h}}{2\mathbf{r}_2} - \frac{\mathbf{h}^3}{2\mathbf{r}_2^3}$$

Taking the ratio:

$$k = \mathbf{r}_1/\mathbf{r}_2$$

we can evaluate $\gamma_1(h)$ for separation distance kh:

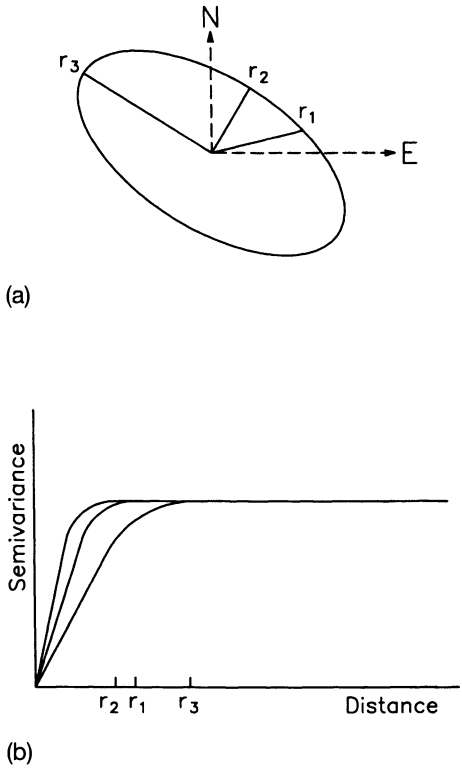

Figure 2.27 Geometric anisotropic model with (a) ranges plotted on polar coordinates and (b) conventional semivariograms.

$$\gamma_1(hk) = \frac{3(kh)}{2\mathbf{r}_1} - \frac{3(kh)^3}{2\mathbf{r}_1^2}$$
$$= \frac{3h}{2\mathbf{r}_2} - \frac{3h^3}{2\mathbf{r}_2^3}$$
$$= \gamma_2(h)$$

Therefore, one can obtain a value of the semivariogram along the minor axis at a separation distance h by multiplying the separation distance by k, and using the semivariogram model for the major axis. The constant k is called the **anisotropy ratio**.

Computer software for geostatistical estimation and simulation requires input of the range, anisotropy ratio, and the direction of the major axis for an anisotropic semivariogram. Some programs assume the ratio to be the minimum range divided by the maximum. Models in three dimensions require an additional anisotropy ratio and yet another angle.

The user must read documentation carefully to determine the convention being used with regard to the anisotropy ratio and both the reference direction and angular direction used to specify the direction of anisotropy.

Fitting a geometric anisotropic model is not hard. The scientist must compute semivariograms for several directions, at least four, and model each using the same sill, and different ranges. Displaying semivariograms on polar coordinates can assist finding the direction with maximum range. The direction of minimum range must be at a right angle to the first direction to be a geometric anisotropy. Once these two ranges have been determined, a useful check on the model is to compute the range for an angle 45 deg to the other directions, i.e. r_{45}. When plotted on polar coordinates, the range of a model of geometric anisotropy falls along an ellipse. The equation for the ellipse gives ranges at intermediate angles, given the length of the major and minor axes, $\mathbf{r}_1$ and $\mathbf{r}_2$, respectively:

$$\mathbf{r}_{45} = \sqrt{\left(\frac{2\mathbf{r}_1^2\mathbf{r}_2^2}{(\mathbf{r}_1^2 + \mathbf{r}_2^2)}\right)}$$

In order to compute the value of a semivariogram model in an arbitrary direction, a linear transformation of coordinates becomes necessary. For two dimensions, the task is to compute new coordinates h'_u and h'_v, which will be used to compute the separation distance $|h'|$. This distance will then be used in an isotropic semivariogram model:

$$\gamma(h_u,h_v) = \gamma'\sqrt{(h'^2_u + h'^2_v)}$$

where $\gamma(h)$ is an anisotropic model, $\gamma'(h)$ is an isotropic model,

$$h'_u = a_{11}h_u + a_{12}h_v$$
$$h'_v = a_{21}h_u + a_{22}h_v$$

and a_{11}, a_{12}, a_{21}, and a_{22} are weighting factors. The transformation is more conveniently expressed in matrix form:

$$[\mathbf{h}'] = [\mathbf{A}]\cdot[\mathbf{h}]$$

where:

$$[\mathbf{A}] = \begin{bmatrix} a_{11} & a_{12} \\ a_{21} & a_{22} \end{bmatrix}$$

$$[\mathbf{h}] = \begin{bmatrix} h_u \\ h_v \end{bmatrix}$$

$$[\mathbf{h}'] = \begin{bmatrix} h'_u \\ h'_v \end{bmatrix}$$

This procedure can be visualized as a stretching of the original coordinate space along a direction perpendicular to the major axis of anisotropy, computing a separation distance in this new space for use in an isotropic semivariogram.

Defining ϕ to be the angle that the major axis of an ellipse makes with the x-axis, and k the ratio of anisotropy of the ellipse, then the matrix multiplication given above uses values:

$$\begin{bmatrix} \mathbf{h}'_u \\ \mathbf{h}'_v \end{bmatrix} = \begin{bmatrix} \cos\phi & \sin\phi \\ -k\sin\phi & k\cos\phi \end{bmatrix} \cdot \begin{bmatrix} \mathbf{h}_u \\ \mathbf{h}_v \end{bmatrix}$$

The separation distance computed from the new coordinates are substituted in the semivariogram model corresponding to the direction along the major axis of the anisotropy ellipse.

This transformation can also be written in the following way:

$$\mathbf{h}' = \begin{bmatrix} h'_u \\ h'_v \end{bmatrix} = \begin{bmatrix} 1 & 0 \\ 0 & k \end{bmatrix} \cdot \begin{bmatrix} \cos\phi & \sin\phi \\ -\sin\phi & \cos\phi \end{bmatrix} \cdot \begin{bmatrix} h_u \\ h_v \end{bmatrix} = \mathbf{SRh}$$

where the first transformation matrix **S** represents the stretching or shrinking, and the second matrix **R** provides the rotation of axes.

In mapping applications, the transformation given above has two purposes. In the presence of anisotropy, a mapping package should consider an elliptical search radius about each locus for estimation. This is easily done by transforming each point (x_u, x_v); to new, isotropic coordinates (x'_u, x'_v), and comparing the distance between (x'_u, x'_v) the point to be estimated against the search radius. A second use for the transformation is that outlined above: calculation of a semivariogram for the kriging system of equations.

In the case of models without a sill, e.g. linear models, all of the directional semivariograms are linear, but with different slopes. One can construct a graph of the inverse of the slope with direction; the result should describe an ellipse if a geometric anisotropy is appropriate.

2.4.2 A convenient notation

Given a particular one-dimensional model with range a, one can show quite easily that evaluating that model for a separation distance h gives that same value as the same model with a range of 1 evaluated for a

separation distance of h/a. Therefore, we can use a shorthand notation for the spherical model:

$$\gamma(\mathbf{h}) = Sph(\mathbf{h}/\mathbf{a})$$

In two dimensions, the same notation can be used, and becomes even more useful. Assume an isotropic spherical model with range 1, h_x is distance along the major axis of anisotropy, h_y is distance along the minor axis, and a_x and a_y are the respective ranges. The spherical model can be written:

$$\gamma(h) = Sph_{\phi}\sqrt{\left(\frac{\mathbf{h}_x}{a_x}\right)^2 + \left(\frac{\mathbf{h}_y}{a_y}\right)^2}$$

where ϕ is the direction of the major axis. The same notation can be used for other models, i.e. *Exp* for the exponential model.

The matrix for stretching now becomes:

$$\mathbf{S} = \begin{bmatrix} 1/a_x & 0 \\ 0 & 1/a_y \end{bmatrix}$$

This notation and transformation matrices are easily extended to three or more dimensions.

2.4.3 Zonal anisotropy

Zonal anisotropy is recognized by a change in sill with direction, and can be expressed in matrix form:

$$\begin{bmatrix} 1/a_x & 0 \\ 0 & 0 \end{bmatrix}$$

In petroleum geology, zonal anisotropies are often observed between the vertical and the two horizontal directions. Hence, the stretch matrix would look like this:

$$\begin{bmatrix} 0 & 0 & 0 \\ 0 & 0 & 0 \\ 0 & 0 & 1/a_z \end{bmatrix}$$

Some computer programs for kriging do not have an explicit provision for zonal models; the user specifies a geometric model, the direction along which the zonal anisotropy is observed, the range along this

direction, and a very large range for the direction orthogonal to the first. In matrix notation this becomes:

$$\begin{bmatrix} 1/a_x & 0 & 0 \\ 0 & 1/a_y & 0 \\ 0 & 0 & 1/a_z \end{bmatrix}$$

where a_x and a_y are very large numbers.

2.4.4 Nested anisotropic models

A semivariogram model can equal the sum of n isotropic models, where each model may be itself isotropic or anisotropic, and is accompanied by a transformation matrix. Take the case of a three-component anisotropic model in two dimensions:

$$\gamma(\mathbf{h}) = \gamma_1(\mathbf{h}) + \gamma_2(\mathbf{h}) + \gamma_3(\mathbf{h})$$

Assume that the first component is isotropic; then:

$$\mathbf{S}_1 = \begin{bmatrix} 1/a & 0 \\ 0 & 1/a \end{bmatrix}$$

The second component, representing geometric anisotropy in direction ϕ_1, has $\mathbf{S}_2$ equal to:

$$\begin{bmatrix} 1/b_1 & 0 \\ 0 & 1/b_2 \end{bmatrix}$$

The third component, zonal anisotropy in direction $\varnothing_2$, has $\mathbf{S}_3$ equalling:

$$\begin{bmatrix} 1/c & 0 \\ 0 & 0 \end{bmatrix}$$

2.4.5 Example of a nested anisotropic model

In this section, a complex model is fitted to a semivariogram computed from 4137 values of the thickness of the Berea sandstone, a Mississippian unit observed in the subsurface under much of southwestern West Virginia. The resultant model includes an anisotropic hole effect nested with other isotropic and anisotropic models. For mapping purposes, modeling the experimental semivariogram could probably be restricted to distances less than 4 km, but this data set presents an opportunity to fit and study a complex model.

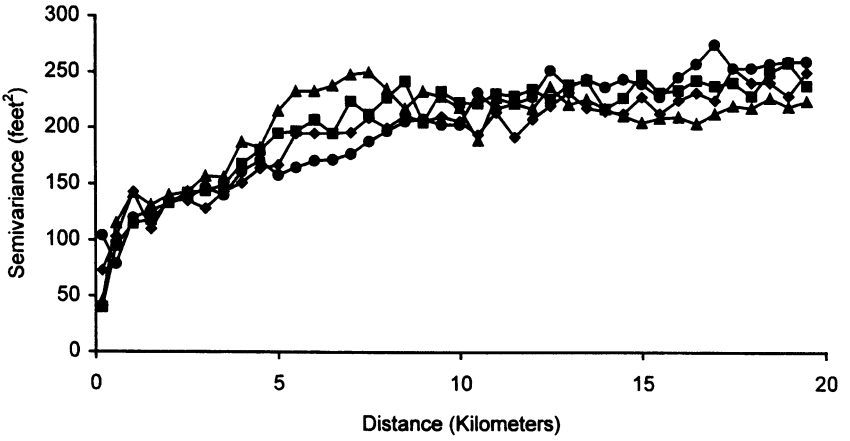

Figure 2.28 Semivariograms of Berea Sandstone thickness. Directions are: north (diamond), northeast (circle), east (square), and southeast (triangle).

The semivariogram (Fig. 2.28) shows several features:

(a) Steep rise from little or no nugget effect
(b) Gradual rise in all directions
(c) A hole effect in the southeast direction
(d) In the northeast direction, values greater than the hole effect at distances beyond 10 km.

An anisotropic nested model with four components was constructed:

1. An isotropic spherical model with a range of 0.75 km and a sill of 95 ft^2,
2. An isotropic exponential model with a range of 5 km and a sill of 90 ft^2,
3. An anisotropic hole effect with a sill of 40 ft^2 and a range of 7.5 km:

$$40\ [1 - \exp\ (-\ b/h_v)\ \cos\ (h_v/7.5)],$$

where $h_v = h\ (\cos\ \Theta_1\ \cos\ \phi + \sin\ \Theta_1\ \sin\ \phi)$, $\Theta_1 = 135°$, $b = 0.1$ and ϕ = direction for which semivariogram is to be drawn. Note that the term $(h_v\ /a)$ acts to damp the hole effect in directions other than 135°. In particular, at 45° (northeast), h_v is equal to zero, and the hole effect disappears. At 135°, the term $(\cos\ \Theta_1\ \cos\ \phi + \sin\ \Theta_1\ \sin\ \phi)$ equals unity, and h_v equals h. This model is therefore a one-dimensional hole effect. The exponential term acts to damp the hole effect with distance h_v.
4. An anisotropic linear model,

$$2.5(h_v\ /1)$$

with:

$$h_v = h\ (\cos \Theta_2 \cos \phi + \sin \Theta_2 \sin \phi)$$

and

$$\Theta_2 = 45°$$

In this case, the model is damped along directions other than 45°. At this angle, the inner product is equal to one, $h_v = h$, and the model becomes

$$\gamma(h) = 2.5h$$

whereas at 135°, the inner product disappears, $h_v = 0$, and

$\gamma(h) = 0$

Figure 2.29 shows the results.

As usual, final values for the sills, ranges and other constants were obtained by repeatedly changing the values and looking at graphs like Fig. 2.29. Journel and Froidevoux (1982) outline a more analytic approach, but the result should be the same. Even an analytic approach can require some iterative adjustments until a satisfactory fit is achieved.

The final semivariogram model can be interpreted in light of inferred depositional environments of the Berea Sandstone in southwestern West Virginia. Averaging 27 ft in the study area, it ranges in thickness from 10 ft in the northeast, to 80 ft in the southwest. This overall trend could account for the anisotropic exponential model. Depositional environments range from fluvial channel, proximal mouth bar, distal mouth bar, and marine (Williamson, 1974).

2.4.6 Another anisotropic model: elevation of a datum

The previous section showed the appearance of a nested model in which a trend is present, but accounts for a small proportion of total variance. Structural data often includes a strong trend, yielding semivariograms with a distinctive appearance.

The Granny Creek field in central West Virginia produces oil from a sandstone reservoir at the top of the Price Formation, Lower Mississippian in age. This is one field of perhaps a hundred that have produced oil and gas from the Price Formation in the Appalachian basin since the 1860s.

A contour map of the base of the reservoir sandstone shows clearly that the field lies in a syncline (Fig. 2.30). Contoured values of the semivariogram (Fig. 2.31) showed the expected north–south anisotropy in this datum, and is useful for determining the principal axis of anisotropy: N10°W.

A nested model with two terms provided a good fit to the directional semivariograms (Fig. 2.32a–d):

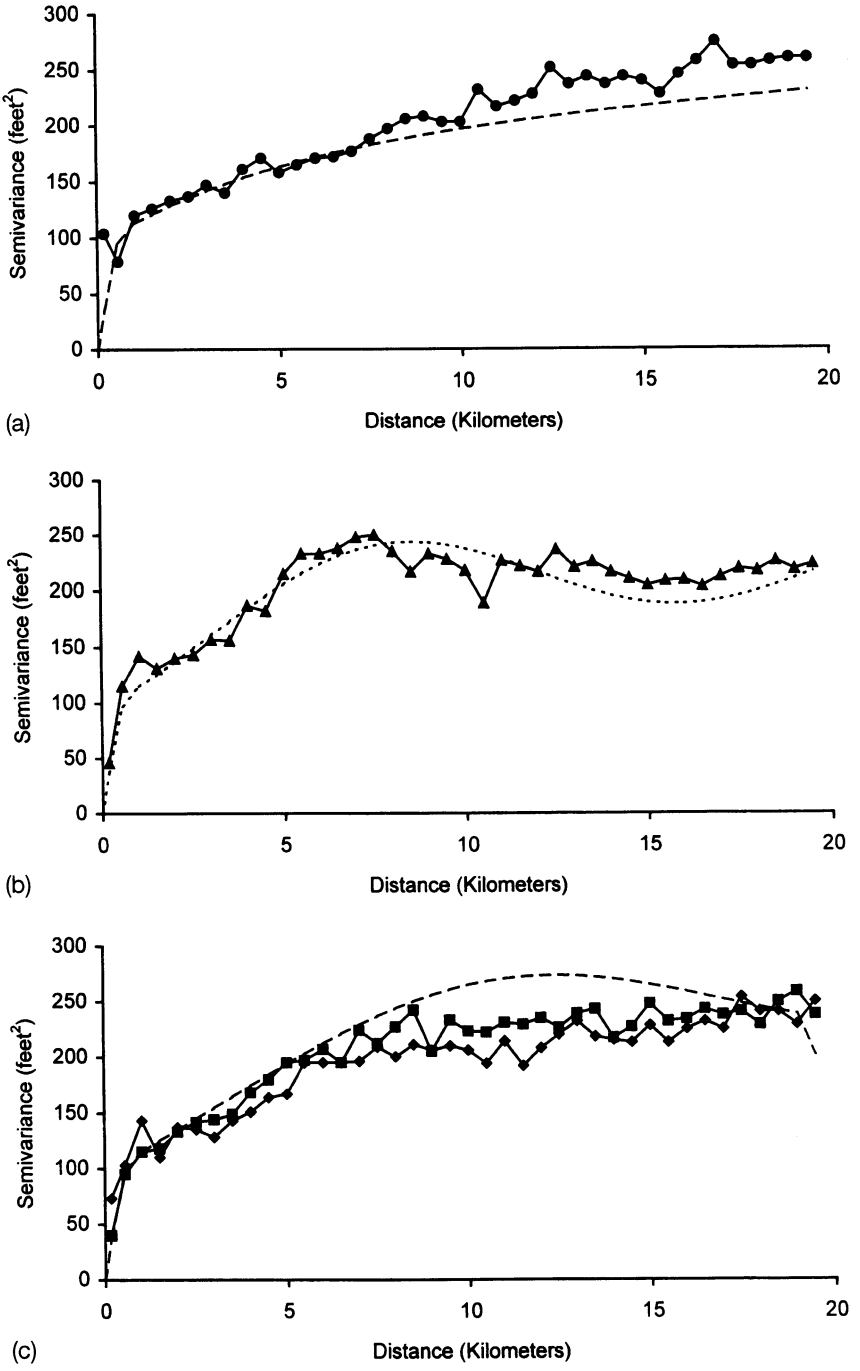

Figure 2.29 Semivariograms and nested anisotropic model for Berea Sandstone thickness. Directions are: (a) northeast; (b) southeast; (c) north (diamonds) and east (squares).

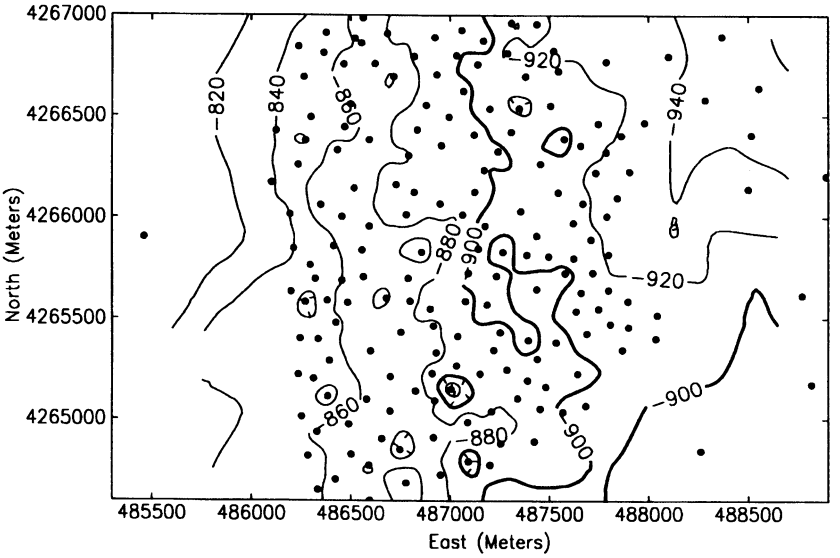

Figure 2.30 Contour map of the base of the reservoir sandstone in Granny Creek Field, central West Virginia. Filled circles represent well locations. Units on map are in feet below sea level.

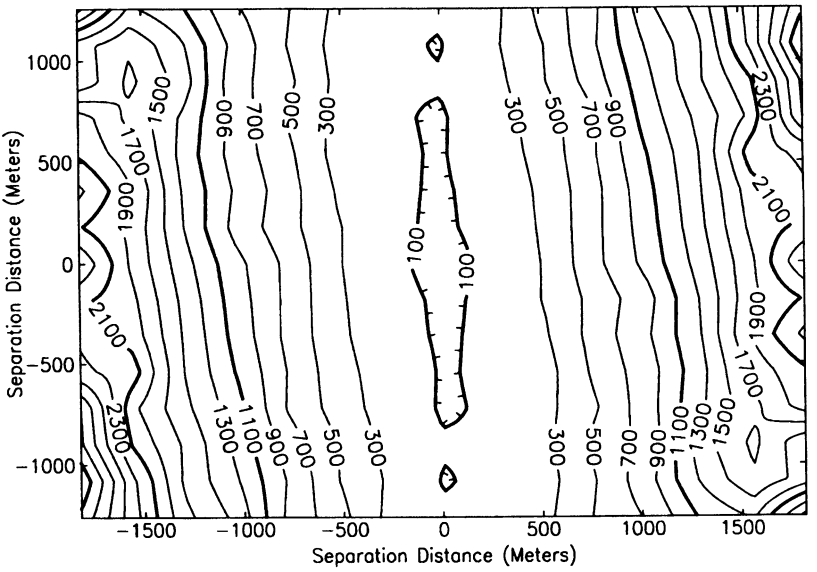

Figure 2.31 Contoured semivariogram of elevation of the reservoir sandstone in Granny Creek Field. Units are ft^2.

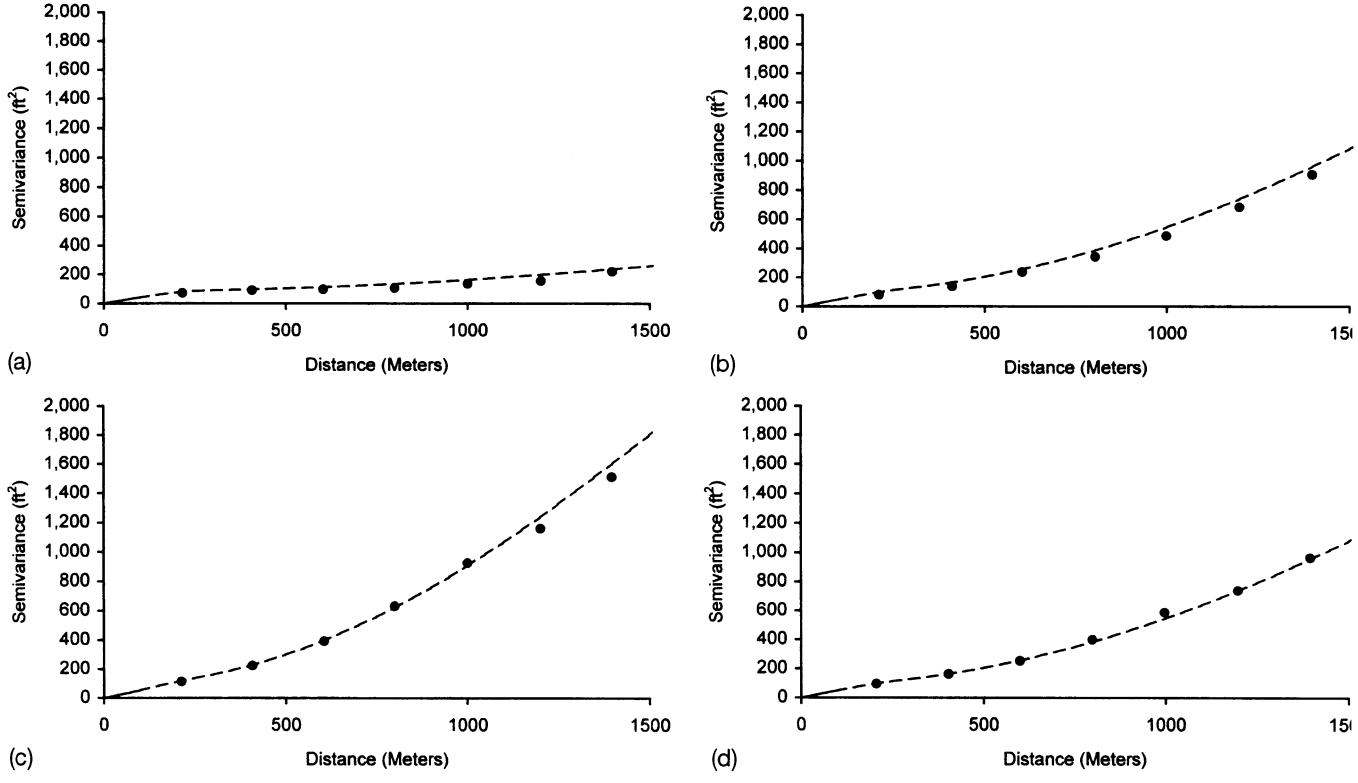

Figure 2.32 Directional semivariograms of the elevation of the base of the reservoir sandstone in Granny Creek Field. Directions are: (a) N 10 deg W; (b) N 35 deg E; (c) N 80 deg E; and (d) N 125 deg E.

$$\gamma(h) = 85Sph_{170}\sqrt{\left(\frac{h_x^2}{286^2} + \frac{h_y^2}{266^2}\right)} + 7100\ \text{Gauss}_{170}\sqrt{\left(\frac{h_x^2}{9500^2} + \frac{h_y^2}{2850^2}\right)}$$

Note the use of the Gaussian semivariogram model; this is often a good choice for a model when well control is excellent in the presence of a strong structural trend. For another published example, see Chu *et al.*, (1994). The Gaussian model represents high continuity in a regionalized variable from well to well at small distances.

Notice also that at the ranges specified, the Gaussian component of the model never reaches a sill; my interest was in exploiting the strong upward concavity of the Gaussian model. This model serves my purposes in a strictly utilitarian way – its shape was useful – rather than a theoretical model of any kind. This is an important theme throughout this book and the field of geostatistics generally: we are building statistical models, not process models.

2.5 THREE-DIMENSIONAL EXAMPLES

2.5.1 Porosity

Geophysical logs were found for 275 wells in Granny Creek Field (Fig. 2.33); porosity was estimated from digitized density logs, giving a database of 13 233 measurements. The field lies in a syncline plunging to the northeast. The reservoir sandstone comprises an upper, relatively coarse-grained unit and a lower, finer-grained unit, deposited in a fluvial-deltaic environment. An angular unconformity truncates the top of the reservoir, with the result that in places the upper, coarser unit is missing. The most productive interval is the lower sandstone unit, which is sandwiched across most of the field by shales below and low-porosity, low permeability coarser sandstones above. Porosity and permeability were reduced in the coarse unit by extensive quartz and calcite cement.

The histogram of calculated porosities (Fig. 2.34) looks as though two populations could be present; one with a mode around 20%, and a second with a mode around 10%. Although the data are not strictly normal, there is no suggestion of a tail or outliers.

The number of wells permits calculation of directional semivariograms. At distances less than 1.5 km, the semivariogram is isotropic (Fig. 2.35), and therefore a single semivariogram was calculated in the horizontal direction (Fig. 2.36). As one must expect in a sedimentary environment, porosity is strongly anisotropic in three dimensions, such that variability over a given distance vertically is much greater than in the same distance horizontally. In fact, because the high-porosity, production portion of the sandstone is sandwiched by low porosity units,

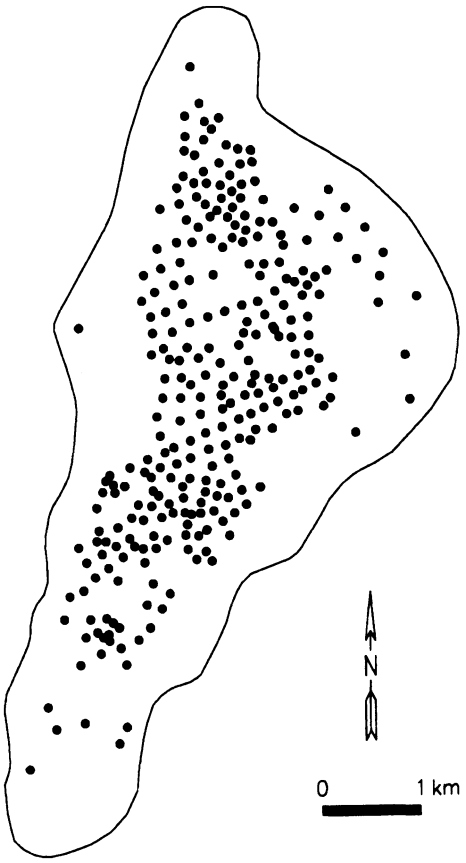

Figure 2.33 Location of wells with geophysical logs for calculation of porosity in Granny Creek oil field.

the vertical semivariogram has the suggestion of a hole effect (Fig. 2.37). Average thickness of the sandstone is about 15 m.

An important feature of the semivariograms is the apparent nugget effect in the horizontal direction, which is not present in the vertical direction. This often happens for three-dimensional data because wells cannot be spaced infinitely close, whereas samples can be taken very close in the vertical direction, especially when the measurements are taken from geophysical logs. Variability from well to well probably represents both actual, small-scale variability, and error caused by inaccuracies in aligning equivalent strata between pairs of wells. In this case, there was no good datum for realigning vertical elevations, and so this task was carried out through automated correlation techniques: basically, internal comparison of geophysical log profiles. Even if a

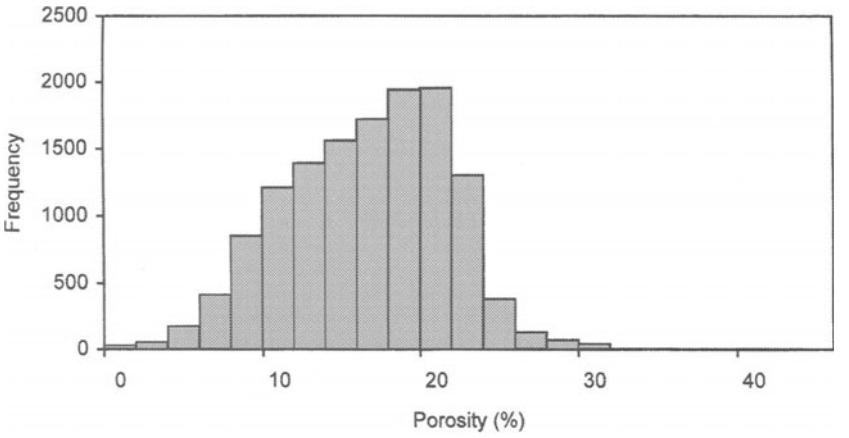

Figure 2.34 Histogram of calculated porosity in Granny Creek oil field.

datum was available, equivalent strata might not be horizontally matched because of off-lapping of depositional units.

One way in which to model the nugget effect is to use a model such as the spherical semivariogram, with a very small range specified for the horizontal direction, and a very long range specified for the vertical direction.

Because of the serious differences in appearance between the horizontal and vertical semivariograms, there is the temptation to model

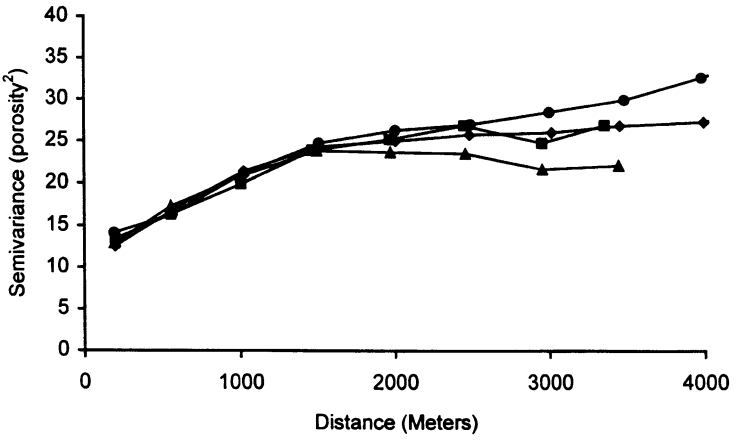

Figure 2.35 Horizontal semivariograms of porosity in Granny Creek oil field. Directions are: north (diamond), northeast (circle), east (square), and southeast (triangle).

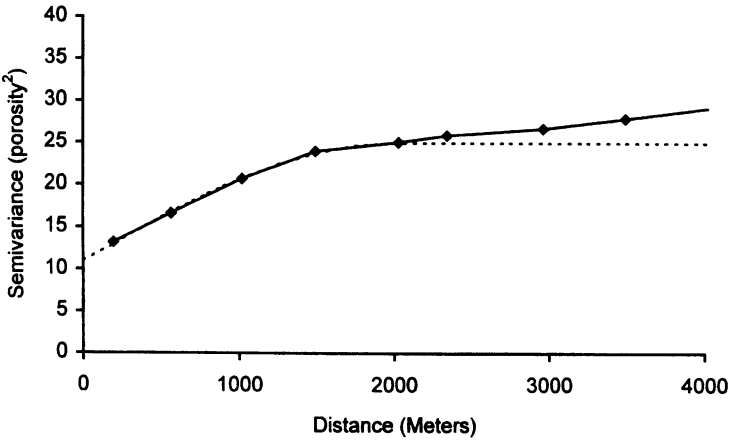

Figure 2.36 Omnidirectional horizontal semivariogram of porosity in Granny Creek oil field. Fitted model is dashed.

each semivariogram separately, and add the results to give a model that might look like this:

$$\gamma(h) = 11Sph\sqrt{\left(\frac{h_h^2}{1^2}+\frac{h_v^2}{\infty^2}\right)} + 14Sph\sqrt{\left(\frac{h_h^2}{2000^2}+\frac{h_v^2}{\infty^2}\right)} + 35Sph\sqrt{\left(\frac{h_h^2}{\infty^2}+\frac{h_v^2}{7.5^2}\right)}$$

where h_h is horizontal separation distance, and h_v is vertical separation distance. This model is shown in Figs 2.36 and 2.37. Although this model fits the observed semivariograms very closely at short distances, it can be

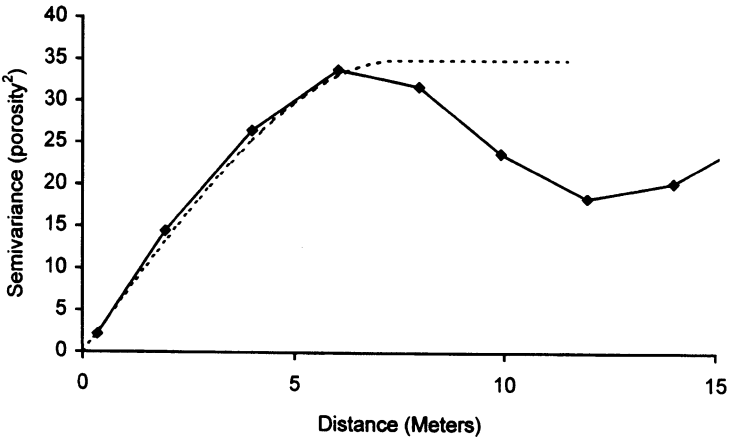

Figure 2.37 Vertical semivariogram with model (dashed line) of porosity in Granny Creek oil field.

shown that nested semivariograms composed entirely of pure geographic and pure stratigraphic semivariograms are not admissible. Semivariograms such as this cannot be used in the estimation stage. Even though the proposed model includes both vertical and horizontal components in each term, the trick of using infinite ranges (or very large ranges) means that at best the matrices used in kriging will be ill-conditioned, i.e. close to being singular. Dimitrakopoulos and Luo (1994) give some guidelines for admissible semivariograms in three dimensions.

The following model is both admissible and simpler:

$$\gamma(h) = 11Sph\left(\sqrt{\frac{h_h^2}{1^2} + \frac{h_v^2}{\infty^2}}\right) + 35Sph\left(\sqrt{\frac{h_h^2}{5500^2} + \frac{h_v^2}{7.5^2}}\right)$$

The graphs show a reasonable good fit in both the horizontal (Fig. 2.38) and vertical (Fig. 2.39) directions. A similar model is provided by:

$$\gamma(h) = 11Sph\left(\frac{|\mathbf{h}|}{7.5}\right) + 24Sph\left(\sqrt{\frac{\mathbf{h}_h^2}{3900^2} + \frac{\mathbf{h}_v^2}{7.5^2}}\right)$$

where:

$$|\mathbf{h}| = \sqrt{(\mathbf{h}_h^2 + \mathbf{h}_v^2)} = \sqrt{(\mathbf{h}_x^2 + \mathbf{h}_y^2 + \mathbf{h}_v^2)}$$

The first term – an isotropic spherical model – acts like a nugget effect in the horizontal direction because the range is much less than any reasonable well spacing.

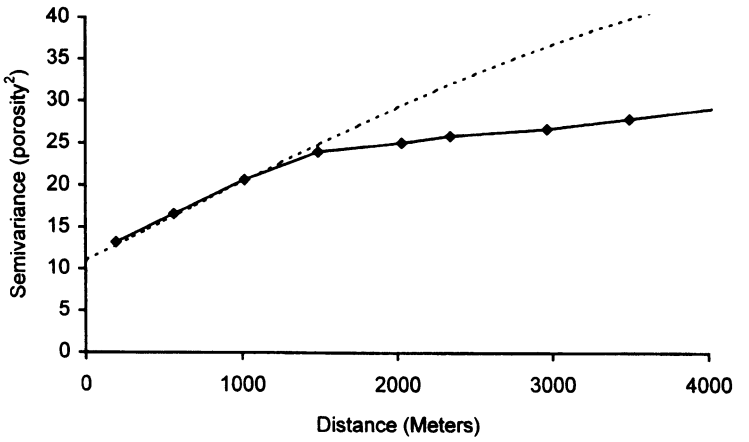

Figure 2.38 Omnidirectional semivariogram of porosity in Granny Creek field, with admissible model (dashed line).

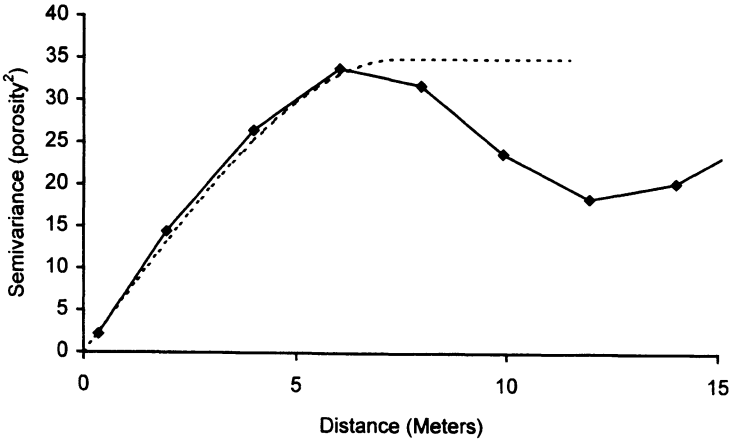

Figure 2.39 Vertical semivariogram with admissible model (dashed line) of porosity in Granny Creek field.

Notice that in creating this model, the overall sill was not given too much attention as long as the fit at smaller distances was reasonable. An equally useful model could have used a smaller sill in order to better fit the horizontal semivariogram, with some downward adjustment to the range in the horizontal direction. No attempt was made here to model the full range of separation distances. In the process of building a three-dimensional interpolation, samples of more than two or three well spacings from the point of estimation will not be given much weight, if any. The same is true in the vertical direction.

In principle, there is little difference between two and three dimensions when computing semivariograms, and in building models. In practice, there can be a large difference stemming from the fact that geographic and stratigraphic variability tend to be very different in scale. As in the example above, one is tempted to model the two directions separately and add models to achieve an omnibus semivariogram model. However, one rarely needs more than two terms: one to provide a nugget effect in one or more directions, and a second for relative large-scale variability. Always remember that the goal is not to obtain an explanatory model, but rather a descriptive model for use in estimation. Understanding the geological phenomenon can perhaps guide the modeling stage.

2.5.2 Permeability

Geologists and petroleum engineers recognize the importance of permeability in oil and gas production, and determining the three-dimensional

variability in permeability is central to reservoir characterization. Unfortunately, sufficient quantities of permeability data are usually hard to obtain. This next example is typical in that regard. In contrast to the porosity data used in the previous example, only values of permeability measured from core are considered here, resulting in data from only eight wells (Fig. 2.40) in Granny Creek field.

The 251 values of core permeability are not normally distributed (Fig. 2.41); the long tail in the histogram suggests that the permeability values might be log-normal. The resulting histogram (Fig. 2.42) looks like a mixture of several log-normal distributions, with the addition of a large spike of low-permeability values representing a lower threshold.

The small number of wells precludes computation of more than a single semivariogram in the horizontal direction. In fact, one can argue that eight wells is not sufficient for even one semivariogram. One

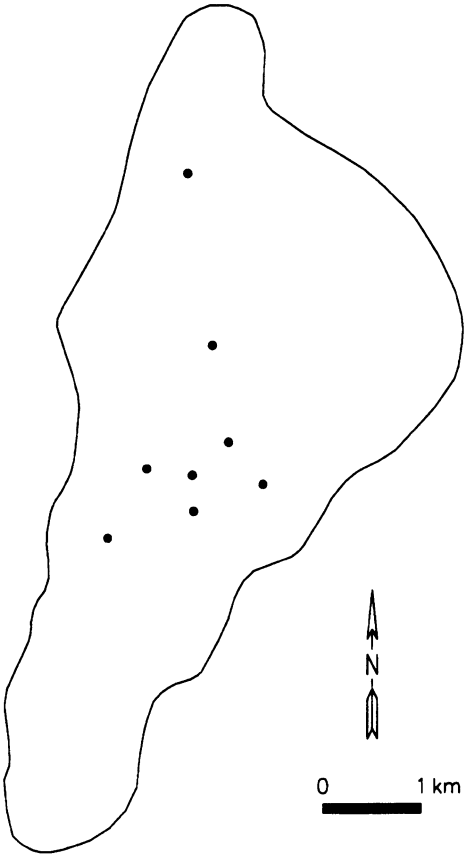

Figure 2.40 Location of wells with core permeability in Granny Creek oil field.

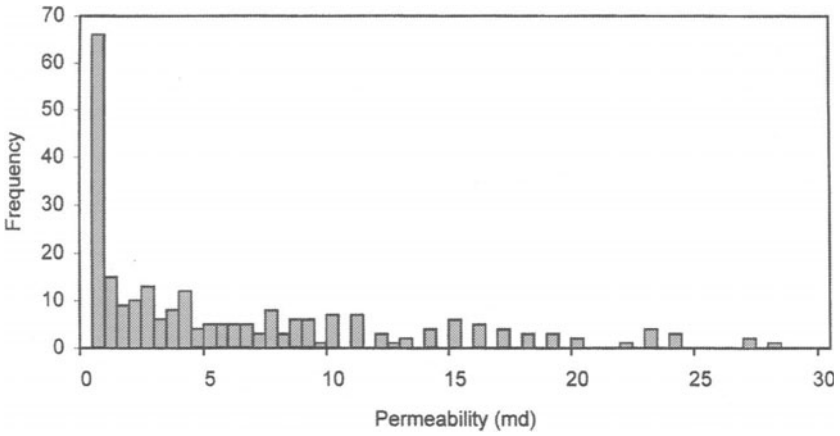

Figure 2.41 Histogram of core permeability in Granny Creek oil field.

difficulty is that no wells are closer than approximately 500 m, so there are no semivariogram values at small geographic distances (Fig. 2.43). Nevertheless, the horizontal semivariogram is relatively smooth except for a jump beyond 2500 m. The northern-most well no doubt accounts for the jump in semivariogram values at large distances.

The vertical semivariogram is fairly smooth at small distances (Fig. 2.44), particularly up to the distance equal to half the average formation thickness of about 15 m.

Semivariograms computed from raw permeability values appear to be easily modelled within the distance range of interest. Sometimes, a log

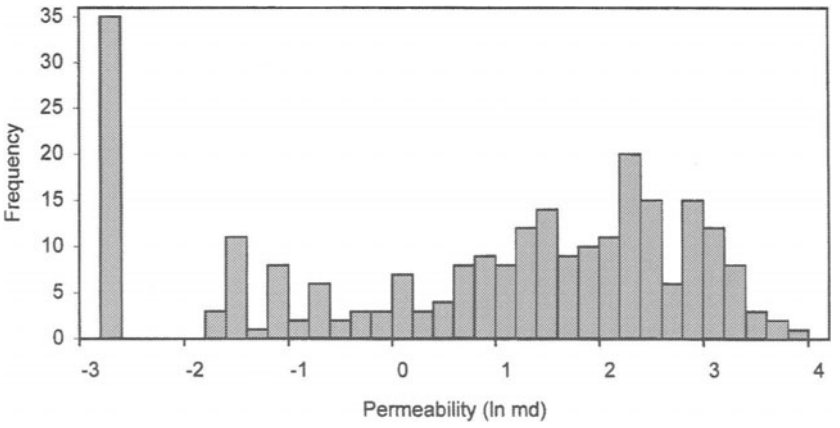

Figure 2.42 Histogram of the natural log of permeability in Granny Creek field.

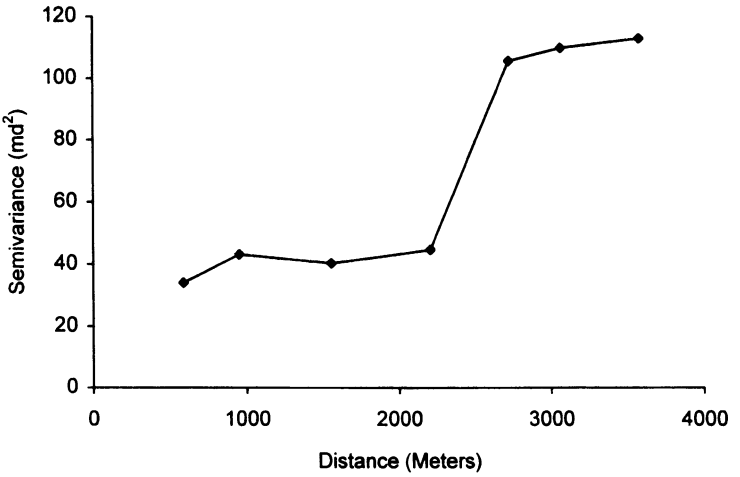

Figure 2.43 Omnidirectional horizontal semivariogram of permeability in Granny Creek field.

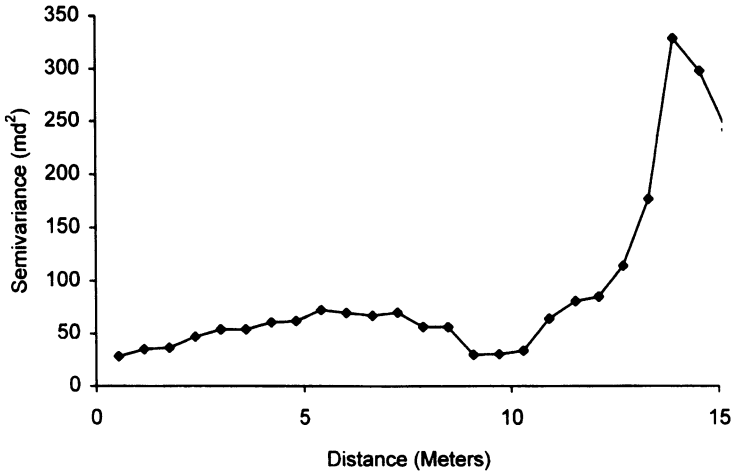

Figure 2.44 Vertical semivariogram of permeability in Granny Creek field.

transform results in a smoother, easier-to-model semivariogram. In this case, the log transform does not make a large difference in the appearance of semivariograms in the horizontal (Fig. 2.45) and vertical (Fig. 2.46) directions. A suggested model shown on these figures includes an isotropic nugget effect, and an anisotropic exponential model:

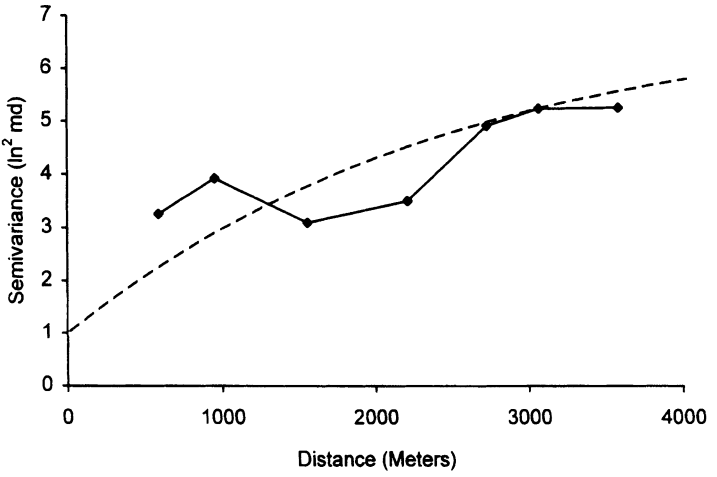

Figure 2.45 Omnidirectional horizontal semivariogram and model (dashed line) of the natural log of permeability in Granny Creek field.

$$\gamma(h) = 1.0 + 6.0 \text{ Exp } \sqrt{\left(\frac{h_h^2}{2500^2} + \frac{h_v^2}{5^2}\right)}$$

where h_h is horizontal distance, and h_v is vertical distance.

Data such as those used in this example are perhaps sufficient for estimating spatial variability within a well: geographic variability has

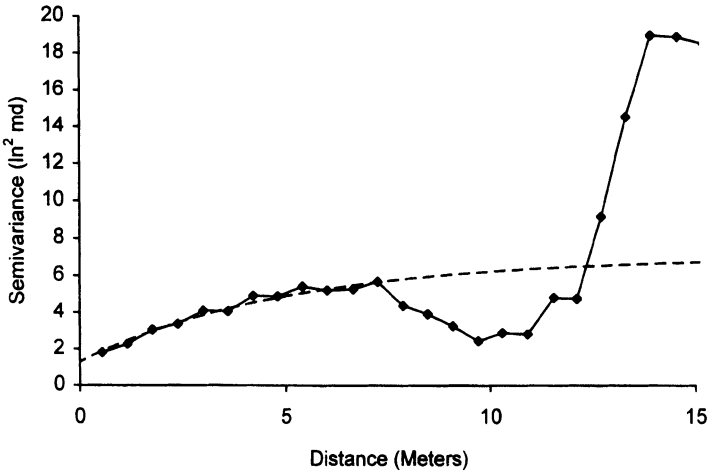

Figure 2.46 Vertical semivariogram and model (dashed line) of the natural log of permeability in Granny Creek field.

probably been inadequately sampled. Porosity at least can be estimated from geophysical logs, which are usually more numerous than cores in mature fields. Several approaches exist for inferring a semivariogram for permeability: by estimating permeability from another variable, by analogy, and by trial and error.

The first option is to uncover an empirical relationship between core permeability and another measurement, such as porosity, which might itself have been estimated from geophysical logs. In many settings, the statistical correlation between porosity and permeability varies among facies; the geologist wants to examine the relationship between core permeability and porosity from samples grouped by lithology or environment of deposition, and calculate a regression equation for each group.

Geostatistical studies for petroleum reservoirs representing many depositional environments now appear in the literature, and can be used as analogues. Semivariograms in the literature can be examined for typical nugget-to-sill ratios and ranges, and used as guides in modeling semivariograms computed with sketchy data from one's own reservoir.

In Chapter 7, the method of conditional simulation is described, in which a surface or volume is fitted to data under the conditions that interpolated values have the same mean, variance and semivariogram as the observed values. Results of such an exercise are often used as input to reservoir flow simulators. When trying to reproduce observed flow patterns, one can specify a variety of semivariograms in building the model of permeability, and compare results with actual events. This is probably the least desirable of the three options, and should be guided by analogues, available data, and experience.

2.6 OUTLIERS, NORMALITY, AND ROBUSTNESS

Plotting a histogram of the regionalized variable under study should precede any calculation of semivariograms or kriged estimates. Frequency distributions of gas or oil volumes, porosity and permeability are generally skewed or include outliers. Anyone attempting to calculate average well initial potential for a field knows the effect that a single very high value has on the statistic. Similarly, a very few observed values of $[z(x) - z(x+h)]$ can account for a large proportion of an average semivariogram value (Krige and Magri, 1982). These large differences may be attributed to a few values on the tail of a non-normal distribution or to outliers. Transformations to normality and rejection of outliers are related topics that can be considered separately and in great depth; interested readers wanting to go beyond the brief survey here should consult, for example Hawkins (1980) on outliers and Huber (1978) on robust procedures.

One of the simplest ways to improve the appearance and stability of the semivariogram is to apply a logarithmic transformation. Krige and Magri (1982) found that 192 lead grades in a South African mine exhibited a two-parameter lognormal distribution except for six high values they treated as outliers. They plotted the cumulative frequency of the differences $[z(x) - z(x + h)]$ for a lag of 15 m in the east–west direction for transformed and untransformed data and also with and without outliers. Out of 543 pairs of untransformed data, the 15 highest differences contributed 64% toward the mean value of the semivariogram at a lag of 15 m. This percentage was reduced considerably after logarithmic transformation. They also found that the presence of one or more outliers can mask the shape of the semivariogram and fitting a nugget effect was impossible. The logarithmic transformation resulted in semivariograms that fitted a De Wijsian model, but the population variance and nugget effect were still inflated because of the presence of outliers. Elimination of these outliers brought additional improvement. They observed a similar improvement by applying a procedure described by Cressie and Hawkins (1980) to untransformed data with outliers.

This procedure begins with a set of squared differences Y_h:

$$Y_h = [z(x) - z(x + h)]^2$$

Examining a class of power transformations:

$$Y_h = \{[z(x) - z(x + h)]^2\}^t$$

Cressie and Hawkins found that $t = 0.25$ yields values of Y_h that fit a normal distribution. They go on to show how to undo this transformation and conclude that an unbiased estimator for the semivariogram is:

$$\gamma(h) = \tfrac{1}{2}[1/n \sum |z(x) - z(x + h)|^{\frac{1}{2}}]^4 \;/\; (0.457 + 0.494/n + 0.045/n^2)$$

One may be able to further improve the estimate of $g(h)$ by using not the mean of Y_h, but some other estimate of expectation, such as the median or a trimmed mean.

Logarithmic transformation and use of the Cressie and Hawkins transformation to Y_h were applied to a set of 467 gas initial potentials measured from wells in Wirt, Roane, and Calhoun counties, West Virginia. A histogram of the raw data shows characteristic non-normality and presence of one large value (Fig. 2.47). The semivariogram (Fig. 2.48) exhibits an apparent hole effect and a very irregular pattern. One good feature appears to be the relatively small nugget effect that needs to be fitted.

The histogram of the data after computing the common log of each observation yields an almost normal distribution (Fig. 2.49). The resulting semivariogram is much smoother (Fig. 2.50) than one calculated from raw data, and the apparent hole effect disappears.

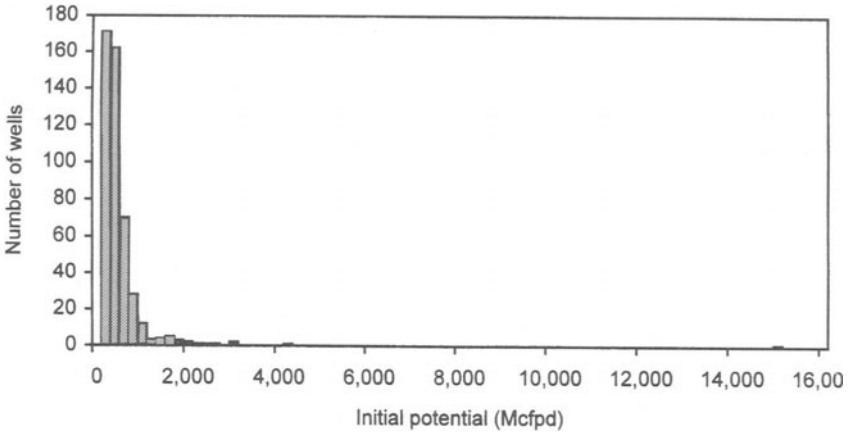

Figure 2.47 Histogram of Devonian shale gas initial potentials from Roane, Wirt and Cathoun Counties, West Virginia.

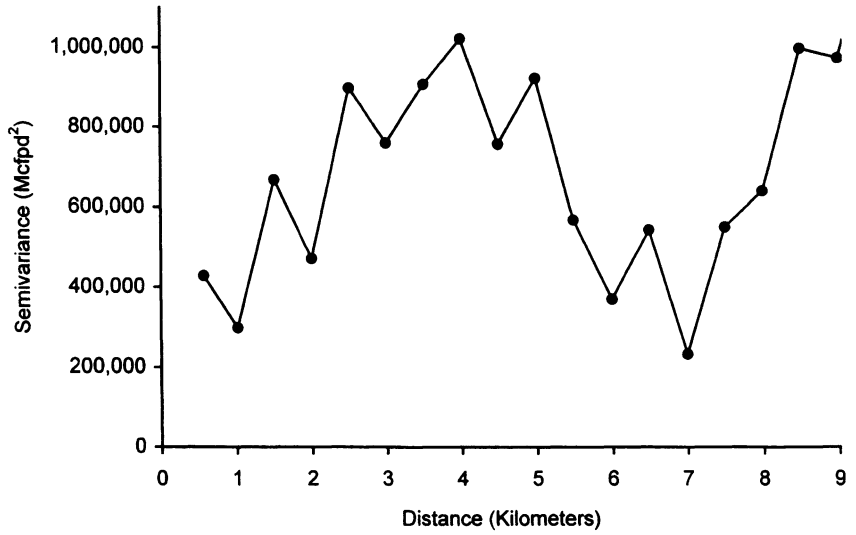

Figure 2.48 Semivariogram of Devonian shale gas initial potentials from Roane, Wirt and Cathoun Counties, West Virginia.

The highest value of $\log_{10}$ (initial potential) may be considered an outlier, so one can use Cressie and Hawkins' transformation to find any improvement. In this example the improvement is minimal; there is some shift downward for the curve as a whole, but the shape remains essentially unchanged (Fig. 2.50). Finally, their transformation can be

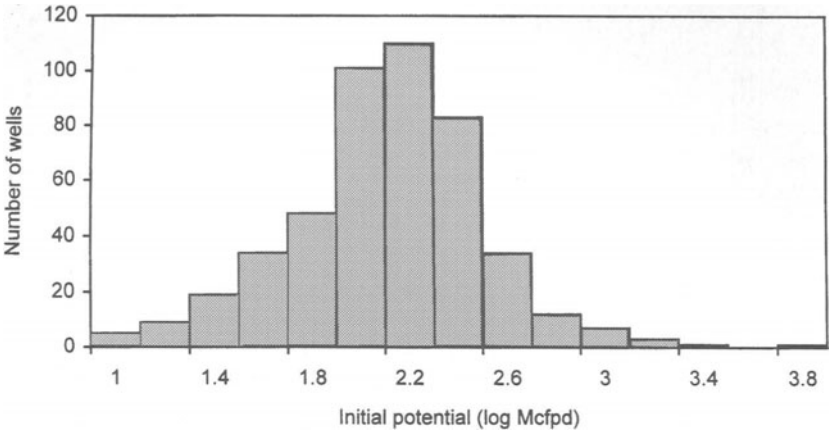

Figure 2.49 Histogram of Devonian shale gas initial potentials after logarithmic transformation.

applied to the raw data, yielding a smooth curve similar to that obtained after logarithmic transformation (Fig. 2.51).

The appearance of a hole effect in semivariograms is probably common for data coming from irregularly distributed sample sites, in the presence of outliers. This may be a serious hazard for variables such as initial potential, highly clustered among fields and dry regions. This

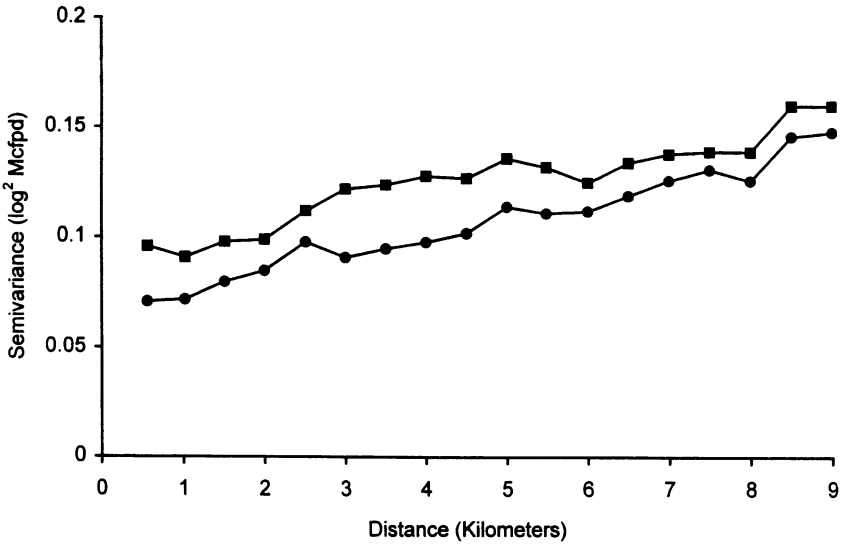

Figure 2.50 Semivariograms of log-transformed gas initial potentials, calculated with robust (filled circles) and conventional estimation (filled squares).

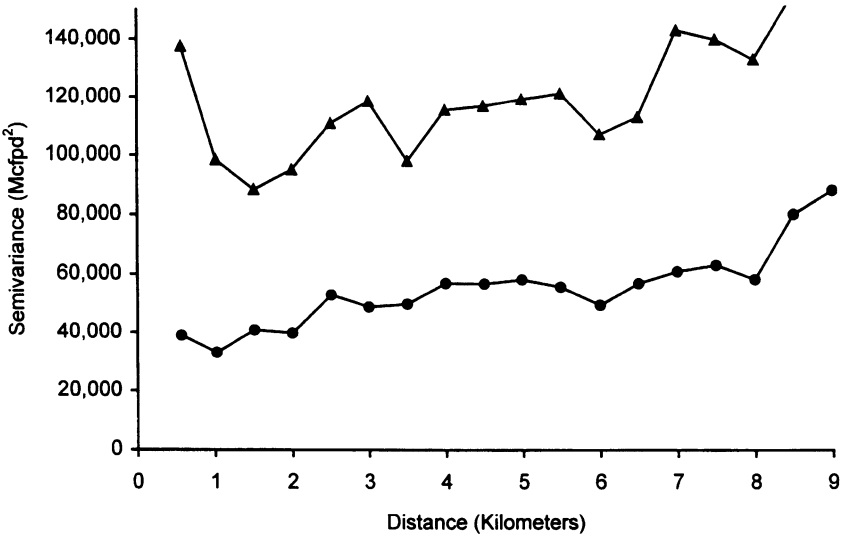

Figure 2.51 Semivariogram of gas initial potentials, using robust estimator (filled circles) and after removal of one outlier (filled triangles).

observation underscores the need for looking at a histogram of raw or transformed data.

2.6.1 The *h*-scattergram

An *h*-scattergram (or *h*-scatterplot) shows the bivariate relationship among pairs of points separated by a specific distance or within a selected distance envelope. It is useful for identifying possible outliers, subsets of the data, and for illustrating the statistical basis of the semivariogram.

Given a separation distance, one plots the pairs $z(x)$ and $z(x + h)$ along two axes of a bivariate scattergram. The shape of the resultant cloud is related to the value of the semivariogram for distance h. The moment of inertia of the bivariate scattergram around a line with a slope of one equals the semivariogram for distance h (Fig. 2.52):

$$
\begin{aligned}
d &= [z(x + h) - z(x)] \cos 45 \\
d^2 &= [z(x + \mathrm{h}) - z(x)]^2 \\
E(d^2) &= \mathrm{E}\{[z(x + \mathrm{h}) - z(h)]^2\} \\
E(d^2) &= \gamma(h)
\end{aligned}
$$

For a semivariogram with small nugget effect and a sill, the scattergram at small values of h should exhibit little deviation from the line of unit slope. With increasing h, the scatter should increase, approaching a

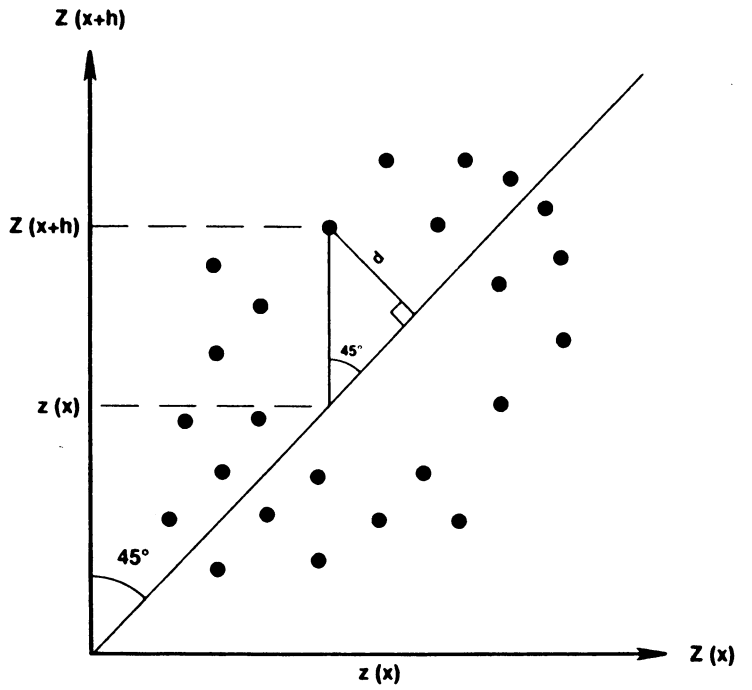

Figure 2.52 An *h*-scattergram.

circular cloud beyond the range. The following sections give several examples illustrating the potential usefulness of the *h*-scattergram.

2.6.2 Outliers

The *h*-scattergram can be used for identifying outliers in data, such as the unusually high value that appears among initial potentials measured in Devonian shale wells.

In this case, it was a simple job of finding the outlier because it appeared to be so extreme compared with the rest of the sample distribution. *H*-scattergrams of raw and log-transformed data (Figs 2.53, 2.54) show a number of things.

First, notice that the transformation has changed the bivariate distribution of initial potentials from a cloud of points near the origin with points straggling off toward higher values (Fig. 2.53), to a distribution that seems to be bivariate normal (Fig. 2.54). The points show almost no clustering about the line of unit slope. Notice also that transformed data cluster very poorly around a line even at short separation distances (Fig. 2.54a), reflecting the very low covariance and the large nugget effect. Finally, the effect of the outliers at 15 000 Mcfpd is largely mitigated by

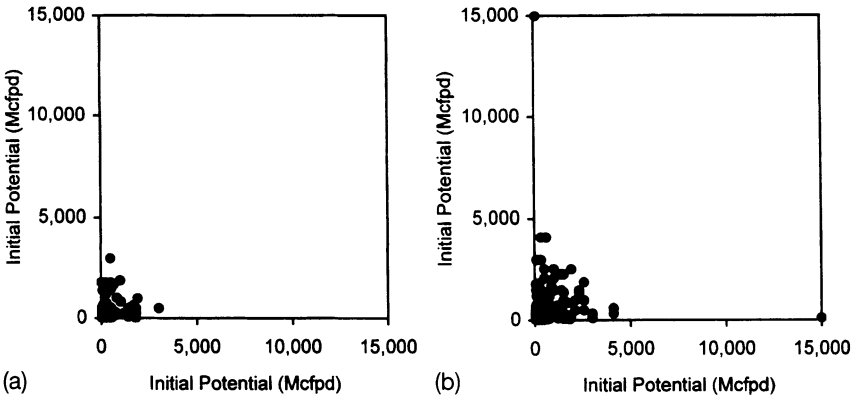

Figure 2.53 *h*-scattergrams of gas initial potential in Devonian shale wells for (a) $0 < h < 0.5$ and (b) $0.5 \leq h < 1$.

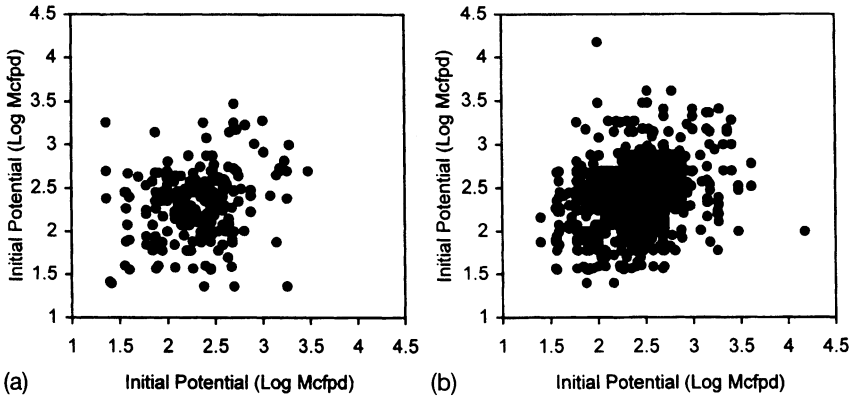

Figure 2.54 *h*-scattergrams of log-transformed gas initial potential in Devonian shale wells for (a) $0 < h < 0.5$ km and (b) $0.5 \leq h < 1$ km.

the transformation, as can be seen by comparing Fig. 2.53a with Fig. 2.54a.

2.6.3 Permeability

Values of permeability from Granny Creek field were found earlier to have a histogram with a large spike of values at the lowest values, apparently a detection threshold. An *h*-scattergram of permeability for values of *h* less than one foot (Fig. 2.55a) shows the presence of two populations: one in which values of similar permeability tend to be adjacent in the core, resulting in a clear correlation on the h-scattergram;

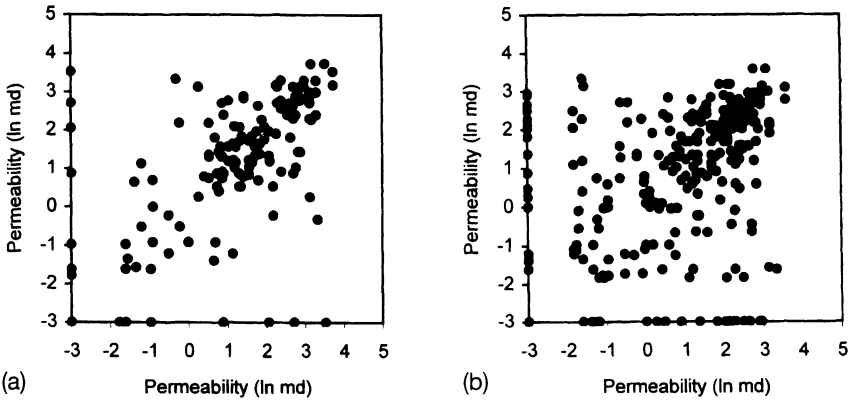

Figure 2.55 h-scattergrams of the log of permeability for (a) $0 < h \leq 1$ ft and (b) $1 < h < 2$ ft.

and a second consisting of the threshold values, which do not appear to be associated with either high or low values of permeability. Hence, one can picture permeability in a given well as a parameter that changes smoothly from sample to sample, except for occasional, very low permeability layers that occur randomly through the stratigraphic section, or at least are not associated with either high or low permeability values.

These observations suggest further lines of enquiry, and could affect how one maps the data in three dimensions. For instance, the geologist might want to discover whether the very low-permeability values correspond to samples of a particular lithology, perhaps shales embedded or interfingering with the reservoir sandstone. Are these samples concentrated in one part of the reservoir? The geologist might decide to strip out these values before mapping, or at least to obtain a semivariogram for the rest of the data. The problem then becomes how to include these low-permeability zones in the final model. They are apparently difficult to predict in the stratigraphic section.

At larger distances (Fig. 2.55b), a number of pairs show up having a moderate to high value for one member, and a low value for the other. These might well correspond to samples lying on either side of a boundary between zones of different permeability. The geologist would want to look at cross sections, and if zones do exist, consider mapping zones separately. In this case, the upper, coarser sandstone facies generally is lower in permeability than the lower facies.

2.6.4 Organic shale thickness

The Huron Shale is a brown to black shale with some interbedded gray shale that averages about 300 ft in thickness in southwestern West

Virginia. Bounded above and below by gray shales, the Huron is easily recognized from gamma ray logs and drillers' logs. It is an important reservoir for Devonian shale gas (Neal and Price, 1986). To explain the occurrence and volume of Devonian shale gas, maps of initial potentials or cumulative production could be compared with an isopach map of the Huron Shale.

Data from 111 wells were selected for analysis. Because the semivariogram has a very small nugget effect (Fig. 2.56), points on the *h*-scattergrams fall close to the line (Figs 2.57, 2.58). Maximum *h* in these figures is 3 km, less than the range. With increasing *h*, the cloud of points changes from a tight configuration about a line of slope one (Fig. 2.58a), to a more elliptical shape (Figs. 2.58b–c).

The *h*-scattergrams show the presence of several outliers. Not all extreme values are the same, however. In Fig. 2.58a, some extreme values fall in line with the trend of the cloud, but others fall well away from the line of unit slope. The first group of points simply represent correct values for organic shale thickness at the upper end of the distribution. Figure 2.58a includes one point in the scattergram that deviates somewhat from the main trend. A closer look at the two wells that this point represents shows that the top of the Huron may have been picked about 30 ft too high in one well. The thickness recorded in the data base was not unambiguously wrong, but the *h*-scattergram suggests some close study of logs from surrounding wells would be in order.

On the other hand, several groups of points plot well away from the main cloud in all scattergrams. These correspond to two wells with incorrect thicknesses recorded in the data base.

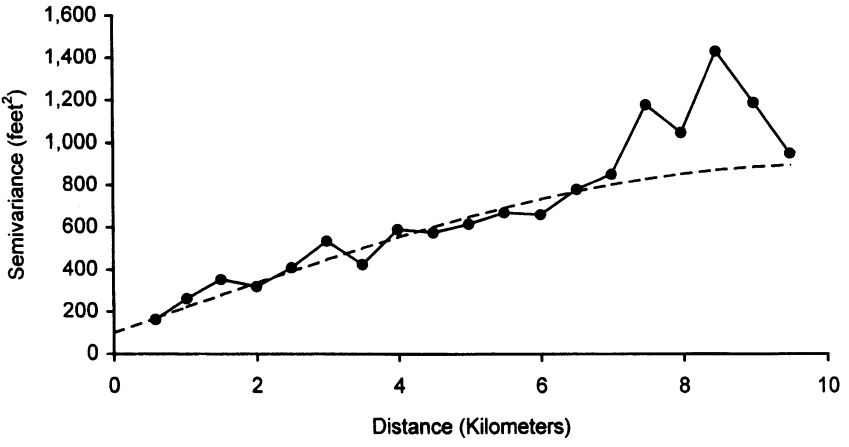

Figure 2.56 Semivariogram of Huron thickness in Mingo County.

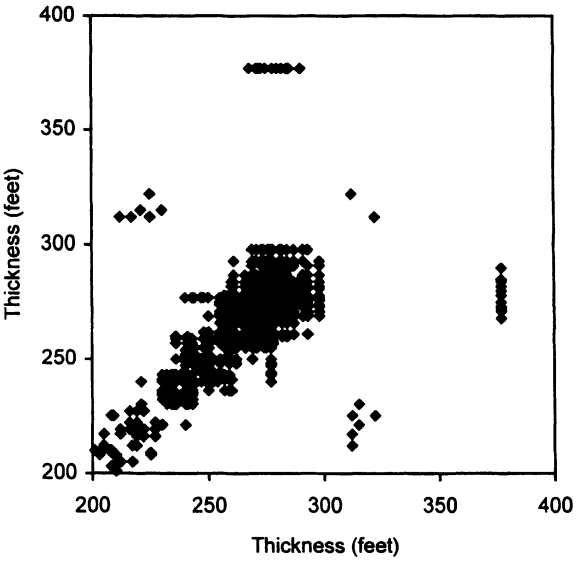

Figure 2.57 Initial display of h-scattergram for thickness of organic-rich shale.

2.7 AUTOMATED FITTING OF SEMIVARIOGRAMS

Many practitioners are bothered by the fact that the semivariogram model is commonly fitted by eye. Purported disadvantages of such an approach are the time spent, and the nonobjectivity of the manual approach. The first criticism is easily dismissed; time spent in fitting semivariograms rapidly decreases with experience, and represents the minimum time one should spend with data. A completely hands-off approach leads all too often to the following scenario: data are collected, semivariograms computed and fitted, kriged values are computed and mapped, strange features are questioned, and the search begins for outliers and incorrect data. Is this an objective approach?

Circumstances that call for an automated, hands-off approach include research that requires comparison of semivariograms, or resampling experiments that involve repeated creation of data sets and model fitting. Neither situation occurs very often in the geological studies I am concerned with in this book.

Nevertheless, computational methods for fitting semivariograms have been proposed, and include ordinary least squares, generalized least squares, weighted least squares, and maximum likelihood. The latter has rather strong distributional requirements, and is not generally used. Among the least-squares approaches, ordinary least squares is the most straightforward, but the most naive. Generalized least squares accounts for covariance between semivariogram values, but the covariance matrix

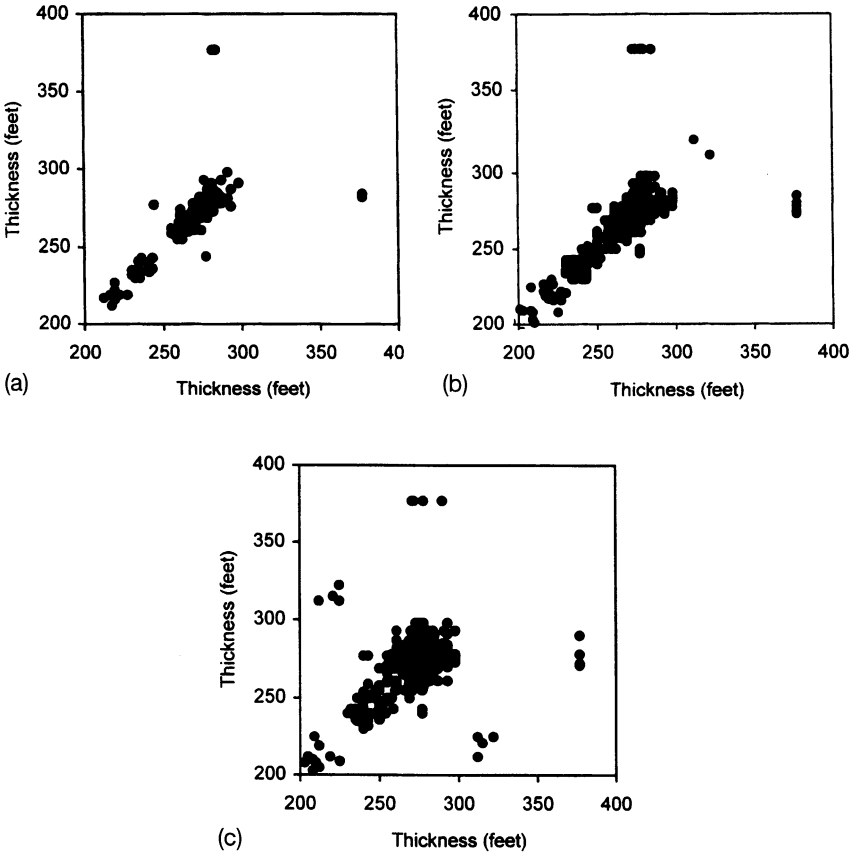

Figure 2.58 Display of h-scattergram for (a) $h < 0.75$ km, (b) $0.75 \leq h < 1.50$ km and (c) $1.50 \leq h < 2.25$ km.

needed can be difficult to obtain. Cressie (1993) considers weighted least squares to be a reasonable compromise between the simplicity of ordinary least squares and the intractability of generalized least squares.

Weighted least squares minimizes the quantity

$$\sum_{j=1}^{k} N(h(j)) \left[\frac{\gamma^*(h(j))}{\gamma(h(j);\Theta)} - 1 \right]^2$$

where $\gamma^*(h(j))$ is the semivariogram computed at distances $h(1),\ldots,h(k)$; $N(h(j))$ is the number of pairs used in calculating $\gamma^*(h(j))$, and $\gamma(h(j);\Theta)$ is a model with parameters Θ. The user must specify a particular model, e.g. a spherical model with sill C, range a, and nugget effect C_0, so that $\Theta = (C_0, C, a)$. This method gives preferential weight to semivariogram values with the largest number of pairs, and also to the smallest values

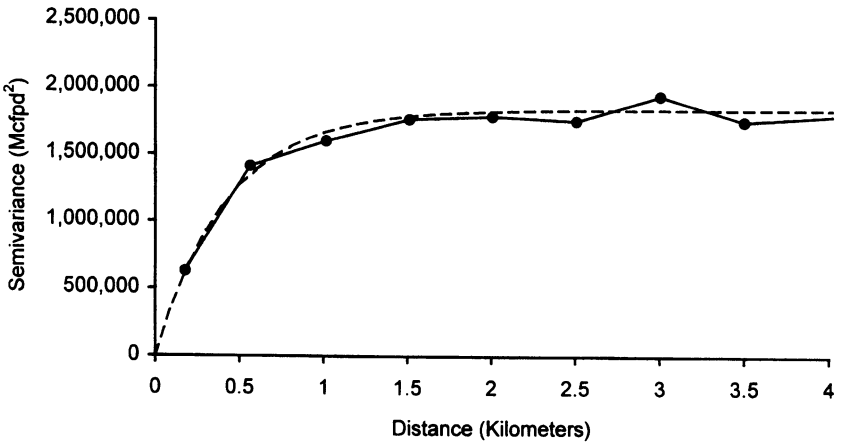

Figure 2.59 Results of automated fitting of a model (dashed line) to semivariogram of Fig. 2.17.

of the observed semivariogram, generally those nearest to the origin. Gotway (1991) provides a computer program for this method.

Recall the manual fit of an exponential model to the semivariogram of gas initial potentials (Fig. 2.19), which gave a constant of 1.8×10^6, and range of 0.4 km. Can weighted least squares do any better in fitting this model? The results of an automated fit are virtually identical to the manual fit; the constant for the exponential model is 1.839×10^6 and the range is 0.428 (Fig. 2.59). Differences in these fitted parameters between the manual and hands-off approach mainly derive from the human operator's tendency not to use as many decimal places. This brief experiment also suggests that once a model has been specified, most of the work is done.

2.8 SUMMARY

Spatial behavior of a regionalized variable can be observed through the semivariogram, a simple graph of between-well distance on the horizontal axis and variance on the vertical axis. For most applications in petroleum geology, sample locations are not situated on a regular grid, so a constant lag cannot be used. Instead, the user selects a lag size and a tolerance, usually one-half the lag size. Selection of a lag size depends upon the number of samples, the dimensions of the study area, and the type and degree of continuity between wells or sample sites. Increasing the lag size yields more pairs at each point on the semivariogram, but the number of points decreases to the point of obscuring the appearance of the semivariogram at small distances.

A regionalized variable may display anisotropic behavior, such as that found on structure maps in folded areas. To detect anisotropy, a semivariogram is constructed for each of several distances, requiring a direction tolerance in addition to a distance tolerance.

Geostatistical estimations require some degree of stationarity in the variable being studied; a constant semivariogram across the area is usually sufficient. Even in the presence of a regional trend, stationarity may be achieved at a local level.

Practical use of an observed semivariogram requires the fitting of a model that captures the main features of the plotted curve. Models can be classified by two characteristics: (1) their appearance at the origin, and (2) presence or absence of a sill. The spherical and exponential models are the most useful in oil and gas applications. Observed semivariograms often call for nested models, in particular one that includes a so-called nugget effect or noise component. Additional models that may be fitted include hole effects, which display pseudoperiodicity, and anisotropic models, which include zonal and geometric anisotropy.

Semivariograms can be fitted for one, two, three, or more dimensions. The complexity of fitting models in three dimensions is increased by the fact that a serious anisotropy usually exists between the horizontal directions and the vertical direction. The user must take care not to construct inadvertently a model that is inadmissible by using purely horizontal and purely vertical terms in a nested model.

As with many statistics, the semivariogram is sensitive to the distribution of the data or the presence of outliers. A simple transform to near-normality can markedly change and improve the semivariogram. For making the semivariogram robust to outliers, a simple procedure exists that can be easily added to any program for calculating the experimental semivariogram. Although normal procedure is for modeling semivariograms by eye, automated methods exist for situations in which the geologist wishes to remain at arm's length from the modeling procedure, or when a large number of models are to be fitted.

Throughout the fitting procedure, the practitioner must keep in mind that the purpose of fitting a model is to obtain a product that can be used in estimation. The purpose of a spatial model in this book is for input to estimation, not to explain a natural phenomenon. The latter is a separate topic beyond the scope of this book. As a result, the geologist should pay close attention to observed semivariograms for small separation distances. The reasons should become more obvious in the next chapter.

REFERENCES

Chu, J., Xu, W. and Journel, A.G. (1994) 3-D implementation of geostatistical analyses – The Amoco case study, in J.M. Yarus and R.L. Chambers (eds),

Stochastic Modeling and Geostatistics. Am. Assoc. Petroleum Geologists, Tulsa, OK, 201–216.

Cressie, N. A. C. (1993) *Statistics for Spatial Data*, revised edition. John Wiley & Sons, New York, 900 pp.

Cressie, N. and Hawkins, D.M. (1980) Robust estimation of the variogram: I. *Math. Geol.*, **12**, 115–125.

Dimitrakopoulos, R. and Xiaochun Luo (1994) Spatiotemporal modelling: covariances and ordinary kriging systems, in Dimitrakopoulos, R., *Geostatistics for the Next Century*. Kluwer Academic Publishers, Dordrecht, 88–93.

Gotway, C.A. (1991) Fitting semivariogram models by weighted least squares. *Computers & Geosciences*, **17**, 171–172.

Gumati, Y.D. and Kanes, W.H. (1985) Early Tertiary subsidence and sedimentary facies – Northern Sirte Basin, Libya. *Am. Assoc. Pet. Geol. Bull.*, **69**, 3952.

Hawkins, D.M. (1980) *Identification of Outliers*. Chapman & Hall, London, 188 pp.

Huber, P.J. (1978) Robust estimates of location: symmetry and asymmetric contamination. *Ann. Math. Stat.*, **42**, 1020–1034.

Journel, A.G. and Froidevaux, R. (1982) Anisotropic hole-effect modeling. *Math. Geol.*, **14**, 217–247.

Journel, A.G. and Huijbregts, C.J. (1978) *Mining Geostatistics*. Academic Press, London, 600 pp.

Krige, D.G. and Magri, E.J. (1982) Studies of the effects of outliers and data transformations on variogram estimates for a base metal and gold ore body. *Math. Geol.*, **14**, 557–564.

Myers, D.E., Begovich, C.L., Butz, T.R. and Kane, V.E. (1982). Variogram models for regional groundwater geochemical data. *Math. Geol.*, **14**, 629–644.

Neal, D. and Price, B. (1986) Oil and gas report and maps of Lincoln, Logan, and Mingo Counties, West Virginia. *W.V. Geol.* and *Econ. Survey Bull. B41*, 68 pp.

Pannatier, Y. (1996) VARIOWIN Software for Spatial Data Analysis in 2D. Springer-Verlag, New York, 91 pp.

Webster, R. and Oliver, M.A. (1993) How large a sample is needed to estimate the regional variogram adequately? in A. Soares (ed.) *Geostatistics Troia '92*, Kluwer Academic Publishers, Dordrecht, pp. 155–166.

Williamson, N. L. (1974) Depositional environments of the Pocono Formation in Southern West Virginia. Unpublished PhD dissertation, West Virginia University.

CHAPTER 3

Linear estimation

Drawing a contour map by hand or by computer uses interpolation. Algorithms for this interpolation range from fitting splines, computing trend surfaces, to drawing flat surfaces within triangulations, all requiring some criterion to be satisfied. The geologist working by hand interpolates between pairs of points, draws connecting contours, does some smoothing to make the map look 'real', and perhaps works in some trends derived from geological experience.

Kriging is a method of calculating estimates of a regionalized variable at a point, over an area, or within a volume, and uses as a criterion the minimization of an estimation variance. Calculated at intersections of a regular grid, kriged estimates can be used for drawing a contour map. The steps in computer mapping are as follows.

1. Collect data, probably irregularly distributed across the study area.
2. Superimpose a regular grid.
3. Interpolate values at each grid node.
4. Construct the contours.
5. If necessary, smooth the lines.
6. Draw the maps.

In this chapter, we are concerned with the third step.

3.1 KRIGING EQUATIONS

Assume that the regionalized variable under study has values $z_i = z(x_i)$, each representing the value at a point x_i. Also assume that this regionalized variable is second-order stationary, with expectation

$$E\{z(x)\} = m$$

a centered covariance

$$E\{Z(x+h)Z(x)\} - m^2 = C(h)$$

and a variogram

$$E\{[Z(x+h) - Z(x)]^2\} = 2\gamma(h)$$

A kriged estimator z_k^* is a linear combination of n values of the regionalized variable:

$$z_k^* = \sum_{i=1}^{n} \lambda_i z_i$$

Weights λ_i are calculated according to these criteria:

1. The estimate is unbiased.
2. The estimation variance is minimized.

The first criterion is satisfied by requiring weights to sum to one, thus ensuring that

$$E\{Z_k^*\} = m \sum_i \lambda_i = m = E\{Z_v\}$$

and

$$E\{[z_v - z_k^*\} = 0$$

The second criterion says that estimation variance:

$$E\{[Z_v - Z_k]^2\}$$

is to be minimized. Writing estimation variance as

$$E\{[Z_v - Z_k]^2\} = E\{Z_v^2\} - 2E\{Z_v Z_k\} + E\{Z_k^2\}$$

it is calculated from:

$$\bar{C}(V,V) - 2 \sum_i \lambda_i \bar{C}(V,v_i) + \sum_i \sum_j \lambda_i \lambda_j \bar{C}(v_i,v_j)$$

where $\bar{C}(A,B)$ is the average covariance between each point in an area A, and each point in an area B. The origin of the terms in this equation will be explained below, along with a discussion of how they are calculated.

The 'kriging system' is a set of $n+1$ linear equations with $n+1$ unknowns, obtained by setting equal to zero each of the partial derivatives:

$$\partial[E\{[Z_v - Z_k^*]^2\} - 2\mu \sum_i \lambda_i]/\partial\lambda_i$$

where the n weights λ_i are to be calculated, and μ is a Lagrange parameter. The system of equations can be written in terms of covariances or in terms of the semivariogram function. The first instance gives the following system of equations to be solved:

$$\sum_{j=1}^{n} \lambda_j \bar{C}(v_i,v_j) + \mu = \bar{C}(v_i,V) \qquad \text{for all } i = 1,n$$

$$\sum_{j=1}^{n} \lambda_j = 1$$

Estimation variance can be rewritten as follows:

$$\sigma_k^2 = \bar{C}(V,V) - \mu - \sum_{i=1}^{n} \lambda_i \bar{C}(v_i,V)$$

With the exception of the first term, all terms in this equation are computed in the course of setting up and solving the system of equations. This way of calculating estimation variance avoids the double summation term and having to save a duplicate n by n array of $\bar{C}(v_i,v_j)$ terms.

Using the semivariogram $\gamma(h)$, the system of equations becomes

$$\sum_{j=1}^{n} \lambda_j \bar{\gamma}(v_i,v_j) - \mu = \bar{\gamma}(v_i,V) \qquad \text{for all } i = 1,n$$

$$\sum_{j=1}^{n} \lambda_j = 1$$

and estimation variance is:

$$\sigma_k^2 = -\bar{\gamma}(V,V) + \mu + \sum_{i=1}^{n} \lambda_i \bar{\gamma}(v_i,V)$$

Although both ways of setting up the system of equations are valid, the first has been preferred for computational reasons, even when the data are not second-order stationary, but follow the intrinsic hypothesis. Writing the system of equations in the form of covariances eliminates the problem of zeroes along the diagonal, which preclude many algorithms that involve dividing by these terms. If the regionalized variable does not obey second-order stationarity and there exist no sill C(0), one can define pseudocovariance as follows:

$$C(h) = A - \gamma(h)$$

where A is some number greater than any value of $\gamma(v_i,v_j)$ or $\gamma(v_i, V)$. The nonbias criterion eliminates the constant A from the system of equations.

The system of equations is perhaps more easily visualized in matrix form. Defining

$$[\lambda] = \begin{bmatrix} \lambda_1 \\ \lambda_2 \\ \cdot \\ \cdot \\ \cdot \\ \lambda_n \\ \mu \end{bmatrix}$$

$$[B] = \begin{bmatrix} \bar{C}(v_1,V) \\ \bar{C}(v_2,V) \\ . \\ . \\ . \\ \bar{C}(v_n,V) \\ 1 \end{bmatrix}$$

and

$$[\mathbf{W}] = \begin{bmatrix} \bar{C}(v_1,v_1) & \bar{C}(v_1,v_2) & \ldots & \bar{C}(v_1,v_n) & 1 \\ \bar{C}(v_2,v_1) & \bar{C}(v_2,v_2) & \ldots & \bar{C}(v_2,v_n) & 1 \\ . & . & . & . & . \\ . & . & . & . & . \\ . & . & . & . & . \\ \bar{C}(v_n,v_1) & \bar{C}(v_n,v_2) & \ldots & \bar{C}(v_n,v_n) & 1 \\ 1 & 1 & \ldots & 1 & 0 \end{bmatrix}$$

then

$$[W]\ [\lambda] = [B]$$
$$[\lambda] = [W]^{-1}\ [B]$$

3.1.1 Terms in the kriging system

All covariances in the kriging system are computed from a semivariogram and the relative distances between samples and the point or block to be estimated.

Each entry in matrix $[W]$ is a sample-to-sample covariance. The distance between well site i and well site j is calculated to give h_{ij} along with the direction of the vector described by the two samples if an anisotropic model is to be used. The value of $\gamma(h_{ij}) = \gamma(v_i,v_j)$ is calculated from the semivariogram model, to give the covariance $C(v_i,v_j) = C(0) - \gamma(v_i,v_j)$. Matrix $[W]$ depends only upon the relative locations of samples and does not contain any information about the geographic locations for which an estimate is desired. In applications where sampled locations lie on a regular grid, this matrix is constant across the area to be kriged except for the edges; exploiting this fact can mean considerable savings in computation time.

Note that $[W]$ remains the same for both point and block kriging. Not so matrix $[B]$, covariances between sample points v_i and the point or block to be kriged, V. If one wants to perform point kriging, $\bar{C}(v_i,V)$ is merely calculated from the distance between location v_i and location V, and the direction of the vector joining these two locations if the semivariogram model is anisotropic, to give $\gamma(v_i,V)$ and the covariance. If we are computing an estimate of the mean value of a regionalized variable

within a block, then $\bar{C}(v_i,V)$ represents the average covariance between any point in the block V and sample v_i. Although in principle computation of point-to-block covariance constitutes an integration, in practice the computation is carried out through a discrete summation. The area or volume of a block is represented by a set of points regularly disposed within the block, the covariance between sample v_i and each point is computed, and an average value is used for $\bar{C}(v_i,V)$. Precision increases with the number of points within the volume or area, but four or five points on a side appears sufficient; this yields 16 or 25 points for an area.

To illustrate terms in the kriging equations, Fig. 3.1 shows sample-point-to-sample-point covariances in matrix [W], sample-point-to-estimated-point covariances [B] in point kriging, and sample-point-to-estimated-block covariance [B] in block kriging. Area V in Fig. 3.1b could have been drawn to include one or more sample points and calculations would remain the same. In the case of point kriging, point V can coincide with a sample point, in which case the estimate equals the known value at that point and kriging variance equals zero. Thus, kriging is an exact interpolator.

Points v_i must be unique so that matrix [W] is strictly positive definite. The kriging system cannot accommodate replicate samples; one must first reduce these to mean values at a location. If kriging is performed from samples stored in a data base, care must be taken that duplicate entries have not been made to the data base. Computer programs for kriging can be written to check that no sample locations lie within a specified distance tolerance. Even when two points do not coincide, they may be close enough relative to other points in the kriging system to make matrix [W] ill-conditioned and the numerical solution of the kriging equations unreliable.

Two of the three terms in the equation for estimation variance are computed while the kriging equations are set up and solved. The remaining term, $\bar{C}(V,V)$, the average covariance of samples within blocks of size V, is computed in the same way as $\bar{C}(v_i,V)$, except that each point

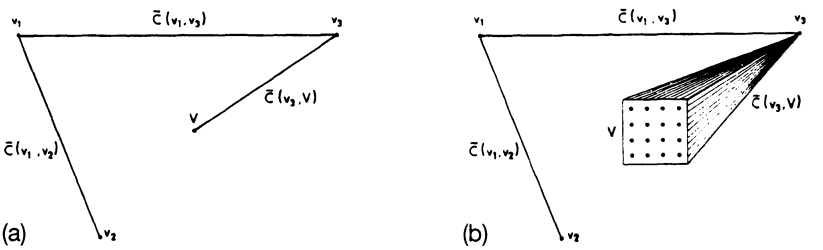

Figure 3.1 Some of the terms in the kriging equations for (a) point kriging and (b) block kriging.

v_i is one of m points used to make a discrete approximation of block V, and these m values are averaged. If a block is approximated by 16 points, then 16 values of $\overline{C}(v_i,v_j)$, $i = 1, m$; $j = 1, m$ are computed and averaged. Block covariance is obviously constant for a given block size, and therefore in mapping an area the value of the block variance can be calculated once at the beginning of a computer program. In the context of point kriging, $\overline{C}(V,V)$ equals covariance at a separation distance of zero.

3.1.2 Properties of kriged estimates

Because kriged estimates minimize estimation variance, considering the three terms of this variance along with the semivariogram model shows that weights depend upon four factors.

The first one is size and shape of the block to be estimated, expressed by the term: $\overline{C}(V,V)$. With decreasing block size, average covariance of points in the block increases, and the estimation variance increases to a maximum when estimating a variable at a point.

Second, distances between points in the block and control points are expressed by the term $\overline{C}(v_i,V)$. With increasing distance between the block and control points, average covariance decreases and estimation variance increases. The farther away the control wells from a point or area, the more uncertainty in an interpolation at that point or block. This accords with geologists' assumption that map reliability increases with the number of control points.

Third, the configuration and distances between control wells are expressed by the term $\overline{C}(v_i,v_j)$. The influence of sample configuration on the estimation variance is explored in some detail below, but for now the following generalization can be made: both the number of control points and their relative dispersion influence estimation variance.

Finally, quality and value of the estimate depends on the semivariogram model. At a given level of precision, estimation of a regionalized variable with a large range can be achieved with fewer widely dispersed wells than a variable having a small range. If a strong directional anisotropy exists in a northeast–southwest direction, an estimate computed from wells in the northwest and southeast directions must have greater uncertainty than one calculated from wells situated the same distance to the northeast and southwest.

Minimization of kriging variance is thus consistent with the geologists' intuition with regard to the spacing of control wells. But where the geologist may have a qualitative sense of overall reliability of a map, computation of estimation variances provides local measures of reliability that may influence the collection of more data, if possible, and interpretation of the map.

For a simple example of kriging at a single point, consider estimating the value of a regionalized variable at point V from the four points in Fig.

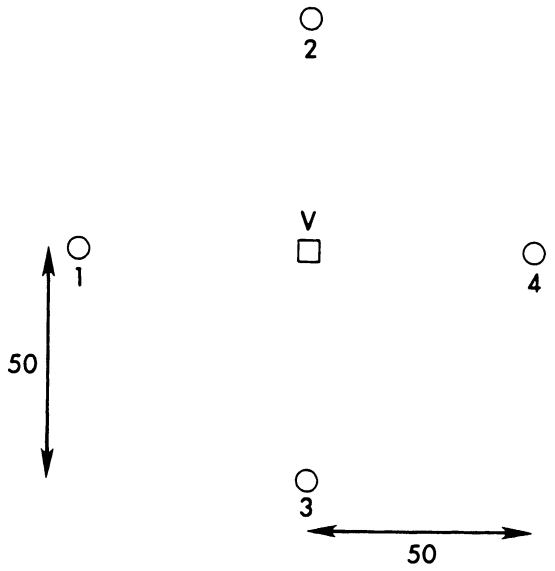

Figure 3.2 Hypothetical configuration of control sites equidistant from a site.

3.2. Assume a spherical semivariogram model having a sill of 1, range of 200, and no nugget effect. Covariance between each point and itself is 1, to give the values in the diagonal of matrix [**W**]. Covariance between points 1 and 4 equals $C(0) - \gamma(v_1,v_4)$, or

$$1 - 1*[(3*100)/(2*200) - (100^3)/(2*200^3)] = 0.3125$$

Completing the calculations gives the following matrix:

$$[\mathbf{B}] = \begin{bmatrix} 1 & .4918 & .4918 & .3125 & 1 \\ .4918 & 1 & .3125 & .4918 & 1 \\ .4918 & .3125 & 1 & .4918 & 1 \\ .3125 & .4918 & .4918 & 1 & 1 \\ 1 & 1 & 1 & 1 & 0 \end{bmatrix}$$

Covariance between V and the samples is a constant because all are the same distance from the point to be estimated:

$$1 - 1*[(3*50)/(2*200) - (50^3)/(2*200^3)] = 0.6328$$

Therefore, matrix [**B**] is simply:

$$\begin{bmatrix} .6328 \\ .6328 \\ .6328 \\ .6328 \\ 1 \end{bmatrix}$$

and the solution is

$$[\lambda] = \begin{bmatrix} .2500 \\ .2500 \\ .2500 \\ .2500 \\ .0588 \end{bmatrix}$$

with an estimation variance of

$$1.0 - 0.0588 - 4*(0.6328*0.25) = 0.3084.$$

As expected, weights are all equal, and the estimate is the mean value of the regionalized variable at the four control wells.

Consider the same point distribution, but in a spherical model with an overall sill of 1 and a nugget effect of 0.25. The matrix of covariances has smaller values off the diagonal, and covariances between control points and point V are lower (Table 3.1A). Kriging weights remain unchanged, but now kriging variance equals 0.54, greater than that calculated for the model without a nugget effect. Thus, uncertainty beyond a very small range as expressed by the nugget effect leads to a greater uncertainty in the final estimate.

The influence of anisotropy can be explored by going back to the spherical model with a sill of 1, range of 200, no nugget effect, and an anisotropic ratio of 1.5 in the east–west direction. The kriging system in Table 3.1B now yields two groups of weights: samples situated east and west of V are given more weight than those to the north and south.

Consider now the configuration of wells in Fig. 3.3, in which two wells are very close to each other and therefore redundant, and two wells are roughly equidistant from each other and the cluster. Using the previous semivariogram model, nugget effect of zero, sill of 1, and range equal to 200, solving the kriging equations (Table 3.1C) gives nearly equal weights to points one and four and the sum of points two and three. Thus, each point in the cluster was downweighted relative to isolated points in other directions. Notice that kriging variance, 0.349, has increased over that of the example with four evenly spaced points, 0.326. Because two points are clustered, the uncertainty in the estimate is about the same as that in an estimate based on three points.

Relative magnitude of nugget effect and range both control the degree of smoothing in kriged estimates. In the case of pure nugget effect, estimates constitute a simple moving average. For example, the configuration of points in Fig. 3.3 was used in conjunction with semivariogram models that differ only in the relative magnitude of the nugget effect (Table 3.2). With an increase in the nugget effect, weights approach the same value until they are equal to 0.25.

Remembering that the nugget effect represents a model with a very small range, one can see that an increase in nugget effect means that

Table 3.1 Systems of equations and solutions for three combinations of semivariograms and well configurations

A. Nugget effect = 0.25

Covariances between samples				*Point-to-point covariances*	*Weights*
1.00	0.37	0.37	0.23	0.47	0.25
0.37	1.00	0.23	0.37	0.47	0.25
0.37	0.23	1.00	0.37	0.47	0.25
0.23	0.37	0.37	1.00	0.47	0.25

B. Anisotropic semivariogram

Covariances between samples				*Point-to-point covariances*	*Weights*
1.00	0.37	0.37	0.09	0.63	0.37
0.37	1.00	0.31	0.37	0.46	0.13
0.37	0.31	1.00	0.37	0.46	0.13
0.09	0.37	0.37	1.00	0.63	0.37

C. Irregular sample spacing

Covariances between samples				*Point-to-point covariances*	*Weights*
1.00	0.51	0.47	0.30	0.63	0.35
0.51	1.00	0.93	0.35	0.63	0.13
0.47	0.93	1.00	0.39	0.63	0.19
0.30	0.35	0.39	1.00	0.59	0.34

more spatial variability in the regionalized variable occurs at short distances, to the limit of complete independence in the case of pure nugget effect. In this situation, the simple mean provides an unbiased

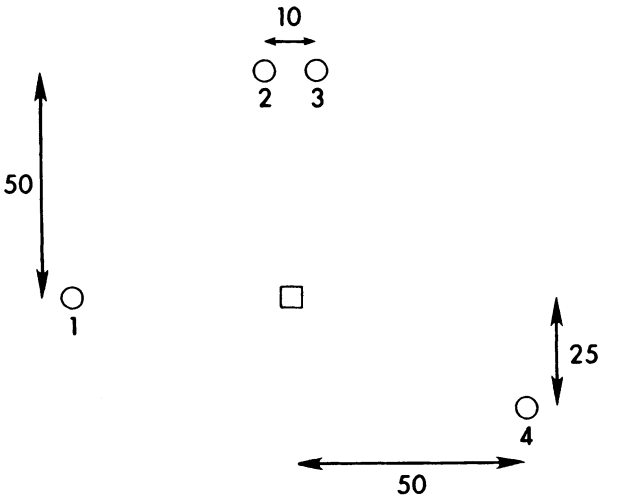

Figure 3.3 A second hypothetical configuration of control points.

Table 3.2 Kriging weights and kriging variance for configurations in Fig. 3.3 using different constants for the semivariogram

Nugget effect	0.00	0.25	0.75	1.00
Sill of spherical model	1.00	0.75	0.25	0.00
Well 1	0.35	0.31	0.27	0.25
Well 2	0.13	0.18	0.23	0.25
Well 3	0.19	0.19	0.23	0.25
Well 4	0.34	0.32	0.27	0.25
Kriging variance	0.35	0.58	1.03	1.25

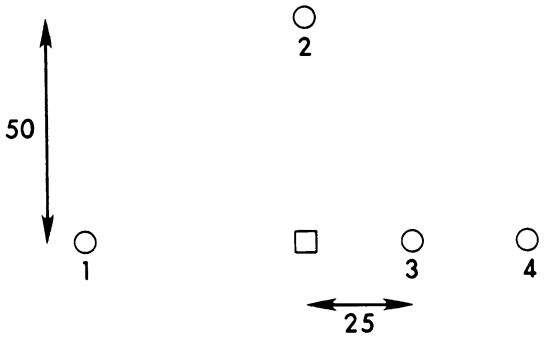

Figure 3.4 A third hypothetical configuration of control points.

estimate. Because all covariances between V and each control well are zero, the second term in the equation for estimation variance drops out, and the estimation variance in our example equals $1 - \mu$, where μ must equal $\frac{1}{n}$. With increasing n, the estimation variance approaches the simple variance. Thus, uncertainty in our estimate depends upon the number of samples when they are independent, as we learned in introductory statistics. Restated, for a given number and configuration of samples, our uncertainty in an estimate decreases with decreasing independence.

When two samples lie in the same direction from the site to be estimated, kriging is said to 'screen' the more distant site relative to the near one. For instance, the configuration of wells in Fig. 3.4 includes two sites that lie due east of V. Solving the system of kriging equations yields the following weights:

well 1 0.278
well 2 0.135
well 3 0.629
well 4 − 0.042

and a kriging variance of 0.244. Notice that well 4 is assigned a weight near zero, even though it lies the same distance from V as wells 1 and 2.

3.1.3 Examples along a transect

The smoothing influence of the nugget effect and the range will now be illustrated for points along a transect of synthetic data. These samples should give some insight into what one might expect to see on a map.

In the first example, a spherical semivariogram model was used with a sill of 25, a nugget effect of zero, and a range of 25 ft. Kriged estimates were calculated every foot, and estimates at sampled footages equal the observed values. Figure 3.5 shows estimates along one 15-ft interval; estimation standard error is plotted as an envelope around the estimates. Of course, estimation variance at control points equals 0. When a nugget effect is absent, and the range is large, interpolation forms a smooth surface, and estimation variance increases away from control points.

Estimates calculated using a nugget effect of 15 and a spherical model with sill of 10 are surrounded by much larger confidence envelopes. Except for excursions through the control points, kriged estimates form a very smooth surface (Fig. 3.6a). If control points are not included with the interpolations but are replaced by values at very close footages, the surface is very smooth indeed (Fig. 3.6b). Thus, the moving average process of kriging dominates interpolation when the nugget effect is large, as shown in the previous section.

Some computer programs give results like those shown in Fig. 3.6b, even when the sites to be estimated include sites of known values, as in

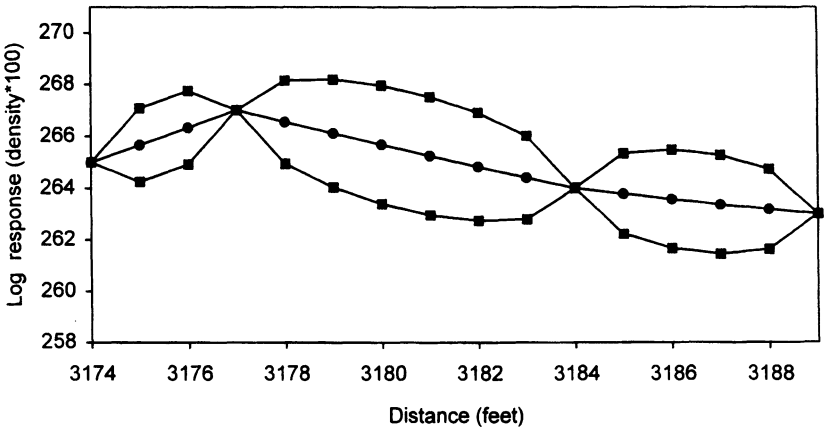

Figure 3.5 Kriged estimates along a transect (filled circles) and estimation standard errors (squares) for one semivariogram model.

Fig. 3.6a. This would seem to contradict an earlier statement that the surface must pass through the control points. The reason for the contradiction is that the nugget effect is a simple way to compute covariances in the presence of a model with a very small, indeterminate range. Properly speaking, the nugget effect should be replaced by a model – a spherical model, say – that passes through the origin. But because the appearance of this very fine-scale model is unknown, it is approximated as a constant C_0. For very small values of h, $\gamma(h) = C_0$, and the covariance C(0) − Y(h) equals $C + C_0 - C_0 = C$, as it should. But the computed covariance for $h = 0$ also comes out being C, when in fact it should be

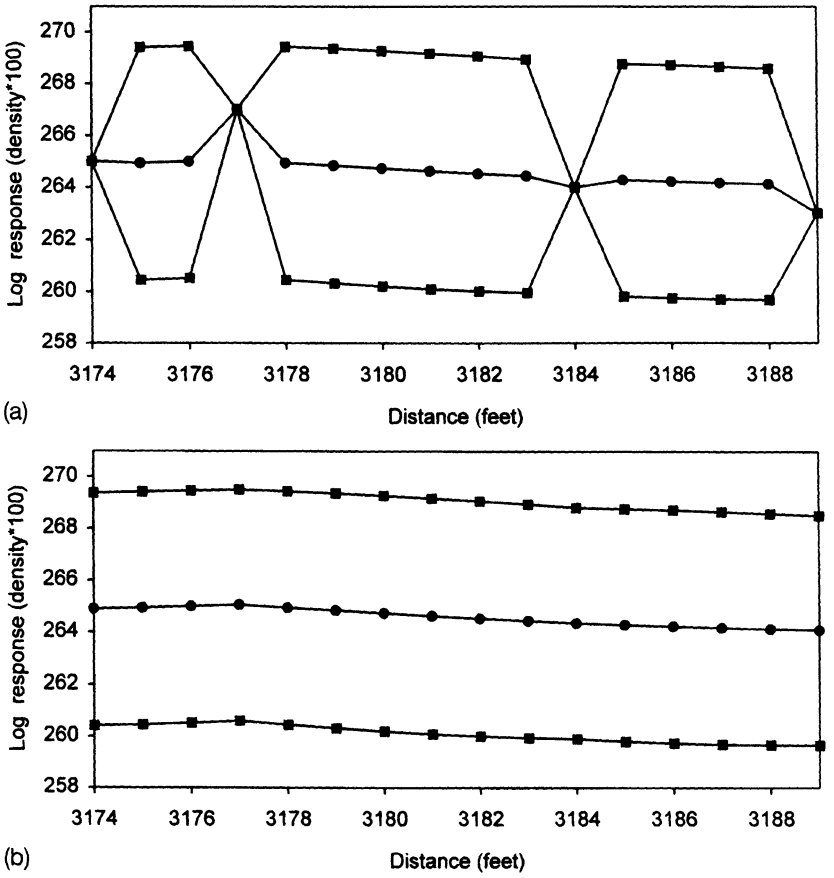

Figure 3.6 Kriged estimates (filled circles) and standard error (squares) along a transect for a semivariogram model with large nugget effect. In (a) some of the estimated locations coincide with the observed points, and therefore estimates equal observed values and estimation variance is zero; in (b) the estimated locations do not coincide with the observed points.

$C + C_0$. Many programs fail to check whether the site to be estimated is coincident with an observation point.

The result is an estimate with non-zero kriging variance. In practice, this discrepancy is rarely a problem; points on a regular grid are unlikely to correspond with sample sites, unless the sample locations are as crudely digitized as those in the present example. However, if one insists that the kriged surface passes through control points, special provision must be made in the computer program.

In Fig. 3.7 the semivariogram model has a nugget effect of zero, sill of 25, and range of 4 ft. The resulting surface has a rougher appearance than that in Fig. 3.5, which was calculated with the same model but a larger range. The shorter range implied less continuity between control sites, and the interpolated surface shows more peakedness. Like the surface that resulted from the large nugget effect, the one in Fig. 3.7 seems to gravitate near the regional mean, only approaching the very high or low values close to control points.

What is the geologic meaning of these profiles? How might they affect the geologists' interpretation of a particular regionalized variable? Given the raw data, most geologists would probably draw a smooth interpolation like that in Fig. 3.5, rather than the one in Fig. 3.7. Why use an algorithm that produces the rougher surface in Fig. 3.7 or the very smooth surface in Fig. 3.6a? The answers lie partially in the geologic meaning and practical value in delineating the geographic or stratigraphic limits of extreme values. Assume for now that data used in this section represents elevation of a formation top. If the petroleum geologist is looking for areas of structural closure, the surface in Fig. 3.5 has a large area of closure within a well-defined anticline, whereas the surface in

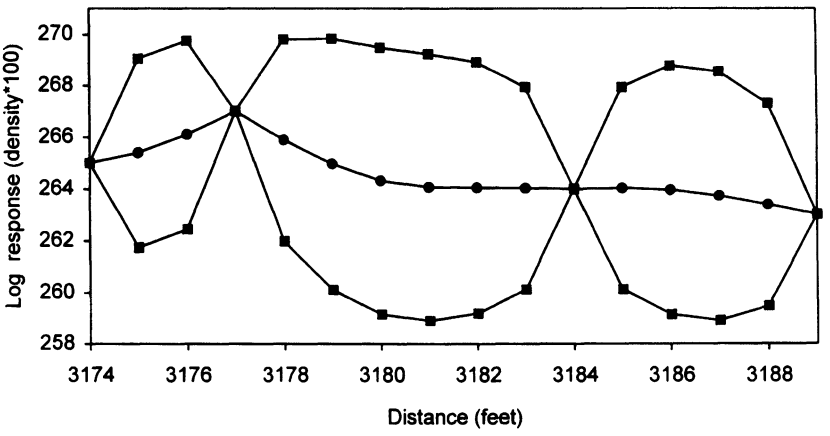

Figure 3.7 Kriged estimates (filled circles) and standard errors (squares) for semivariogram model with a short range and no nugget effect.

Fig. 3.6b appears to be a gentle monocline, with no closure within the geographic window we are peering through. In specifying a large nugget effect the geostatistician is saying that autocorrelation is low beyond a very short distance, and therefore extreme values should not be taken as more than local features. At the time of mapping these extreme values are limited to very small areas (Fig. 3.6a) or ignored altogether (Fig. 3.6b). In either case the maps show very conservative estimates in the presence of a large nugget effect.

To take another example, assume that the regionalized variable in these figures is initial potential (although the absolute scale makes little sense). Using a cutoff of 266 units, four of the estimates in Figure 3.5 lie above this value, three values lie above this value in Fig. 3.7, and only the observed value lies above this value in Fig. 3.6. In the presence of a large range and little small-scale uncertainty, one can delineate a rather large area of higher potential. The smaller the range and the greater the small-scale uncertainty, the less emphasis one places on these extreme values.

Note that kriged estimates do not imply that the actual surface in Fig. 3.6 is a monocline with bumps and depressions; rather, they imply that small-scale features do exist but cannot be determined very far from the control points. The problem lies not in the map but in the number of control wells relative to the scale of the structure. In the case represented by Fig. 3.6 many bumps and depressions probably lie between the second and third control points, but the program cannot draw them in any more than a geologist can. The large envelope around the estimates shows that almost anything can happen between the control points. One way to visualize what might be taking place between the control points is to perform conditional simulation, the subject of Chapter 7.

On a transect or map of kriged estimates, the geologist could report only those estimates with an estimation variance less than a given value. This procedure parallels that of the geologist who limits contouring to areas a certain distance from control points.

To summarize this section, the kriging system of equations and the kriging variance depend upon the size and shape of the area V, distances between V and control points, the configuration of the control points, and the semivariogram model. With a number of examples I have attempted to clarify the computations and to show the effect of these factors on the kriging weights. Given a configuration of points, the semivariogram model can have a profound influence on map appearance and estimation variance. Kriging places less importance on extreme values in the presence of large degrees of indeterminate, small-scale variation. These examples are not meant to suggest that the geologists experiment with semivariogram models until the map 'looks right'. Rather, one should attempt to model the regionalized variable conscientiously. If the resulting model does not yield a map of the expected

appearance, perhaps some fault lies in the data, or perhaps an attempt must be made to obtain more data, thereby reducing the nugget effect. The next section illustrates kriging applied to actual data.

3.2 EXAMPLES

3.2.1 Thickness of a clastic section

A spherical semivariogram with a sill of 300 000 ft^2, no nugget effect, and range of 8 units describes the regional behavior of data extracted from a study of Paleocene clastics (Gumati and Kanes, 1985) (Fig. 3.8). This simple semivariogram model was used with 39 observations to generate kriged estimates on a regular grid of 6×6 points (Fig. 3.9). Kriging variance ranges from a low of 0, where a node of the grid coincides with a control point, to a high of 338 278, where the regionalized variable was poorly sampled in the northern part of the study area (see Fig. 2.2).

Block kriging provides an average value of clastic thickness within an area or, multiplied by the dimensions of the two-dimensional block, estimates volume of rock. If estimates of blocks are combined, the result is a so-called global estimate of reservoir thickness or volume. Such parameters can be estimated through simple arithmetic averages, but the results would be biased in the presence of significant clustering of control points.

Block kriging was performed on the thickness data using the same semivariogram model used in point kriging, and 5×5 blocks centered on the grid nodes used above. Two observations may be made from the map of kriged estimates (Fig. 3.10). The standard error of estimation is

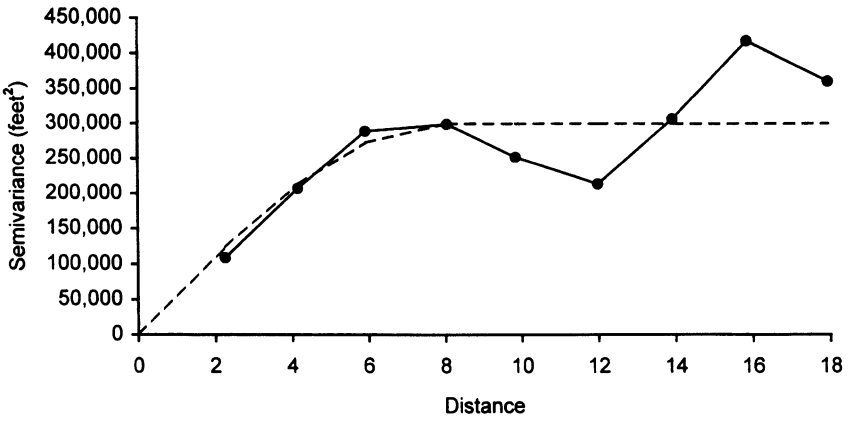

Figure 3.8 Semivariograms of the thickness of Paleocene clastics.

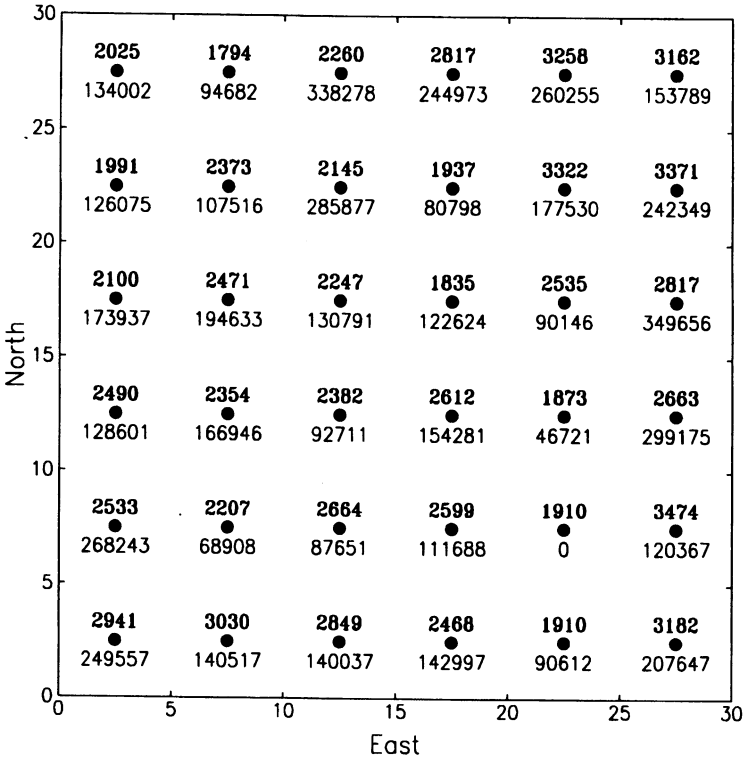

Figure 3.9 Estimates (above symbols) and estimation variances for point kriging of Paleocene thickness data.

lower for each block relative to that for the point centered within the block. With increasing block size, estimation variance should decrease.

Observe from Fig. 3.10 that block estimates vary less than point estimates. Whereas raw data range between 1439 and 3941, point estimates range between 1794 and 3474, and block estimates range between 1887 and 3332. The calculation of kriged estimates for points on a coarse grid accounts for the limited range in the estimates; an infinitely fine grid would yield at least the same range of estimates as the original data because kriging is an exact interpolator. However, the smaller range in the block estimates results from the smoothing that kriging performs when estimating average block values. As block size increases, the range further decreases to the limit of a regional average. Histograms of point (Fig. 3.11) and block (Fig. 3.12) estimates show that the latter estimates cluster more about a median value of 2400 ft.

How do block estimates compare with a naive average of values within a block? We can take the three values that lie within the 20×20

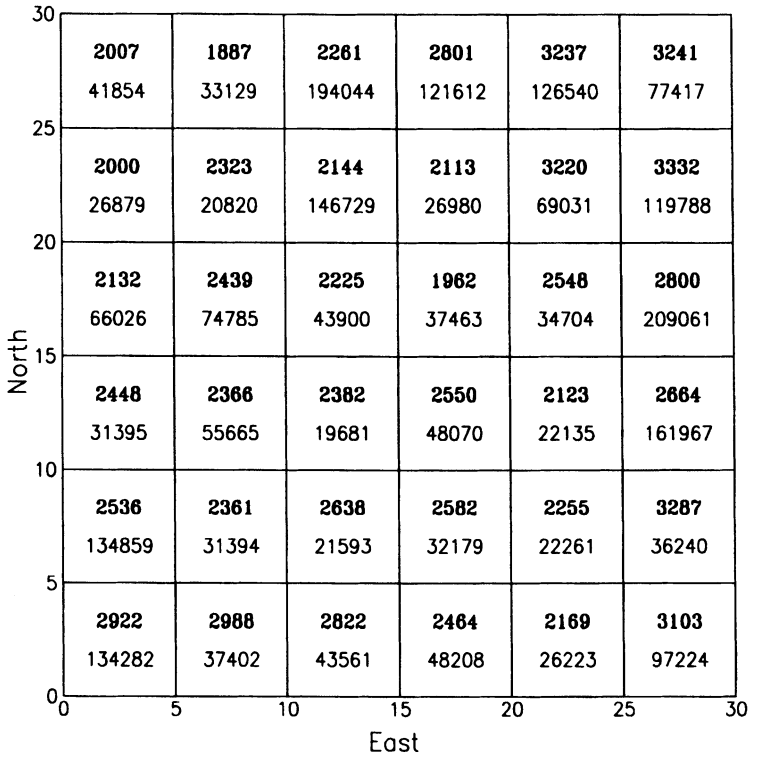

Figure 3.10 Block kriged estimates and estimation variances for thickness of Paleocene clastics.

area in the extreme northeast corner of the total area. The average of the three values, 3632, 3048, and 3890, equals 3523 ft, whereas the average of the four blocks in this area equals 3278 ft, less than the naive estimate because kriging includes the points surrounding the area in question in computing an average thickness. When control points are distributed uniformly throughout the limits of a block, points outside the block are screened, and contribute very little to the calculation. On the other hand, if control points are clustered to one side of the block, consideration of surrounding values better defines the regionalized variable and improves the estimate.

Block kriging is not used often with oil and gas data. It was developed in the context of mining, where interest lies in computing the average value of a regionalized variable such as gold within a volume of rock. Even if we are interested in computing the average porosity in a volume of reservoir, for example, we usually choose a block size so small relative to well spacing, that point and block estimates are virtually identical.

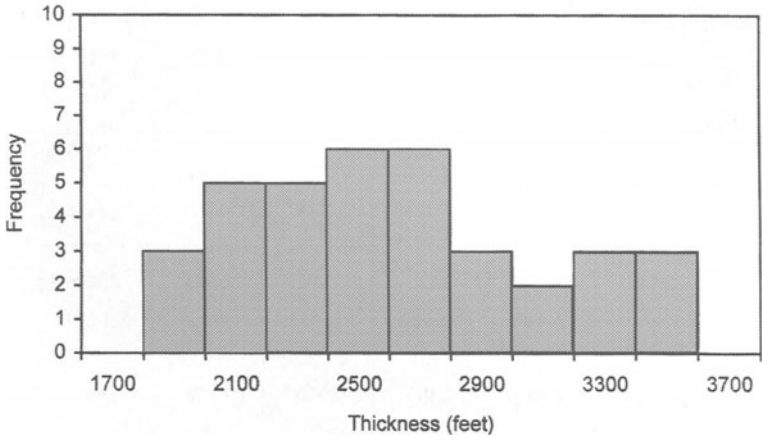

Figure 3.11 Histogram of estimates from point kriging Paleocene thicknesses.

3.2.2 Initial potential of Upper Devonian gas

In Chapter 2 a simple exponential semivariogram model was found to fit closely the spatial behavior of initial potential of gas observed in wells producing from Upper Devonian clastics in Barbour County, West Virginia. These data are used to further illustrate kriging of two-dimensional data, and to introduce a procedure called 'validation'.

A subset of the original data was used to compute a new semivariogram (Fig. 3.13); the locations selected fall within the region to be

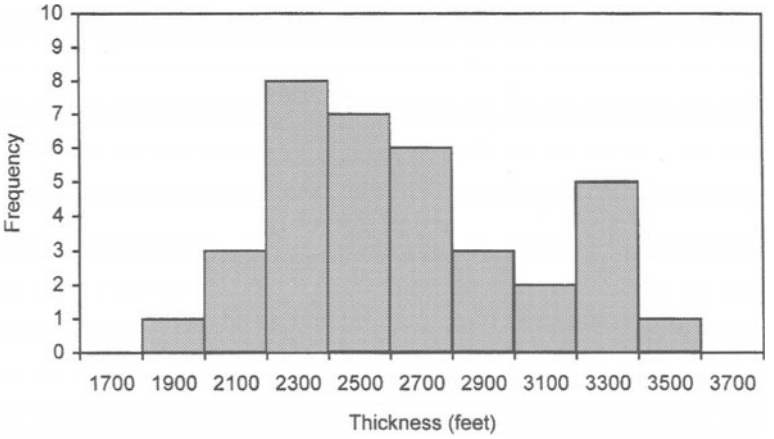

Figure 3.12 Histogram of estimates from block kriged Paleocene thicknesses.

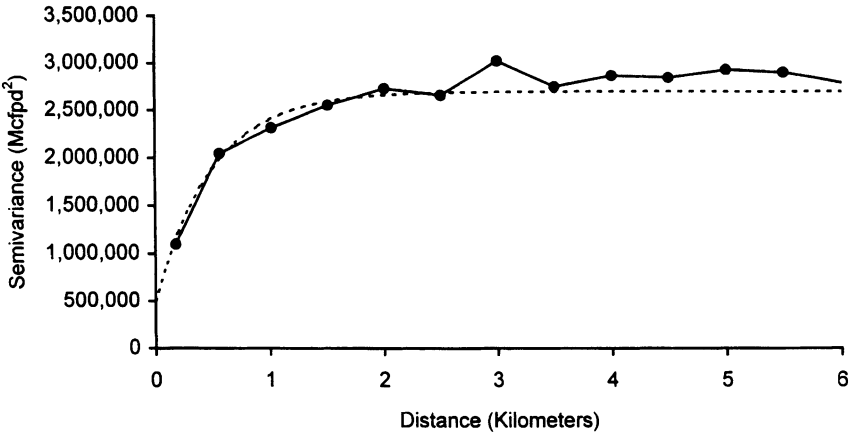

Figure 3.13 Semivariogram of initial potentials in a portion of Barbour County, West Virginia.

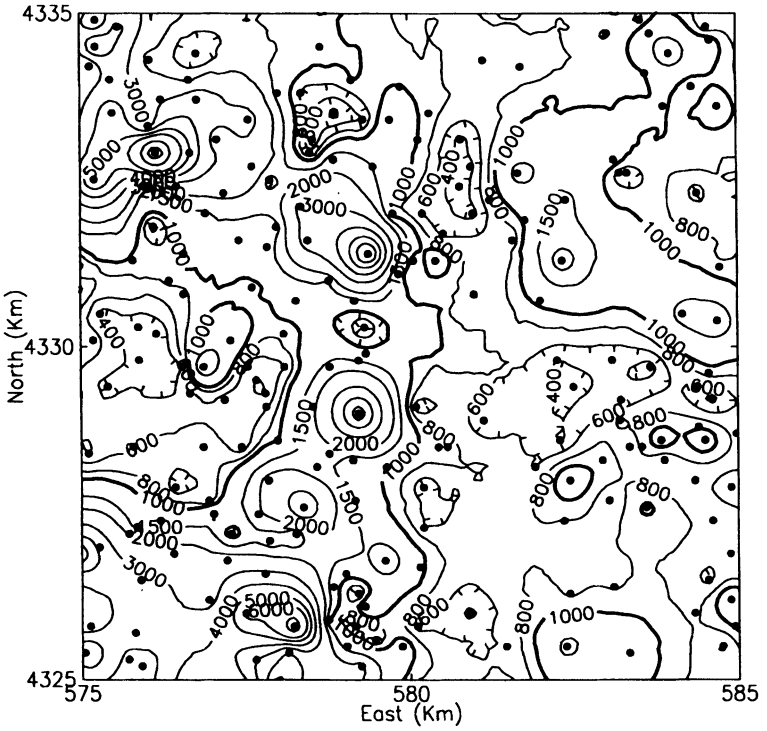

Figure 3.14 Contour map of kriged estimates of gas initial potentials in a portion of Barbour County, West Virginia. Area mapped is 10 km on a side. The contour interval is irregular; units are thousands of cubic feet of gas per day.

mapped as well as in adjacent areas to avoid edge effects. Kriged estimates were computed for each point on a regular grid covering a 100 km^2 region (Fig. 3.14). The grid was 91 rows by 91 columns, thus providing an estimate every 0.11 km, a spacing much finer than the sample spacing. To eliminate edge effects, wells within a distance equal to the practical range, 4.5 km, were included along with wells falling within the area to be mapped.

Kriged estimates show the large degree of smoothing one expects to find when the nugget effect equals about half the sill. A map of well locations annotated with the initial potentials shows the large variation among even closely spaced wells (Fig. 3.15). Nevertheless, the map of kriged estimates shows trends in initial potential within the area mapped. Those needing the surface to exactly honor the data might be out of luck, although as demonstrated in earlier examples, if the grid is fine enough, the contour map will honor each point. Of course, with such a large nugget effect, each well would be surrounded by a bull's-eye.

In Chapter 2, we looked at the possibility of using a log transform on raw data to smooth the semivariogram, and expedite model-fitting. In

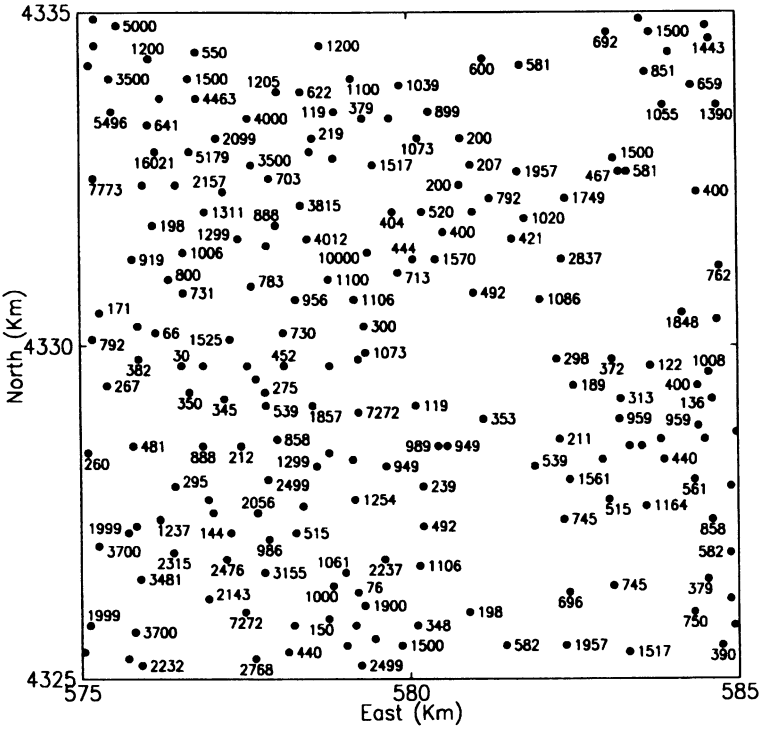

Figure 3.15 Well locations annotated with gas initial potential data. Units are thousands of cubic feet of gas per day.

the present example, some exploratory work showed little difference between semivariograms computed from untransformed and transformed data.

3.2.3 Log transform?

Nevertheless, using the log transform in kriging has a long, if checkered history. It was observed several decades ago that many data sets were highly skewed, and approach a lognormal distribution.

This fact has several consequences, one of which is that the semivariogram can be hard to model with confidence. Another is that assumptions of stationarity that are made may be violated. In geographic terms, the effect of this is that maps may show large areas of high values centered about a few observations, i.e. what we call bull's-eyes. In addition, and perhaps more serious, is that estimation variances are unrealistically small in areas of high values in the regionalized variable. The noticeable nonnormality of data sets in many fields – including petroleum geology – has caused part of the concern over use of estimation variance in any way, and has led to the development of nonlinear methods of estimation, including lognormal kriging (Rendu, 1979).

Lognormal kriging uses a forward transform of calculating the logarithms of each raw value. Semivariograms and linear estimates are computed from transformed data. Estimates must then be back-transformed to the original units. If the original data are represented by z_i and logtransformed data by y_i, kriged estimates in the original units of measure are calculated from:

$$z_k^* = 10^{(y_i^* + \sigma_k^2/2 - \mu)}$$

where z_k^* and y_k^* are kriged estimates, σ_k^2 is the estimation variance, and μ is the Lagrange parameter. To simply compute the antilog of y_k^* yields a biased estimate and is incorrect. A concern of many practitioners is that because the back-transform involves the estimate and estimation variance in the exponent, that back-transformed values may be overly sensitive to minor perturbations in data values and locations.

Lognormal kriging was carried out on the initial potential data, and results are compared in with disjunctive kriging in Chapter 5 and indicator kriging in Chapter 6.

3.2.4 Cross validation

The practice of 'cross validation', or simply 'validation', is a commonsense procedure for comparing estimated values with observed values, just as one computes residuals between predicted and observed values in regression or analysis of variance. The procedure is as follows: for each sample in the data set, compute a kriged value at the same

location from the rest of the data, ignoring that sample. The result is an estimated value for comparison with the corresponding true value.

Comparison of observed errors and kriging variance can be made in a number of statistical and graphical ways. If the kriged estimates are unbiased, averages of the estimates and the observations should be equal. The 674 values of initial potential used in the previous section average 1239.3 Mcfpd; the average kriged estimate from cross-validation of untransformed data is nearly identical: 1232.3 Mcfpd.

Graphical displays are useful and often humbling. After fitting the exponential model to the experimental semivariogram in Chapter 2, the observation was made that although a very satisfying fit of the theoretical model to the data was found, the interpretation of the model was less encouraging. Specifically, the very large nugget effect relative to the sill means that there exists a large proportion of the fine-scale variation not captured by the well density. As a result, kriged estimates largely represent moving averages, leading to large deviations between estimated and observed values.

Indeed, this is the case. A graph of observed versus estimated values should result in a straight line with a slope of 1. Such a plot for the initial potential data (Fig. 3.16) displays very little correlation. Moreover, there appears to be a conditional bias: low values of initial potential are overestimated, and high values are underestimated.

However, such a plot can be dissected by considering estimation variance, which is relatively low for locations surrounded by a number of nearby wells, and higher for locations having well control that is sparse or poorly distributed. Figure 3.17a shows results for the 100 wells with the smallest estimation variances; these wells should have the best

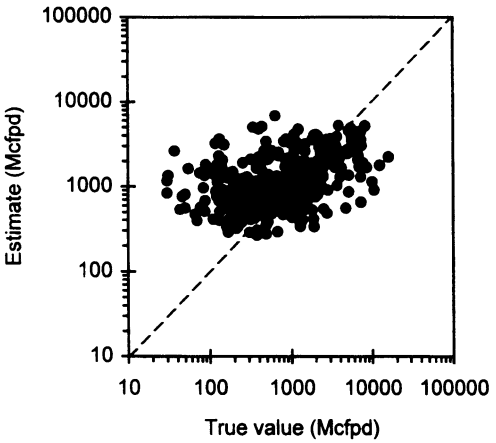

Figure 3.16 Scattergram of observed values of initial potential against estimated values.

agreement between observed and estimated values because they have the best control. The cloud of points does indeed lie along a line with slope of 1, although there is a lot of scatter. Three points with low observed values fall away from the main group of points, and might represent errors in the data. For the 100 wells with the highest estimation variances, the cloud of points bears no relationship with the line of slope 1 (Fig. 3.17b). Well control was so poor for these wells that the estimate is basically a regional average. The conditional bias depends upon the degree of well control.

Clark (1986) reviews the history of validation and its usefulness in geostatistics. She points out that this type of comparison was used initially to compare methods of estimation (David, 1977; Journel and Huijbregts, 1978) and to justify the use of kriging as an estimation method (e.g. Parker *et al.*, 1979, and others in the same volume). Validation is still used in this way.

Because statistics and displays used in validation depend upon both estimation method and semivariogram model, the procedure has also been used in supporting the selection of a particular semivariogram model, or for adjusting the parameters of a model. Clark (1986) demonstrates that use of validation procedures for selecting a semivariogram model may not be incorrect, but they also may not be sensitive enough to be very useful. In one example, she modeled an obviously anisotropic semivariogram in three ways: with an isotropic linear model, an anisotropic linear model, and a pure nugget effect. Standard validation procedures did show that the third model had problems but could find little difference between the first model and the second, correct one. She urges caution. Nevertheless, the statistics and displays generated by validation efforts provide excellent tools for peering into the results of a

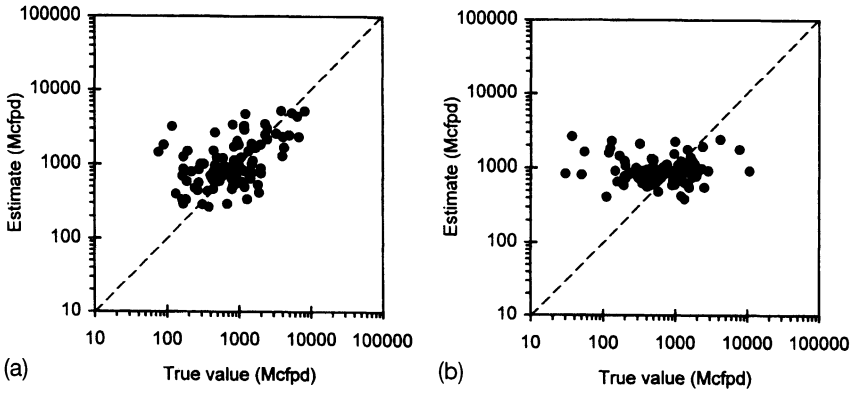

Figure 3.17 Scattergram of observed and estimated initial potentials for (a) the 100 wells with the smallest estimation variances, and (b) the 100 wells with the largest estimation variances.

geostatistical study and may have more value in exploratory data analysis than in testing the hypothesis 'My semivariogram model is right'. Davis (1987) comes to a similar conclusion.

3.3 KRIGING IN THREE DIMENSIONS

Estimation in three dimensions is no different than that in two dimensions, except some practical aspects of the search and gridding algorithm become important. These include the search radius and adjusting for structural deformation of the reservoir to be mapped.

In Chapter 2, the following model for the semivariogram of porosity was fitted:

$$\gamma(h) = 11Sph\left(\frac{|h|}{7.5}\right) + 24Sph\sqrt{\left(\frac{h_h^2}{3900^2} + \frac{h_v^2}{7.5^2}\right)}$$

which showed unsurprisingly that porosity is strongly anisotropic in the vertical versus the horizontal directions. This anisotropy has an important implication in the practical use of estimation on a grid and the choice of search radius. To force the search algorithm to 'find' more than the nearest well to the node being estimated, the search radius or window in the vertical direction must be much smaller than that horizontally. This makes sense, because we want the search to take place at least approximately along directions representing original bedding, if possible.

Because the typical oil or gas reservoir is structurally deformed, a process known as flattening must be applied before gridding. This procedure is usually accomplished by selecting a datum internal or external to the reservoir, and computing new elevation relative to this datum, the same as hanging a stratigraphic cross-section from a datum. Where chronostratigraphic units cross lithostratigraphic units, care must be taken in selecting a surface for this vertical adjustment (Bashore *et al.*, 1994). Because the data are approximately normal in distribution, data were not transformed in any way. A block 1 km by 1 km by 17 m was kriged and the results are displayed here as a map and two cross-sections (Figs 3.18–3.20). The map represents a slice 7.5 m from the base of the block, where porosity is relatively high. The two cross-sections show north–south and east–west slices through the block. This block is approximately in the middle of Granny Creek field.

3.4 SUMMARY

Linear estimation, or kriging, minimizes estimation variance by solving a set of kriging equations. These equations include covariances between

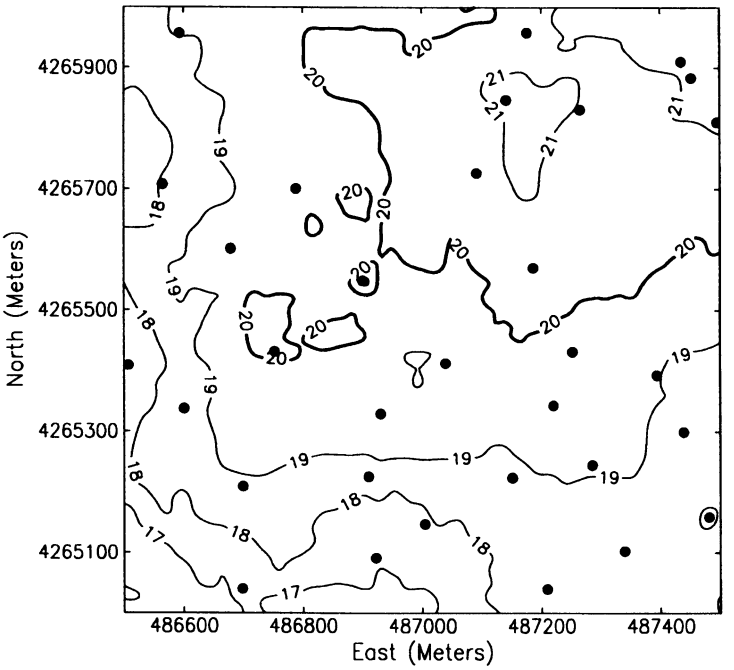

Figure 3.18 Map of three-dimensional model of porosity in Granny Creek oil field at an elevation of −257.5 m (see Figs 3.19 and 3.20). Filled circles show well locations. Units are per cent porosity. The contour interval is 1% porosity.

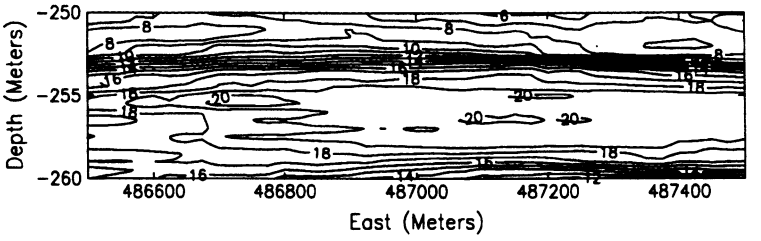

Figure 3.19 East–west cross-section through three-dimensional model of porosity in Granny Creek field at coordinate 4265500 North in Fig. 3.18. Units are per cent porosity. The contour interval is 1% porosity.

the point or volume to be estimated and the sample points and covariances between each pair of sample points. The weights calculated through solving the system of equations depend upon the size and shape of the volume to be estimated, the distance and direction of each sample from the volume to be estimated, the distance between samples, and the semivariogram.

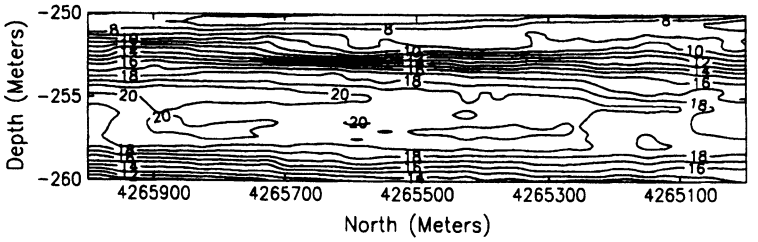

Figure 3.20 North–south cross-section through three-dimensional model of porosity in Granny Creek field at coordinate 487000 East in Fig. 3.18.

Kriging is an exact estimator in the sense that the estimate at a control point equals the observed value. Kriging also smoothes the data when the semivariogram includes a large nugget effect.

Validation procedures exist for the user to assess the quality of the kriged estimates. These 'leave one out' procedures have been used in the past in modeling semivariograms, but results can be misleading. Validation is more useful for viewing the effect of smoothing on the estimates.

Linear estimation in three dimensions usually requires that depths be adjusted relative to a datum so that the search parallels original bedding planes. The search radius for gridding must generally be much larger in the horizontal directions than the vertical.

REFERENCES

Bashore, W.M., Araktingi, U.G., Levy, M. and Schweller, W.J. (1994) Importance of geological framework and seismic data integration for reservoir modeling and subsequent fluid-flow predictions, in Yarus, J.M. and Chambers, R. (eds), *Stochastic Modeling and Geostatistics*. American Association of Petroleum Geologists, Tulsa, OK, pp. 159–175.

Clark, I. (1986) The art of cross validation in geostatistical applications. *Proceedings 19th APCOM*, pp. 211–220.

David M. (1977) *Geostatistical Ore Reserve Estimation*. Elsevier, New York, 364 pp.

Davis, B.M. (1987) Use and abuses of cross-validation in geostatistics. *Math. Geol.*, **19**, 241–248.

Gumati, Y.D. and Kanes, W.H. (1985) Early Tertiary Subsidence and Sedimentary Facies – Northern Sirte Basin, Libya. *Am. Assoc. Pet. Geol. Bull.*, **69**, 39–52.

Journel, A.G. and Huijbregts, C.J. (1978) *Mining Geostatistics*. Academic Press, London, 600 pp.

Parker, H.M., Journel, A.G. and Dixon, W.C. (1979) The use of the conditional lognormal probability distribution for the estimation of openpit ore reserves in stratabound uranium deposits – a case study. *Proceedings 16th APCOM*, pp. 133–148.

Rendu, J.M. (1979) Normal and lognormal estimation. *Math. Geol.*, **11**, 407–422.

Multivariate geostatistics

There are several situations where one may want to study and exploit the covariance between two or more regionalized variables.

1. The variable of interest is a linear combination of regionalized variables. Direct estimation of the linear combination is usually not optimal (Myers, 1983).
2. A variable is poorly sampled but correlates highly with a second variable that is much better sampled. One can take advantage of this correlation to improve estimation of the undersampled variable.
3. A variable exhibits low spatial autocorrelation, but correlates highly with one that exhibits relatively high continuity. Again, the observed values or the second variable may help to improve estimates of the first variable, particularly if the first one is undersampled.

The mutual spatial behavior of regionalized variables is called coregionalization. A number of methods exist for estimating a coregionalized variable from two or more variables, including cokriging, kriging with external drift, and collocated cokriging.

4.1 COREGIONALIZATION

Consider the two-variable case in which we want to estimate a value z^* from $z_1, z_2 \ldots z_n$, and there are also m observations of a second variable: $y_1, y_2 \ldots y_m$. Call this estimate z^*_{ck} to indicate that the estimate is to be computed through cokriging. The task at hand is to compute two sets of weights $\lambda_1, \lambda_2 \ldots \lambda_n$, and $\kappa_1, \kappa_2 \ldots \kappa_m$, which are used to compute the cokriging estimate:

$$z^*_{ck} = \sum_{i=1}^{n} \lambda_i z_i + \sum_{j=1}^{m} \kappa_j y_j$$

Cokriging makes use of the covariance between the main or primary variable z, and the secondary variable y. If the primary variable is seriously undersampled relative to y, the hope is that the secondary variable is sufficiently well sampled and covariance between the two

variables is high enough to improve the estimate of the primary variable. Put another way, the goal is to minimize the uncertainty in the estimate.

The following quantities are defined under second-order stationarity. For random functions $Z(x)$ and $Y(x)$, the second-order moments are the cross-covariance:

$$C_{ZY}(h) = E\{Z(x+h)Y(x)\} - m_Z m_Y$$

and the cross-variogram:

$$2\gamma ZY(h) = E\{[Z(x+h) - Z(x)]\ [Y(x+h) - Y(x)]\}$$

If $Z = Y$, these two expressions reduce to the ordinary covariance and variogram.

The cross-covariance is calculated from

$$C_{ZY}(h) = \tfrac{1}{n} \sum [z(x+h)\ y(x)] - m_z m_y$$

and the cross-semivariogram from

$$\gamma_{ZY}(h) = \tfrac{1}{2n} \sum [z(x_i+h) - z(x_i)]\ [y(x_i+h) - y(x_i)]\}$$

The cross-variogram and cross-covariance display some interesting properties. In contrast to a semivariogram, the cross-semivariogram can take on negative values. Such behavior is observed when two variables are negatively correlated. For instance, one would expect a negative cross-semivariogram between percentages of illite and quartz in a clastic unit.

The cross-semivariogram is equal when z and y are switched; the cross-covariance is not:

$$\gamma_{zy}(h) = \gamma_{yz}(h)$$

but

$$C_{zy}(h) = C_{yz}(-h)$$

Similarly, the following are true:

$$\gamma_{zy}(h) = \gamma_{zy}(-h)$$

and

$$C_{zy}(h) \neq C_{zy}(-h)$$

Cokriging uses matrices of cross-covariances. Strictly speaking, such matrices are not necessarily symmetric. However, cross-covariances are usually calculated from cross-semivariograms using the equation:

$$2\gamma_{zy}(h) = 2C_{zy}(0) - C_{zy}(h) - C_{yz}(h),$$

which simplifies to

$$\gamma_{zy}(h) = C_{zy}(0) - C_{zy}(h)$$

if we assume $C_{zy}(h) = C_{yz}(h)$, which is usually reasonable.

4.2 COKRIGING EQUATIONS

The cokriging system of equations is fairly simple, and resembles that for kriging:

$$\sum_{i=1}^{n} \lambda_i \bar{C}(v_i,v_j) + \sum_{i=1}^{m} \kappa_i \bar{C}(u_i,v_j) + \mu_1 = \bar{C}(V,v_j) \qquad \text{for } j = 1, n$$

$$\sum_{i=1}^{n} \lambda_i \bar{C}(v_i,u_j) + \sum_{i=1}^{m} \kappa_i \bar{C}(u_i,u_j) + \mu_2 = \bar{C}(V,u_j) \qquad \text{for } j = 1, m$$

$$\sum_{i=1}^{n} \lambda_i = 1$$

$$\sum_{i=1}^{m} \kappa_i = 0$$

There are two unbias conditions, for a total of n + m + 2 equations.

The following equation gives the estimation variance:

$$\sigma_{ck}^2 = \bar{C}(V,V) + \mu_1 - \sum_{i=1}^{n} \lambda_i \bar{C}(v_i,V) - \sum_{i=1}^{m} \kappa_i \bar{C}(u_i,V)$$

All of the cautions relating to interpretation and use of estimation variance from kriging also hold in the case of cokriging. However, estimation variance as an index of uncertainty is useful for gauging the relative effectiveness of cokriging in reducing uncertainty.

As stated earlier, cokriging is generally used for estimating a variable that is sampled sparsely in comparison to a secondary variable with which it is correlated. At least one observation of the primary variable *must* be included in the cokriging system of equations.

Interested readers might want to consult the papers by Myers (1982, 1983) for a general statement of cokriging in matrix form. He considers the case where more than two variables are to be mapped, and no clear distinction exists between primary and secondary variables. This might be the case in which one variable was observed in one set of wells, and a second variable in a different set of wells. In some areas, one or another variable is undersampled.

4.3 MODELING A COREGIONALIZATION

Continuing with the most common case of a primary variable and one secondary variable, the first step in cokriging is computing and modeling a semivariogram for each variable. In addition, the cross-semivariogram must be calculated and modeled. If more than one secondary variable is

to be included, a cross-semivariogram must be computed for each pair of variables, including the primary variable. If the total number of primary and secondary variables equals n, there will be $n(n+1)/2$ semivariograms and cross-semivariograms to examine. This can become a lot of work, and is thought to be the major drawback to cokriging by many workers.

Consider also that for the set of semivariograms and cross-semivariograms to be positive definite, the following relationship must hold for any variable j and k:

$$|\gamma_{jk}(h)| \leq \sqrt{(\gamma_j(h)\,\gamma_k(h))}$$

This is most easily accomplished by using the linear model of coregionalization with positive definite coefficients. In words, this approach uses the same nested model for all semivariograms and cross-semivariograms, differing only in the coefficients. For the two-variable case with three nested structures, the models are:

$$\gamma_z(h) = a_1\gamma_1(h) + a_2\gamma_2(h) + a_3\gamma_3(h)$$
$$\gamma_y(h) = b_1\gamma_1(h) + b_2\gamma_2(h) + b_3\gamma_3(h)$$
$$\gamma_{zy}(h) = c_1\gamma_1(h) + c_2\gamma_2(h) + c_3\gamma_3(h)$$

For this model to be positive definite, the following must be true for every i:

$$a_i > 0$$
$$b_i > 0$$
$$|c_i| < \sqrt{(a_i b_i)}$$

Fitting these models can be tedious, but a few rules of thumb are important and help in the modeling.

First, include only variables that are clearly correlated with the primary variable as determined from scattergrams or correlation coefficient.

Second, do not overfit the semivariograms or cross-semivariograms. Here is one place to remember that accurate models are needed only up to the search radius to be employed. Also, screening effects limit the need to find accurate semivariograms beyond typical well-spacing distances. This is particularly true for the secondary variables, for which sampling is the most dense. For most applications, a simple model with nugget effect is probably sufficient. Three-dimensional data probably require more complex models.

Start with fitting the semivariograms and then do the cross-semivariograms. Or, if you start with cross-semivariograms, work in an organized and consistent fashion, checking for positive definiteness as you go. The requirements for positive definiteness mean that any cross-semivariogram model must also appear in the semivariogram, but not all semivariogram models must have non-zero coefficients for all cross-semivariograms.

4.4 A SIMPLE EXAMPLE

A set of artificial data was constructed to illustrate the undersampled case and to suggest when cokriging has some advantage over ordinary kriging of one variable. Two regionalized variables are sampled on a regular grid (Fig. 4.1); one variable has been sampled at every node on the grid, whereas the second was sampled at only 11 nodes. Estimates are to be calculated at the center of each cell. From the configuration of samples, one can see that some cells should yield good estimates for each variable, whereas others should yield relatively high estimation variances for the undersampled variable.

The following semivariogram models were assumed for the two variables. The fully sampled variable has a nugget effect of zero, sill of 1.8, and range of a spherical model equal to two units; the undersampled variable has the same model with a sill of 1.1; and the cross-semivariogram has a nugget effect of zero, a sill of 1.4, and a range of two units. This cross-semivariogram model has the highest value of the sill that satisfies the requirement for positive definiteness.

The advantage of cokriging over kriging and the effect of semivariogram models on the results are examined through comparison of estimation variances. One must use estimation variance as an absolute measure of error with caution. Kriging variance can represent little more than an index of sample configuration. However, using estimation variance for the purpose of comparison is appropriate.

Estimation variances were calculated for the undersampled variable through kriging (Fig. 4.2) alone and cokriging (Fig. 4.3). In well-sampled cells, such as that in the extreme lower left, the reduction in estimation

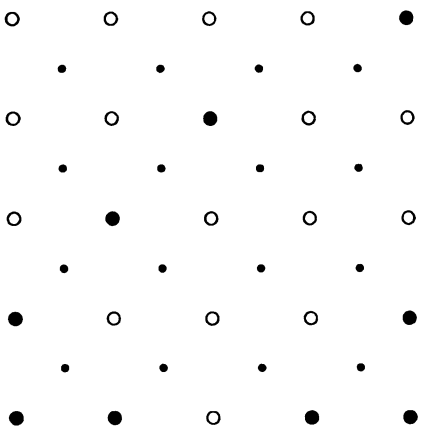

Figure 4.1 Sample locations for two regionalized variables; grid nodes have been sampled for one (open circles) or both variables (large closed circles). Small closed circles show locations where estimates are calculated.

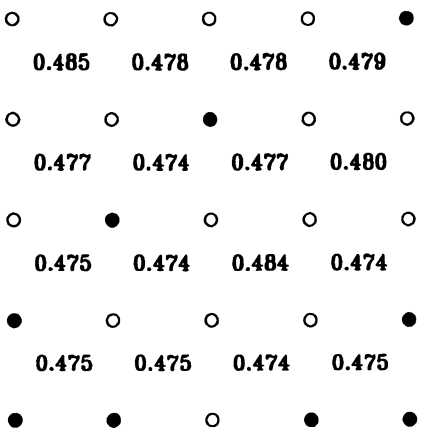

Figure 4.2 Estimation variance of the undersampled variable obtained by cokriging with a relatively large cross-covariance.

variance from 0.560 to 0.475 is small. In contrast, the upper left-hand cell shows a reduction from 1.223 obtained by ordinary kriging, to 0.485 by cokriging. In general, the effect of cokriging is to reduce all the estimation variances to a relatively small value averaging 0.48.

With such a high cross-covariance between the variables, the secondary variable can be virtually substituted for the first. When cross-covariance equals zero, cokriging gives the same results as kriging. Most real-world cases are somewhere between these two extremes.

Consider now the case when the cross-semivariogram has a sill of 0.55 and semivariograms remain unchanged. The gain in cokriging is now

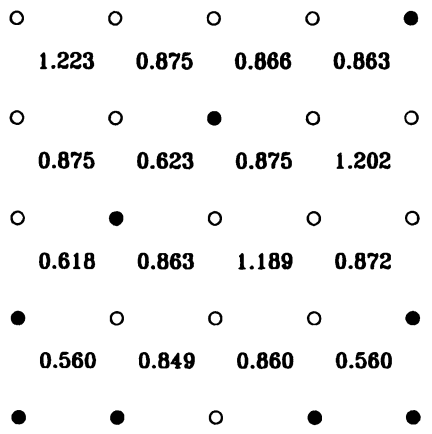

Figure 4.3 Estimation variances obtained by kriging the undersampled variable.

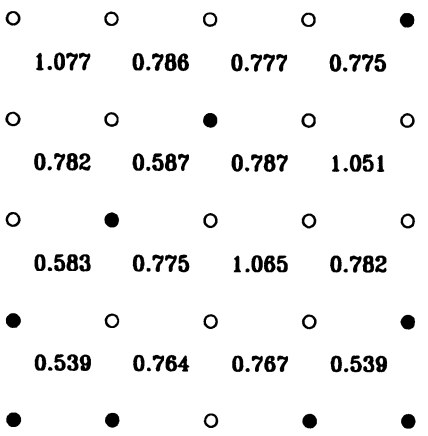

Figure 4.4 Estimation variances obtained by cokriging in the presence of low cross-covariance between an undersampled variable and a secondary variable.

much reduced, reflecting lower cross-covariance between the two variables (Fig. 4.4). Indeed, one might decide in such a case that the work required in cokriging does not warrant the expected improvement in the estimates.

Cokriging equations in matrix form are illustrated for the configuration of three points that includes two fully sampled locations and one undersampled location (Fig. 4.5). An estimate is to be calculated for the point labeled V. Assume a model of coregionalization used earlier: sills of 1.1, 1.8, and 0.55 for the undersampled variable, fully sampled variable, and the cross-semivariogram, respectively; ranges of two units; and no nugget effects.

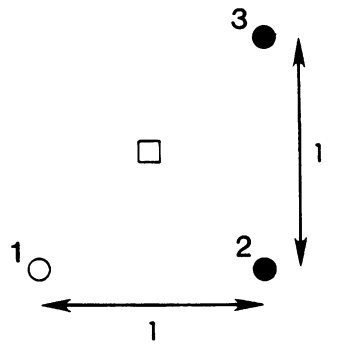

Figure 4.5 Simple configuration of two fully sampled locations (closed circles); an undersampled location (open circle); and a site for estimation (square).

The cokriging equations for the problem in Fig. 4.5 are:

$$\begin{bmatrix} \bar{C}(v_2,v_2) & \bar{C}(v_3,v_2) & \bar{C}(u_1,v_2) & \bar{C}(u_2,v_2) & \bar{C}(u_3,v_2) & 1 & 0 \\ \bar{C}(v_2,v_3) & \bar{C}(v_3,v_3) & \bar{C}(u_1,v_3) & \bar{C}(u_2,v_3) & \bar{C}(u_3,v_3) & 1 & 0 \\ \bar{C}(v_2,u_1) & \bar{C}(v_3,u_1) & \bar{C}(u_1,u_1) & \bar{C}(u_2,u_1) & \bar{C}(u_3,u_1) & 0 & 1 \\ \bar{C}(v_2,u_2) & \bar{C}(v_3,u_2) & \bar{C}(u_1,u_2) & \bar{C}(u_2,u_2) & \bar{C}(u_3,u_2) & 0 & 1 \\ \bar{C}(v_2,u_3) & \bar{C}(v_3,u_3) & \bar{C}(u_1,u_3) & \bar{C}(u_2,u_3) & \bar{C}(u_3,u_3) & 0 & 1 \\ 1 & 1 & 0 & 0 & 0 & 0 & 0 \\ 0 & 0 & 1 & 1 & 1 & 0 & 0 \end{bmatrix} \begin{bmatrix} \lambda_1 \\ \lambda_2 \\ \kappa_1 \\ \kappa_2 \\ \kappa_3 \\ \mu_1 \\ \mu_2 \end{bmatrix} = \begin{bmatrix} \bar{C}(V,v_2) \\ \bar{C}(V,v_3) \\ \bar{C}(V,u_1) \\ \bar{C}(V,u_2) \\ \bar{C}(V,u_3) \\ 1 \\ 0 \end{bmatrix}$$

Plugging in values gives:

$$\begin{bmatrix} 1.1000 & 0.3437 & 0.1719 & 0.5500 & 0.1719 & 1 & 0 \\ 0.3437 & 1.1000 & 0.0639 & 0.1719 & 0.5500 & 1 & 0 \\ 0.1719 & 0.0639 & 1.8000 & 0.5625 & 0.2090 & 0 & 1 \\ 0.5500 & 0.1719 & 0.5625 & 1.8000 & 0.5625 & 0 & 1 \\ 0.1719 & 0.5500 & 0.2090 & 0.5625 & 1.8000 & 0 & 1 \\ 1 & 1 & 0 & 0 & 0 & 0 & 0 \\ 0 & 0 & 1 & 1 & 1 & 0 & 0 \end{bmatrix} \begin{bmatrix} \lambda_1 \\ \lambda_2 \\ \kappa_1 \\ \kappa_2 \\ \kappa_3 \\ \mu_1 \\ \mu_2 \end{bmatrix} = \begin{bmatrix} 0.5409 \\ 0.5409 \\ 0.2705 \\ 0.2705 \\ 0.2705 \\ 1 \\ 0 \end{bmatrix}$$

and the solution is:

$$\begin{bmatrix} \lambda_1 \\ \lambda_2 \\ \kappa_1 \\ \kappa_2 \\ \kappa_3 \\ \mu_1 \\ \mu_2 \end{bmatrix} = \begin{bmatrix} 0.500 \\ 0.500 \\ 0.113 \\ -0.072 \\ -0.040 \\ -0.139 \\ -0.001 \end{bmatrix}$$

4.5 INITIAL POTENTIALS AND CUMULATIVE PRODUCTION

Initial potentials and ten-year cumulative production figures have been made available for about 452 wells producing gas from Devonian shales in an area covering four 7.5-min quadrangles in southwestern West Virginia (Columbia Gas System Service Corp., 1985).

In contrast to most of the data used in this book, these data are not taken from public records. The company providing this information was responsible for drilling, completing, and producing gas from these wells, in addition to using the data for mapping. Although some wells were shot or hydraulically fractured and other wells completed naturally, two sources of variation – company and reporting practice – have been eliminated, giving an above-average set of data.

Both initial potential and cumulative production of gas after ten years were available for 377 wells; initial potential was available for an additional 75 wells. Over most of a four-quadrangle study area, well control is sufficient for mapping cumulative production without the aid of initial potentials. In some areas, wells were drilled almost exclusively by other companies, and so cumulative production figures were not available. Cokriging improves estimates of cumulative production across these areas.

Using initial potential to estimate cumulative production conforms to the common practice of using initial potentials to informally predict gas production. Cokriging makes the procedure more explicit and objective and exploits the positive correlation between these two variables (Fig. 4.6).

Semivariograms and the cross-semivariogram were fitted with a spherical model having a range of 1.5 km and no nugget effect (Figs 4.7–4.9). Constants for the spherical models are:

Cumulative production:	20 000
Initial potential:	175 000
Cross-semivariogram:	27 000

A 36-km^2 area was chosen for evaluating use of cokriging cumulative production (Fig. 4.10). Within this area, wells represented only by initial potentials lie in a northwest–southeast band. Estimates of cumulative production were calculated through both ordinary kriging and cokriging at a 0.1-km spacing, and then contoured.

Estimation variance for kriged cumulative production (Fig. 4.11) reflects the poor well control over much of the area mapped. More than half has variances exceeding 20 000 Mmcf^2. Estimation variances for cumulative production obtained through cokriging exceed 20 000 Mmcf^2

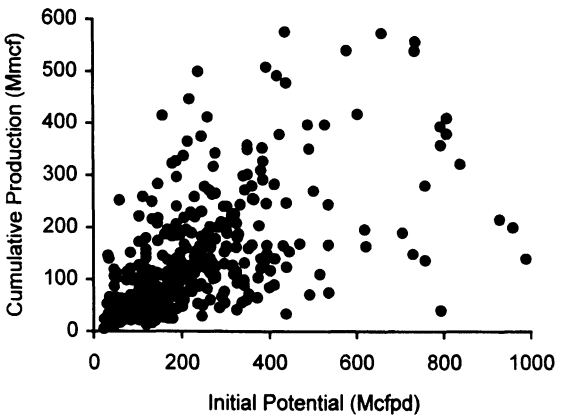

Figure 4.6 Scattergram of initial potential and cumulative production of gas.

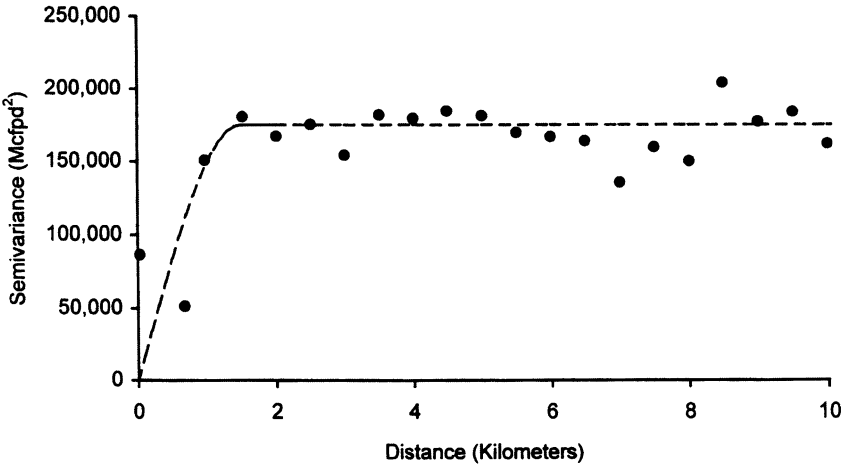

Figure 4.7 Semivariogram of initial potential of gas.

over less area (Fig. 4.12), but the improvement appears small. Within the area of good well control, there is no improvement.

Maps of cumulative production after kriging (Fig. 4.13) and cokriging (Fig. 4.14) are nearly identical in the southwest corner, where control for both variables is good. As expected, the maps differ most in areas of poor control on cumulative production. The map of kriged estimates shows numerous artifacts of the estimation and contouring, caused by the short range in the semivariogram, and the lack of wells. Adding several wells in the north-central part of the area improves the estimates, but leaves some artifacts where control remains poor.

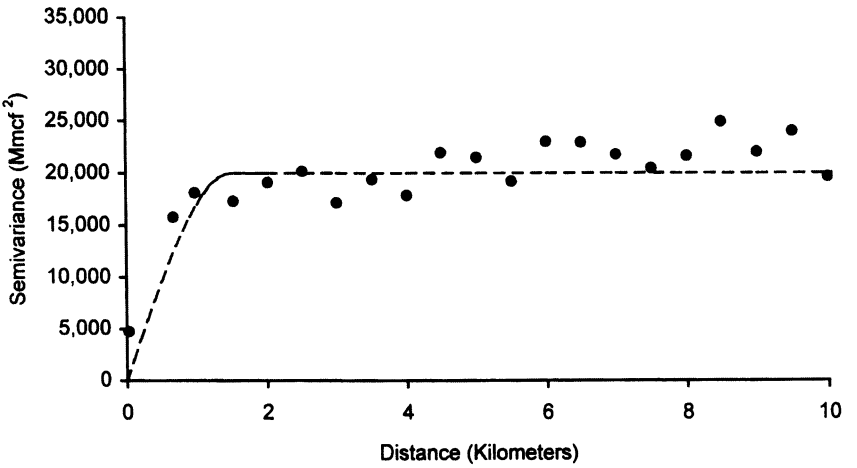

Figure 4.8 Semivariogram of cumulative production of gas.

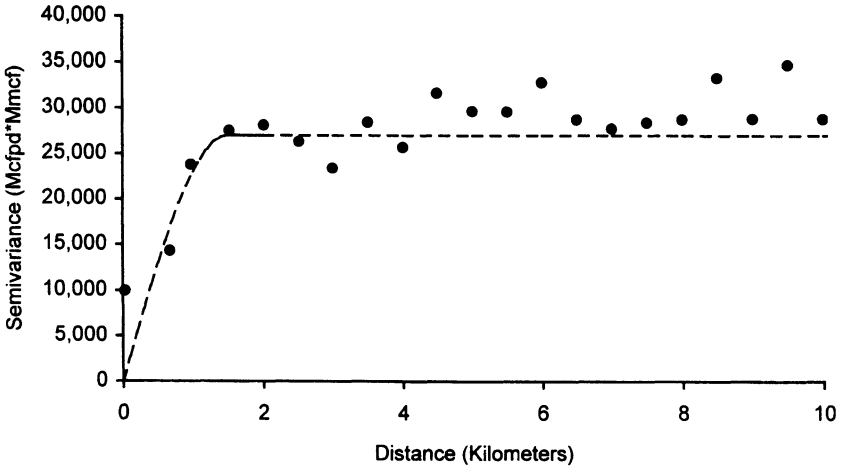

Figure 4.9 Cross-semivariogram of initial potential and cumulative production.

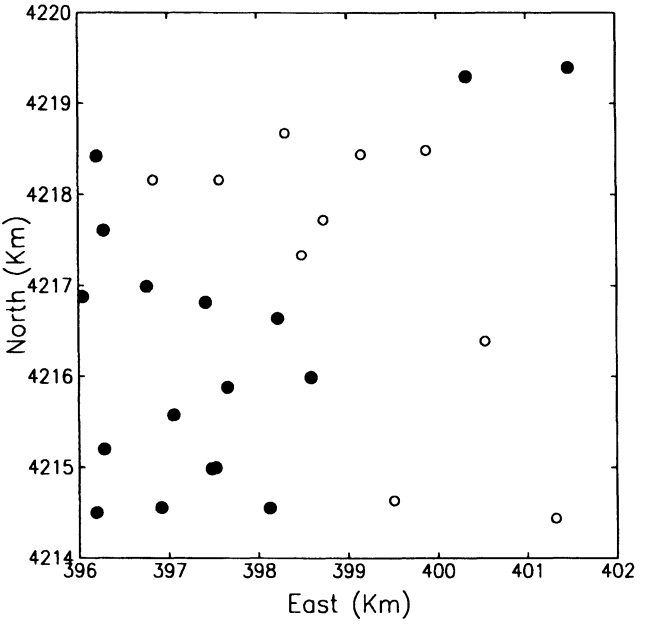

Figure 4.10 Locations of control wells used in cokriging cumulative production. Initial potentials were available for all wells, cumulative production for wells represented by open circles.

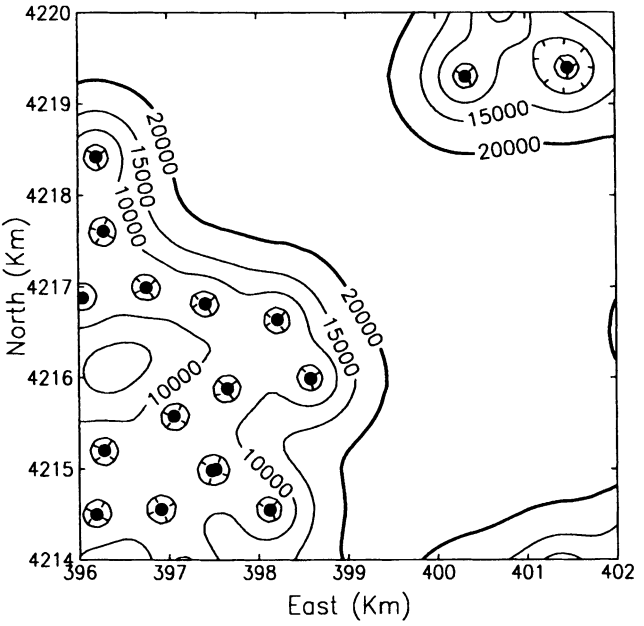

Figure 4.11 Contoured estimation variances for kriged estimates of cumulative production. Contour interval is 5000 $Mmcf^2$.

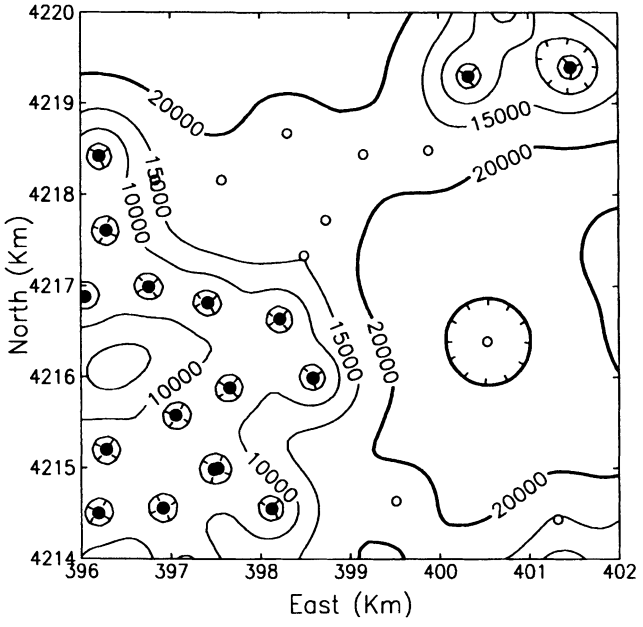

Figure 4.12 Contoured estimation variances for cokriged estimates of cumulative production. Contour interval is 5000 $Mmcf^2$.

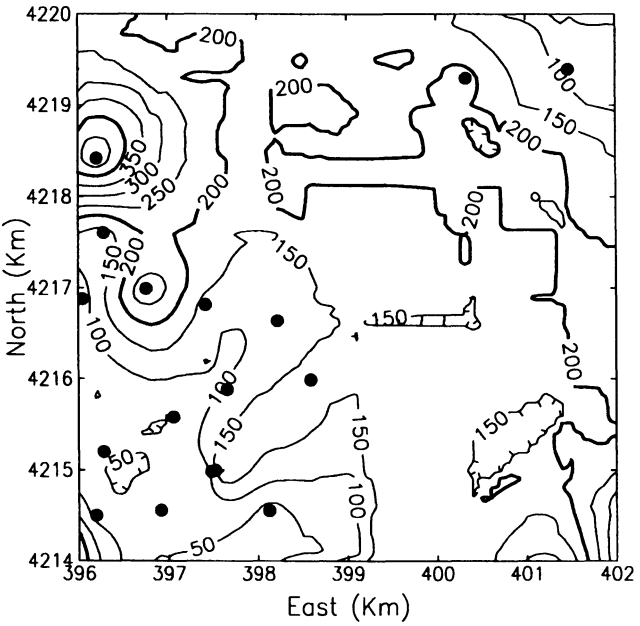

Figure 4.13 Kriged estimates of gas cumulative production. The contour interval is 50 Mmcf.

4.6 A STRATIGRAPHIC APPLICATION

When drawing a structure contour map, the geologist may not have good control in some areas because the datum is hard to pick from logs or because the rock unit lies deeper than most wells. A shallower horizon may be much better sampled because of its distinctive lithology or because it is an important target for drilling. The geologist can use elevations of the shallower unit if the interval between the two horizons is thought to be roughly constant. Such a procedure can be formalized through cokriging.

The top of the Upper Devonian shales in much of West Virginia can be found easily on drillers' lithologic logs because of the presence of the overlying Berea Sandstone. In areas where the Berea is absent, wire-line logs are generally necessary to accurately pick the top of the shales.

The Greenbrier Limestone is a distinctive formation that occurs a variable distance above the Devonian shales in much of West Virginia. In the central part of West Virginia, the Greenbrier is about 2200 ft above the top of the shales. Despite this thick interval of intervening rock, elevation of these two formation tops are statistically correlated (Fig. 4.15). Data used in this example comprise of 2335 tops of the Greenbrier Limestone, and 206 tops of the Devonian shales.

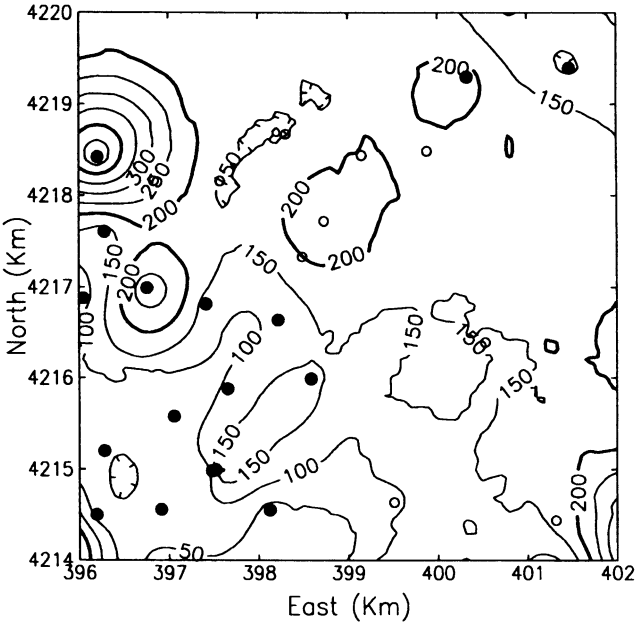

Figure 4.14 Contoured estimates of gas cumulative production calculated through cokriging. Contour interval is 50 Mmcf.

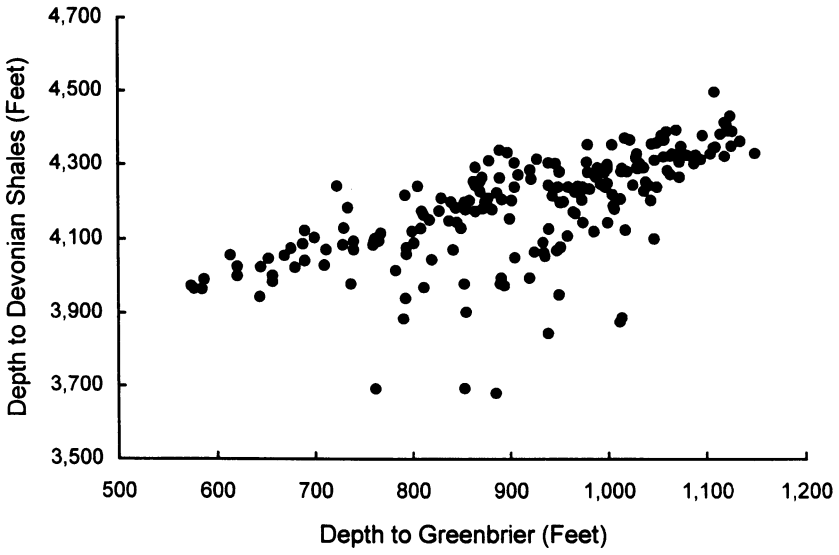

Figure 4.15 Scattergram of the subsea top of the Greenbrier Formation versus top of the Devonian shales in Doddridge County, West Virginia.

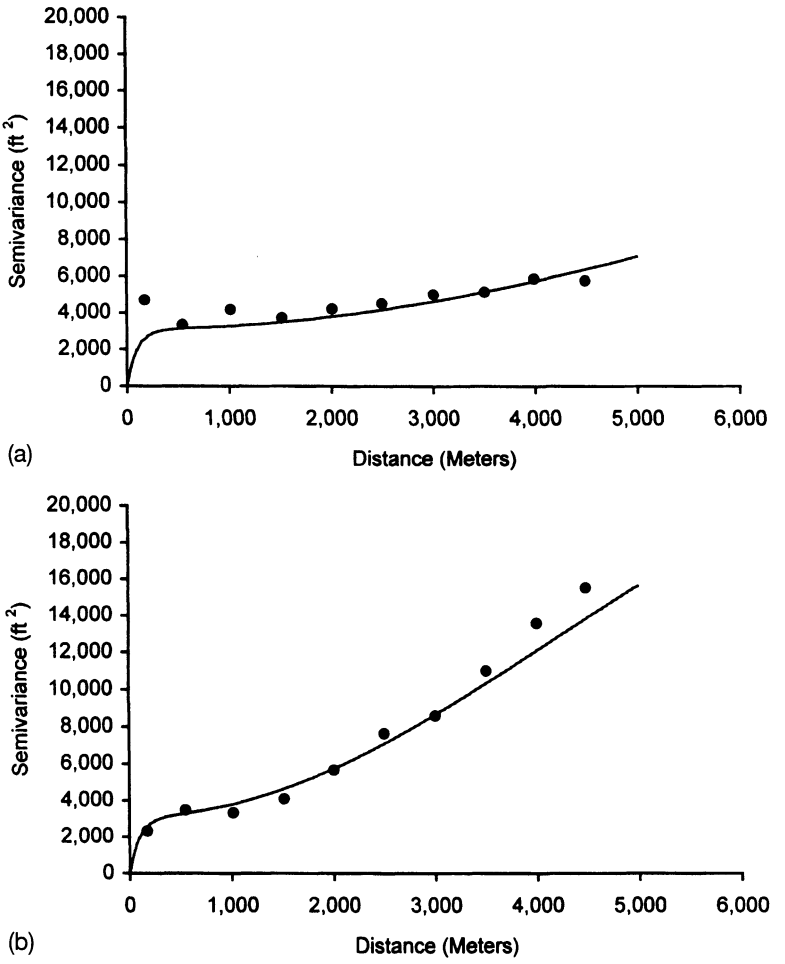

Figure 4.16 Directional semivariograms of subsea elevation of the top of the Greenbrier Formation. Directions are: (a) N 30 deg East; and (b) N 120 deg East.

Wells used in this example are situated in an area of broad folds oriented northeast–southwest. Consequently, directional semivariograms for the top of the Greenbrier Limestone show definite anisotropy, with the major direction equal to N30°E (Fig. 4.16). The large number of data available results in a relatively smooth semivariogram. Directional semivariograms for the top of the Devonian shales are more erratic because of the relatively small number of data (Fig. 4.17). Cross-semivariograms are intermediate in appearance (Fig. 4.18). The semivariogram for the top of the Greenbrier Limestone was modeled first in order to provide some guidance in modeling the other semivariograms.

After a lot of experimentation and iteration, the linear model of coregionalization decided upon includes two terms: an isotropic exponential model with a range of 100 m, and an anisotropic Gaussian model with a range of 12 000 m along the major axis of N30°E, and 6000 m along the minor direction. Let $\gamma_1(\mathbf{h})$ stand for the exponential model, $\gamma_2(\mathbf{h})$ stand for the Gaussian model, $\gamma_D(\mathbf{h})$ the model for the top of the shales, $\gamma_G(\mathbf{h})$ the model for the Greenbrier Limestone, and $\gamma_{DG}(\mathbf{h})$ the cross-semivariogram. The complete models are:

$$\gamma_D(\mathbf{h}) = 2{,}500\gamma_1(\mathbf{h}) + 300{,}000\gamma_2(\mathbf{h})$$
$$\gamma_G(\mathbf{h}) = 3{,}100\gamma_1(\mathbf{h}) + 25{,}000\gamma_2(\mathbf{h})$$
$$\gamma_{DG}(\mathbf{h}) = 500\gamma_1(\mathbf{h}) + 80{,}000\gamma_2(\mathbf{h})$$

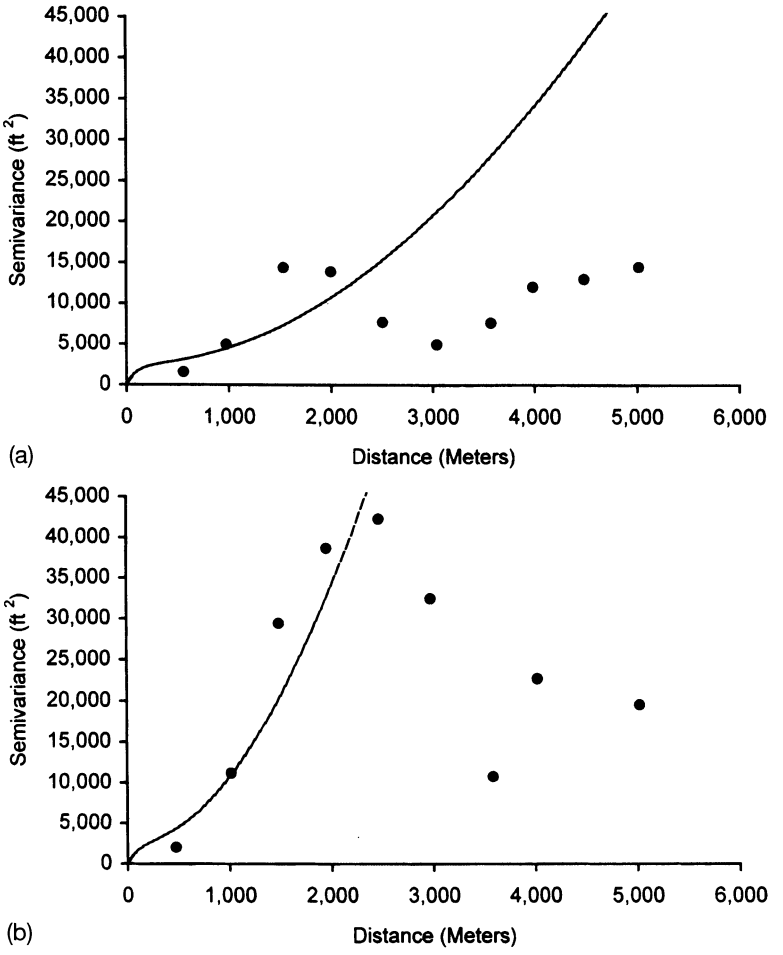

Figure 4.17 Directional semivariograms of subsea elevation of the top of the Devonian shales. Directions are: (a) N 30 deg East; and (b) N 120 deg East.

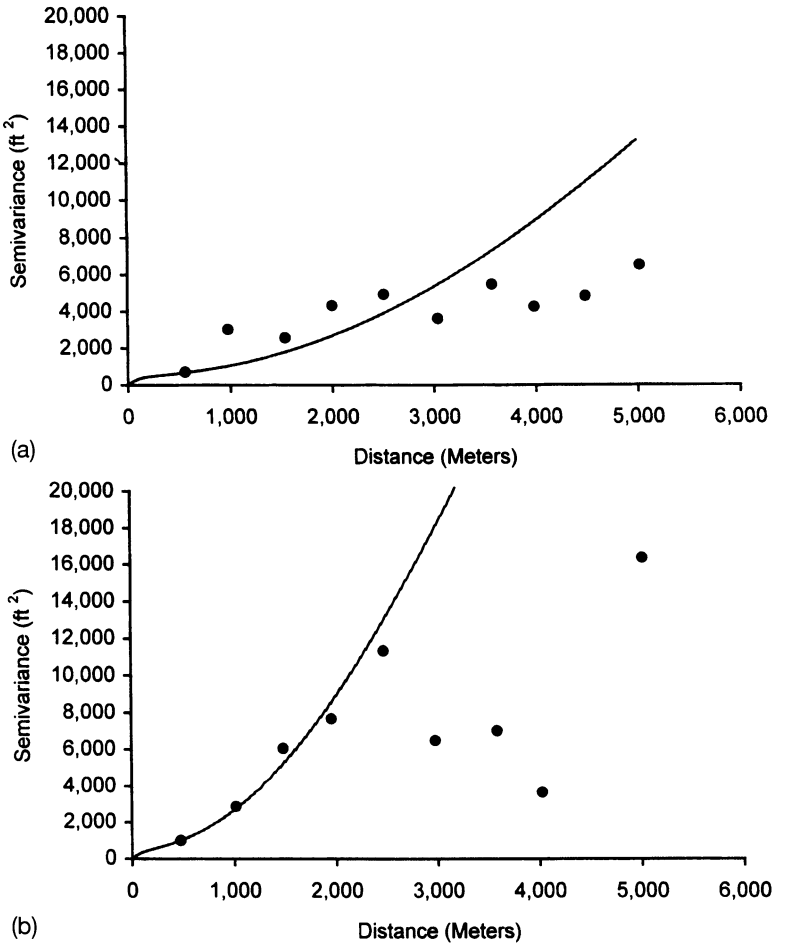

Figure 4.18 Directional cross-semivariograms between elevation of the top of the Greenbrier Formation and elevation of the top of the Devonian shales. Directions are: (a) N 30 deg East; and (b) N 120 deg East.

For an area 10 km by 10 km, subsea tops of the Devonian shale and the Greenbrier Limestone were estimated through kriging, and the top of the shales through cokriging. The Devonian shale top (Fig. 4.19) shows a broad syncline running from the northeast corner to roughly the southwest corner of the map of kriged estimates. Well control in the western part of the area mapped is relatively poor.

The kriged estimates of the top of the Greenbrier Limestone (Fig. 4.20) shows the same synclinal structure and a much better well control. A number of targeted gas reservoirs lie between the two formation tops

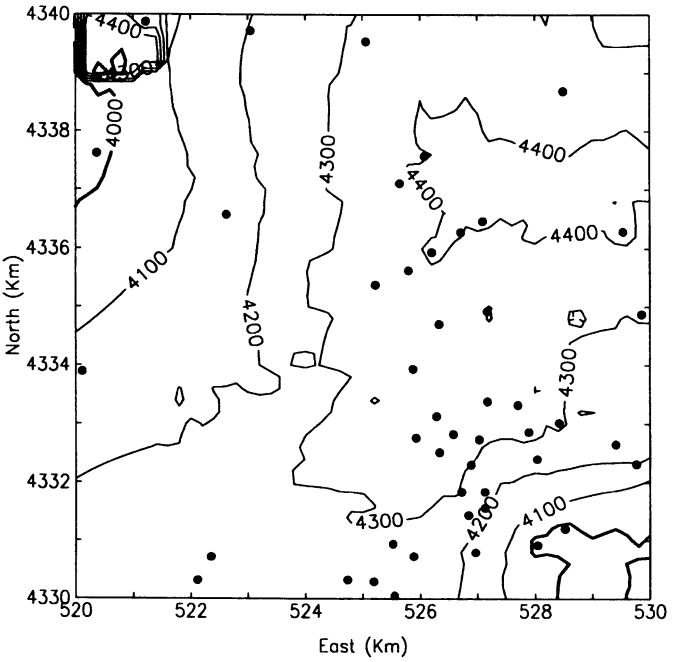

Figure 4.19 Contour map of elevation of the top of the Devonian shales calculated through ordinary kriging. Well locations are shown as closed circles. Contour interval is 100 ft.

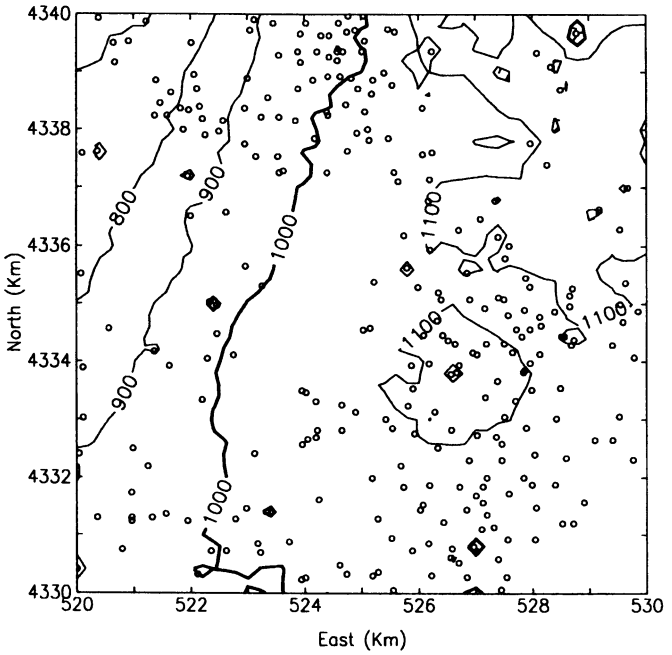

Figure 4.20 Contour map of elevation of the top of the Greenbrier Limestone calculated through ordinary kriging. Well locations are indicated by the open circles. Contour interval is 100 ft.

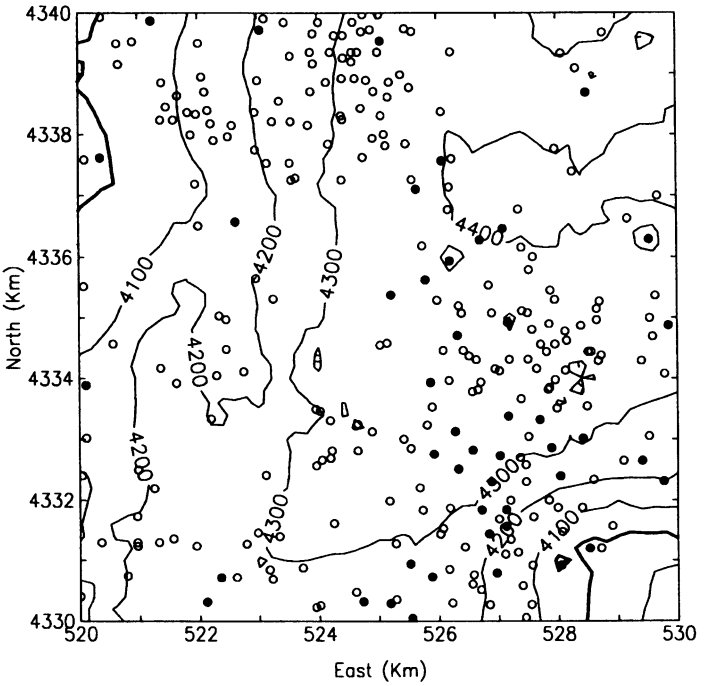

Figure 4.21 Contour map of elevation of the top of the Devonian shales calculated through cokriging. The top of the shales is known at locations indicated by a closed circle. The top of the Greenbrier Limestone was observed at all well locations posted. Contour interval is 100 ft.

considered here, and therefore many wells do not go as deep as the shales.

The map of estimates from cokriging (Fig. 4.21) exhibits the same fundamental structure as the kriged estimates, but the syncline appears to be better defined in the south-central part of the map. Look at the 4300 ft contour line; it is blunt and ragged on the map of kriged estimates. Cokriging appears to have eliminated an edge effect in the northwestern corner of the map of kriged estimates. Although estimation included wells outside of the area mapped, an area of sparse data in the primary variable remained directly to the west of this corner.

A peculiar north–south structure lies in the western part of Fig. 4.21 which one would probably investigate further before accepting.

4.7 KRIGING WITH EXTERNAL DRIFT

Picture the case in which the secondary variable is known everywhere in the study area, such as the travel time to a horizon in seismic data. Hence, we know the value of this variable at every node on an arbitrary

grid, as well as at locations where the primary variable was measured. The primary variable in our example is depth to the same horizon; because these depths are observed directly in wells only, we want to use the complete coverage provided by the seismic data to supplement our measured depths during estimation.

Kriging with external drift is a linear estimator like all we have looked at so far (Galli and Meunier, 1987):

$$z_{kt}^{*} = \sum_{i=1}^{n} \lambda_i z_i$$

The divergence from ordinary kriging comes in the system of equations:

$$\sum_{j=1}^{n} \lambda_j \bar{C}(v_i,v_j) + \mu_1 + \mu_2 y(v_i) = \bar{C}(v_i,V) \qquad \text{for all } i = 1,n$$

$$\sum_{j=1}^{n} \lambda_j = 1$$

$$\sum_{j=1}^{n} \lambda_j y(v_j) = y(V)$$

Notice that there is only one set of weights; the secondary variable is not used in estimation directly, but rather shows up in one of the constraints. This system of equations is a special case of methods such as **universal kriging** that attempt to account for trend in the data through polynomials.

The external drift method requires two sets of data. The first is the value of both the primary and secondary variables at each well location. The second is a grid of values of the secondary variable which matches the locations at which the primary variable is to be estimated. The user must also provide a semivariogram for the primary variable. This method requires neither a semivariogram for the secondary variable, nor a cross-semivariogram.

The following example of kriging with external drift uses seismic and well data to estimate porosity in a siltstone reservoir within the west Texas Permian basin. The data were studied previously by Chambers *et al.* (1994), and were provided by the senior author of that paper.

The goal is to estimate average porosity in a siltstone over an area of 10 000 by 10 000 ft. Porosity was observed in 55 wells. Chambers *et al.* (1994) describe acquisition and scaling of the acoustic impedance data between -1 and 0. The complete data set was sampled to give an 86 by 86 node grid for estimation of porosity using acoustic impedance as an external drift.

The 55 values of porosity are barely enough to yield a variogram (Fig. 4.22), to which a spherical model was fitted with a range of 3 000 ft, and sill of $2\%^2$. Kriged estimates of porosity from the well data show broad

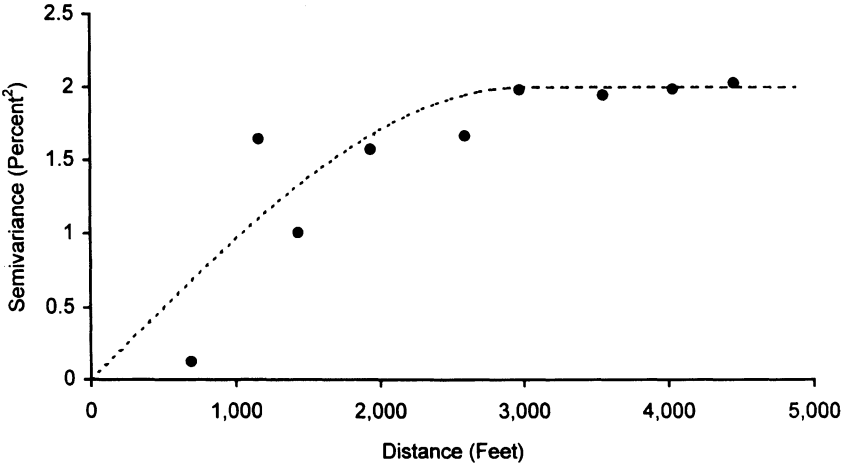

Figure 4.22 Semivariogram of average porosity measured in 55 wells from a clastic reservoir in the West Texas basin.

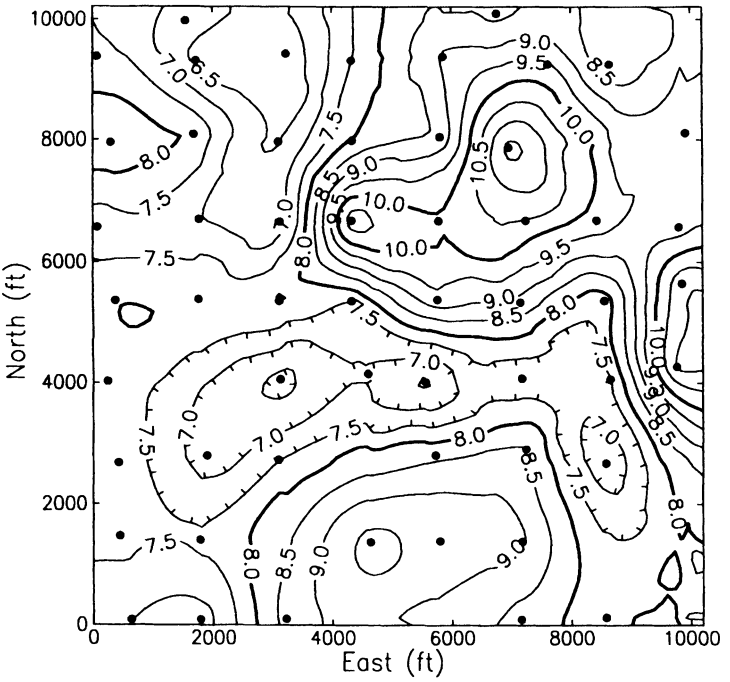

Figure 4.23 Kriged estimates of percent porosity. Well locations are shown as filled circles. Contour interval is 0.5%.

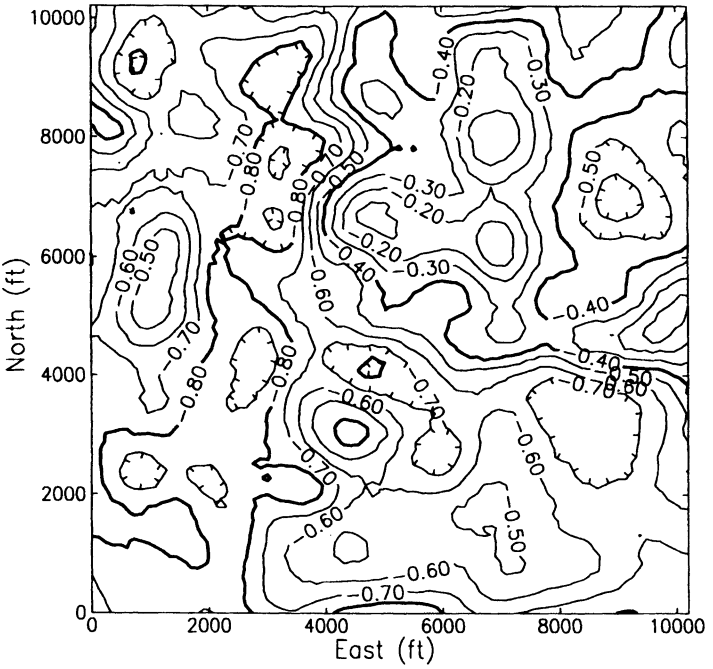

Figure 4.24 Contoured grid of scaled acoustic impedance values.

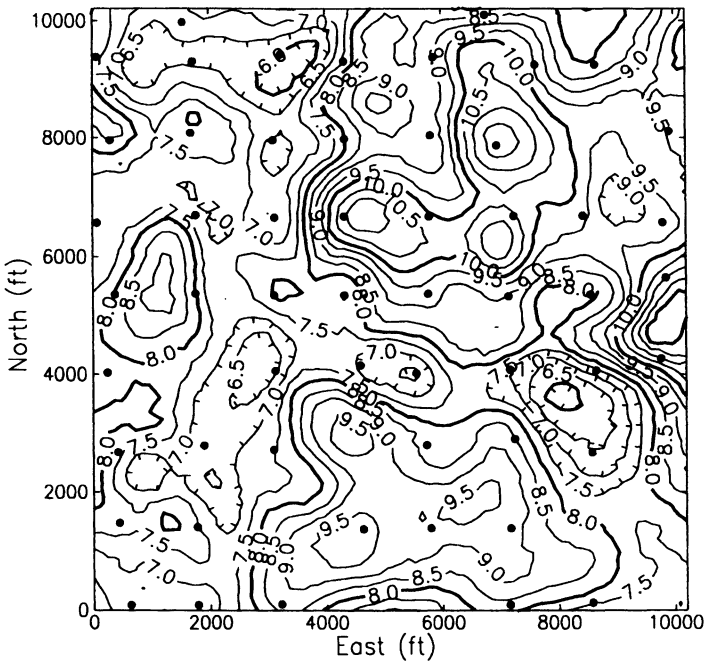

Figure 4.25 Contoured estimates of porosity calculated through kriging with external drift, with acoustic impedance as the drift variable. Contour interval is 0.5%.

trends such as the high values in the northeast corner of the area mapped, and an east–west low in the center of the map (Fig. 4.23). The map of acoustic impedance (Fig. 4.24) was drawn directly from the grid of values provided, and suggests some detail on a scale smaller than that of the well spacing.

The contour map of porosity estimated by the external drift method (Fig. 4.25) uses the same contour interval as the map of kriged estimates. Kriging with external drift has added some complexity, local trends follow those in acoustic impedance in many places, and porosity is less smoothed. The histogram of estimated values of porosity by ordinary kriging looks very similar to that for porosity calculated with the help of

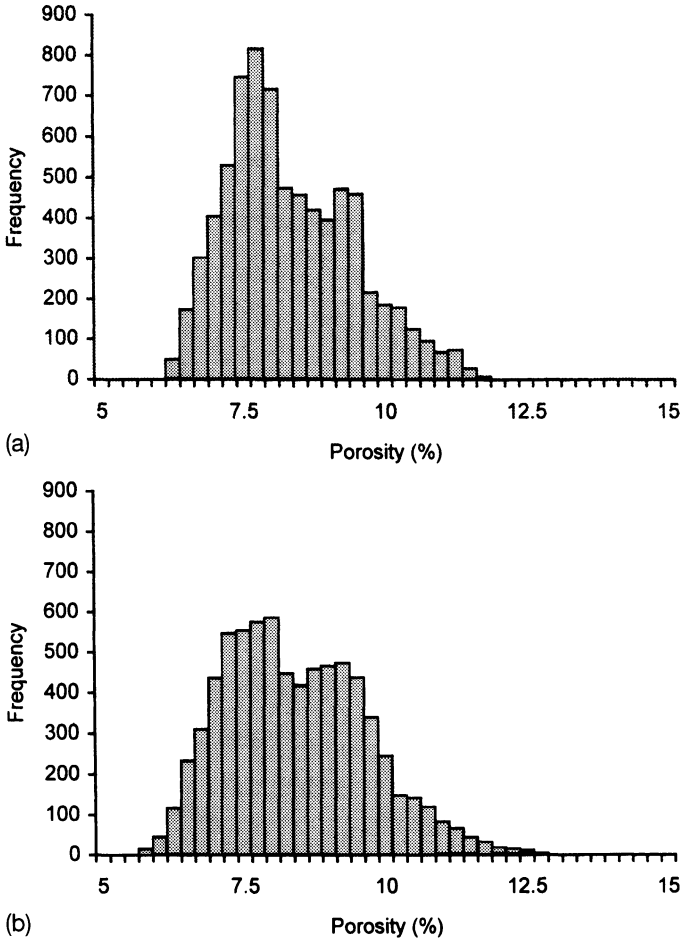

Figure 4.26 Histograms of gridded values of porosity calculated by (a) ordinary kriging, and (b) kriging with external drift.

the seismic data, but note that the latter histogram is heavier in the tails (Fig. 4.26).

4.8 COLLOCATED COKRIGING

It should be obvious that standard cokriging can be used for improving well data such as porosity with seismic information. The fact that seismic data are sampled densely in comparison with well data, combined with the screening effect of kriging, means that few values of the secondary data need to be used in the cokriging equations. Only the value of the secondary variable closest to the grid node being estimated receives very much weight. If the grid for estimation corresponds to that on which the secondary variable is sampled, the grid nodes are collocated.

This observation means that the cokriging equations can be significantly simplified by including neighboring values of the primary variable, and only one collocated value of the secondary variable. A further simplification for the practitioner is possible when the cross-covariance between the two variables is equal to the product of the covariance for the primary variable and the correlation coefficient between the primary and secondary variables, scaled by the variance of the two variables:

$$C_{ZY}(h) = \sqrt{\left(\frac{C_Y(0)}{C_Z(0)} \rho_{ZY} C_Z(h) \right)}$$

where $C_Y(0)$ and $C_Z(0)$ are variances, and ρ_{ZY} is the correlation coefficient. Hence, only the semivariogram for the primary variable needs to be modeled; the cross-semivariogram is obtained through this equation. The practitioner should check that the resulting cross-semivariogram model adequately fits observed values. **Collocated cokriging** is described by Xu *et al.*(1992); and an example appears in Chu *et al.* (1994) and Bashore *et al.* (1994).

One advantage of collocated cokriging over a full cokriging is that seismic data can display a high degree of continuity. As a result, cokriging equations are approximately singular and become unstable. Utilizing only a collocated value of the secondary variable avoids this problem.

4.9 DIFFICULTIES AND SOLUTIONS

4.9.1 Noncoincident well locations

Primary and secondary variables may be sampled at a different network of sites. This can happen when a set of data is constructed from multiple

samplings. Take, for example, the case in which porosity is available from one set of wells, permeability from another. In this situation, the conventional cross-semivariogram cannot be computed because it requires the variables to be sampled at some of the same locations. This is an extreme case. In others, the number of coincident samples might be too small for a cross-semivariogram to be calculated.

The **pseudo cross-semivariogram** was proposed by Clark *et al.* (1989) as a substitute for the usual estimator of covariance between two variables:

$$\lambda_{zy}^{p}(h) = \frac{1}{2n(h)} \sum [z(x_i) - y(x_i + h)]^2$$

A number of authors have suggested alternative definitions of the pseudo cross-semivariogram, looked at the properties of this statistic, proposed ways of modeling it, and examined its appropriateness in cokriging (e.g. Myers, 1991; Papritz *et al.*, 1993).

4.9.2 Too many variables

The most time-consuming part of cokriging is computing and modeling $n(n+1)/2$ semivariograms and cross-semivariograms. This task becomes very tedious for n greater than 3. Unlike ordinary kriging, where the model only needs to fit the experimental semivariogram to a reasonable degree, cokriging requires that all of the cross-semivariograms obey the inequality constraint. The simplest solution is to drop some of the variables, namely those that show little statistical correlation with the variable of interest.

Davis and Greenes (1983) present a way of cokriging without having to model cross-semivariograms. Briefly, their method begins with an initial orthogonalization of the variables through principal components analysis. For each of the new variables, one computes and models a semivariogram. Ordinary kriging of the transformed data is followed by a back-transform to the original units. Computations can be performed with programs for ordinary kriging along with subroutines for eigenvector analysis and matrix multiplication.

This procedure depends upon the transformed data having no spatial cross-covariance; this can be checked by computing the cross-semivariograms. Wackernagel (1995) summarizes the major approaches to geostatistical analysis of multivariate data.

4.9.3 Secondary variables insufficiently weighted

Cokriging can sometimes give results that appear nearly identical to those obtained through ordinary kriging, as though the secondary variable was ignored. The secondary variables can be given more weight

by imposing a different nonbias condition. Take the simple case of a single secondary variable. If the observed values of the secondary variable are adjusted such that their mean equals that of the primary variable, then the cokriging estimate is calculated from:

$$z^*_{ck} = \sum_{i=1}^{n} \lambda_i z_i + \sum_{j=1}^{m} \kappa_j (y_j - m_z - m_y)$$

where m_z is the mean value of the primary variable, and m_y is the mean of the secondary variable. The nonbias condition is now:

$$\sum_{i=1}^{n} \lambda_i + \sum_{i=1}^{n} \kappa_i = 1$$

Yet another approach is to go without nonbias conditions altogether. **Simple cokriging** requires that all variables be adjusted to a mean of zero. All three methods are available in the GSLIB software of Deutsch and Journel (1998).

4.10 SUMMARY

Mutual behavior of two or more variables in space – a coregionalization – can be used to obtain better estimates of a given variable than if that variable is estimated alone. Cokriging estimates a regionalized variable from two or more coregionalized variables, and is useful when a primary variable is undersampled relative to secondary variables.

Cokriging requires semivariograms for both the primary variable, and each of the secondary variables. In addition, one must calculate and model cross-semivariograms between all variables. Modeling is often tedious and difficult because of the requirement for admissibility. The linear model of coregionalization helps this process along providing several simple rules are obeyed. The advantage of cokriging can disappear in the presence of large nugget effects in semivariograms, low cross-correlation, or large range in the undersampled variable relative to sample spacing.

Kriging with external drift and collocated cokriging are methods related to conventional cokriging. The first is used when values of a secondary variable are available on a grid. Collocated cokriging is used when the grid of values to be estimated coincides with that of the secondary variable, and only a single coincident value of the secondary variable is used with the primary variable for estimation at each location on the grid. Both methods are appropriate for drawing maps of structure or porosity, in which well data are sparse in comparison with a grid of data obtained through a 3-D seismic survey.

Common problems with cokriging are noncoincident sample locations across variables, several secondary variables, and an apparent underweighting of the secondary variables during estimation. The first problem can be handled with the pseudo cross-semivariogram. The number of variables can be reduced through principal components analysis. Rewriting the cokriging equations increases the weight given to the secondary variables during estimation.

REFERENCES

Bashore, W.M., Araktingi, U.G., Levy, M. and Schweller, W.J. (1994) Importance of a geological framework and seismic data integration for reservoir modeling and subsequent fluid-flow predictions, in J.M. Yarus and R.L. Chambers (eds), *Stochastic Modeling and Geostatistics*. American Association of Petroleum Geologists, Tulsa, OK, pp. 159–175.

Chambers, R.L., Zinger, M.A. and Kelly, M.C. (1994) Constraining geostatistical reservoir descriptions with 3-D seismic data to reduce uncertainty, in J.M. Yarus and R.L. Chambers (eds), *Stochastic Modeling and Geostatistics*. American Association of Petroleum Geologists, Tulsa, OK, pp. 143–157.

Chu, J., Xu, W. and Journel, A.G. (1994) 3-D implementation of geostatistical analyses – the Amoco case study, in J.M. Yarus, and R.L. Chambers (eds), *Stochastic Modeling and Geostatistics*, American Association of Petroleum Geologists, Tulsa, OK, pp. 201–216.

Clark, I., Basinger, K.L. and Harper, W.V. (1989) MUCK – a novel approach to cokriging, in B.E. Buxton, (ed.), Proceedings of the Conference on *Geostatistical, Sensitivity, and Uncertainty Methods for Ground-Water Flow and Radionuclide Transport Modeling*, Battelle Press, Columbus, OH, pp. 473–493.

Columbia Gas System Service Corporation (1985) *Southwest West Virginia Data Book, Issue 2*, April 1985, for Gas Research Institute Contract No. 5083-213-0856.

Davis, B.M., and Greenes, K.A. (1983) Estimation using spatially distributed multi variate data: an example with coal quality. *Math. Geol.* **15**, 287–300.

Deutsch, C.V. and Journel, A.G. (1998) *GSLIB: Geostatistical Software Library and User's Guide*. Oxford University Press, New York, 369 pp.

Galli, A. and Meunier, G. (1987) Study of a gas reservoir using the external drift method, in G. Matheron and M. Armstrong (eds), *Geostatistical Case Studies*. D. Reidel, Dordrecht, pp. 105–119.

Myers, D.E. (1982) Matrix formulation of co-kriging. *Math. Geol.*, **14**, 249–257.

Myers, D.E. (1983) Estimation of linear combinations and co-kriging. *Math. Geol.*, **15**, 633–637.

Myers, D.E. (1991) Pseudo-cross variograms, positive-definiteness, and cokriging. *Math. Geol.* **23**, 805–816.

Papritz, A., Künsch, H.R. and Webster, R. (1993) On the pseudo cross variogram. *Math. Geol.*, **25**, 1015–1026.

Wackernagel, H. (1995) *Multivariate Geostatistics: An Introduction with Applications*. Springer-Verlag, New York, 256 pp.

Xu, W., Tran, T., Srivastava, R.M. and Journel, A.G. (1992) *Integrating Seismic Data in Reservoir Modeling: the Collocated Cokriging Alternative*. Proceedings of Society of Petroleum Engineers Technical Conference, pp. 833–842.

CHAPTER 5

Nonlinear estimation: disjunctive and lognormal kriging

Linear estimation through ordinary kriging provides local averages of a regionalized variable, and calculated estimation variance gives some idea of the expected precision of the estimates. However, some applications may call for knowledge of local spatial distributions. Placing confidence intervals around local estimates; stating the probability that a regionalized variable lies below, between, or above some values; computing mean values of a variable above a cutoff; drawing a map of estimated local medians rather than estimated local averages; and handling extreme values in markedly nonnormal data all require consideration of local distribution.

At first, estimation variance reported by most kriging programs seems to provide a confidence interval about the estimate. However, kriging variance gives a proper confidence interval only under condition of multivariate normality (Journel, 1986); we have observed in previous chapters the rarity of univariate normal distributions. Simple transforms can fit data to a univariate normal distribution, but they cannot guarantee multivariate normality, and correct back-transforms are needed. These back-transforms can themselves require specific distributional assumptions, and can be numerically unstable. Kriging variance of a linear estimate might only represent a measure of the goodness of local sample distribution (Journel, 1986).

Drawing a map of local averages may not answer the question asked by the geologist. A map of initial potential shows locations of high and low interpolated values, but gives a very poor impression of the probability of drilling a well above some value. Presence of a few very high values tends to inflate local averages, and simple interpolation gives a misleading impression of the chance of drilling a well with high initial potential. Because of the highly skewed distribution of initial potential, most observed values are very low. Rather than the map of average or interpolated initial potential, a geologist might consider an isoprobability

M. E. Hohn, *Geostatistics and Petroleum Geology*

map, which shows the probability that initial potential is greater than some threshold at any given location in a region.

Finding local spatial distributions is also necessary for calculating the average value of a regionalized variable above or below a specified cutoff. For instance, one may want to know average thickness of a reservoir sand where it is thicker than some minimum required as an indicator of economic production. When an area is being considered for exploration or development, well control is sparse and ordinary linear estimates are highly smoothed. Thus, no area may appear to have a sand thickness greater than the selected threshold except for very small areas around the control wells. Linear estimators do not reproduce the degree of local variability reflected in control wells.

An average might not be the best measure of central tendency; in some cases the median is more useful and closer to what the petroleum geologist wants to measure and express. Sometimes, the median comes closer than the average to the geologist's idea of 'typical'. Maps of median values provide an obvious alternative to maps of averages or hand-drawn interpolations.

Extreme values pose a difficult problem in that they may persist even after a transform, suggesting that they belong to a population other than the one under analysis. Very large production values may be trimmed from the data set, but this trimming makes some assumption about the distribution of the main population, and the trimmed values may contain the most valuable information. Untrimmed, these extreme values can inflate the apparent extent of highly productive areas.

Several avenues exist for computing local estimates for contouring that allow some kind of probabilistic judgments. In this chapter we consider two methods, disjunctive and lognormal kriging. Both involve a transformation of raw data to a normal distribution, modeling semivariograms computed from transformed data, and solving kriging equations, but differ in how the transform is done, and how kriging results are back-transformed to the original scale. Disjunctive kriging is described below in some detail because it includes an important step: calculation of normal scores from raw data. Lognormal kriging are discussed briefly, just enough to show its potential usefulness, and to point out the hazard of incorrect back-transformation.

5.1 DISJUNCTIVE KRIGING

Disjunctive kriging comprises four main steps: (1) normalizing raw data, (2) computing and modeling a semivariogram of normalized data, (3) calculating coefficients, and (4) estimating local averages and frequency distributions. After outlining the method, I present an example using the initial potential data from Barbour County.

5.1.1 Methodology

5.1.1.1 Overview

Central to disjunctive kriging is transforming sample values z in a space S' to normalized values y in a space S''. Whereas the data can have any probability distribution, including the normal distribution, values y have a normal distribution with a mean of 0 and variance 1. Values in S' and S'' are related through a function ϕ:

$$z = \phi(y)$$

which is expressed as a linear combination of an infinite number of Hermite polynomials:

$$\phi(y) = \sum_{k=0}^{\infty} C_k H_k(y)$$

where $H_k(y)$ is a Hermite polynomial of order k, and each C_k is a coefficient calculated from sample values. A value z_i has coordinates $C_k H_k(y)$ in space S', and its corresponding value y_i has coordinates $H_k(y)$ in space S''. An estimate y^*_{dk} has coordinates H_{kv} in S''. Each coordinate is a linear combination of corresponding coordinates of sample values, i.e.

$$\boldsymbol{H}_{kv} = \sum_{i=1}^{n} \lambda_i \boldsymbol{H}_k(y_i)$$

The estimate z^*_{dk} in S' is calculated through:

$$z^*_{dk} = \sum_{k=0}^{K} \boldsymbol{C}_k \boldsymbol{H}_{kv}$$

The following sections present disjunctive kriging in some detail through the three steps of transforming raw data to normal scores, computing a semivariogram, and estimation, including back-transformation.

5.1.1.2 Normal scores transform

Given n values z_i, sorted in increasing order from z_1 to z_n, the number of values of z_i less than or equal to a value z_0 equals i_o, and the estimated probability that z_i is less than or equal to z_0 is $(i_o - 0.5)/n$. The observed values are sorted, and a value p_i is calculated for each z_i. From a table of the cumulative distribution of the standard normal variate, the corresponding value of y_i is found for each p_i. This procedure can be carried out graphically (Fig. 5.1), or from a table of the standard normal variate, or more likely, with a computer program such as that in Kim *et al.*, 1977; Yates *et al.*, 1986, or GSLIB (Deutsch and Journel, 1998). The **normal scores** transform is an important step in other geostatistical techniques, such as sequential Gaussian simulation (Chapter 6).

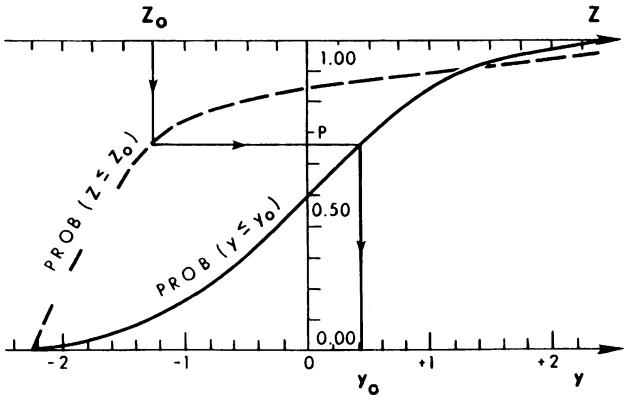

Figure 5.1 Graphical transformation of raw data to a normal distribution.

The estimation stage is going to require us to represent the transform ϕ with a linear combination of Hermite polynomials

$$\phi(y) = \sum_{k=0}^{\infty} C_k H_k(y)$$

In practice, this transformation is approximated through a finite number of terms:

$$\phi(y) = \sum_{k=0}^{k} C_k H_k(y)$$

where $H_k(y)$ is calculated from the relationships:

$$\begin{aligned} H_0(y) &= 1 \\ H_1(y) &= y \\ H_{k+1}(y) &= yH_k(y) - kH_{k-1}(y) \end{aligned}$$

Coefficients C_k are calculated through Hermite integration:

$$C_k = \frac{1}{[k!\sqrt{(2\pi)}] \sum_{j=1}^{J} w_j e^{(y_j^2/2)} \phi(y_j) H_k(y_j)}$$

where $k = 1, K$. Values of w_j are given by Rendu (1980) and Abramowitz and Stegun (1970), and are imbedded in any computer program, along with a value for J. Values of $\phi(y_j)$ are computed through the inverse of the procedure described above for obtaining normal scores.

The user must specify the number of terms K in the expansion that affect accuracy of the transformation. With increasing K, the fit between raw data and $\phi(y)$ improves. Goodness of fit for a given number of

coefficients depends on the shape of the raw data distribution; complex or skewed distributions require more coefficients than approximately normal distributions. Rendu (1980) points out that the important factor should be accuracy of estimation, not goodness of fit to the function ϕ; he uses ten coefficients in his example.

5.1.1.3 The Semivariogram of transformed data

Autocorrelation among normalized data must be modeled for the estimation step. Stationarity is an important assumption in disjunctive kriging. The user simply graphs the semivariogram of the normalized data; because the values have a variance of 1, the sill should equal 1, and the autocorrelogram $\rho(h)$ has the relationship

$$\rho(h) = 1 - \gamma(h)$$

5.1.1.4 Estimation

Once sample values have been normalized and coefficients calculated, estimation is straightforward. For each value of $k > 0$, one must solve a system of m linear equations:

$$\sum_{j=1}^{m} \lambda_j(\rho_{ij})^k = (\rho_{iv})^k \qquad \text{for } i = 1, m$$

where m equals the number of sample values Y_i in the neighborhood of the location to be estimated; ρ_{ij} is the value of $\rho(h)$ between sample i and sample j; and ρ_{iv} is the value of $\rho(h)$ between sample i and the point to be estimated. Weights λ are used in the equation:

$$H_{kv} = \sum_{i=1}^{n} \lambda_i H_k(y_i)$$

to give the kth coordinate of the normalized block estimator in the space S''. Using the Hermite polynomial approximation to ϕ, the disjunctive kriging estimate is simply:

$$z^*_{dk} = \sum_{k=0}^{K} C_k H_{kv}$$

Because $K + 1$ systems of equations must be solved, run-time efficiency requires that K be kept to a minimum. However, for large K, values for ρ_{ij} and ρ_{iv} approach zero, and kriging weights also tend to zero. Therefore, large values of K are unnecessary.

An important output from disjunctive kriging is a local frequency distribution, which is said to be conditioned on the local, available data, and provides such information as the probability that the regionalized

variable exceeds a given value. Recall that this kind of information can be computed from the estimate and estimation variance given by ordinary kriging, but to use estimation variance requires the assumption of multivariate normality that is untestable, perhaps unrealistic, and unlikely for many univariate distributions. The local frequency distribution is calculated from the following:

$$P^*_{dk}(z_c) = 1 - G(y_c) - e^{(-y_c^2/2)} / \sqrt{(2\pi)} \sum_{k=1}^{K} [H_{k-1}(y_c)/k!\ H_{kv}]$$

where $P^*_{dk}(z_c)$ is the probability that an estimate exceeds a cutoff z_c, and $G(y_c)$ is the Gaussian cumulative distribution function.

In summary, disjunctive kriging looks to the user much like ordinary kriging with the addition of an initial step to transform data, requiring selection of the number of coefficients to use. Output from this step includes normal scores and a set of coefficients. From the normal scores, the user computes a semivariogram and fits a model. Input to the estimation procedure comprises normal scores, coefficients, and the semivariogram model. The user obtains as output an estimate, and optionally probabilities of exceeding specified cutoffs of the regionalized variable.

5.2 EXAMPLE: INITIAL POTENTIAL

A data set comprising 674 values of initial potentials of gas in Barbour County, West Virginia, shows far from a normal distribution (Fig. 5.2). Individual values range between 10 and 16 022 Mcfpd. Values in Fig. 5.3 are normal scores as calculated using 18 coefficients. Although the distribution is not ideal, transformed data (Fig. 5.3) approach a normal distribution, and is certainly much better than the skewed distribution of the raw data.

One can judge the efficacy of the transformation from the first several moments of transformed data. Data plotted in Fig. 5.3 have a mean of −.002, a variance of 1.03, and a skewness of −.058, reasonably close to 0, 1 and 0, respectively.

The mean of initial potential calculated with the Hermite model, 1243 Mcfpd, is within 0.3% of the actual value of 1239 Mcfpd. The variance given by the model, 2 438 421 Mcfpd^2, is within 4.3% of the observed value, 2 549 088 Mcfpd^2. Theoretical values for the mean and variance are given by:

$$\mu = C_0$$

$$\sigma^2 = \sum_{k=0}^{\infty} k! C_k^2$$

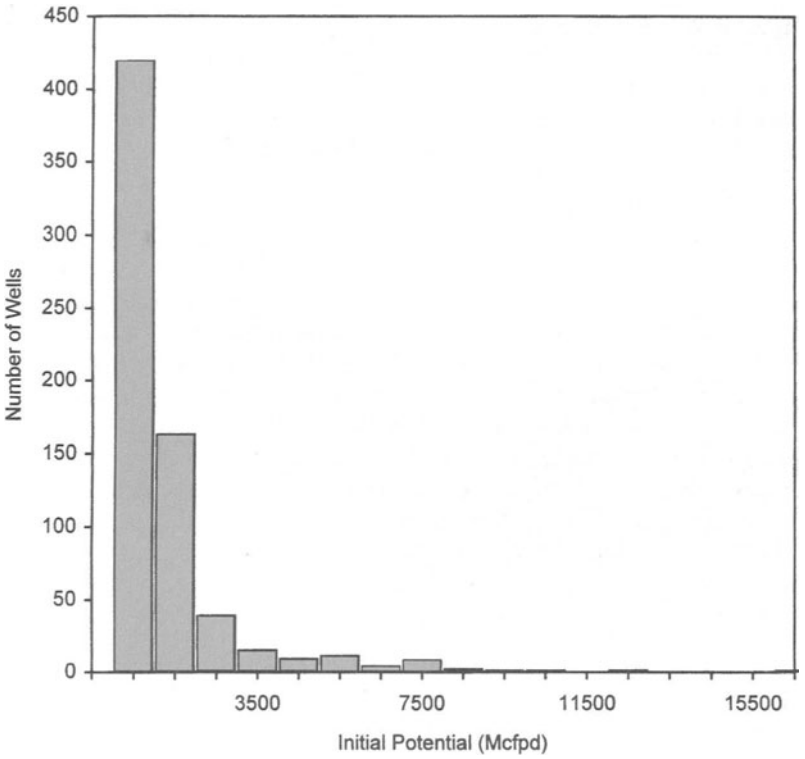

Figure 5.2 Histogram of gas initial potentials in Upper Devonian rocks of Barbour County, West Virginia.

Rendu (1980) suggests that ten coefficients are far more than adequate, a conclusion borne out in part by the small absolute values beyond the first several terms in Table 5.1. On the other hand, inspection of Fig. 5.3 shows that even 18 coefficients appear inadequate for a fully satisfactory transformation. Others have reported difficulties in obtaining an accurate fit for highly skewed data and see this as a drawback to disjunctive kriging.

The semivariogram of initial potentials in Barbour County (Fig. 5.4) displays the same large nugget effect noted in Chapter 2. An exponential model with a range of 1.5 km, constant of 0.56 $Mcfpd^2$, and nugget effect of 0.54 $Mcfpd^2$, provide a good fit to observed values. Note the overall sill does not equal the variance of 1. This can happen if there exists a trend in the data, or if only part of the variogram is plotted and modeled. Although disjunctive kriging requires stationarity, these data do not appear trended sufficiently to discourage use of the method.

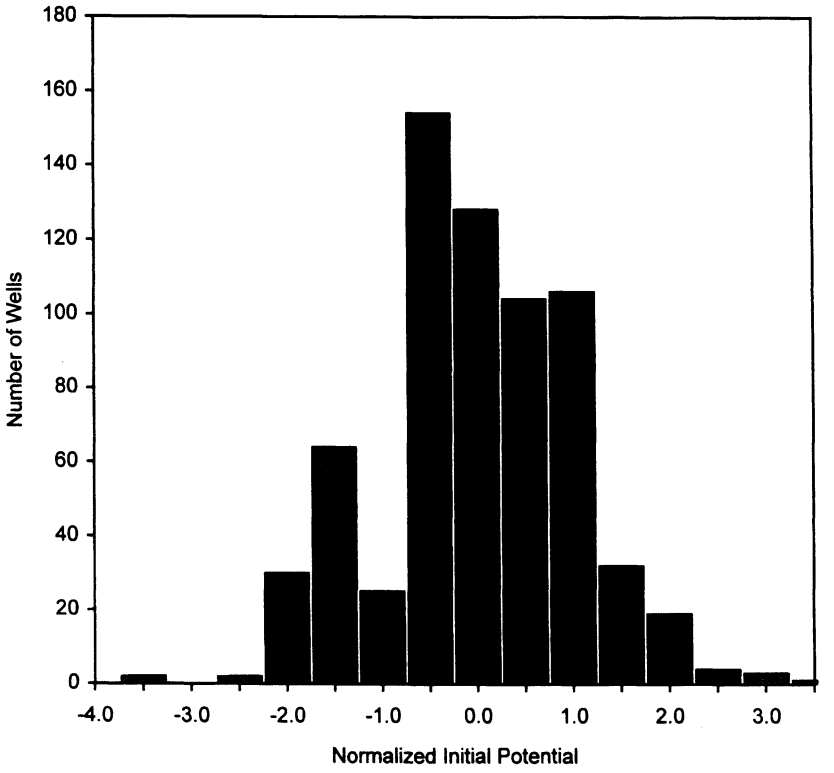

Figure 5.3 Histogram of normalized values of gas initial potential.

Table 5.1 Ten Hermite coefficients for Barbour County initial potential data

C_0	1242.79	C_5	− 12.76
C_1	1245.00	C_6	− 3.39
C_2	590.81	C_7	− 0.01
C_3	148.34	C_8	0.05
C_4	70.25	C_9	− 0.06

The map of initial potentials computed through disjunctive kriging (Fig. 5.5) looks similar over much of the area to that obtained from ordinary kriging (Fig. 3.14). As before, the grid has 91 rows by 91 columns, providing an estimate every 0.11 km, much finer than the sample spacing. To eliminate edge effects, wells outside the mapped area up to a distance equal to the practical range, 4.5 km, were included with wells falling within the area to be mapped. The similarity of the two

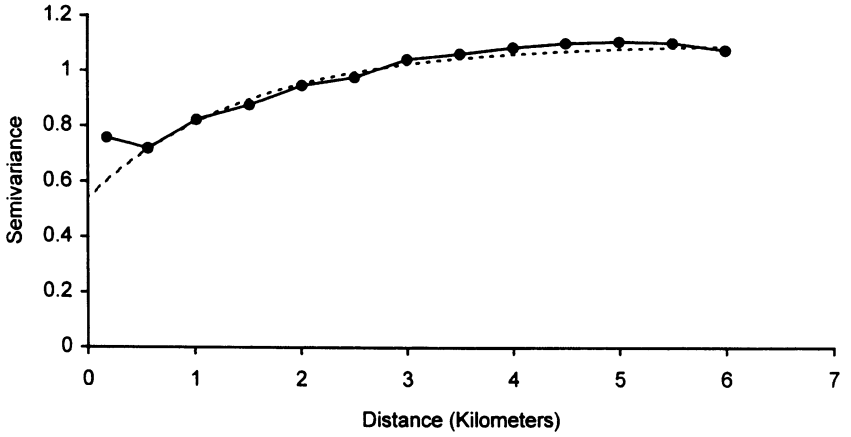

Figure 5.4 Semivariogram of normalized values of initial potential.

maps should not surprise us; ordinary kriging has often been found to be insensitive to lack of normality, except where large data spikes occur.

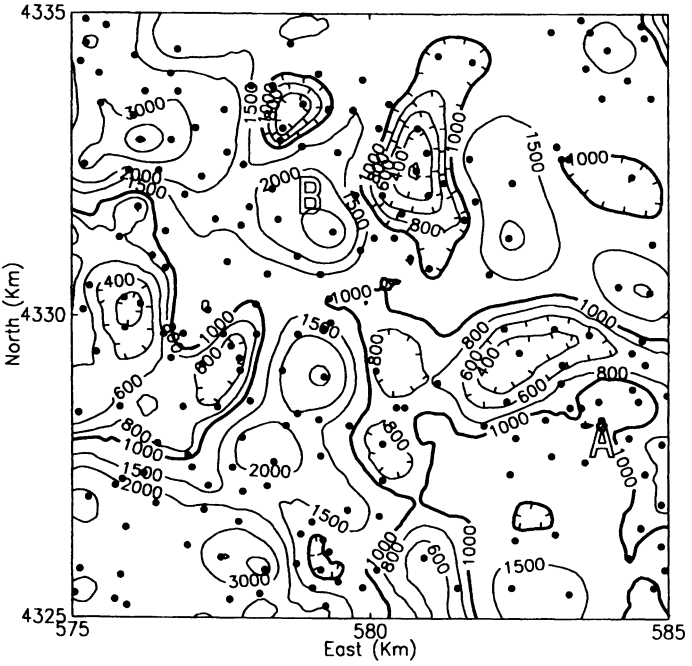

Figure 5.5 Contour map of initial potentials estimated by disjunctive kriging. Units are thousands of cubic feet per day (Mcfpd). The contour interval is irregular.

Indeed, the map of ordinary kriged estimates seems to have larger spikes around the locations of very high-volume wells.

The problem with ordinary kriging is in trying to obtain exceedance probabilities, such as the probability of exceeding a given volume of gas. Disjunctive kriging gives these probabilities explicitly, without having to compute an estimation variance. Hence, at specified locations, we can draw a graph showing the probability that initial potential falls within given intervals, or a cumulative frequency graph for exceedence probabilities.

At each location, disjunctive kriging was used to compute the probability of exceeding each of nine values for initial potential: 198; 327; 467;

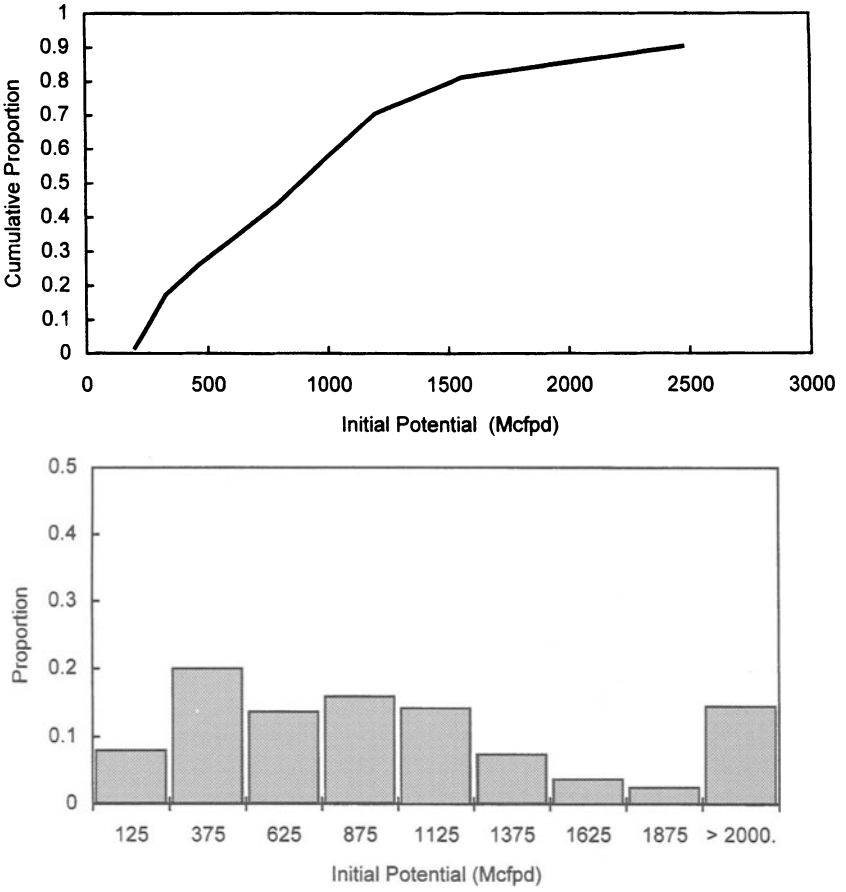

Figure 5.6 Results from disjunctive kriging at location 'A' in Fig. 5.4. (a) Conditional cumulative distribution function; (b) histogram of relative frequencies.

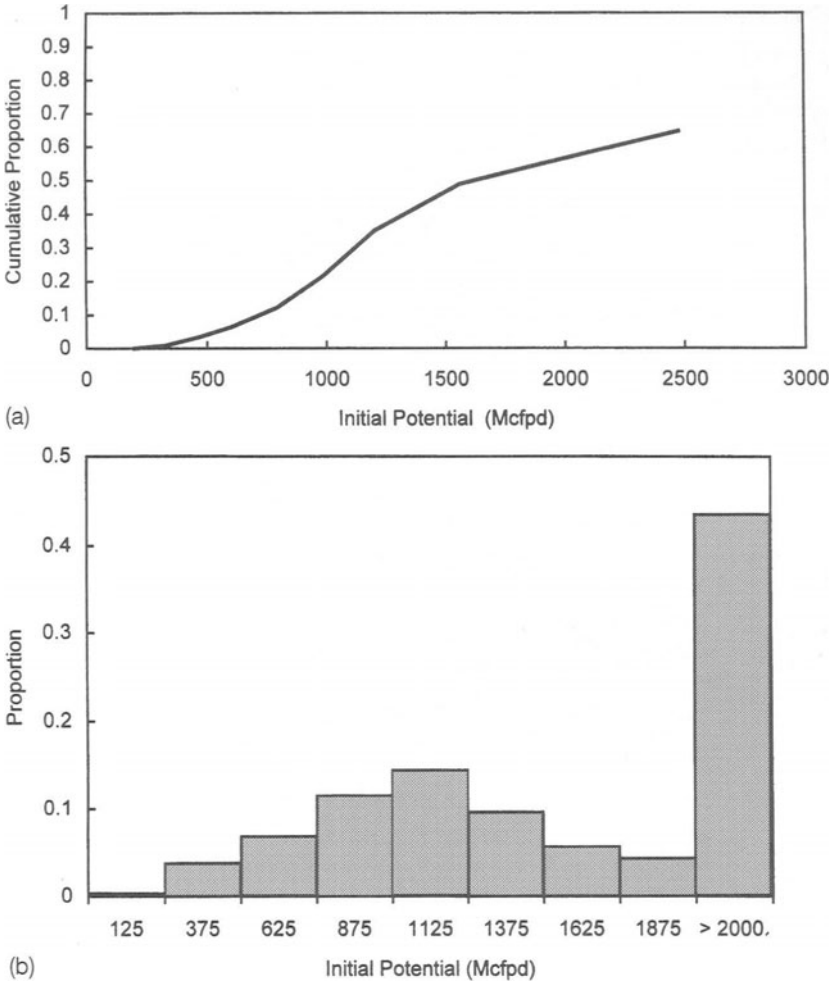

Figure 5.7 Results from disjunctive kriging at location 'B' in Figure 5.4. (a) Conditional cumulative distribution function; (b) histogram of relative frequencies.

600; 792; 986; 1200; 1561; and 2477 Mcfpd. These values break up the distribution of initial potentials into deciles. Results are shown for two locations designated 'A' and 'B' on Fig. 5.5, representing spots with low and high estimated initial potential, respectively. Note that like the overall data distribution, these locally conditioned frequency distributions are skewed, and histograms in Figs 5.6 and 5.7 have a spike for the region above 2000 Mcfpd. Comparing these two figures, we see that the center of mass at location 'A' is less than 1000 Mcfpd, whereas the same at location 'B' exceeds that rate. In addition, the histogram at location 'B'

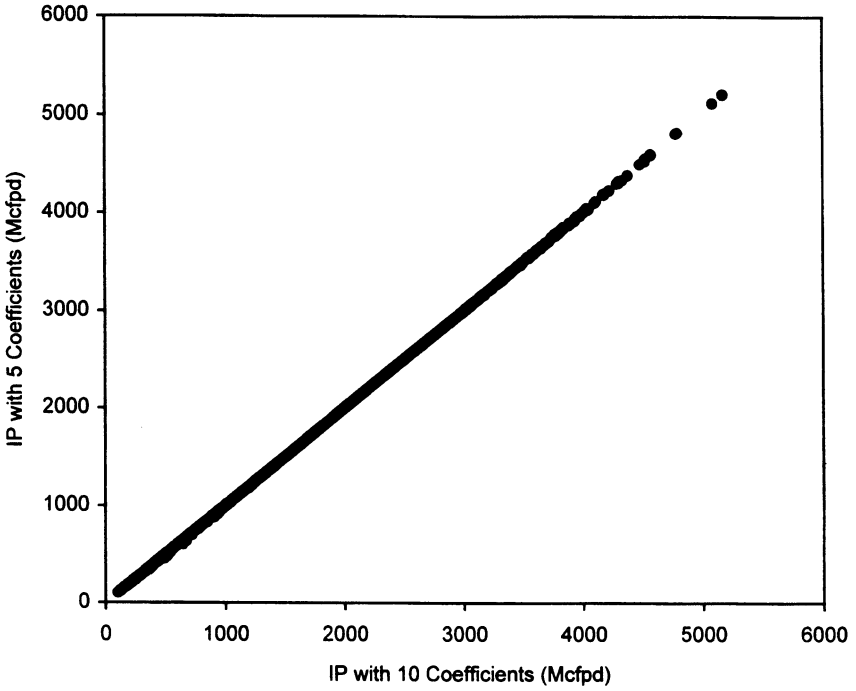

Figure 5.8 Scattergram comparing results of disjunctive kriging using ten Hermite polynomials with kriging using five coefficients.

has a relatively long tail; the probability that initial potential exceeds 2000 Mcfpd is almost 50%.

One of the problems I experienced was in selecting the number of coefficients to use. A reasonable fit between the raw data and the theoretical distribution was only achieved with a minimum of 18 coefficients. Yet, the program I was using to carry out the actual kriging could handle no more than 10; including more than that resulted in attempts to divide by zero. Previous authors have stated that few coefficients are actually needed for estimation, and so, because the Hermite polynomials are orthogonal, I could simply use the largest 10 coefficients for the kriging stage.

This poses the question: did I lose much by reducing the number of coefficients? To find out, I computed kriged estimates using five coefficients, and obtained results virtually identical to those in Fig. 5.5. Estimates given by using five coefficients are nearly equal to those obtained by using 10 coefficients (Fig. 5.8). Dropping down to three coefficients appears to cause a conditional bias in the results; larger values of initial potential are underestimated, smaller values are overestimated (Fig. 5.9). Even so, mapped estimates change little when the

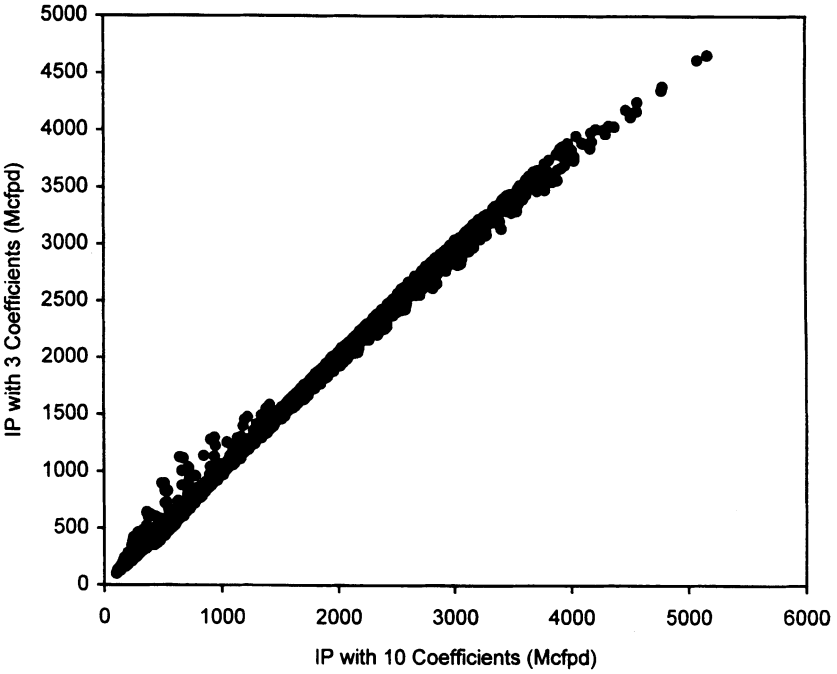

Figure 5.9 Scattergram comparing results of disjunctive kriging using ten Hermite polynomials with kriging using three polynomials.

number of coefficients is as few as three (Fig. 5.10). Table 5.2 shows the effect of the number of coefficients on conditional probabilities. It appears that 10 coefficients are far more than necessary for these data.

5.3 LOGNORMAL KRIGING

Taking the logarithms of the initial potential data yields close to a normal distribution (Fig. 5.11), suggesting that this might be a useful transform for kriging. **Lognormal kriging** has been around for several decades, and has many variants. The method consists of calculating logarithms, modeling the semivariogram computed from transformed data, kriging, and back-transforming to the original units. This back-transform is more than simply taking the antilogs of kriged estimates, as explained in Chapter 3.

Using the Barbour County data once again, I found that an exponential model with constant of 0.11, range of 1.5 km., and nugget effect of 0.10, were found to fit closely the observed semivariogram (Fig. 5.12).

Kriged estimates computed for each point on a regular grid covering the same 100 km^2 region looked at before (Fig. 5.13) show the large degree of smoothing one expects to find when the nugget effect equals

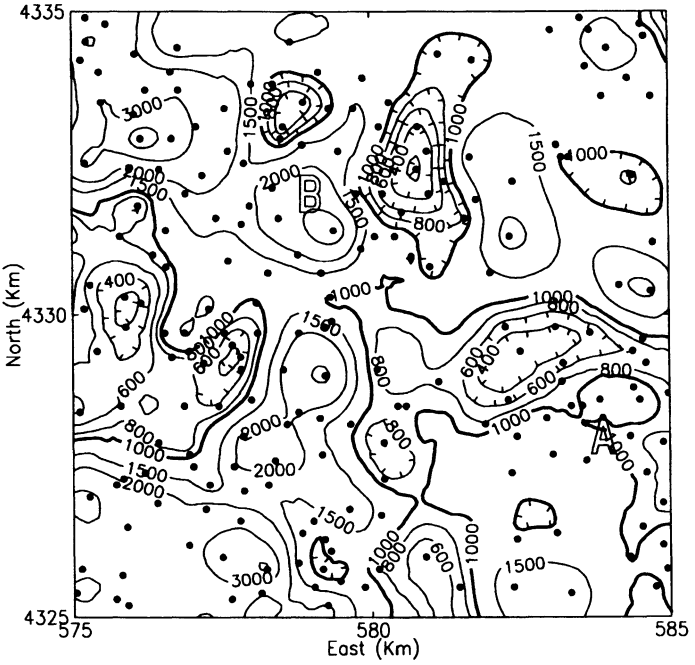

Figure 5.10 Contour map of initial potentials estimated by disjunctive kriging using three Hermite polynomials. Units are thousands of cubic feet per day (Mcfpd). The contour interval is irregular.

Table 5.2 Comparison of disjunctive kriging results for differing numbers of coefficients at two locations. Numbers are calculated probabilities of exceeding cutoff

	Location 'A'		*Location 'B'*	
Cutoff (Mcfpd)	*3 Coeff.*	*5 Coeff.*	*3 Coeff.*	*5 Coeff.*
198	0.98	0.98	1.00	1.00
327	0.82	0.83	0.99	0.99
467	0.73	0.74	0.97	0.97
600	0.66	0.67	0.94	0.94
792	0.56	0.56	0.88	0.88
986	0.43	0.43	0.79	0.78
1200	0.30	0.30	0.65	0.65
1561	0.19	0.19	0.51	0.51
2477	0.10	0.10	0.35	0.35

about half the sill. A map of well locations annotated with the initial potentials shows the large variation among even closely spaced wells (Fig. 3.15). Nevertheless, the map of kriged estimates shows trends in

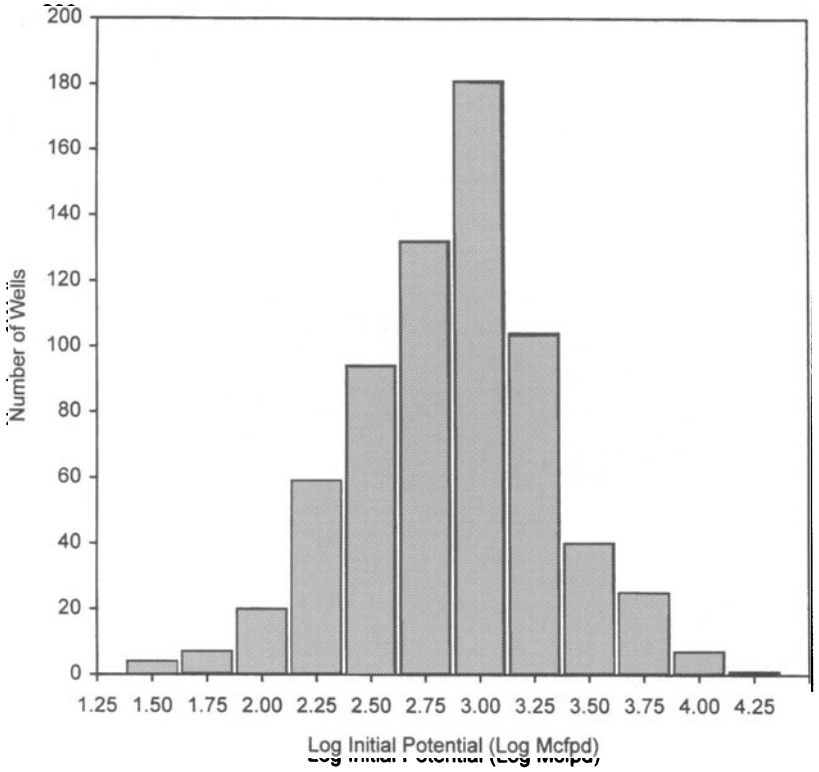

Figure 5.11 Histogram of gas initial potentials after log transform.

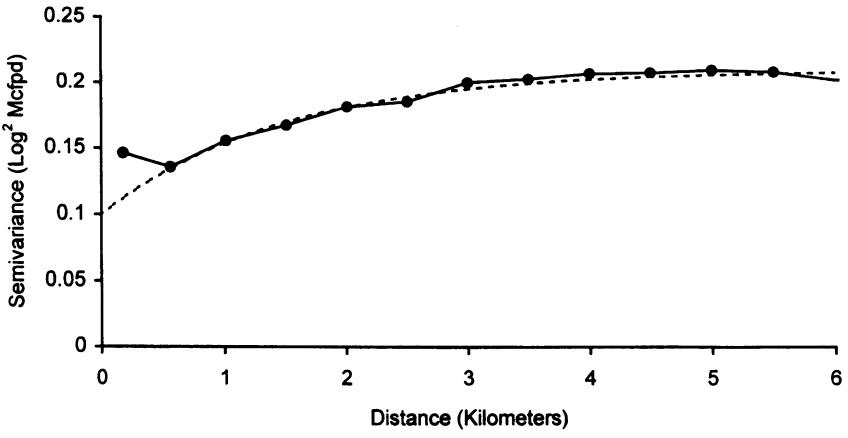

Figure 5.12 Semivariogram of log-transformed initial potentials.

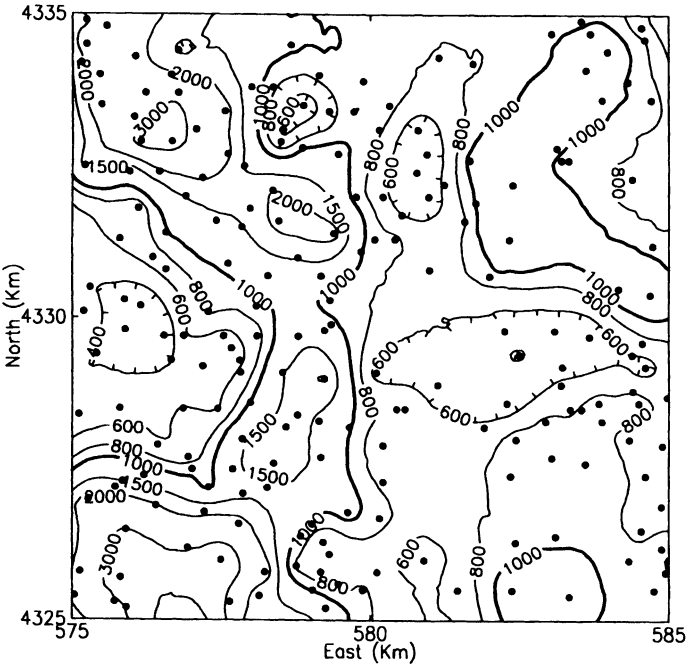

Figure 5.13 Contour map of initial potentials estimated by lognormal kriging. Units are thousands of cubic feet per day (Mcfpd). The contour interval is irregular.

initial potential within the area mapped. Those needing the surface to exactly honor the data might be out of luck, although as demonstrated in earlier examples, if the grid is fine enough, the contour map will honor each point. Of course, with such a large nugget effect, each well would be surrounded by a bull's-eye.

5.4 SUMMARY

In this chapter we have considered the problem of estimating local frequency distributions, which transcends simple estimation of local averages. By estimating local frequency distributions, one can draw maps of medians, probability of exceeding a cutoff value, and others. Nonlinear estimation provides a means to such estimates, but at a computational cost.

Disjunctive kriging begins with a transformation of sample data to normality; the transformation function is approximated by a linear combination of Hermite polynomials. Transformed data are used in calculating a semivariogram and fitting a model. Estimation requires solving K-1 sets of equations, where K equals the number of terms in the

Hermite expansion used to approximate the transformation between normalized and raw data.

Fitting a set of Hermite polynomials to raw data generally does a good job of approximating the mean and variance, but a plot of the frequency distribution function calculated from the polynomials can look only crudely normal. The main problem appears to be with the one or more extremely large values that can occur in sets of highly skewed data such as initial potential.

Estimation needs no more user intervention than does ordinary kriging, although the computer must do a lot more work. The results include not only estimates of local averages, but percentiles of local frequency distributions.

REFERENCES

Abramowitz, M., and Stegun, I.A. (1970) *Handbook of Mathematical Functions*, National Bureau of Standards Applied Mathematics Series 55, V.S. Government Printing Office, Washington, D.C., 1,046 pp.

Deutsch, C.V. and Journel, A.G. (1998) *GSLIB: Geostatistical Software Library and User's Guide*. Oxford University Press, New York, 369 pp.

Journel, A.G. (1986) Geostatistics: Models and tools for the Earth Sciences. *Math. Geol.* **18**, 119–140.

Kim, Y.C., Myers, D.E. and Knudsen, H.P. (1977) *Advanced Geostatistics in Ore Reserve Estimation and Mine Planning (Practitioners Guide)*. Report to U.S. Energy and Research and Development Administration, subcontract no. 76-003-E.

Rendu, J.-M. (1980) Disjunctive kriging: Comparison of theory with actual results. *Math. Geol.* **12**, 305–320.

Yates, S.R., Warrick, A.W. and Myers, D.E. (1986) A disjunctive kriging program for two dimensions. *Computers & Geosciences*, **12**, 281–313.

CHAPTER 6

Indicator kriging

Examples in the previous chapters used data that vary along a continuous scale. However, in many situations one is presented with nominal data or with data that are more easily treated if converted to a nominal scale. As a simple example of such an indicator variable, the presence or absence of a show of gas may be represented by the two values 0 and 1. Statistics such as success ratio assume a value for economic threshold that may not be stated. A more explicit use of a threshold appears in Kumar (1985), where fields had to exceed 1 million barrels (159 000 m^3) in recoverable reserves to be economical at 1979 prices. A continuous variable can be converted to an indicator variable for a number of thresholds, yielding a new variable for each threshold chosen; this procedure forms the basis for an important estimation method described in the second part of this chapter.

6.1 ANALYSIS OF AN INDICATOR VARIABLE

To introduce the idea of an indicator variable, consider a map of successful and dry wells (Fig. 6.1) adapted from an illustration in Kumar (1985; Fig. 3). Kumar studied the northwest shelf of the Delaware basin in New Mexico, a region that is generally densely drilled but has some sparsely drilled areas. The Permian Age San Andres Formation, one of three major oil-producing intervals in Kumar's study area, contains oil accumulations in updip pinchouts zones with above-average porosity. In addition, some structural anomalies are present in the study area. Areas deemed prospective had low drilling density, were updip from established fields, and contained a structural anomaly.

In Kumar's Fig. 3, each section with at least one test of the San Andres Formation was shaded one color if all tests were dry and a second color if at least one producer was drilled. To create a small set of data, I simply laid a sheet of graph paper over Kumar's figure and read off coordinates of successful and dry sections in a central area of about 65 km^2. The resulting sample distribution (Fig. 6.1) provides a close approximation to Kumar's map. The intent was not to repeat Kumar's study, which stands on its own, nor to provide a new interpretation.

M. E. Hohn, *Geostatistics and Petroleum Geology*

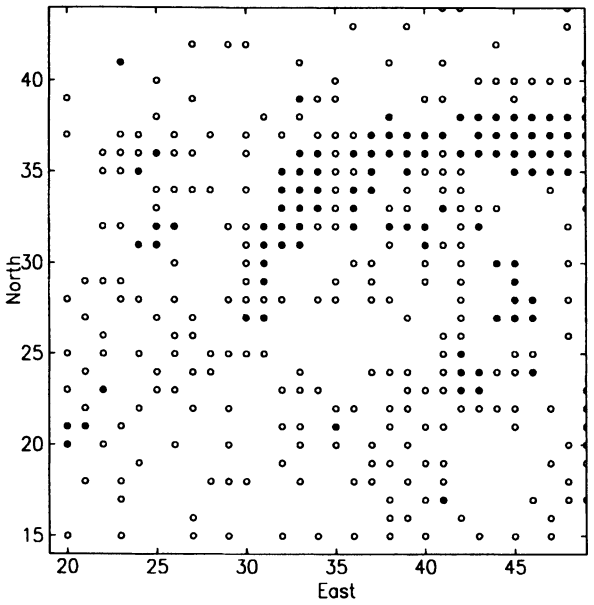

Figure 6.1 Locations of successful (solid circles) and unsuccessful oil wells in the Delaware basin of New Mexico; data adapted from Kumar (1985).

Geostatistical analysis of the data set follows the same procedures described in Chapters 2 and 3. Based on 333 values, the experimental semivariogram conforms to an exponential model with a range of 1.33, sill of 0.21, and nugget effect of zero (Fig. 6.2). The first three points of the experimental semivariogram are calculated from 596, 873, and 1070 pairs, respectively. Each field in the study area is represented by numerous samples. The number and spacing of the samples account in part for the smoothness of the semivariogram. In addition, the data cannot include any outliers because all values must equal 0 or 1.

The sill in Fig. 6.2 equals the sample variances, 0.21. The following simple relationship holds true between the mean m and variance σ^2 of an indicator variable:

$$\sigma^2 = m - m^2$$

Kriging an indicator variable does not result in values of 0 and 1, but rather estimates along a continuous scale that generally lie between 0 and 1. In the present situation, linear estimates represent success rates for blocks or predicted probabilities of success at points. Thus, linear estimation from an indicator variable yields probabilities. A map of point estimates (Fig. 6.3) clearly shows fields conforming to densely drilled areas with at least one successful well per section. Surrounding these

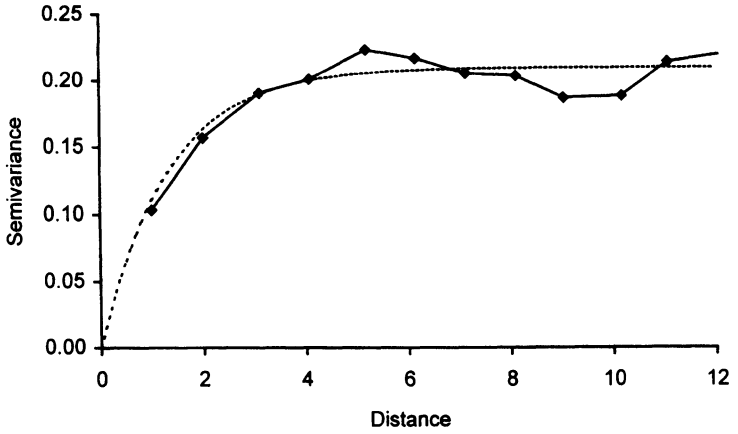

Figure 6.2 Indicator semivariogram for data in Fig. 6.1.

fields are haloes with lower values of predicted success, grading into interfield areas of dry holes.

Drawing maps of success rates is one situation where the computer possesses a clear advantage at all steps over hand contouring. Between raw data presence and absence and the final map, one must calculate frequencies at a point or a block. As this task is only practical through a

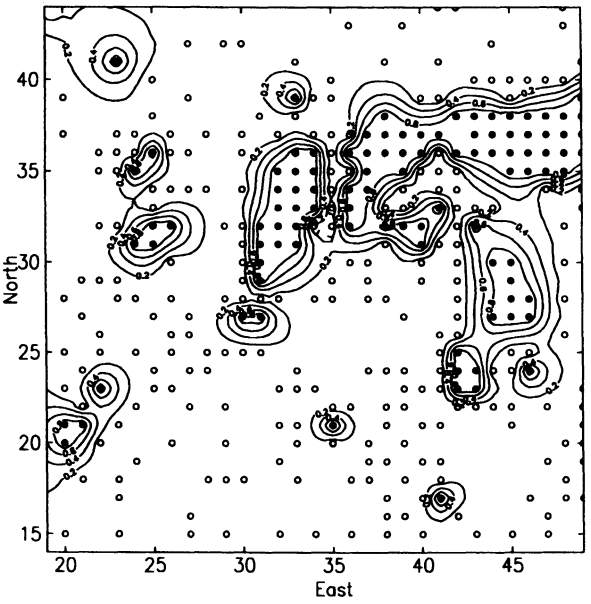

Figure 6.3 Contour map of point-kriged estimates of success probabilities.

computer program, linear estimation is a reasonable path to follow and provides the advantages of unbiased results and a measure of precision in the form of estimation variance.

One of three basic considerations in Kumar's choices for prospective areas, drilling density, is measured indirectly through estimation variance. The map of estimation variance or standard error (Fig. 6.4) may be useful in finding areas adjacent to known fields with high estimation variance and correspondingly low drilling density.

Kriging indicator variables is seen to be an exercise in defining the limits of a field. Where wells judged successful by some criterion are located near unsuccessful wells, field limits are sharply defined. Where successful and unsuccessful wells lie some distance from each other, field limits are rather more fuzzy, and better represented by a probabilistic estimate as performed here. The criterion for success might be whether the well was completed, or whether the well exceeds some threshold in production, oil saturation, porosity, or reservoir thickness.

Pawlowski *et al.* (1993) proposed an interesting use of indicator kriging to solve the general problem of defining a field boundary for contouring reservoir thickness of the oil column. Assigning wells within the field a value of one, and wells outside a value of zero, they performed kriging on this indicator variable. They multiplied kriged estimates of oil column thickness by the probability estimates, giving a map showing a gradual decrease in oil column thickness towards the limits of the field.

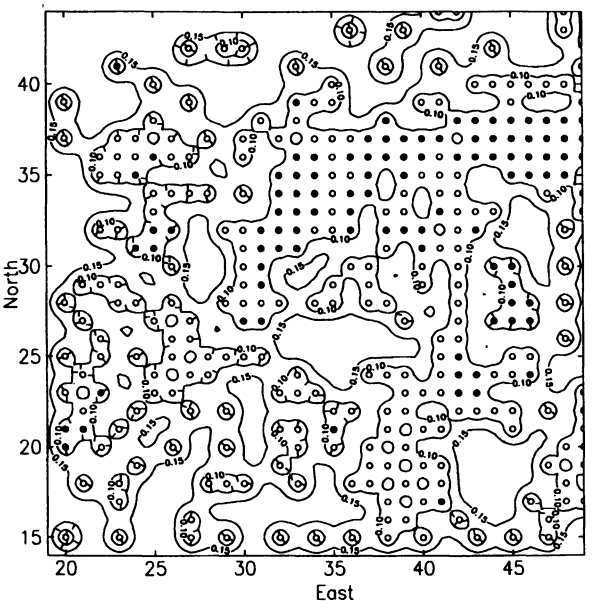

Figure 6.4 Contour map of standard error of estimated success probabilities.

6.2 INDICATOR KRIGING WITH MULTIPLE CUTOFFS

A number of issues in geostatistics can be boiled down to the basic problem of computing a cumulative distribution function at a specific location, conditioned on surrounding observations, i.e. computed from observed values of the regionalized variable. Having a conditional cumulative distribution function (ccdf), one can not only compute an estimate, but also a confidence interval, and probabilities of exceeding (or not exceeding) certain values. For a while, estimation variance seemed to be the route to a ccdf, but it requires assumptions such as multivariate normality.

The method of indicator kriging was proposed as a so-called non-parametric estimation of regionalized variables. It has the advantages that any distribution can be handled; it is easy to use; it gives exceedence probabilities and therefore confidence intervals directly; it provides a local ccdf from which at least two measures of central tendency are easily calculated, mean and median; and it is robust to outliers.

Given a regionalized variable that is measured on a continuous scale, assume that instead of a single threshold or cutoff, L cutoffs z_l are applied to the observed data, such that

$$i(x; z_l) = 1 \text{ if } z(x) < z_l$$
$$0 \text{ if not,}$$

where $z(x)$ is the value of a regionalized variable such as initial potential (IP) at location x. Thus, raw data are transformed into L new variables, each taking on values of 0 and 1. Cutoffs are not necessarily imposed by nature or a measuring device, nor necessarily suggested by the purpose of estimation, such as mapping the frequency of wells with first-year production above z. Although some cutoffs may be chosen to satisfy some goal of the mapping, the main purpose is to obtain a reasonable picture of the frequency of wells below or above each cutoff. The proportion P of values below a cutoff z_l within an area or volume equals

$$P(V; z) = \frac{1}{V} \int_V i(x; z_i) \mathrm{d}x$$

With knowledge of $P(V; z)$, one can compute the proportion of wells with a value of the regionalized variable above cutoff z_l:

$$\text{proportion } z(x) > z_l = P(V; z)$$

The proportion can be estimated from n observed values of $z(x)$:

$$P^*(V; z_l) = \frac{1}{n} \sum_{k=1}^{n} i(x_k; z_l)$$

i.e. a simple arithmetic average of the indicator variable. In fact, V does not need to be an area, but can be a point, in which case, the quantity being estimated is the probability that the regionalized variable at a point exceeds a given cutoff.

We know that spatially autocorrelated, probably clustered data should not be treated as though they were independent; instead, they should be weighted according to whether they lie in or near V, and according to the spatial continuity of $z(x)$, to give the estimate:

$$P^*(V;z_l) = \sum_{k=1}^{n} \lambda_k(z_l) i(x_k;z_l)$$

with n weights $\lambda_k(z_l)$ corresponding to the number of points in the neighborhood of V. For each cutoff, a system of ordinary kriging equations is set up and solved for the weights. Each cutoff also requires calculating, graphing, and modeling a semivariogram.

Although most of the computations in indicator kriging can be done with computer programs for linear kriging, the work is most efficiently carried out with programs written specifically for the method, such as those in Deutsch and Journel (1998), particularly at the estimation stage. Searching for samples within a neighborhood takes up a large proportion of the computer time required in kriging. Therefore, all sets of equations should be set up and solved after each search. Modifying an existing kriging program or obtaining a program for indicator kriging has clear advantages over simply running a standard program once for each cutoff. Aside from a savings in time, a program for indicator kriging must check for problems in order relations, described next.

Assume that the rank-ordered cutoffs are $\{z_1 < z_2 < z_3 < \ldots z_L\}$; estimated probabilities must obey the order relations:

$$P^*(v;z_l) \leq P^*(V;z_{l+1})$$

for all l. Because the systems of equations are solved separately, proper order relations are not guaranteed. Violations are usually minor and can be corrected by using an approximation:

$$\begin{aligned} P^{**}(V;\, z_l) &= \text{Max } \{P^*(V;\, z_l),\, 0\} \\ P^{**}(V;\, z_l) &= \text{Max } \{P^{**}(V;\, z_{l-1}),\, P^*(V;\, z_l)\} \\ P^{**}(V;\, z_L) &= \text{Min } \{P^{**}(V;\, z_L),\, 1\} \end{aligned}$$

The first and third corrections ensure that the estimated probabilities lie between 0 and 1. This procedure must start with the lowest cutoff. With modification, this procedure can start with the highest cutoff. Finally, the average of the upward- and downward-corrected values can be calculated, the approach used in GSLIB (Deutsch and Journel, 1998).

Ways of avoiding order relation problems include constraining weights to be non-negative and using median kriging. Constraining the weights requires special programming, and is not often implemented.

Order relations occur when different semivariograms are used for each cutoff; a single weighting scheme corresponding to the median cutoff resolves this problem but also loses one of the advantages of indicator kriging, i.e. the covariance models provide a more detailed description of the spatial continuity of the variable than the one model corresponding to the median. Rather than trying to avoid order relation problems, one is probably better off using conventional indicator kriging and making the required corrections.

6.2.1 Working with the cdf

The result of indicator kriging is a set of cutoff values, and an estimate of the probability of not exceeding that cutoff. Depending upon the number of cutoffs, these results give a more-or-less complete picture of the expected value of the regionalized variable at a given location, and can be graphed as either a conventional histogram or a cumulative distribution function. From this cdf, we can compute some measure of central tendency such as a mean or median, and a measure of uncertainty such as an estimation variance.

We can also draw several types of maps, including maps of the probability of exceeding or not exceeding each cutoff. Because we want to map an estimate of the regionalized variable at each location, we must compute a mean in the following way:

$$z_{ik}^{*} = \sum_{l=1}^{L} z'_l [P^{*}(V;z_{l+1}) - P^{*}(V;z_l)]$$

where z'_l is a central value of the interval $[z_l, z_{l+1}]$. This central value can be set equal to the midpoint of the interval or to the observed mean of all values between the two cutoffs. The lower and upper tails of the distribution must be handled by one of several possible ways. Taking the upper tail, for instance, one can use the midpoint between the uppermost cutoff specified and the maximum value in the observed data. A hyperbolic model is useful for the upper tail in positively skewed data. By adjusting constants in the hyperbolic model, one can control the length of the tail and how quickly it declines.

An option provided in GSLIB is to use the observed data above the upper cutoff to divide the interval between this cutoff and a specified maximum value into several sub-intervals of equal probability. These sub-interval probabilities must sum to that for the interval as a whole. This approach of interpolating between tabulated quantiles can be used for interpolating between cutoffs, and for the lower tail.

Percentile maps can be drawn from the conditional distribution function fitted at each grid node. For instance, the median can be found by interpolating between z_a and z_{a+1}, where $P^{*}(V; z^a)$ is the highest value of

$P^*(V; z_l)$ less than 0.5. The same procedure yields a percentile for any value; it is not limited to the 50*th* percentile. With appropriate choice of percentages, we can compute and map upper and lower confidence intervals.

Indicator kriging gives risk-qualified estimates without the assumption of multivariate normality required for using estimation variances from linear kriging. A desirable side-effect obtained from indicator kriging is robustness of semivariograms and estimates to extreme values in the regionalized variable. Because transformation from raw values to indicator variables uses the rank order of the data, extreme values affect only the number of cutoffs one wants to consider.

6.3 EXAMPLES

The case studies that follow illustrate semivariograms for indicator variables defined by a number of cutoffs. In the first two examples, I stop with the fitting of models; the third example uses the models and indicator kriging to map initial potentials.

6.3.1 Initial potential in Barbour County

The 674 values of gas initial potential in Devonian clastics of Barbour County, West Virginia, show no pronounced trends with direction. Semivariograms were calculated for four cutoffs. These cutoffs and percentages of values below each cutoff are as follows:

400 Mcfpd	25%
792	50
1399	75
2477	90

At the lowest cutoff, a nugget effect dominates the semivariogram (Fig. 6.5), which is described by an exponential model.

Nugget effect = 0.13
Constant = 0.015
Range = 3 m

The other cutoffs were also fitted with exponential models and nuggets effects. For cutoff 2 (Fig. 6.6) the following constants were used.

Nugget effect = 0.19
Constant = 0.10
Range = 3 km
Anisotropy ratio = 0.33
Major axis is north–south

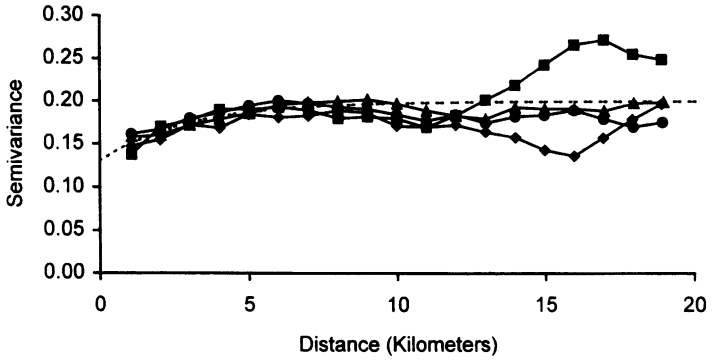

Figure 6.5 Directional semivariograms and model of gas initial potential in Barbour County for the 400 Mcfpd cutoff. Directions are diamonds: north–south; filled circles: northeast–southwest; squares: east–west; and triangles: southeast–northwest. Dashed line shows the isotropic model.

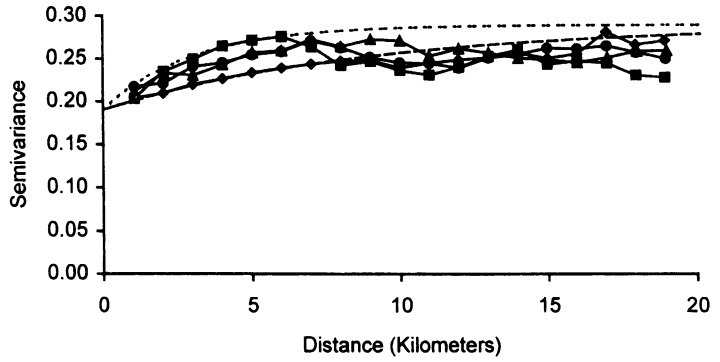

Figure 6.6 Directional semivariograms and anisotropic model of gas initial potential for the 792 Mcfpd cutoff. Directions are diamonds: north–south; filled circles: northeast–southwest; squares: east–west; and triangles: southeast–northwest. The model represented by the long dashes is for the north–south direction, the other for the east–west direction.

For cutoff 3 (Fig. 6.7):

Nugget effect = 0.11
Constant = 0.09
Range = 1.5 km
Anisotropy ratio = 0.5
Major axis is north–south

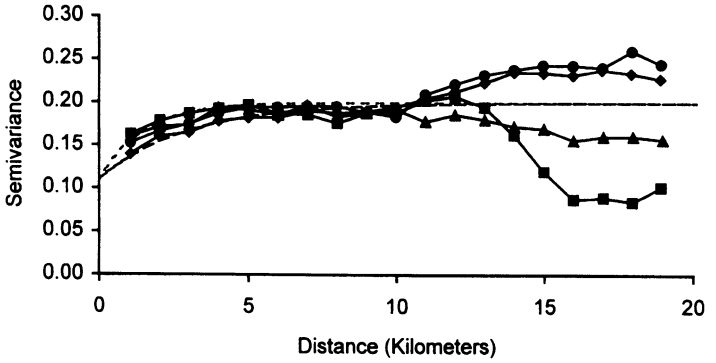

Figure 6.7 Directional semivariograms and anisotropic model for gas initial potential for the 1399 Mcfpd cutoff. Directions are diamonds: north–south; filled circles: northeast-southwest; squares: east–west; and triangles: southeast–northwest. The model represented by the long dashes is for the north–south direction, the other for the east–west direction.

For cutoff 4 (Fig. 6.8):

Nugget effect = 0.07
Constant = 0.025
Range = 2 km (isotropic)

Semivariograms for the highest and lowest cutoffs have the largest nugget effects relative to the constants for the exponential model. This is not unusual for variables constructed through the indicator transform. In this case, the observation can be interpreted as there being a background level of gas accumulation throughout the study area. Superimposed on this background are poorly-defined north–south trends in gas quantity

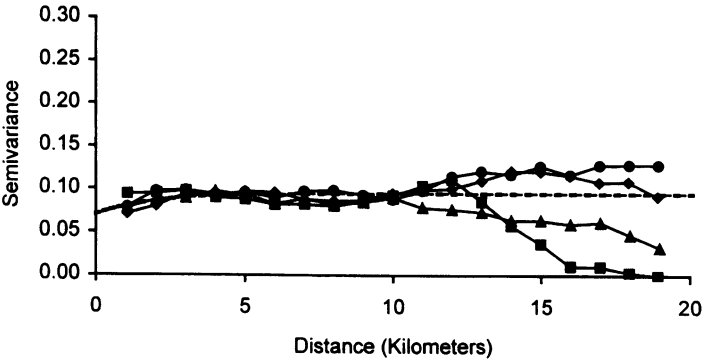

Figure 6.8 Directional semivariograms and model for gas initial potential at 2477 Mcfpd cutoff. Directions are diamonds: north–south; filled circles: northeast–southwest; squares: east–west; and triangles: southeast–northwest. Dashed line shows the isotropic model.

(spatial covariance is low). Several sweet-spots are more-or-less randomly scattered across the area represented by these data.

Semivariogram models do not need to be understandable, nor explanatory. However, we can sometimes ask ourselves if the observed semivariograms and the models appear to make sense. It is possible to invest a lot of time in modeling a semivariogram and constructing estimates, only to discover that the computer program was reading the wrong data. When carrying out a multiple-step procedure such as indicator kriging, one should occasionally step back from the work at hand, and ask whether the expected results are being obtained.

Kriging each indicator variable gives a separate map that is interpreted to be the probability that initial gas potential will exceed that cutoff for a new well (Figs. 6.9–6.12). Each map can look different from the others, in part because semivariogram models differ in range, anisotropy, and relative nugget effect. Indeed, maps for the 50*th* and 75*th* percentiles have a more north–south trend than maps for the other two cutoffs.

Computed probabilities and midpoints of each interval were used as described above to compute an estimate of initial potential across the area mapped (Fig. 6.13). Trial and error showed that good results were obtained when values above and below the minimum and maximum cutoffs were computed by interpolating between tabulated quantiles as

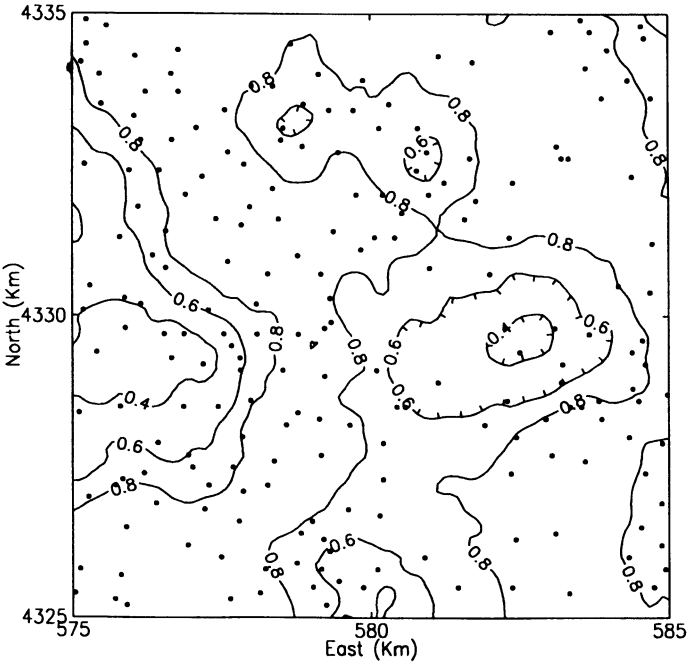

Figure 6.9 Probability that initial potential will not exceed 400 Mcfpd.

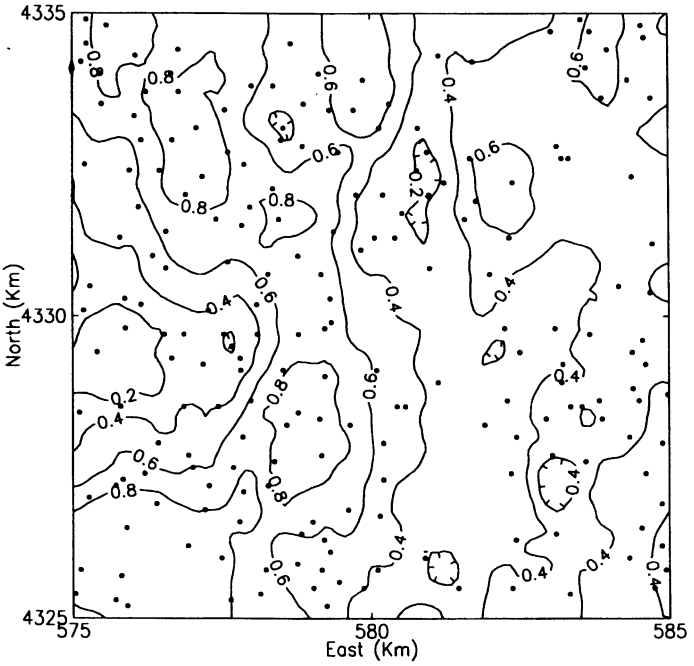

Figure 6.10 Probability that initial potential will not exceed 792 Mcfpd.

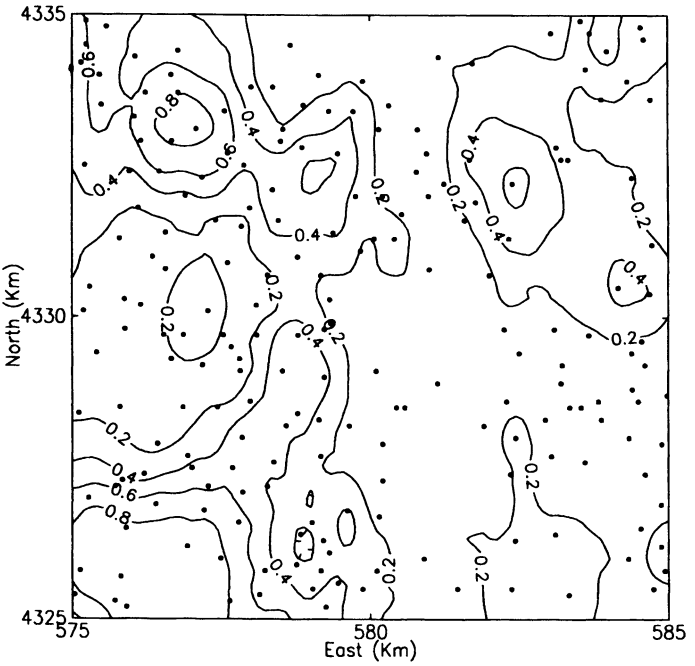

Figure 6.11 Probability that initial potential will not exceed 1399 Mcfpd.

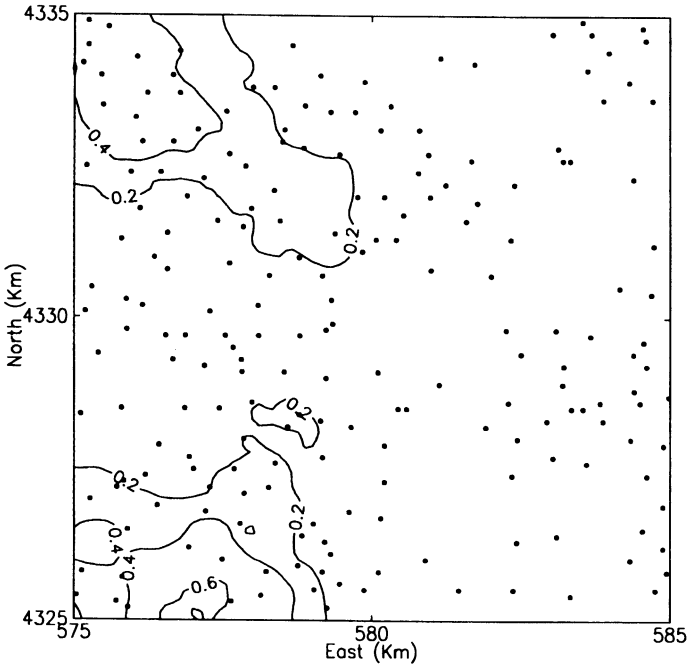

Figure 6.12 Probability that initial potential will not exceed 2477 Mcfpd.

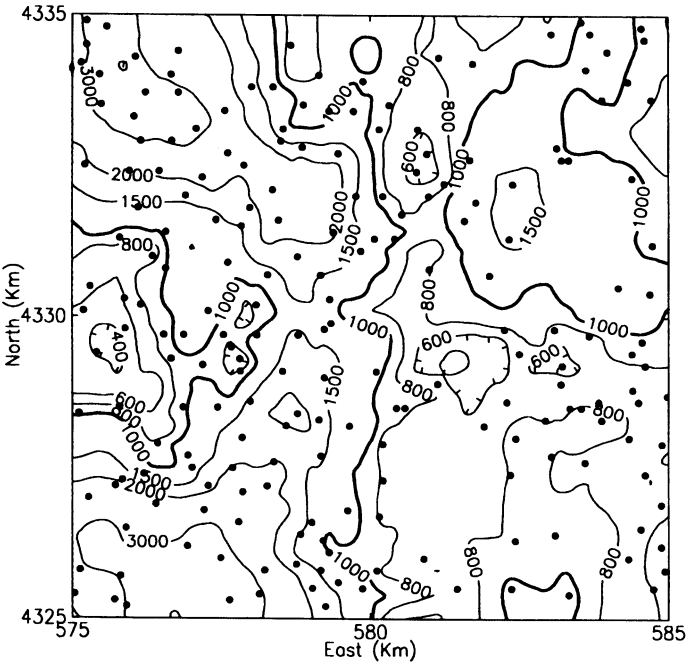

Figure 6.13 Contoured initial potential of gas from indicator kriging. Units are thousand cubic feet of gas per day (Mcfpd). The contour interval is irregular.

described earlier. Comparing results of indicator kriging with ordinary kriging of log-transformed data (Fig. 6.14) shows very similar maps.

Ordinary kriging of raw, untransformed data yields a measure of estimation variance that is constant for a given spatial configuration of data. Hence, maps of estimation variance, or estimation standard deviation, consist of concentric circles around individual points, coalescing in areas between points. Because indicator kriging provides a cdf at each grid location, we can compute the lower and upper 16% quantiles, and map this quantity. This quantity is like the estimation standard deviation of conventional kriging. Results show that uncertainty in the estimates depends not only upon data configuration, but also the values of initial potential (Fig. 6.15). Notice how the estimation standard deviation increases along trends to the northwest and to the southwest. Our measure of uncertainty no longer shows those rather unbelievable concentric rings around individual data points.

By the way, the estimation variance for lognormal kriging shares with indicator kriging this property of dependence on data values. Unlike the formula for estimation variance in ordinary kriging, that for lognormal kriging includes the log estimate as a term. Why, then, not use lognormal

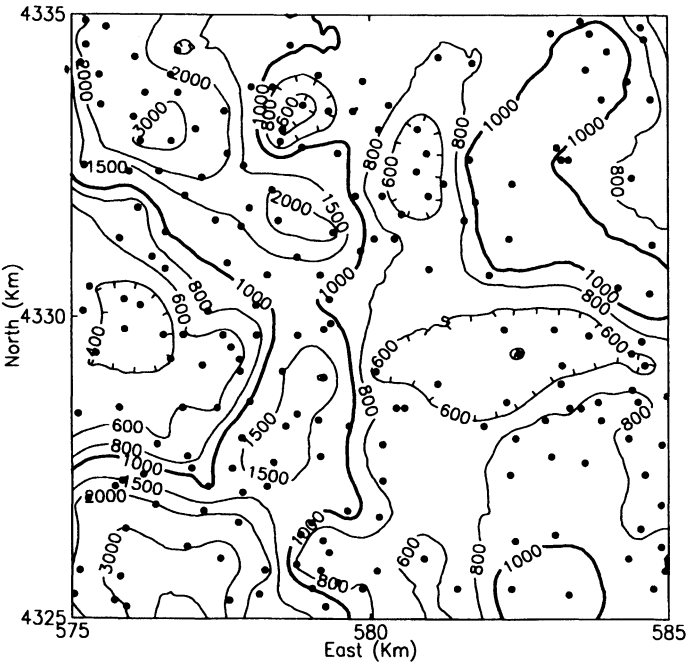

Figure 6.14 Contoured initial potential of gas from lognormal kriging. Units are thousand cubic feet of gas per day (Mcfpd). The contour interval is irregular.

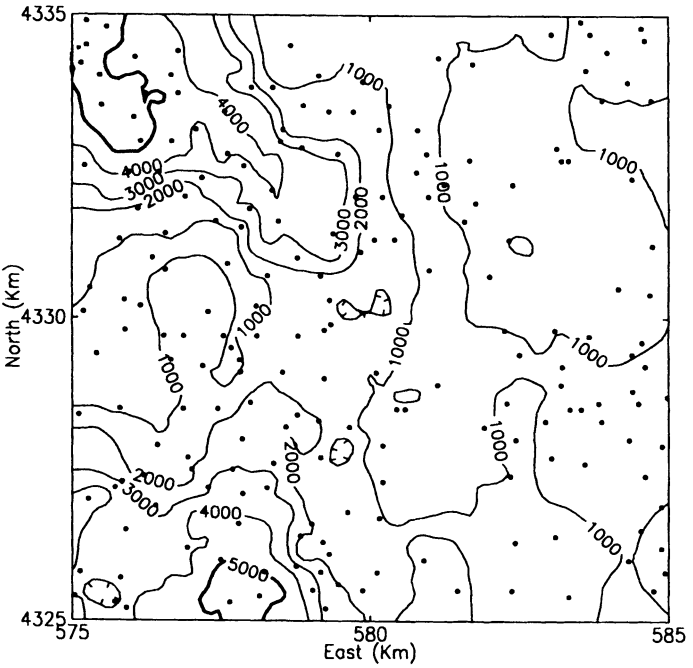

Figure 6.15 Contoured 'estimation standard deviation' of estimates of initial potential calculated with indicator kriging. The contour interval is 1000 Mcfpd.

kriging? Indicator kriging makes few distributional assumptions, and permits greater flexibility in modeling spatial dependence.

6.4 MEDIAN KRIGING

The flexibility and sensitivity that indicator kriging offers in modeling spatial dependence comes with a cost: the number of semivariograms that must be modeled, and the number of sets of equations that must be solved. **Median indicator kriging** (Journel, 1983) has been proposed as a practical shortcut for many data sets. Using this approach, one computes and models the semivariogram for the median of the data. Kriged estimates are still calculated for a number of cutoffs, but now the same semivariogram model is used for all cutoffs, meaning that only one set of equations needs to be solved.

If semivariograms calculated for a number of cutoffs are very similar, median indicator kriging should give results very similar to indicator kriging, and for the initial potential data, this is indeed true (Fig. 6.16). Estimates illustrated in this map were calculated by using nine cutoffs representing deciles of the data, and the anisotropic model for the 792 Mcfpd cutoff was used. The map of estimated initial potentials from

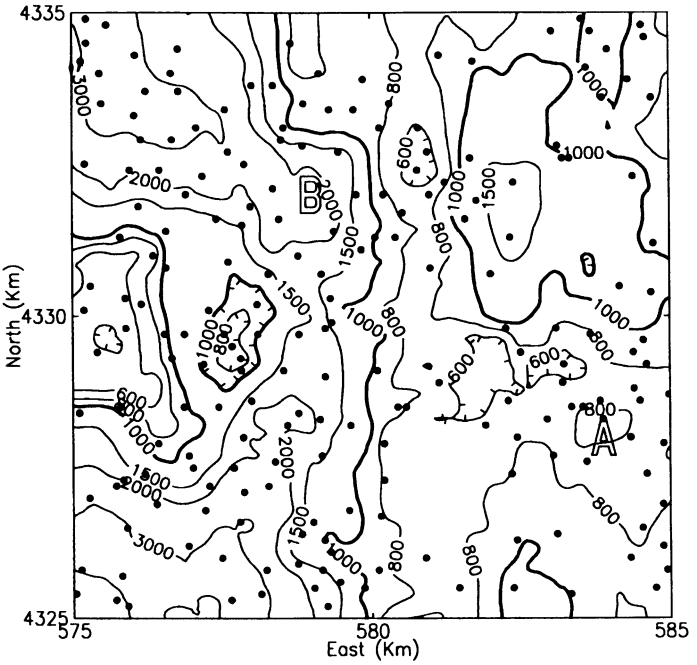

Figure 6.16 Contoured initial potential of gas from median indicator kriging. Units are thousand cubic feet of gas per day (Mcfpd). The contour interval is irregular.

median indicator kriging appears to have somewhat more of a north–south trend than the previous map. This is explained by the use of an anisotropic model for all cutoffs. Obviously, median indicator kriging is inappropriate if we were primarily interested in computing the probability of exceeding, or not exceeding particular cutoffs. Semivariograms for the higher cutoffs do not display noticeable anisotropy, and it would be incorrect to use an anisotropic model for estimating such probabilities.

Interested readers might want to consult Goovaerts (1994) for relative performance of methods for indicator kriging and Lajaunie (1990) for a comparison with disjunctive kriging.

6.5 CUMULATIVE DISTRIBUTION FUNCTIONS

One of the interesting features of indicator kriging is that cumulative distributions functions can take on very different, sometimes bizarre shapes from place to place in a study area. In contrast, we assume normal cdfs for ordinary kriging, and so, armed with an estimate and estimation variance at a location, we must draw a normal curve to

represent the cdf. For lognormal kriging, cdfs across our map have the same general shape, but are skewed to a lesser or greater degree from place to place. Disjunctive kriging is much the same; cdfs vary from place to place in the mean and variance, with a corresponding change in skewness.

Figures 6.17 and 6.18 compare cdfs for two locations: one with a low estimate for initial potential (location A on Fig. 6.16), and one for a high estimate (location B). The distributions can be viewed as cumulative functions, or in histogram form. They show that the two cdfs differ in both location and scale, and the one with the higher estimate has the larger spread in values, characterized by a large tail that goes beyond the interval graphed. In addition, neither cdf is normal, especially the one with the higher average.

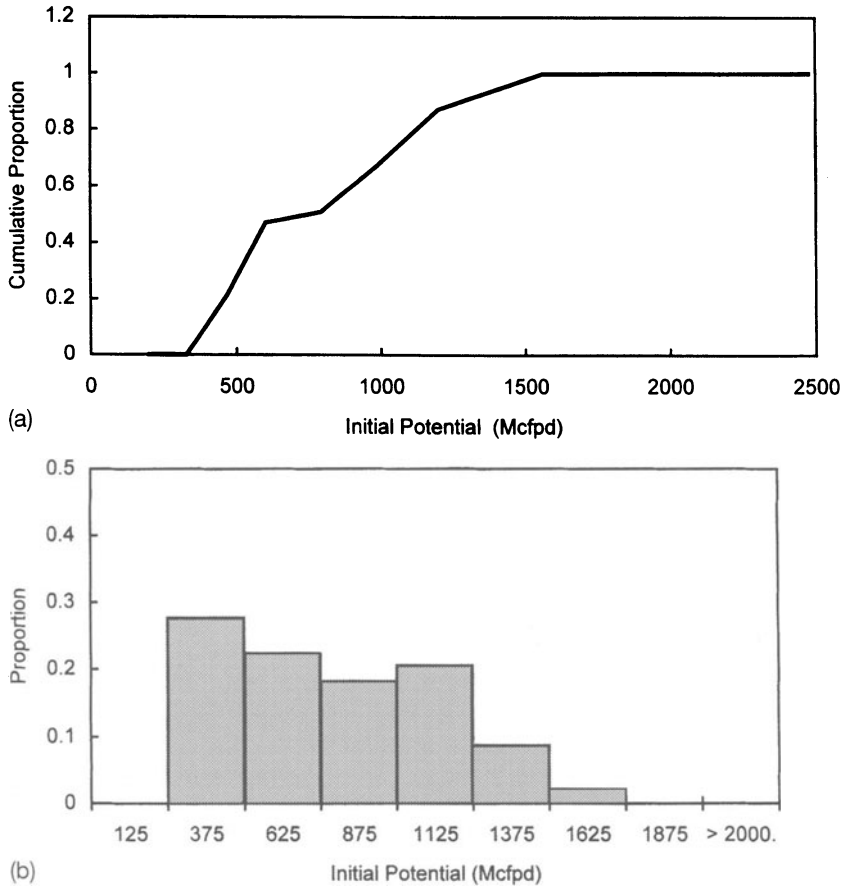

Figure 6.17 Local cumulative distribution and histogram of initial potential at location A in Fig. 6.16.

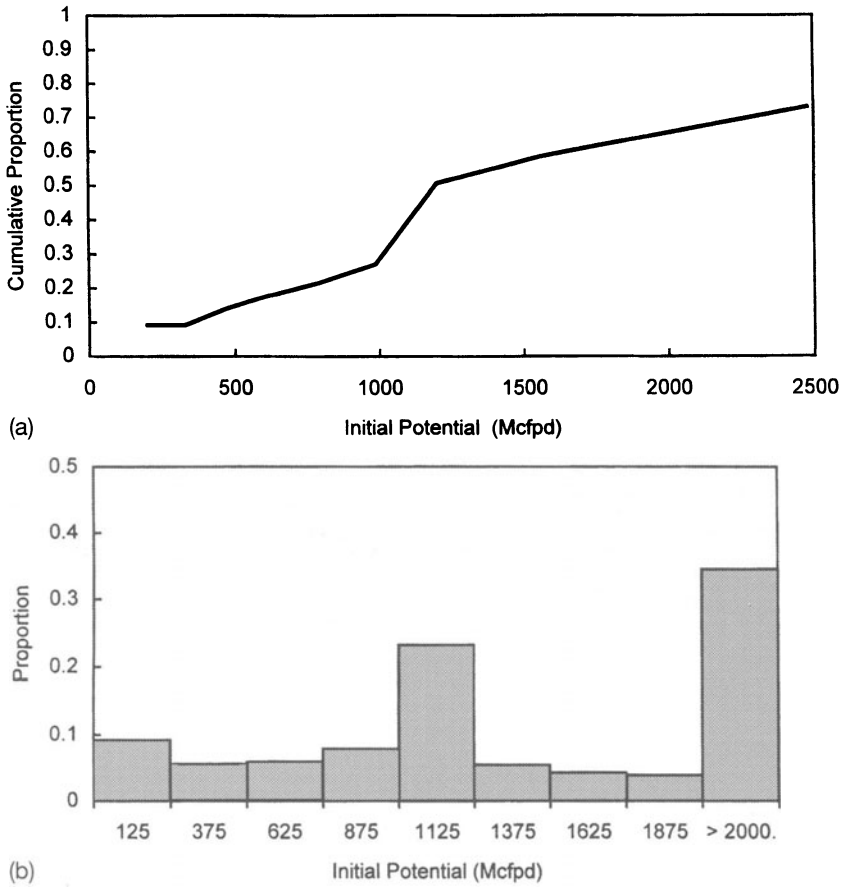

Figure 6.18 Local cumulative distribution and histogram of initial potential at location B in Fig. 6.16.

6.6 SOFT DATA

Some data – formation tops come to mind – can include both 'hard' information, for which we know a value, and 'soft' information, for which we know the true value lies within certain limits. Taking structural data as an example, we might know the top of a particular formation in some wells, and the top of an overlying formation in others. The first set of wells provide hard data, the second soft data. When we draw a structure contour map, we would like to use all available data, but we can only use the soft data very easily if we contour by hand. Most computer programs cannot utilize soft data. Yet, we know that shallower formation tops can provide constraints on the elevation of the top of the formation of interest at some locations.

However, indicator kriging provides a way out of this problem. Because one must transform formation tops to a set of indicator variables that specify whether the top is above or below each specified elevation, soft data is easily incorporated in the analysis. Assume that we are mapping the formation top in terms of distance below sea level. For all subsea depth cutoffs less than total depth below sea level, we can record a value for the corresponding indicator variable. For cutoffs greater than total depth, we record a missing value that is not considered during estimation.

6.7 FACIES MODELING

The spatial relationships between two or more sedimentary facies often determine recovery efficiency within an oil field. In studies of reservoir heterogeneity, determining vertical and horizontal distribution of permeability plays an important role. In some cases, permeability is linked to facies; for instance, low permeability shales within predominantly sandstone units can act as barriers to flow, or high-permeability sandstones interbedded with low-permeability clastic sediments can lead to deleterious water breakthrough during waterflooding. In other cases, empirical relationships between porosity and permeability can differ among lithologic units. Accurate prediction of permeability from porosity requires determination of lithofacies.

Mapping lithofacies in a petroleum reservoir is an obvious application of indicator kriging. The simplest case is when only two facies are present. For example, the Granny Creek oil field described in earlier chapters can be divided vertically into a lower, distal facies deposited in distributary mouth bars. These intergrade with proximal mouth bar sediments, overlain by fluvial channel deposits. In the original study, four facies were identified from geophysical logs (Hohn *et al.*, 1997), but for this example, I assigned the two most distal facies a value of one, and the two proximal facies a value of zero.

Based on data from the entire field, semivariograms were fitted with the following model (Figs 6.19 and 6.20):

$$\gamma(h) = 0.025Sph\left(\sqrt{\frac{h_h^2}{0.001^2} + \frac{h_v^2}{\infty^2}}\right) + 0.035Sph\left(\sqrt{\frac{h_h^2}{250^2} + \frac{h_v^2}{1^2}}\right)$$

$$+ 1.0Sph\left(\frac{\sqrt{h_h^2}}{100000^2} + \frac{h_v^2}{90^2}\right)$$

Indicator kriging of a volume of the reservoir gives a set of probability maps such as that in Fig. 6.21. This is the probability that the lithofacies

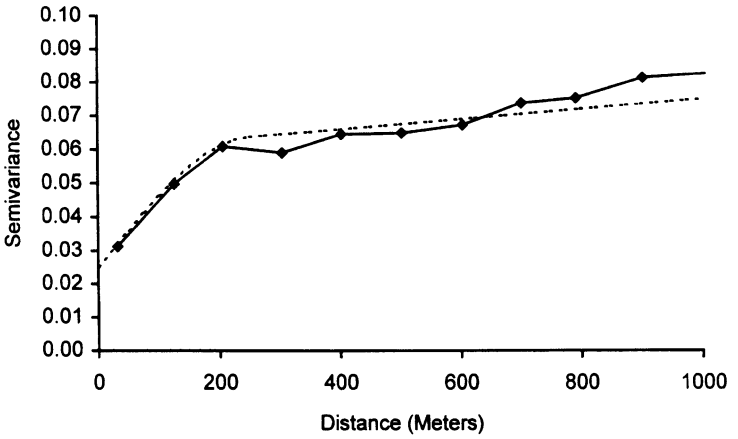

Figure 6.19 Directional semivariogram of a facies indicator variable in the horizontal direction. Dashed line shows model.

is the distal one. By assigning this facies to each coordinate where the probability exceeded 0.5, a map like Fig. 6.22 results. Figure 6.23 represents the lithofacies at another level within the reservoir. Vertical slices through the middle of the volume show the interfingering of the two lithofacies (Figs 6.24, 6.25).

Most problems of this type require more than two lithofacies. If lithofacies can be placed in some kind of order, conventional indicator kriging is straightforward. For each coordinate in a volume, a predicted lithofacies is assigned based on which one has the largest probability. Given three lithofacies numbered 1, 2, and 3, for instance, we can use

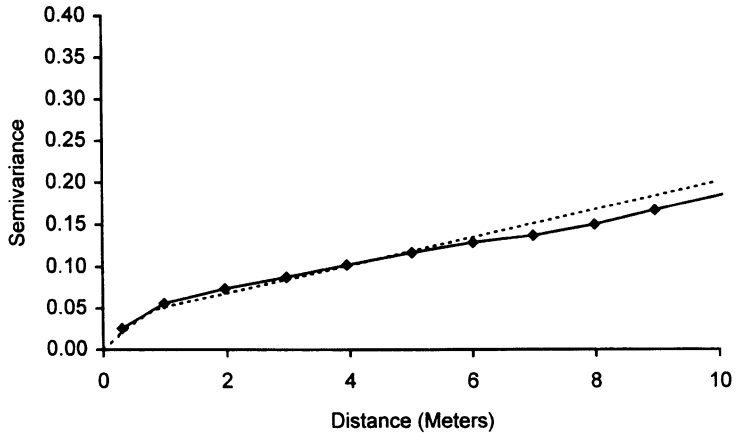

Figure 6.20 Directional semivariogram of a facies indicator variable in the vertical direction. Dashed line shows model.

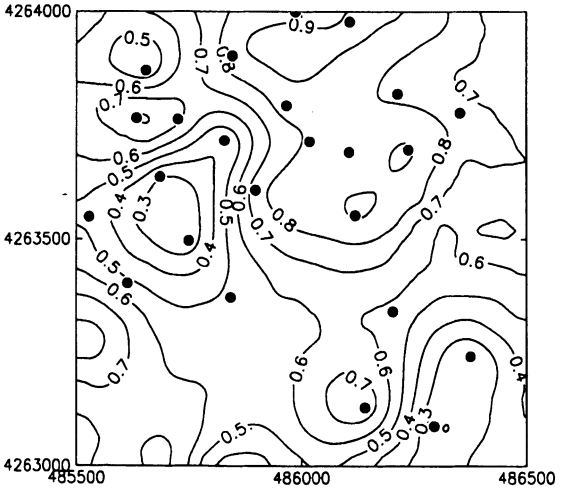

Figure 6.21 Contoured probability that rock at an elevation 2.5 m above the base of the reservoir represents the distal facies. Solid circles are well locations.

indicator kriging as described above with two cutoffs, 1.5 and 2.5, gives the probability that the lithofacies is equal to 1, equal to 1 or 2, or equal to three. The difference between the first two probabilities gives the probability that the lithofacies equals 2. The lithofacies with the highest predicted probability would be assigned to each coordinate on a surface or within a volume.

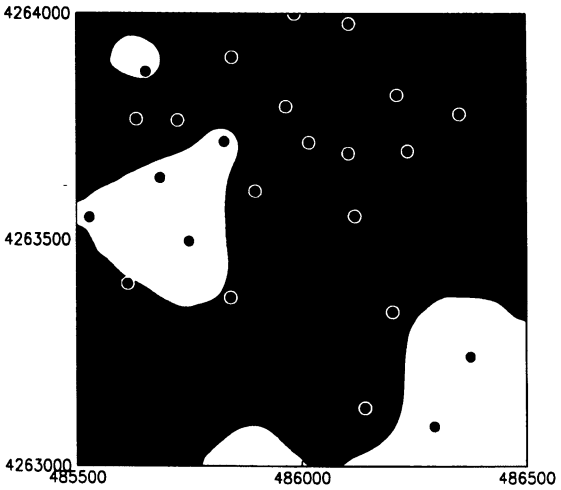

Figure 6.22 Facies map derived from Fig. 6.21. Black areas represent the distal facies.

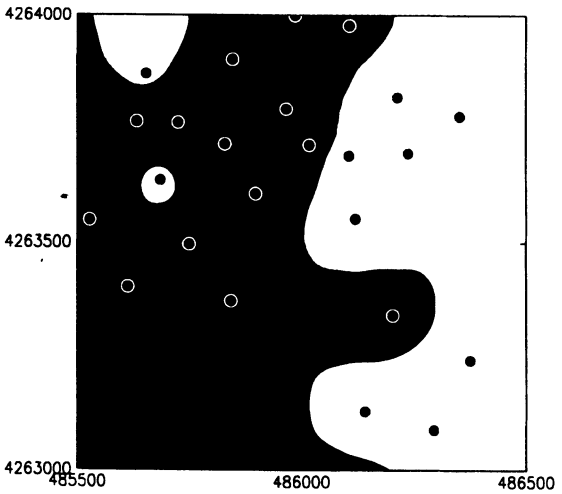

Figure 6.23 Facies map at an elevation 4 m above the base of the reservoir.

Although *ad hoc*, this approach makes sense in many situations. Within a clastic reservoir, for instance, lithofacies are often defined on the basis of average grain size, and might range from shales, to shaley siltstones, siltstones, silty sandstones and sandstones. These discrete categories in fact represent a discretization of a continuum of rocks differing in grain size, and are in a sense indicator variables with upper and lower cutoffs. If we could quickly measure grain size in the well, true indicator variables could be defined and mapped using straightforward indicator

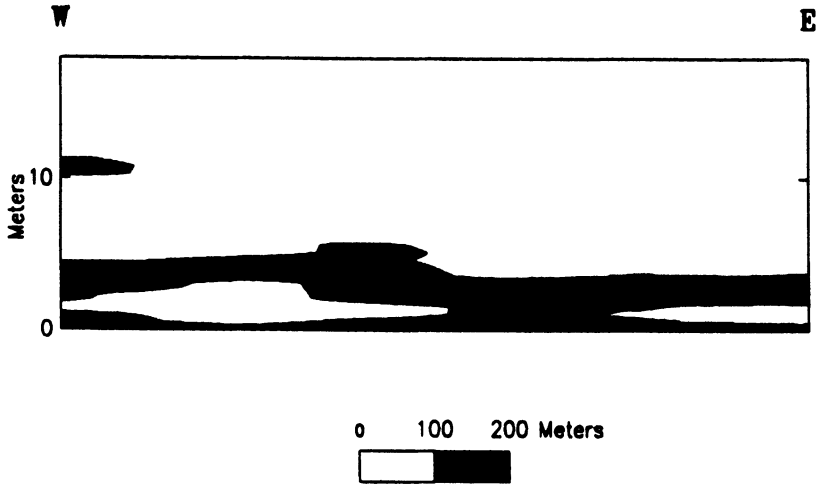

Figure 6.24 East–west cross-section of facies at northing 4263500.

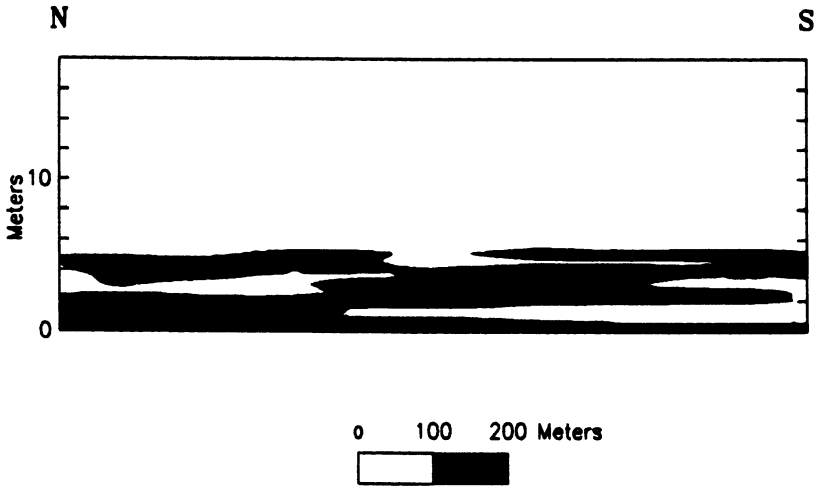

Figure 6.25 North–south cross-section at easting 486000.

kriging. More often, geophysical logging tools are used to infer grain size or rock type indirectly. This was the case for the data used in the preceding example, in which rock types were determined from density and gamma-ray logs (Hohn *et al.*, 1997).

Dimitrakopoulos and Dagbert (1993) took a different approach; they recognized similarities between mapping rock types and indicator kriging, but viewed the problem as one having to do with rock types that define proper subsets of the space or volume. They called their rock types relative indicator variables. The method they proposed begins with a set of rock types D_K, ordered such that the space occupied by D_k is contained within the space occupied by rock type D_{k+1}. Presence or absence of rock type 1 is first estimated. Within the subspace that rock type 1 is estimated to be absent, rock type 2 is estimated. Where rock type 2 is absent within this subspace, rock type 3 is estimated. And so forth. The advantage of relative indicator kriging is that order relations are maintained. Obviously, results depend on the sequencing of lithotypes, and the effects of mis-specification – getting the sequence wrong – are unknown.

Soares (1992) defined an indicator variable as simply the presence or absence of a given rock type, without any implication of ordering of rock types. Spatial dependence is measured with a covariance or semivariogram, as usual, but with a difference. Semivariograms representing each rock type are summed to give a **multiphase variogram**, which measures the probability that locations x and $x + h$ manifest different rock types. Solving a single set of kriging equations yields a set of probabilities for each rock type at each location.

For a given location, one can assign the rock type having the highest probability of occurrence. To preserve the overall proportion of lithologies in a study area, a more sophisticated approach is probably needed. Soares (1992) proposed a scheme in which the probabilities of each rock type are sorted into descending order. If lithology k has a proportion p among n locations, it is assigned to the p^*n locations at which the probability of lithology k exceeds that of all other lithologies. Dimitrakopoulos and Dagbert (1993) used the same method for going from probabilities to an allocation of lithologies.

Similarly, I could be more sophisticated in assigning my two lithologies to each location, using the overall proportion of the distal lithotype to determine a probability level for going from Fig. 6.21 to Fig. 6.22. This proportion equals 0.14, the probability level exceeded by 14% of the values equals 0.62; the resulting map has less of this lithotype than before (Fig. 6.26).

Because the proportion of lithotypes changes from the top of the reservoir to the bottom, it makes even more sense to compute a proportion at each level of the reservoir, and use these proportions as thresholding probabilities. Beucher *et al.* (1993) and Le Loc'h and Galli (1997) used a **vertical proportion curve** in their work, and in fact extend the concept to three dimensions.

The number of methods for estimating lithologic types is increasing. A potential difficulty with many approaches is the assumption of an order relationship among the facies. This assumption often makes sense for facies based on grain size or environment of deposition. Although they

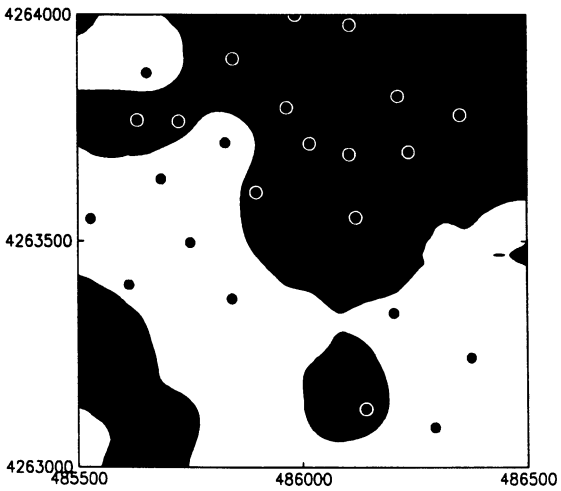

Figure 6.26 Facies map derived from Fig. 6.21, assigning the distal facies to every location where the probability of this facies exceed 0.62.

do not always require that transitions between facies are only between adjacent facies within the order, it is not clear what the effect on the results would be if, for example, a fluvial facies cut across several more distal facies.

Rivoirard (1993) summarized the types of arrangements that can occur among rock types, ranging from complete disorder to a strict ordering with transitions. At the one end are **mosaic models**, in which there is no requirement that particular rock types occur adjacent to each other, or that there exists ordering or sequence of rock types. If one could travel around the space occupied by the lithologies, as one left one lithology, the new lithology could not be predicted. At the other end are his **diffusion** models, in which there is not only a sequence of rock types, but to travel from rock type i to rock type $i + 2$, one must travel through rock type $i + 1$. Between these extremes are models in which there is a sequence of rock types, but one can skip categories in the sequence while traveling around the reservoir. Rivoirard gave examples of the semivariograms one might expect under these models, and the appropriate analyses.

Rivoirard's diffusion model fits the cross-section shown in Fig. 6.27, where rocks of the finest grain size are surrounded by rocks of slightly coarser grain size, and so forth; transitions between lithologies are smooth. In Fig. 6.28, there is a definite order of lithologic types, but transitions can be abrupt. This is the picture we see in stacked, fining-upward sequences typical of many fluvial deposits.

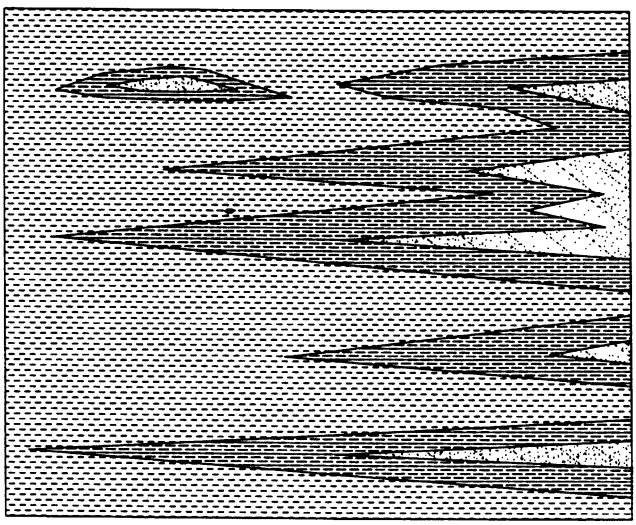

Figure 6.27 Hypothetical cross-section illustrating the diffusion model of facies architecture. Not to scale.

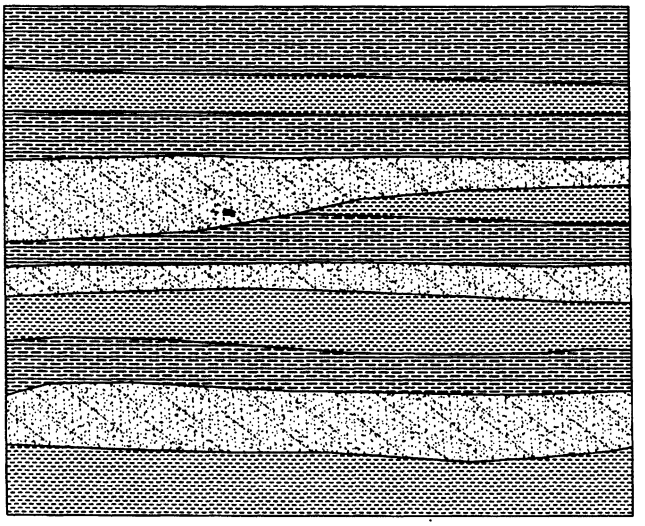

Figure 6.28 Hypothetical cross-section illustrating a model of facies architecture less severe in requirements than the diffusion model of Fig. 6.27. Not to scale.

6.8 PROBABILITY KRIGING

Consider the uniform transform:

$$y(x) = \text{estimated probability } [z(x) \geq z]$$

where the values $y(x)$ are uniformly distributed in the interval (0, 1). For n data, the quantity $n{\cdot}y(x)$ is simply the rank order of $z(x)$. As in nonparametric univariate statistical tests, geostatistics based on ranks are robust to the presence of outliers and nonnormal distributions. Used in conjunction with the transform to indicator variables, the uniform transform leads to an estimator called 'probability kriging' (Sullivan, 1984; Journel, 1985):

$$P^*(V;z_l) = \sum_{k=1}^{n} \lambda_k(z_l) i(x_k;z_l) + \sum_{k=1}^{n} \kappa_k(z_l) y(x_k)$$

with

$$\sum_{k=1}^{n} \lambda_k(z_l) = 1 \qquad \sum_{k=1}^{n} \kappa_k(z_l) = 0$$

for each cutoff l. This estimator utilizes a cokriging system of equations of dimensions 2n + 2, and requires not only an indicator semivariogram for each cutoff, but a semivariogram for the uniform transformation, and a cross-semivariogram between transformed data and each indicator

variable, to give a total of $2L+1$ semivariograms and cross-semivariograms.

Other than the greater burden in modeling spatial continuity, this new estimator requires the same computations as indicator kriging, including the check for problems in order relations and subsequent adjustments. Because the transform must be one to one, a step must be added when duplicate values are present in the data. A frequent occurrence in geological data is the presence of a 'spike' in the histogram below some lower level of detection. Although one can remove such a spike by assigning ranks at random, a more sophisticated approach exploits spatial autocorrelation of the data. Given two data values that are equal, this approach assigns the higher rank to the point surrounded by the larger observed values. A program in Verly (1984) finds all samples within a specified radius from a point and calculates a local average. These local averages are used to break tied ranks.

Probability kriging represents an attempt to calculate estimates that are less sensitive than indicator kriging to the choice and number of cutoffs and estimates that more fully reflect local variability of the raw data while maintaining robustness to outliers and nonnormality. In a comparison of these nonparametric estimators, Sullivan (1984) graphed estimated versus observed values for a number of cutoffs. One drawback to indicator kriging occurs when sample spacing is nearly uniform and approaches the range of the semivariogram for a given cutoff. Because only a small number of samples lie within the range, a limited number of possible 0, 1 outcomes, and therefore estimated values, are possible for a given sample configuration. The result is a very noisy map for that cutoff. The estimator employing rank order largely avoids this difficulty. Sullivan also shows that indicator kriging yields smoother estimates than does the more complex estimator. All kriging methods give smoothed estimates such that the variance of the estimates is less than that of the actual data: large values are underestimated, and low values are overestimated. In general, one prefers to lessen the smoothing property of an estimator while maintaining some robustness to extreme values. It can be shown in theory and actual examples (Sullivan, 1984) that the variance of estimates from probability kriging lies between those for indicator kriging and ordinary kriging. As in any method of estimation, the degree of smoothing depends upon the relative magnitude of the nugget effect to the sill and the range.

I have not included detailed examples of probability kriging because it consists of a simple extension of computational methods discussed in this and earlier chapters, and results look similar to those from indicator kriging. Sullivan's dissertation discusses both methods in detail, and provides FORTRAN code for computing indicator semivariograms and cross-semivariograms, indicator kriging, and probability kriging. FORTRAN code for despiking is found in the dissertation by Verly (1984).

GSLIB (Deutsch and Journel, 1998) provides most of the tools for probability kriging.

6.9 SUMMARY

An indicator variable takes on values of 0 or 1 depending upon the presence or absence of a feature. Although a variable may be nominal a priori, more often it results from a threshold applied to continuous data. An indicator variable can be estimated and mapped like any variable; results are probabilities of exceeding the cutoff.

The idea of applying a cutoff to continuous data can be developed further to give nonparametric estimates of the full range of a continuous variable. The geostatistician merely applies a number of cutoffs and computes semivariograms and kriged estimates for each cutoff. For a given locality, the result is a set of probabilities of exceeding each cutoff; these estimates are used to construct local frequency distributions and to construct mean, median, and isoprobability maps. The advantages of nonparametric estimation include robustness to nonnormality and outliers. The principal disadvantage is the large number of semivariograms that must be fitted if the number of cutoffs is large. However, one is left in the end with a clear picture of the univariate and bivariate distribution of a given set of data.

Median indicator kriging eliminates the chore of modeling several semivariograms by using the model at the median for all cutoffs. Probability kriging is a method that attempts to retrieve some of the information lost by transforming data to a set of indicator variables.

REFERENCES

Beucher, H., Galli, A., Le Loc'h, G., Ravenne, C. and HERESIM Group (1993) Including a regional trend in reservoir modelling using the truncated Gaussian method. in A. Soares (ed.), *Geostatistics Troia '92*, Kluwer Academic Publishers, Dordrecht, pp. 555–566.

Deutsch, C.V. and Journel, A.G. (1998) *GSLIB: Geostatistical Software Library and User's Guide*. Oxford University Press, New York, 369 pp.

Dimitrakopoulos, R. and Dagbert, M. (1993) Sequential modelling of relative indicator variables: Dealing with multiple lithology types, in A. Soares (ed.), *Geostatistics Troia '92*. Kluwer Academic Publishers, Dordrecht, pp. 413–424.

Goovaerts, P. (1994) Comparative performance of indicator algorithms for modeling conditional probability distribution functions. *Math. Geol.*, **26**: 389–411.

Hohn, M.E., McDowell, R.R., Matchen, D.L. and Vargo, A.G. (1997) Heterogeneity of fluvial-deltaic reservoirs in the Appalachian Basin: A case study from a Lower Mississippian Oil Field in Central West Virginia. *Amer. Assoc. Pet. Geol. Bull.*, **81**.

Journel, A.G. (1983) Nonparametric estimation of spatial distributions. *Math. Geol.*, **15**, 445–468.

Journel, A.G. (1985) Recoverable reserves estimation: The geostatistical approach. *Mining Engineering*, June 1985, 563–568.

Kumar, N. (1985) Estimating exploration potential in mature producing area, Northwest Shelf of Delaware Basin, New Mexico. *Amer. Assoc. Pet. Geol. Bull.*, **69**, 1903–1916.

Lajaunie, C. (1990) Comparing some approximate methods for building local confidence intervals for predicting regionalized variables. *Math. Geol.*, **22**, 123–144.

Le Loc'h, G. and Galli, A. (1997) Truncated plurigaussian method: Theoretical and practical points of view, in E. Baafi (ed.), Wollongong '96: 5th International Geostatistics Congress Preprints.

Pawlowski, V., Olea, R.A. and Davis, J.C. (1993) Boundary assessment under uncertainty: a case study. *Math. Geol.*, **25**, 125–144.

Rivoirard, J. (1993) Relations between the indicators related to a regionalized variable, in A. Soares (ed.), *Geostatistics Troia '92*, Kluwer Academic Publishers, Dordrecht, pp. 273–284.

Soares, A. (1992) Geostatistical estimation of multi-phase structures. *Math. Geol.*, **25**, 149–160.

Sullivan, J. (1984) Non-parametric estimation of spatial distributions. Unpublished PhD dissertation, Stanford University, 367 pp.

Verly, G.W. (1984) Estimation of spatial point and block distributions: The multigaussian model. Unpublished PhD dissertation, Stanford University, 416 pp.

CHAPTER 7

Conditional simulation

In the past ten years, conditional simulation has come be used in analysis and mapping of regionalized variables. An important advantage to the geostatistical approach to mapping lies in the modeling of spatial covariance that precedes interpolation; semivariogram models derived from this step can make the final estimates sensitive to directional anisotropies present in the data. On the other hand, the smoothing property of kriging can also mean that one throws away detail at the mapping stage.

In earlier chapters, I argue that the smoothing property of kriged estimates in the presence of a large nugget effect can be desirable when the geologist wants to estimate reserves. In other situations, the geologist may want to enhance extreme values, emphasize directional anisotropies, and otherwise exploit the fine-scale variation in data. In the place of local estimates with minimal estimation variance, the geologist wants a map that honors observed values of the regionalized variable, has the same degree of fine-scale variability as the observed data, and obeys the same spatial law. By relaxing the requirement of minimal squared error, conditional simulation sacrifices some certainty for more detail.

A simulation is said to be 'conditional' when it honors the observed values of a regionalized variable.

7.1 METHODS OF CONDITIONAL SIMULATION

This discussion of methods for simulation considers only the case in which we want to create a realization that passes through data provided by a user. As we will see, at least one method requires an initial realization that is not conditioned to data, but the results are usually conditioned in a subsequent step. Usually, we are interested in conditional simulations.

A taxonomy of simulations can divide methods into those that result in a conditioned result in the first step, and those that first yield a nonconditioned simulation, and then condition this result to the data. In

the first class belong so-called **sequential** methods and LU decomposition; to the second class belongs the now-classic **turning bands** method. Another method, **simulated annealing,** does not fit very well into this taxonomy. It begins with an initial realization, and trades values at pairs of grid nodes to satisfy a goodness-of-fit criterion, the objective function. Each of these methods is described below.

7.1.1 Sequential methods

In sequential simulation, a simulated value at each location u is drawn from a probability distribution function computed from actual and previously simulated values in the neighborhood of this location. The algorithm begins with a randomly selected location, and progresses sequentially across the grid representing the area to be simulated. The order of this progression is not specified by theory, but a random sequence is usually followed (Isaaks, 1990).

At each location, the computer program searches for points in a user-specified neighborhood; these points can include both data input to the program, and data that have been simulated in earlier steps. A probability distribution is computed from these points by way of one of a number of methods. How one computes this probability distribution distinguishes between types of sequential simulation, two of which are sequential indicator and sequential Gaussian simulation.

The **sequential indicator** method uses indicator kriging to compute the local probability distribution. This method requires input of a semivariogram model for each cutoff specified by the user. As in indicator kriging, one can elect to input for all cutoffs the semivariogram model for the cutoff corresponding to the median of the data, with some loss in accuracy. In simulating petrophysical variables such as permeability, one is interested in extreme values, and usually wants to provide accurate spatial models for the extremes in order to best capture the effect of permeability barriers or high-permeability zones on fluid flow through a reservoir. The time needed to model semivariograms for the tails is probably worth the effort.

Sequential Gaussian simulation computes a conventional kriged estimate and estimation variance from data transformed to normal scores. This approach requires a single semivariogram model based on transformed data. Once simulation at every node is complete, results are back-transformed to the original units.

Both sequential indicator and sequential Gaussian simulation require some decisions to be made about the tails of the distributions. Because the number of grid nodes to be simulated vastly outnumbers the number of input data in most situations, information provided by the input data is usually insufficient to yield reasonable values at the tails. Data sets in

petroleum applications are often long-tailed at the upper end, but with few values. As a result, the probability distribution in the tails is poorly known on a purely empirical basis from data at hand. The user must bring in some additional information gleaned from previous experience, or developed from the goals of the simulation. In cases where the number of control wells is large, the user can perform linear interpolation between quantiles computed from input data; this was explained in the chapter on indicator kriging (Chapter 6).

Programs such as GSLIB (Deutsch and Journel, 1992) give the user a menu of extrapolation such as a power model, a hyperbolic model, and linear extrapolation. In addition, parameters required by the power and hyperbolic models can create short or long tails. Here the judgment of the user comes into play. When reservoir parameters are to be used to compute volumetrics, one might want to select a conservatively short upper tail to avoid unrealistic overestimations of reservoir potential. On the other hand, when extreme values of permeability lead apparently to problems during secondary recovery, long tails are appropriate so that one can assess the total range of possible scenarios.

Whatever approach is used for computing a local probability distribution, the shape, mean, and spread of this distribution depends on the semivariogram input to the program, the locations of points in the neighborhood, and the values of the regionalized variable at these points. Where points are sparse, the spread tends to be wide, and the center near that of the regionalized variable. Near one or more control points or a previously determined simulation point, the spread tightens, and the center approaches that of these points. Of course, grid nodes coinciding with control points (within a reasonable tolerance) have centers equalling values at the controls points, and zero spread.

These probability distributions are then used to select a point at random. The range of values that might be selected is wide in areas of poor control, very narrow where data densities are high. As a result, results from repeated simulation of an area differ most from each other in areas of poorest control.

7.1.2 LU decomposition

This method uses a matrix algebra method called LU or Cholesky decomposition, using as input covariance between data locations and grid locations, a vector of independent normal random variables, and the conditioning data. First, a covariance matrix **C** is calculated:

$$\mathbf{C} = \begin{bmatrix} C_{11} & C_{12} \\ C_{21} & C_{22} \end{bmatrix}$$

Where C_{11} is covariance between data at control points, C_{22} is covariance between nodes on a grid, and C_{12} is covariance between data locations and grid nodes. LU decomposition gives matrices **L** and **U**, which when multiplied equal the matrix **C**:

$$\mathbf{C} = \mathbf{LU} = \begin{bmatrix} L_{11} & 0 \\ L_{21} & L_{22} \end{bmatrix} \begin{bmatrix} U_{11} & U_{12} \\ 0 & U_{22} \end{bmatrix}$$

Using the vector of known data z, and a vector of random variables w obtained from a random number generator, a vector of simulated values z_{cs} is given by:

$$z_{cs} = L_{21}L_{11}^{-1}z + L_{22}w$$

Notice that vector w has a number of entries equal to the number of nodes on the grid for simulation. Similarly, the covariance matrices can become very large, creating storage and computation time problems on the computer, as well as numerical inaccuracies when the covariance matrix has a large number of zero entries, i.e. dimensions of the area being mapped are much larger than the ranges of the covariance model used.

Nevertheless, this method has the advantages that it conditions in one step, it handles any kind of covariance function, and it is easy to implement using libraries of standard mathematical algorithms. Davis (1987) and Dowd and Saraç (1994) show practical ways to increase the size of grid that LU decomposition can handle, but at the cost of adding some complexity to the calculations.

7.1.3 Turning bands

At one time, the turning bands method was synonymous with simulation; it can handle problems of virtually any size, and was available in the literature. Error simulation methods such as the turning bands algorithm account for the smoothing effect of kriging by adding an error component having a mean of zero and an appropriate variance and semivariogram. The turning bands method thus has two steps: initial computation of a nonconditional simulation, and conditioning this simulation to the input data.

The turning bands method uses the fact that given a set of random numbers T_i and a weighting function f, a one-dimensional random function $Y(u)$ is:

$$Y(u) = \int_{-\infty}^{\infty} f(u + r)T(r)\mathrm{d}r = T^{*}f'$$

where $f'(u)$ is the transpose of $f(u)$; i.e. $f'(u) = f(-u)$, $T(r)dr$ is a stationary random measure that when discretized yields T_i, and * is the convolution product. Covariance of $Y(u)$ is:

$$C_1(S) = \sigma^2 f * f'$$

where σ^2 is the variance of Y. Thus, one can construct a one-dimensional sequence of values having a specified covariance.

A discrete approximation for $Y(u)$ is obtained by forming a series of random variables, T_i, independent of each other and belonging to the same distribution with a mean of zero and a specified variance. These values are computed by assigning points at regular intervals along a line to give $t_{i-k} \ldots t_i \ldots t_{i+k}$ and calculating the moving average:

$$Y_i = \sum_{k=-R}^{R} t_{i+k} f(kb)$$

The value b, is the distance of separation between adjacent values of t_i. When b is set to $\frac{a}{2R}$, where a is the range of a covariance or semivariogram model, the discrete approximation is simply:

$$Y_i = \sum_{k=-R}^{R} k t_{i+k}$$

A small bias in the one-dimensional covariance of Y_i can be corrected by a multiplicative factor (Journel and Huijbregts, 1978, p. 536).

The turning bands method extends the one-dimensional simulation to three dimensions. Given N lines D_1, D_2, ..., D_N corresponding to unit vectors uniformly distributed over the unit sphere, a simulated value $z_s(x)$ can be constructed from independent simulations along the lines:

$$z_s(x) = \frac{1}{\sqrt{N}} \sum_{i=1}^{N} z_i(x)$$

where $z_i(x)$ is the simulated value along line i which is within a band that is perpendicular to the line and that includes point x. Although one can choose large N, a value of 15 gives good results.

Adjusting values $z_s(x)$ to have the same approximate distribution as observed values, $z(x)$ requires two steps. First, minor deviations of simulated values from a zero mean and unit variance are eliminated by subtracting the actual mean of the simulated values, and multiplying by the variance. Second, adjusted values are scaled and centered to the desired mean and variance, usually the mean and variance of the conditioning data. When observed values of the regionalized variable

follow a normal distribution, only this centering and rescaling is needed.

When a regionalized variable does not follow a normal distribution, a transform to normality is applied to the conditioning data before calculating the mean, variance, and the semivariogram used in simulation. Once simulation is completed including conditioning, described next, simulated values are transformed by the inverse of the original transform. Hermite polynomial expansions may be used for the general case. Whatever the transform, simulation uses transformed values, and requires a semivariogram model computed from transformed values of the regionalized variable.

Conditioning output from the turning bands method at a location g requires:

1. the simulated value at g obtained through turning bands: $z_s(g)$
2. an estimate of the regionalized variable at g obtained by kriging nearby wells: $z^*(g)$
3. an estimate of the simulated variable at g obtained by kriging simulated values at locations coinciding with sample locations: $z_s^*(g)$.

In general, sample locations do not coincide with grid locations, as required by the calculation of $z_s^*(g)$. However, the node nearest each sample location is sufficient if the grid is fine relative to sample spacing.

Conditioned values, $z_c(g)$ are simply calculated from:

$$z_c(g) = z_s(g) + z^*(g) - z_s^*(g)$$

Examining the formula shows that the conditionally simulated values equal observed values everywhere grid nodes coincide with sample locations. Journel and Huijbregts (1978, p. 496) show that the estimation variance of the simulated values is twice that for kriged estimates.

7.1.4 Simulated annealing

The method of **simulated annealing** has become popular in recent years for generating simulations like those given by sequential and turning bands techniques, and also for improving results obtained by these other approaches. Simulated annealing begins with an initial image, input data, and a semivariogram to be reproduced. During the analysis, the annealing algorithm attempts to modify the intial image to one that better reproduces the variogram, while also maintaining the same univariate distribution as that of the input data.

Unlike methods described above, simulated annealing does not have a predetermined number of steps which can be calculated before a simulation. Rather, annealing operates iteratively, attempting to minimize an

objective function within a reasonable number of iterations, while trying to avoid falling into a local minimum.

A computer program first creates an initial image by assigning each node a value of the regionalized variable randomly drawn from a frequency distribution provided by the user. Where grid nodes and input data coincide within some tolerance, grid nodes are assigned the input values. Obviously, this initial image does not conform to a specified semivariogram.

The simulated annealing algorithm now attempts to reproduce a given semivariogram by exchanging values chosen at random from the grid; values corresponding to locations of conditioning data are left alone throughout iteration. Not every drawing of a pair of grid nodes results in a swap. The algorithm first computes the value of an **objective function**:

$$O = \sum_h \frac{[\gamma^*(h) - \gamma(h)]^2}{\gamma(h)^2}$$

where $\gamma^*(h)$ is the semivariogram model specified by the user, and $\gamma(h)$ is the semivariogram for the simulated image. This function should go to zero with the number of iterations. Remember, the goal of the annealing procedure is to find a near-perfect fit between the semivariogram of simulated data, and the one input by the user.

If the swap at a particular step reduces the objective function, the swap is made. To reduce the chance that the simulation ends before the objective function is sufficiently close to zero – i.e. the algorithm falls into a local minimum – some swaps are accepted that actually increase the objective function. The probability of accepting is given by the formula:

$$P = \begin{matrix} 1 & \text{if } O_n \leq O_o \\ e^{(O_o - O_n)/t} & \text{if } O_n > O_o \end{matrix}$$

where O_n is the value of the objective function if the swap is made, O_o is the old value, i.e. the swap is not made. The value t determines how quickly the algorithm reaches a solution. The higher this value, the more often an unfavorable value for the objective function is accepted, and the more slowly the algorithm reaches a minimum. If it is lowered too quickly, the probability of falling into a local minimum increases. The number of iterations required increases with the size of the grid, but only indirectly. The number of iterations vastly outnumbers the number of grid nodes.

As with all simulation methods outlined in this chapter, the user must input conditioning data, a semivariogram, and a random number seed to start the random selection off. Annealing also requires t, and parameters that control the decrease in t as the simulation progresses. The number

and effect of these parameters depends on the particular implementation of simulated annealing.

7.2 EXAMPLES

The three case studies in this section are used to illustrate sequential indicator simulation and sequential Gaussian simulation. The reader should already be familiar with data used in these examples because they have been used in previous chapters. The first set is the initial potential data from Barbour County, West Virginia, an example of skewed data in two dimensions. The second set of data is the three-dimensional distribution of porosity in a sandstone reservoir in Granny Creek field. The third example shows the use of simulation for generating lithofacies models in three dimensions.

7.2.1 Sequential indicator simulation: initial potential in Barbour County

Recall that gas initial potentials are available from 674 wells within one county. These wells were used in Chapter 6 to compute and fit semivariograms for four cutoffs corresponding to the 25*th*, 50*th*, 75*th*, and 90*th* percentile of the input data. Constants for exponential models with nugget effects are repeated here for convenience:

Cutoff: 400 Mcfpd
Nugget effect: 0.13
Constant: 0.015
Range: 3 km

Cutoff: 792 Mcfpd
Nugget effect: 0.19
Constant: 0.10
Range: 3 km with anisotropy ratio = 0.33
Major axis is north–south

Cutoff: 1399 Mcfpd
Nugget effect: 0.11
Constant: 0.09
Range: 1.5 km with anisotropy ratio = 0.5
Major axis is north–south

Cutoff: 2477 Mcfpd
Nugget effect: 0.07
Constant: 0.025
Range: 2 km

For each cutoff, the nugget effect is a large proportion of the variance, and two cutoffs show minor anisotropy at smaller separation distances.

These semivariogram models were used to generate simulations within the 10 by 10 km area used in previous chapters (Fig. 7.1). Although only 206 gas wells lie within this area, the complete set of wells in Barbour County was used to avoid edge effects. GSLIB (Deutsch and Journel, 1992) with some modifications was used to generate simulations; interpolation in the tails and between cutoffs followed tabulated quantiles.

An important feature of simulation is that the user can generate as many realizations as desired, each merely requiring a new random number seed. The four simulations in Fig. 7.2 are all different, but because they are conditioned to the same set of data, they share the same trends in high and low gas volumes. For instance, they all have the same meandering trend of high values in the western part of the area mapped. Within these trends, initial potential is very noisy, consistent with the

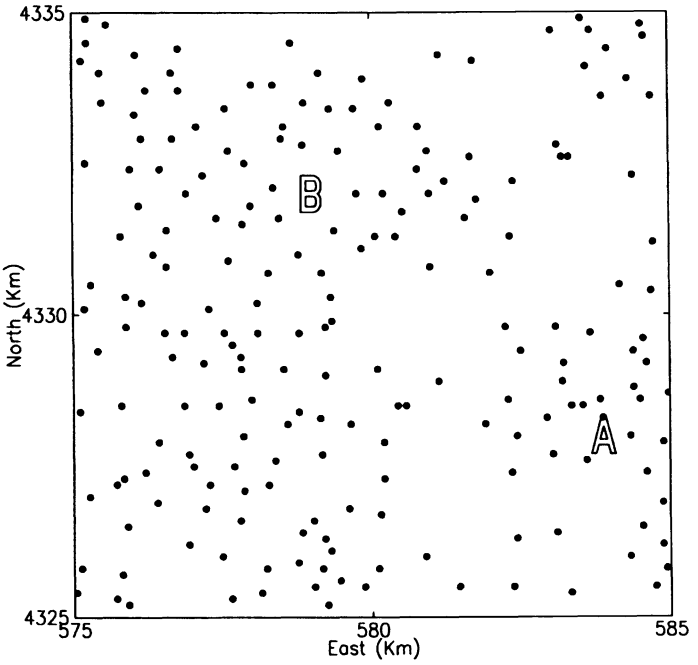

Figure 7.1 Locations of wells used to simulate gas initial potentials in a portion of Barbour County, West Virginia. Wells near location 'A' are generally low in gas potential, and wells near location 'B' are relatively high in potential.

general observation that gas volumes from adjacent wells can have very different values. Despite this large variability over small distances, areas exist with a better-than-average chance of encountering a high volume.

To aid in comparing these results with those obtained through kriging, the contour map of initial potential estimated by median indicator kriging in Chapter 6 was superimposed on these maps. One can see both the relative smoothness of kriged estimates, and the general correspondence between trends on the two types of maps.

It is good practice to compare the semivariogram of a conditional simulation with the one provided as input to the computer program. In this case, semivariograms for each cutoff used in the simulation (Fig. 7.3) fail to match the anisotropy of the input models for the middle cutoffs, but they have approximately the correct sills and nugget effects. These discrepancies probably arise because the simulation only covered a small part of the total area represented by the Barbour County. Ways to refine the analysis include computing a semivariogram for this specific 10×10 km area; dividing the area into subregions, each with a different model; or employing a moving-window method such as that described by Haas (1990).

Another check is to compare the semivariogram of initial potential (not the indicator variables) from the simulation with that of the original data (Fig. 7.4). This illustration has both a semivariogram computed from the complete set of data, and one for the 206 wells within the area mapped. This small area includes some of the largest values of initial potential in the data, and thus has a higher sill. Simulated data yield a higher value of the semivariogram at the smallest distances. At distances greater than about 0.5 km, all three semivariograms have nearly reached their respective sills. The first point on the semivariogram for the subset of data is based on only 45 pairs. In general, semivariograms show that the simulation has captured the low spatial covariance of initial potential beyond a few hundred meters shown by the well data.

Yet another check on the results is the comparison of the histogram for wells in the area mapped (Fig. 7.5), and the histogram for the simulated grid (Fig. 7.6). The two histograms look very similar. They both differ from the histogram drawn for the data as a whole shown in Chapter 5 (Fig. 5.2), which includes wells located outside the area mapped.

A P–P plot is convenient for making such comparisons of histograms (Fig. 7.7). In this graph, the cumulative relative frequencies of gas volumes from wells are plotted against those for the simulation results. If the two distributions are the same, the P–P plot displays a straight line. In this case study, the distributions of well data and simulated values are very similar.

Given a large number of simulations, one can generate a cumulative probability distribution at each location in an area, similar to those created in the previous chapters. At a sample location, the resulting

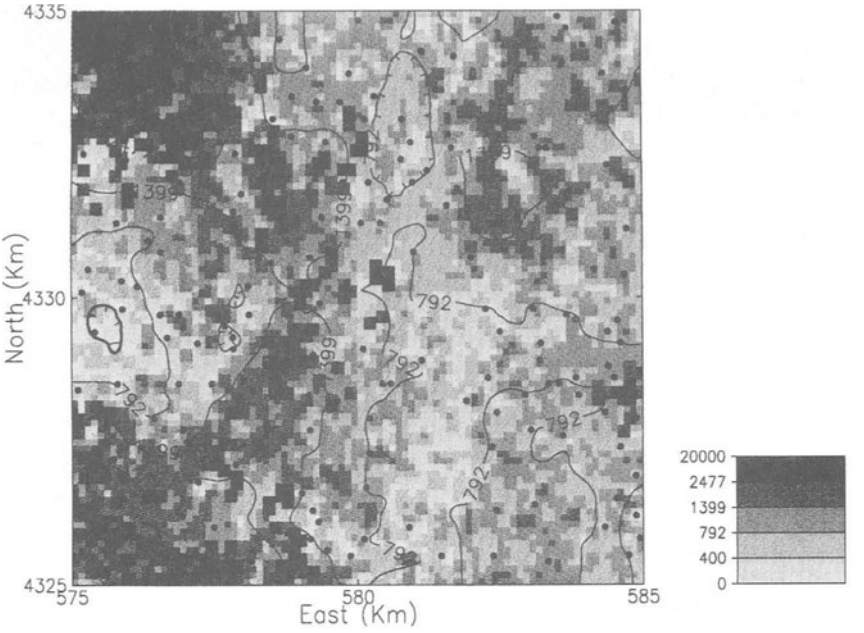
4335
4330
4325
North (Km)
575
580
585
East (Km)
399
792
20000
2477
1399
792
400
0

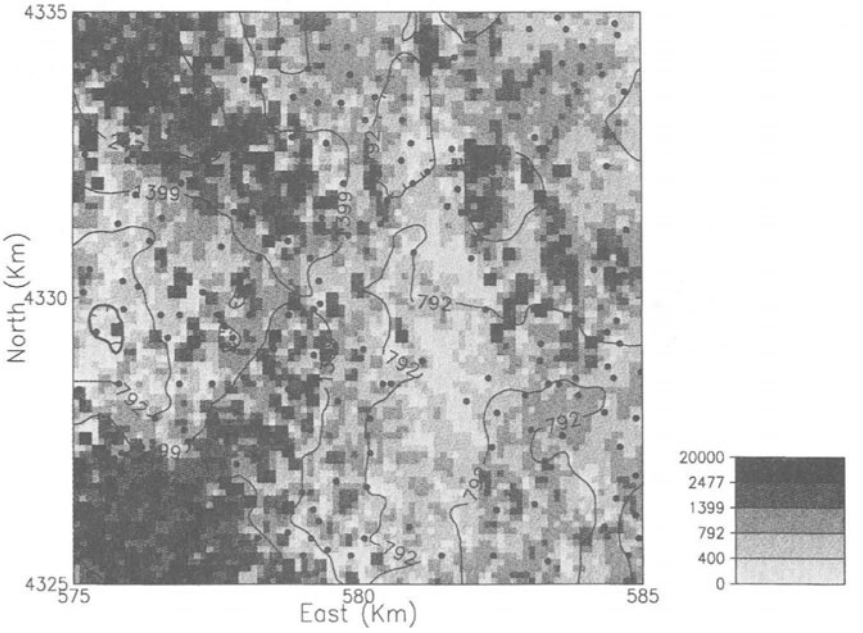
4335
4330
4325
North (Km)
575
580
585
East (Km)
399
792
20000
2477
1399
792
400
0

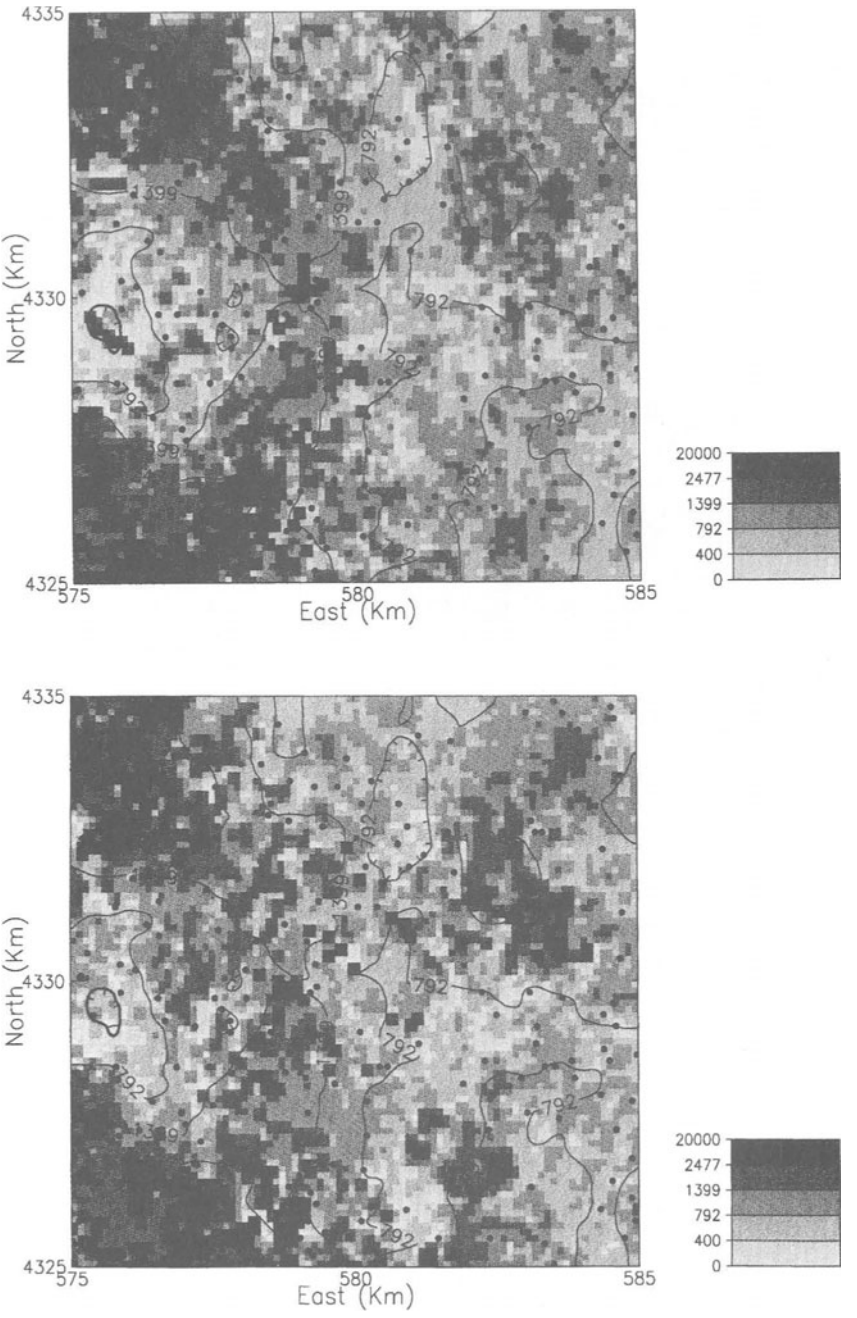

Figure 7.2 Four conditional simulations of gas initial potential, generated with different random number seeds. Well locations are shown as solid circles. Units are Mcfpd. Superimposed are contours of kriged estimates of initial potential corresponding to quartiles of the histogram of initial potential.

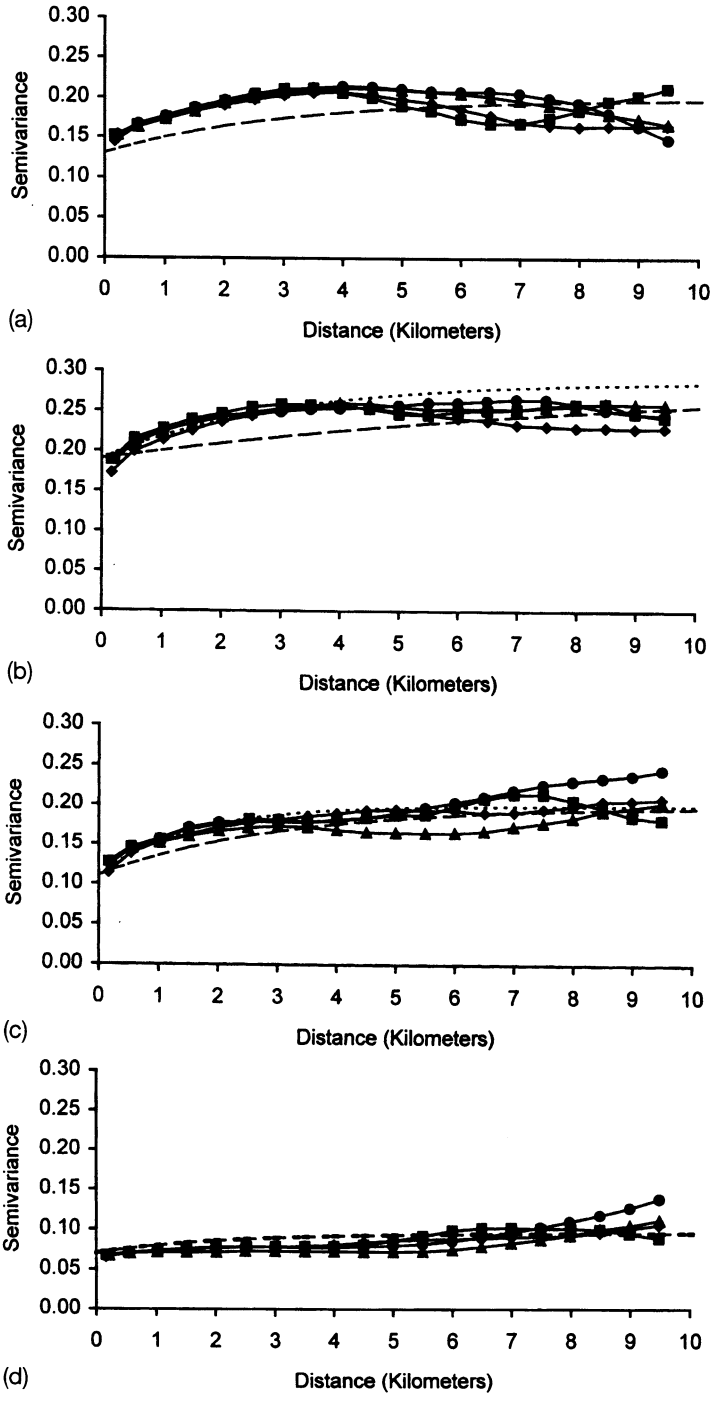
Semivariance
0.30
0.25
0.20
0.15
0.10
0.05
0.00
0 1 2 3 4 5 6 7 8 9 10
Distance (Kilometers)
(a)
(b)
(c)
(d)

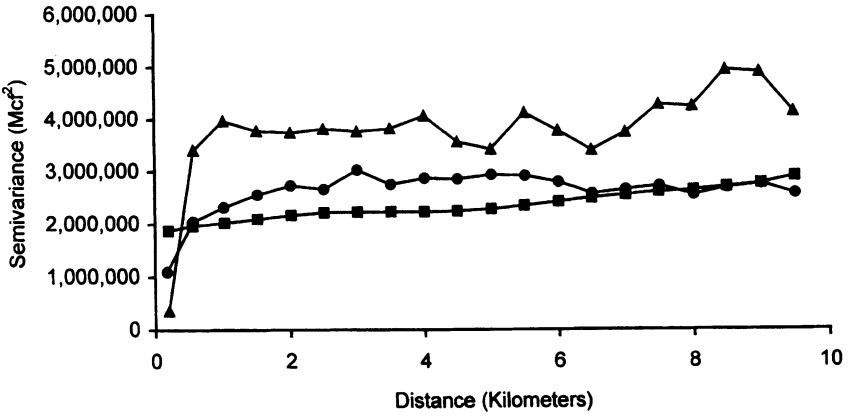

Figure 7.4 Semivariograms of simulated gas initial potentials for the complete data set (solid circles), data within the area mapped (triangles), and the simulation (squares).

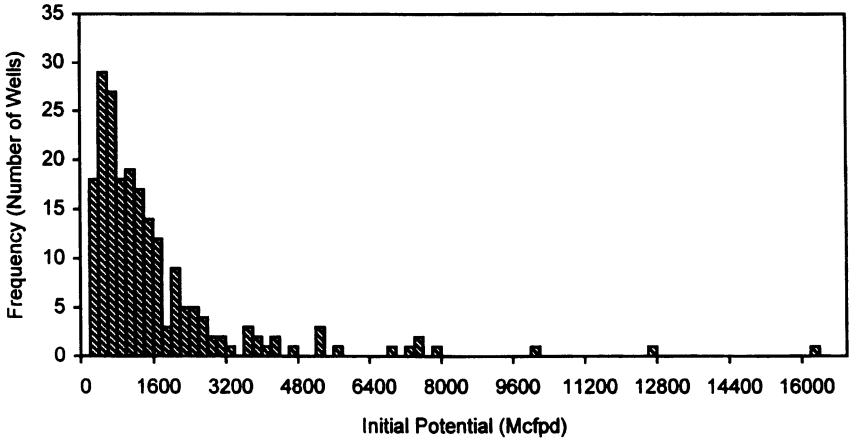

Figure 7.5 Histogram of initial potential within area simulated and mapped.

Figure 7.3 Directional semivariograms (solid lines) of simulated initial potential and model (dashed line) for each indicator variable (cutoff) used in conditional simulation. Directions are: north–south (diamonds); northeast–southwest (solid circles); east–west (squares); and southeast–northwest (triangles). Cutoffs are: (a) 400 Mcfpd; (b) 792 Mcfpd; (c) 1399 Mcfpd; (d) 2477 Mcfpd.

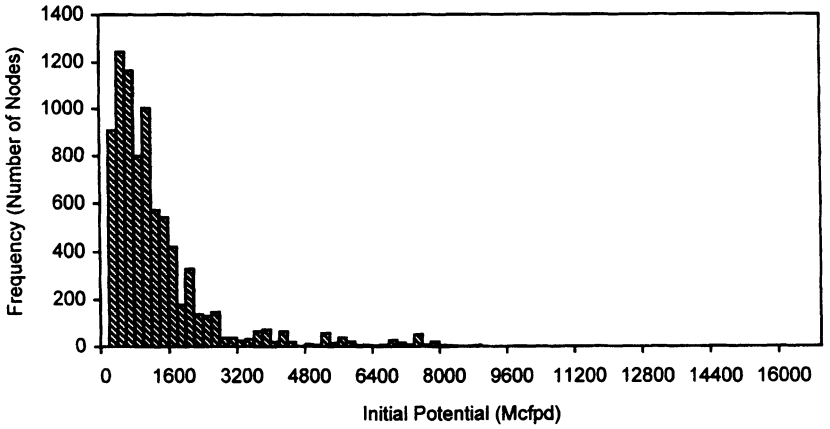

Figure 7.6 Histogram of simulated initial potentials.

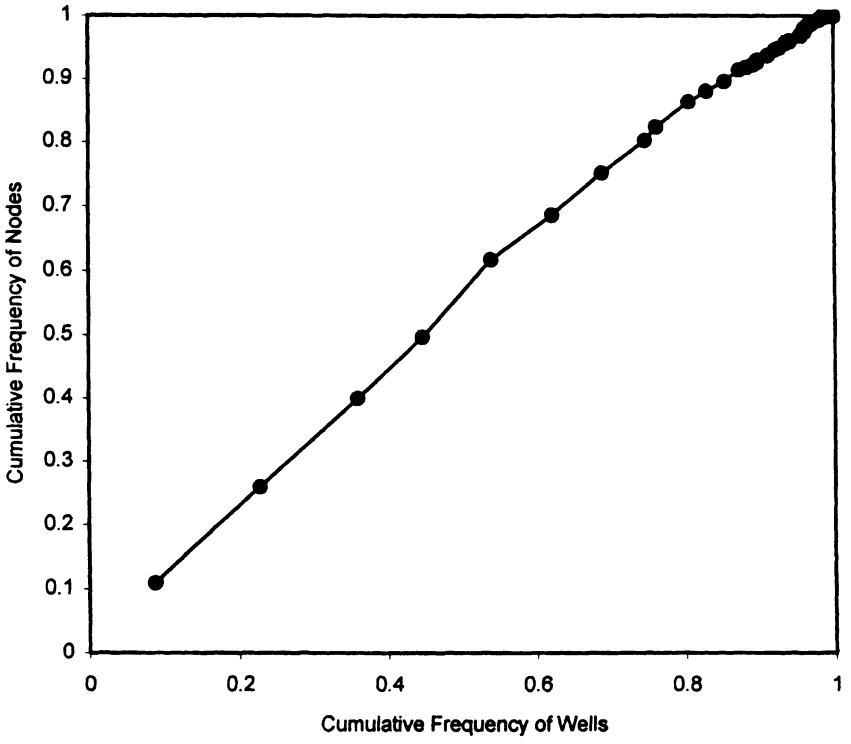

Figure 7.7 P–P plot of well initial potentials and simulated initial potentials.

histogram should have a single spike at the value observed. The histogram spreads out as one moves into areas of sparse well control or large variance in observed values. Histograms in Figs 7.8 and 7.9 were made from 100 simulated values of initial potential at each of the two locations studied in previous chapters. Location A has a center of mass around 875 Mcfpd, and very little tail, although two values exceeded 2000 Mcfpd. Location B is located in an area of generally high gas volumes, and has a large tail; almost a third of the values exceed 2000 Mcfpd. The appearance of these histograms roughly match those in Chapters 5 and 6 for disjunctive and indicator kriging.

7.2.2 Sequential Gaussian simulation: porosity in Granny Creek Field

To reduce computing time, the complete set of three-dimensional log porosity data from Granny Creek field used in previous chapters was reduced in size to those wells occurring within a ten kilometer area, plus some wells in the surrounding area. Sequential Gaussian simulation requires an initial calculation of normal scores from porosity data. Resulting horizontal and vertical semivariograms of normal scores resemble those calculated from raw data and graphed in Chapter 2 (Figs 7.10, 7.11). The following model was fitted:

$$\gamma(h) = 0.35Sph\left(\frac{|h|}{3.0}\right) + 0.65Sph\sqrt{\left(\frac{h_h^2}{1750^2} + \frac{h_v^2}{7^2}\right)}$$

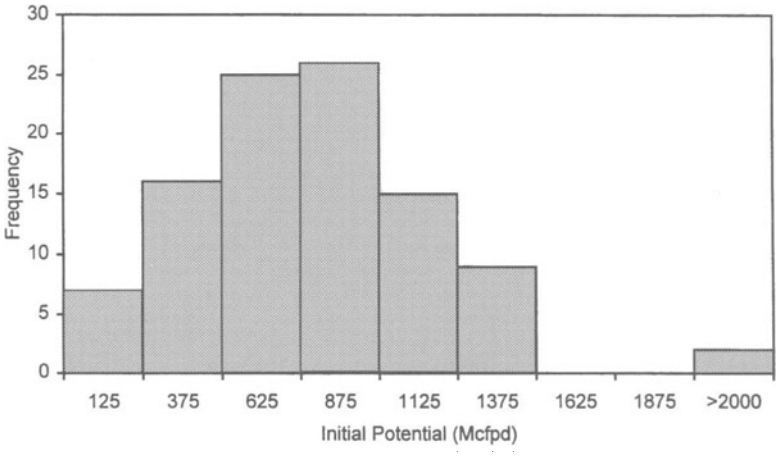

Figure 7.8 Local cumulative distribution and histogram of initial potential at location A in Fig. 7.1.

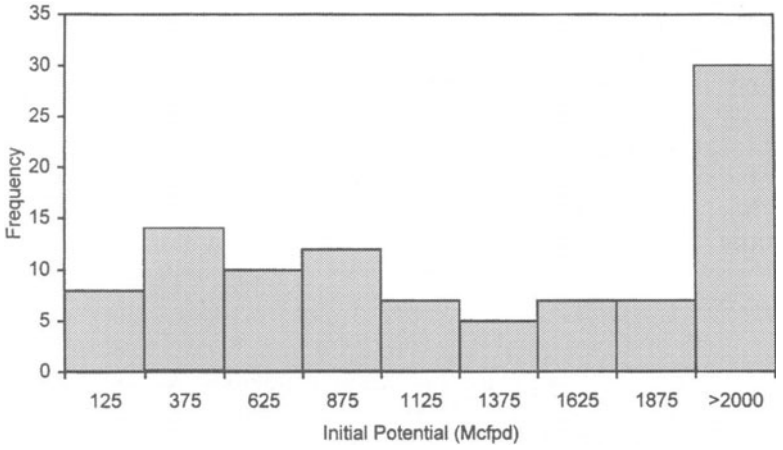

Figure 7.9 Local cumulative distribution and histogram of initial potential at location B in Fig. 7.1.

Notice that the vertical semivariogram shows a pseudoperiodicity arising from zonation of the sandstone reservoir represented by these data. I made no attempt to model this oscillation about the sill because vertical distances greater than two to three meters were not to be used in the search that takes place in simulating porosity at a given node.

The practitioner must be careful in specifying an appropriate search radius for simulation. In this situation, the search radius I used was 300 m horizontally, and 3 m vertically. It is also important not to go

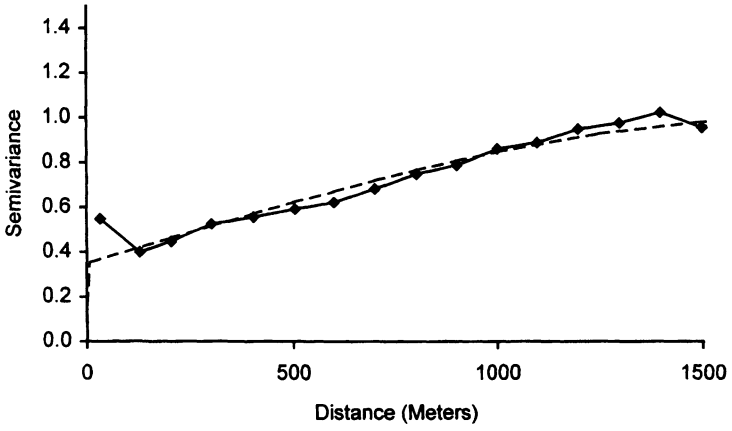

Figure 7.10 Semivariogram of normal scores of porosities computed from geophysical logs (solid line) and fitted model (dashed line) in the horizontal direction.

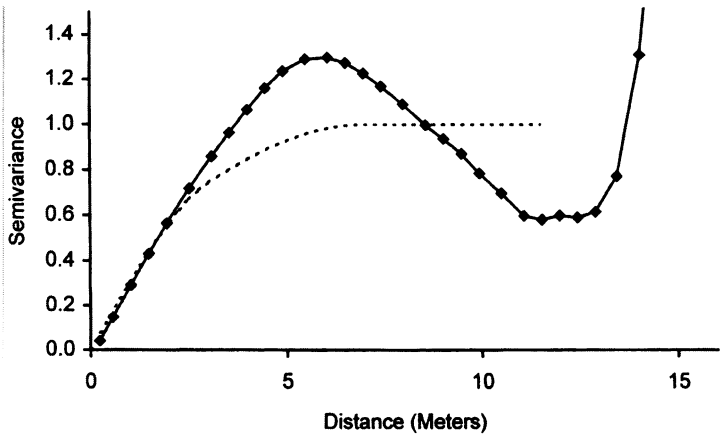

Figure 7.11 Semivariogram of normal scores of porosities computed from geophysical logs (solid line) and fitted model (dashed line) in the vertical direction.

beyond the vertical range of available data; resulting extrapolations contain artifacts that can mislead the unwary user. In early runs with this set of data, I inadvertantly went too deep, and 'found' a new high-porosity zone.

The same volume kriged in Chapter 3 was simulated here for comparison. Figure 7.12 shows a map view of a slice 3 m from the base of the reservoir. Small-scale variability occurs where the map of kriged estimates is fairly smooth.

Vertical slices (Figs 7.13, 7.14) show the strong vertical zonation of the reservoir; the zone of relatively high porosity in the lower part of the reservoir is the one in which most of the wells in the field were completed. Again, simulated porosities vary more locally than kriged estimates. Horizontal (Fig. 7.15) and vertical (Fig. 7.16) semivariograms of simulated log porosity compare roughly with specified models.

Reservoir characterization usually requires knowledge about the spatial distribution of permeability. Because core permeability data are generally limited in number and spatial distribution, it has been found useful to infer a three-dimensional model of permeability from porosity; Almeida and Frykman (1994) published an example which used geostatistical methods to generate realizations of permeability in a reservoir.

An easy way for coming up with a three-dimensional model of permeability is to regress permeability on log porosity, and using a fitted regression equation, compute a value of permeability at each node from the three-dimensional realization of log porosity. One drawback to this approach is that permeabilities calculated in this way have the same

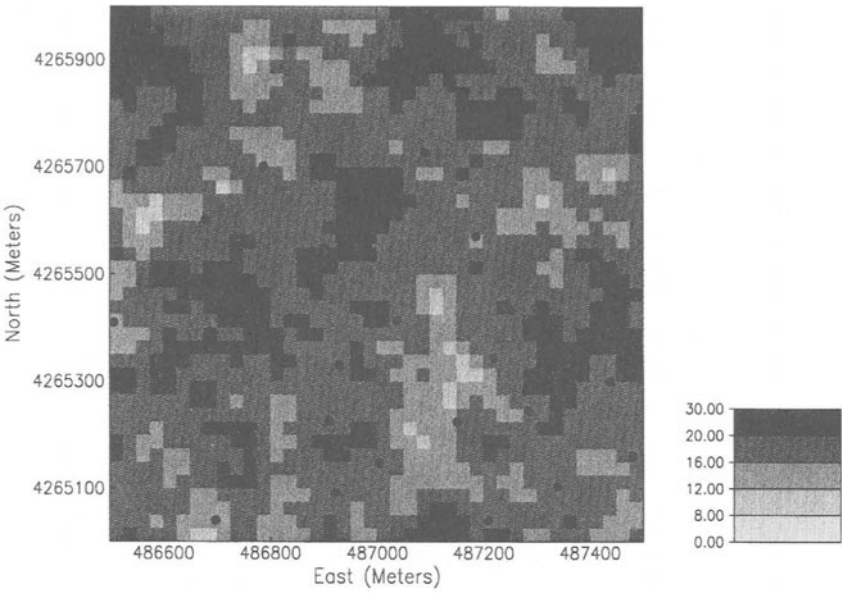

Figure 7.12 Map of log porosities from sequential Gaussian simulation with well locations.

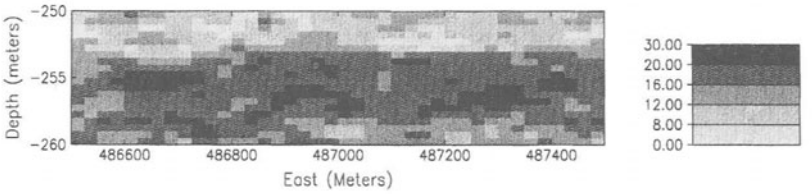

Figure 7.13 East–west cross section of log porosities (in per cent) from sequential Gaussian simulation. Cross-section is located at 4265500 m North.

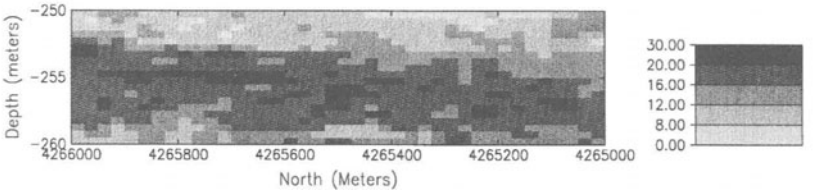

Figure 7.14 North–south cross-section of log porosities (in per cent) from sequential Gaussian simulation. Cross-section is located at 487000 m East.

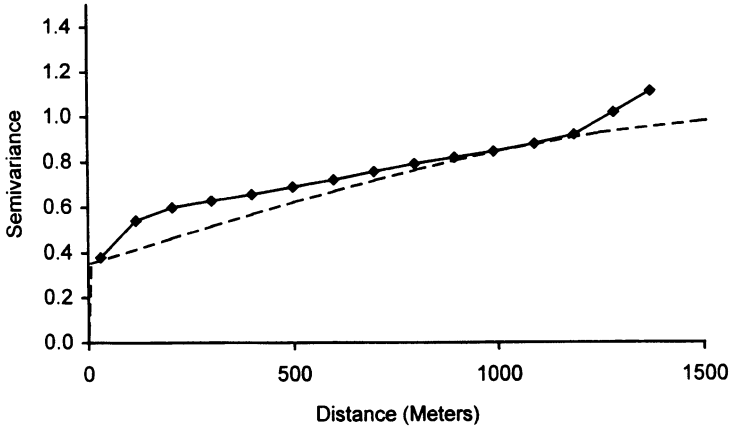

Figure 7.15 Semivariogram of simulated normal scores of porosities computed from geophysical logs (solid line) and fitted model (dashed line) in the horizontal direction.

spatial covariance as porosity, up to a multiplicative factor, because the permeabilities are essentially recentered and rescaled porosities. This is not a problem if in fact permeability and porosity have about the same semivariograms. A second drawback is the fact that what little permeability data are available go unused during simulation. This approach has the advantage of being easy to understand and implement. In some instances, so little permeability data might be available within an area to be simulated that this simple method works as well as any.

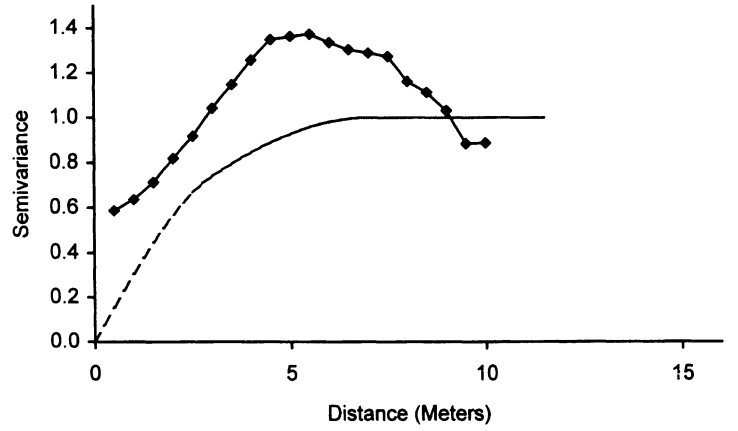

Figure 7.16 Semivariogram of simulated normal scores of porosities computed from geophysical logs (solid line) and fitted model (dashed line) in the vertical direction.

Sequential Gaussian cosimulation is a general method (Verly, 1993) that combines the principles and practice of simulation and cokriging to generate realizations of several regionalized variables simultaneously. Recall from Chapter 4 the following nomenclature: the variable of direct interest, e.g. permeability, is the primary variable, which is usually undersampled. A secondary variable such as log porosity is to be used indirectly while estimating simulating the primary variable.

The initial step in sequential Gaussian cosimulation is to compute and model semivariograms from normal scores of the primary and secondary variables. Also needed is a cross-semivariogram between the primary and secondary variables. All sequential methods compute a kriged estimate at each grid node from surrounding data and previously simulated values. Cosimulation uses cokriging to compute an estimate of the primary variable from surrounding actual and simulated values, and nearby values of the secondary variable. This method can be extended to more than one secondary variable, e.g. core and log porosity.

Almeida and Frykman (1994) simplified the sequential Gaussian cosimulation approach by computing estimates at each node through collocated cokriging, hence avoiding having to calculate and model cross-semivariograms. They computed a realization of the secondary variable on the same grid to be used for the primary variable. If data are already available on this grid, such as with seismic data, this step is skipped. Semivariograms are necessary for the primary and secondary variables, but correlation coefficients are used in place of cross-semivariograms.

Chambers *et al.* (1994) combined sequential simulation and kriging with external drift as yet another approach to the general problem of incorporating secondary information. In their situation, acoustic impedance served as the secondary variable in simulating porosity. Theirs is an interesting study because they demonstrated the effect of different numbers of control wells, and compare the results of kriging with conditional simulation. They drew a map representing an average of a number of simulations, and showed that this map approximates one of kriged estimates, as it should.

Strictly speaking, Gaussian methods require data that are multivariate normal. Although this requirement cannot be checked, a necessary condition for a distribution to be multivariate normal is that it is univariate and bivariate normal. The normal scores transform used in sequential Gaussian simulation must result in a set of values that are univariate normal. Bivariate normality can be checked by comparing indicator semivariograms with a theoretical indicator semivariogram computed from the model fitted to the normal scores semivariogram. This was done for the porosity dataset using the **bigaus** program in GSLIB (Deutsch and Journel, 1992).

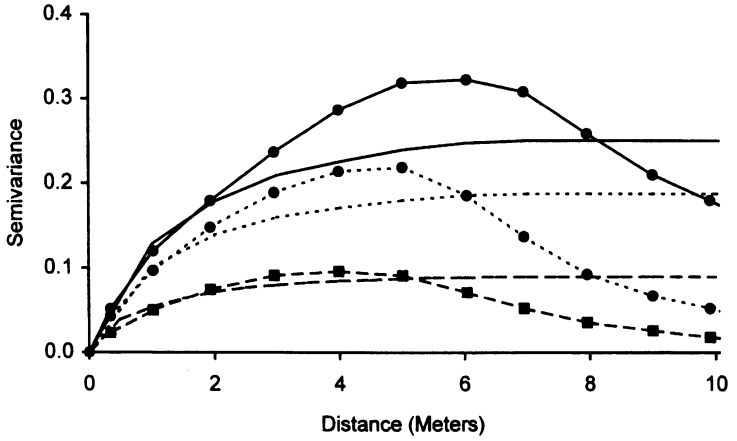

Figure 7.17 Vertical semivariograms used in check for bivariate normality of log porosity normal scores. Semivariograms with solid circles are calculated from normal score indicator variables, semivariogram without symbols are computed from semivariogram model. Cutoffs correspond to the 50th (solid lines), 75th (dotted lines), and 90th (dashed line) percentiles.

Because of the extreme sensitivity of observed semivariograms in the horizontal direction to the vertical window tolerance, vertical semivariograms were used for the comparison. Beyond two or three meters, semivariograms respond to the strong vertical trends in porosity (Fig.

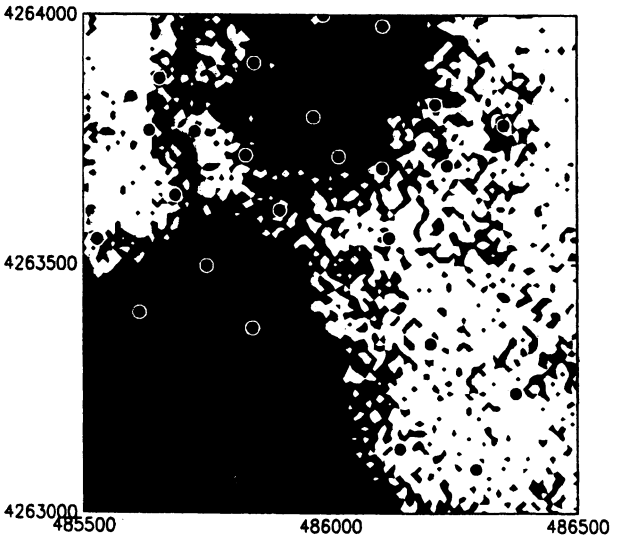

Figure 7.18 Map of simulated facies at an elevation 4 m above the base of the reservoir. Black areas represent the distal facies. Solid circles are well locations.

7.17), and therefore the theoretical semivariograms and those computed from the normal scores for three cutoffs should only be compared for small separation distances. Although there are no formal tests proposed in the literature for the comparison, it seems reasonable to conclude from the graph that the transformed data are bivariate normal.

7.2.3 Sequential indicator simulation of sandstone facies

In Chapter 6, indicator kriging was used to map two facies within a sandstone reservoir using the following model for the semivariogram:

$$\gamma(h) = 0.025Sph\sqrt{\left(\frac{h_h^2}{0.001^2} + \frac{h_v^2}{\infty^2}\right)} + 0.035Sph\sqrt{\left(\frac{h_h^2}{250^2} + \frac{h_v^2}{1^2}\right)}$$

$$+ 1.0Sph\left(\frac{\sqrt{h_h^2}}{100\,000^2} = \frac{h_v^2}{90^2}\right)$$

Facies were determined from geophysical logs in a study of reservoir heterogeneity within a Lower Mississippian sandstone reservoir. This model will now be used for sequential indicator simulation of facies in three dimensions within the same volume of reservoir used in the previous example.

Results show an expected similarity with the model obtained through indicator kriging, but with a large number of small-scale features (Figs

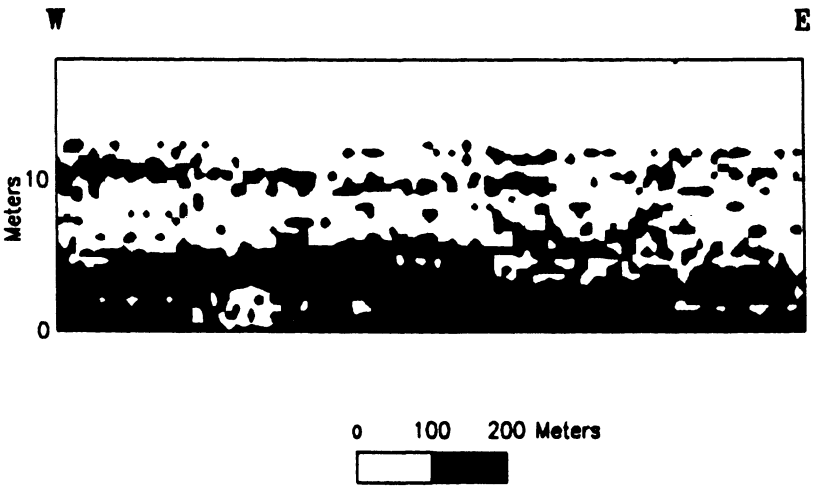

Figure 7.19 East–west cross-section of simulated facies at northing 4263500 of Fig. 7.18.

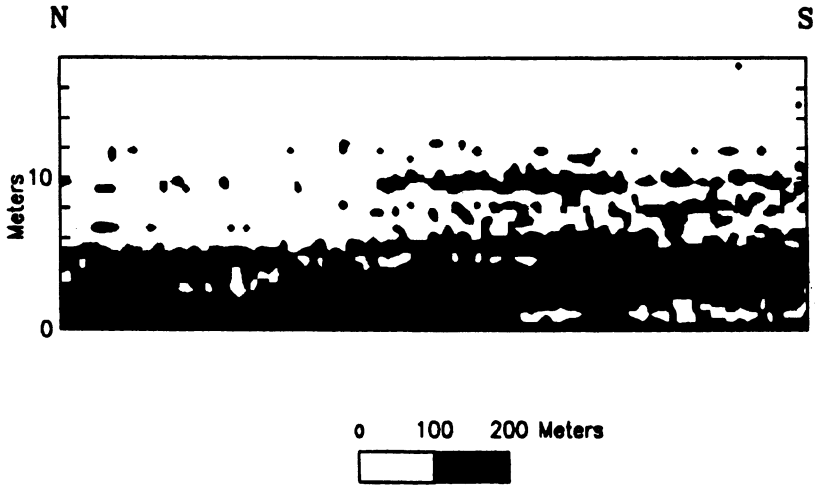

Figure 7.20 North–south cross-section of simulated facies at easting 486000 of Fig. 7.18.

7.18–7.20). These features accord with the geologists observations that transitions between facies tend not to be very well defined. The upper, proximal facies interfinger with the lower, distal facies. The resulting three-dimensional model has many discontinuities that could affect flow of oil and water through the reservoir.

7.3 WHICH METHOD TO USE?

Research into methods of conditional simulation is at the stage that kriging was ten years ago; a number of methods and variations on a theme have been proposed, but the features unique to each are not all known. Only a handful of comparative studies are available in the literature. However, a few guidelines are possible.

Applications using the turning bands method have declined in numbers for two reasons: the directions of anisotropy are limited to the coordinate axes of the grid; and the limited number of lines can lead to artificial and unrealistic-looking bands in the results. Although it might be possible to rotate coordinate axes before variography and simulation for simple semivariogram models, the resulting grid would probably have to be rotated back and regridded. This is not worth the effort with other simulation methods available.

Sequential methods are easy to use and software is widely available. The Gaussian methods require a normal scores transform before variography, but as we have seen, such transforms can be beneficial for a

number of reasons when working with skewed distributions. The indicator approach takes more work at the variography stage. The tediousness of modeling a number of semivariograms can be eliminated if one uses the model for the cutoff at the median is used for all cutoffs. It is a good idea to check whether this model fits those for the other cutoffs reasonably well.

Simulated annealing requires a few more decisions by the user than the other methods, for example, an initial grid, parameter t, and an objective function. It has been used in place of the other simulation methods, but the most important applications of simulated annealing will be in situations where objective functions other than the semivariogram are required, and where results of a simulation by another method must be adjusted for some reason. The salient feature of simulated annealing is the ability to create quite complex objective functions beyond the simple semivariogram.

Use of a sophisticated objective function is illustrated by Deutsch (1993). Wanting to create realizations of permeability, he used both a semivariogram and effective permeabilities in the objective function, weighted to ensure that both contributed equally. Because calculated effective permeabilities are nonlinear averages, conventional simulation methods could not be used to incorporate this information. Realizations generated by this process were used in flow simulators to predict breakthrough time and remaining oil in place after 50 years of production.

In simulating rock types within a sandstone reservoir, Murray (1994) was able to obtain reasonable results with sequential indicator simulation. Although semivariograms were not reproduced exactly, they were close, and the proportions of lithologies were correct. A problem with the realizations was the fact that the least-favorable rock type was often found within the most-favorable rock type, i.e. vertical transition probabilities between the two rock types were too high in the realizations compared with what was observed in wells. Therefore, Murray used simulated annealing to **postprocess** the initial realizations, utilizing the frequency of transitions as part of the objective function. Both the transition probabilities and vertical semivariograms were much improved in the final realizations.

The interested reader should consult the paper by Gotway and Rutherford (1994), who compared several methods of conditional simulation with several data sets of different types and probability distributions. This is probably the most extensive comparative study published to date.

7.4 SUMMARY

Conditional simulation is used to generate multiple realizations of a regionalized variable for points within an area or volume. It is often used to create realizations of permeability for input to flow simulators.

Whereas kriging tends to result in smoothed maps of a regionalized variable, simulation attempts to preserve variablity at all scales. In general, simulation algorithms create realizations that reproduce the mean, variance and semivariogram of observed data. When the simulation also reproduces the observed data, it is said to be conditioned.

The turning bands method was once used almost exclusively, but is less used today because of artifacts in the results and limitations on the semivariogram model that can be used. It creates an initial realization that is then conditioned to the data through a simple calculation.

Sequential simulation methods are frequently used. Gaussian simulation and indicator simulation use a normal scores transform and indicator transforms respectively on data prior to actual simulation. Hence, these methods are particularly suited to the skewed data distributions often observed in geologic data.

Simulated annealing starts with an initial image of the correct mean and variance, and updates this image according to an objective function. This objective function usually includes the semivariogram, but can use additional functions of the realization. This flexibility makes it useful in situations where a nonlinear criterion must be satisfied, and for post-processing realizations generated by other simulation algorithms.

REFERENCES

Almeida A.S. and Frykman, P. (1994) Geostatistical modeling of chalk reservoir properties in the Dan Field, Danish North Sea, in J.M. Yarus, and R.L. Chambers (eds), *Stochastic Modeling and Geostatistics*. American Association of Petroleum Geologists, Tulsa, OK, pp. 273–286.

Chambers, R.L., Zinger, M.A. and Kelly, M.C. (1994) Constraining geostatistical reservoir descriptions with 3-D seismic data to reduce uncertainty, in J.M. Yarus and R. Chambers (eds), *Stochastic Modeling and Geostatistics*. American Association of Petroleum Geologists, Tulsa, OK, pp. 143–157.

Davis, M. (1987) Generating large stochastic simulations – the matrix polynomial approximation method. *Math. Geol.*, **19**(2), 99–108.

Deutsch, C.V. (1993) Conditioning reservoir models to well test information, in A. Soares (ed.) *Geostatistics Troia '92*. Kluwer Academic Publishers, Dordrecht, pp. 505–518.

Deutsch, C.V. and Journel, A.G. (1992) *GSLIB: Geostatistical Software Library and User's Guide*. Oxford University Press, New York, 340pp.

Dowd, P.A. and Saraç, C. (1994) An extension of the LU decomposition method of simulation, in M. Armstrong and P. A. Dowd (eds) *Geostatistical Simulations*. Kluwer Academic Publishers, Dordrecht, p. 23–36.

Gotway, C.A. and Rutherford, B.M. (1994) Stochastic simulation for imaging spatial uncertainty: Comparison and evaluation of available algorithms, in M. Armstrong and P.A. Dowd (eds) *Geostatistical Simulations*. Kluwer Academic Publishers, Dordrecht, pp. 1–21.

Haas, T.J. (1990) Lognormal and moving window methods of estimating acid deposition. *Journal of the American Statistical Association*, **85**, 950–963.

Isaaks, E. (1990) *The application of Monte Carlo Methods to the Analysis of Spatially Correlated Data*. Unpublished PhD dissertation, Stanford University.

Journel, A.G. and Huijbregts, C.J. (1978) *Mining Geostatistics*. Academic Press, London, 600 pp.

Murray, C.J. (1994) Identification and 3-D modeling of petrophysical rock types, in J.M. Yarus and R.L. Chambers (eds) *Stochastic Modeling and Geostatistics*. American Association of Petroleum Geologists, Tulsa, OK, pp. 323–337.

Verly, G.W. (1993) Sequential Gaussian cosimulation: A simulation method integrating several types of information, in A. Soares (ed.) *Geostatistics Tróia '92, Vol. 1*. Kluwer Academic Publishers, Dordrecht, pp. 543–554.

Locations and initial potentials of Devonian wells in a West Virginia gas field

Easting (km)	Northing (km)	Initial potential (Mcfpd)
568.869	4360.153	100
559.100	4355.079	102
535.641	4365.509	103
561.432	4353.771	110
562.071	4342.616	118
574.727	4345.594	119
565.212	4345.477	133
562.264	4345.422	133
565.081	4358.239	150
564.085	4357.214	150
567.922	4350.865	154
558.686	4352.763	158
560.245	4355.549	158
536.995	4352.106	193
563.636	4356.439	198
564.574	4358.852	200
579.492	4353.132	200
562.185	4358.370	215
560.153	4351.880	225
565.858	4342.801	225
561.002	4350.469	227
565.791	4356.427	232
564.645	4344.517	245
569.092	4359.322	246
565.282	4357.131	246
571.558	4356.540	250
559.251	4350.948	250

Easting (km)	Northing (km)	Initial potential (Mcfpd)
566.532	4345.335	266
569.471	4354.424	267
566.099	4348.321	270
560.808	4350.899	286
554.354	4352.453	298
564.726	4343.408	320
571.468	4353.918	327
560.436	4349.385	335
562.811	4351.993	353
564.806	4356.788	353
570.392	4358.409	360
572.447	4348.409	400
565.831	4348.720	412
566.250	4347.521	425
561.981	4344.835	440
568.626	4347.017	444
572.289	4355.220	444
574.984	4351.176	448
559.938	4354.930	450
560.480	4349.909	467
561.144	4353.737	470
569.345	4349.768	482
566.554	4348.356	489
560.141	4350.431	492
569.951	4346.320	492
567.038	4347.775	500
561.383	4356.915	500
571.342	4346.148	516
568.767	4347.327	516
573.577	4350.608	519
562.266	4348.321	531
560.463	4345.933	539
574.689	4347.011	550
571.410	4354.410	581
560.320	4348.891	582
557.679	4349.703	582
563.866	4357.613	600
562.941	4347.679	622
566.860	4349.006	622
574.057	4350.458	638
576.991	4346.941	650
559.818	4345.680	650

Easting (km)	Northing (km)	Initial potential (Mcfpd)
560.549	4350.342	660
563.120	4343.395	671
568.518	4348.342	678
559.528	4349.131	696
569.834	4345.980	696
565.154	4346.680	696
561.915	4350.199	697
561.825	4349.488	730
569.247	4347.300	764
560.800	4345.750	787
566.960	4348.545	793
560.774	4349.079	793
565.771	4347.393	793
566.587	4347.216	808
572.179	4354.171	822
570.139	4346.723	822
565.995	4349.183	852
568.225	4346.305	875
565.752	4346.777	880
564.503	4347.259	907
561.422	4348.869	907
557.857	4351.585	910
563.008	4342.377	919
561.007	4349.883	919
569.895	4347.152	1000
563.311	4346.449	1008
559.884	4349.535	1055
564.073	4347.040	1100
569.587	4354.856	1131
566.519	4346.814	1154
563.743	4346.359	1185
563.667	4346.852	1185
564.891	4340.758	1200
568.172	4355.153	1320
568.572	4355.865	1402
561.440	4349.702	1476
569.517	4346.563	1516
560.529	4346.703	1517
569.177	4347.022	1517
563.188	4346.848	1569
570.240	4346.076	1594
569.135	4349.057	1600

Easting (km)	Northing (km)	Initial potential (Mcfpd)
561.714	4342.212	1639
568.477	4355.833	1782
569.159	4349.088	1825
563.555	4342.936	1900
564.149	4346.578	1975
568.847	4354.603	1980
566.478	4348.849	2000
561.473	4348.499	2208
561.855	4348.717	2300
563.669	4343.615	2700
564.489	4351.760	3011

Thickness of Paleocene clastics in Libya

No.	East	North	Thickness
1	0.0	24.0	1848
2	2.5	20.0	1806
3	4.0	25.0	2220
4	1.0	11.0	2513
5	6.0	0.0	3209
6	5.0	2.0	3080
7	10.0	2.0	3164
8	8.0	7.0	2164
9	5.5	11.0	2400
10	4.0	14.5	2434
11	20.0	30.0	3632
12	27.5	26.0	3048
13	24.0	21.0	3890
14	11.0	17.0	2480
15	8.0	20.5	2573
16	5.0	23.0	2270
17	8.0	24.5	2134
18	3.5	29.0	1967
19	7.0	28.5	1684
20	19.0	1.5	2435
21	14.0	4.0	2640
22	16.5	8.5	2530
23	13.5	8.0	2629
24	11.0	9.0	2706
25	20.0	11.5	2911
26	11.0	13.5	2209
27	16.0	17.0	1674
28	14.0	12.5	2436
29	18.5	20.5	2110
30	17.5	23.5	1870

No.	East	North	Thickness
31	20.0	12.5	2658
32	22.5	16.5	2234
33	23.0	12.5	1690
34	29.0	8.0	3941
35	20.5	7.0	2572
36	21.5	3.0	1439
37	22.5	7.5	1910
38	26.0	5.0	2995
39	25.0	2.5	3001

Initial Potential of Gas from Wells in Barbour County, West Virginia

Easting (Km)	Northing (Km)	Initial Potential (Mcfpd)
571.50	4331.60	163
588.38	4323.50	870
574.02	4337.20	800
571.45	4331.80	169
577.93	4322.30	1233
588.28	4323.50	600
577.67	4329.50	370
579.17	4325.80	293
573.97	4337.10	169
577.81	4329.30	275
583.54	4328.50	933
577.79	4322.30	6787
572.72	4327.30	133
588.47	4321.20	1200
572.77	4327.20	381
579.31	4326.10	1900
587.40	4329.50	950
577.17	4324.20	5500
577.05	4324.10	3890
583.35	4328.50	470
579.21	4326.30	76
578.97	4324.20	118
573.24	4338.50	4000
571.83	4331.90	684
576.26	4323.40	467
576.58	4323.00	4100

Easting (km)	Northing (km)	Initial potential (Mcfpd)
575.93	4322.80	1500
587.54	4329.40	1000
579.82	4323.00	683
589.17	4321.50	670
571.55	4331.40	268
577.93	4324.40	2316
576.53	4323.40	3300
577.59	4324.60	6500
570.53	4332.00	1303
575.84	4327.30	1000
583.21	4332.60	467
586.36	4323.30	875
588.59	4321.10	600
578.17	4322.40	4224
577.36	4324.50	8245
573.31	4338.40	1200
570.95	4334.30	184
584.40	4328.80	959
575.72	4327.20	2000
575.87	4323.70	850
578.54	4333.10	219
579.46	4325.60	283
583.83	4328.60	1399
588.23	4321.30	900
578.50	4332.90	169
577.54	4329.70	275
578.66	4324.20	2477
570.65	4332.30	431
571.71	4332.00	244
576.39	4322.80	820
579.94	4322.90	839
577.44	4338.00	850
579.03	4325.50	1200
577.73	4322.80	1186
584.50	4328.60	1390
587.82	4329.90	712
579.23	4329.80	1356
589.38	4323.70	800
587.07	4333.00	900
577.01	4327.50	2000
578.20	4324.50	2800
583.69	4334.70	1500

Easting (km)	Northing (km)	Initial potential (Mcfpd)
575.85	4323.30	1469
577.88	4324.90	492
587.04	4328.50	492
583.54	4334.90	490
570.99	4334.20	311
577.82	4329.10	539
576.09	4324.20	5244
575.24	4334.90	400
586.26	4323.40	1100
584.61	4329.20	136
588.90	4321.80	1200
584.39	4329.40	400
575.83	4338.30	2000
577.71	4323.00	2477
588.02	4325.00	920
577.22	4323.60	3450
589.41	4321.50	678
578.83	4326.40	1000
578.78	4328.40	1710
570.59	4331.70	200
583.20	4328.90	959
572.71	4338.00	947
575.24	4334.50	6731
580.07	4331.30	444
576.94	4327.70	193
577.47	4337.50	1500
577.01	4338.00	2000
577.63	4338.20	787
587.18	4329.20	1237
580.98	4332.00	200
578.76	4325.90	150
579.34	4329.90	1073
576.87	4329.70	2768
587.53	4330.10	950
575.71	4325.30	2477
579.11	4324.00	5175
572.63	4339.40	769
579.56	4337.40	1205
576.66	4334.00	1500
577.55	4321.90	5673
579.70	4337.40	327
581.24	4332.20	792

Easting (km)	Northing (km)	Initial potential (Mcfpd)
583.88	4328.30	440
578.59	4328.20	1299
574.33	4337.10	400
570.97	4332.10	134
574.33	4337.50	189
586.47	4328.00	1547
572.21	4327.50	70
577.28	4327.20	144
588.55	4323.20	1500
580.53	4331.70	400
579.02	4326.60	1061
589.53	4323.50	246
575.68	4323.90	421
588.13	4330.30	823
580.78	4332.40	200
576.54	4324.00	5750
579.23	4324.70	1900
580.41	4331.30	1570
573.13	4334.80	1033
577.86	4327.10	986
586.85	4332.90	163
578.75	4324.70	3000
584.88	4326.20	1594
580.44	4328.50	989
588.78	4323.60	1400
577.98	4331.80	888
586.74	4321.70	1476
583.13	4332.80	1500
583.33	4332.60	581
576.15	4330.20	66
586.69	4321.40	1975
575.96	4322.40	1500
584.60	4334.60	1443
588.21	4331.50	750
579.25	4325.20	2500
576.61	4322.40	5537
577.69	4327.50	2057
580.58	4328.50	949
575.67	4322.80	2144
573.60	4333.00	190
583.22	4329.20	313
583.78	4324.00	762

Easting (km)	Northing (km)	Initial potential (Mcfpd)
579.31	4333.40	379
576.43	4337.80	2000
586.15	4322.20	1087
583.98	4334.40	2316
577.26	4337.20	1100
575.59	4337.90	1000
586.85	4328.70	990
575.73	4338.50	680
589.21	4322.20	700
589.00	4321.00	1500
576.54	4329.70	30
575.88	4330.30	232
575.91	4325.20	2232
573.70	4337.20	1007
572.90	4339.00	2000
588.27	4330.70	769
576.23	4333.70	3000
588.36	4325.00	1986
577.84	4323.80	984
575.45	4335.20	3610
576.78	4333.70	4464
571.11	4335.20	222
586.91	4329.60	900
576.30	4322.10	7428
571.99	4327.30	320
578.10	4329.70	452
576.94	4323.00	3100
577.81	4337.10	1000
574.82	4323.40	2141
586.70	4323.10	600
570.70	4332.80	516
578.51	4322.20	875
582.94	4328.30	1061
578.35	4323.90	3400
575.58	4334.80	5000
573.63	4334.80	166
573.83	4323.40	90
584.55	4334.80	300
584.94	4325.80	1032
571.96	4331.50	516
588.91	4331.50	762
587.09	4322.00	793

Easting (km)	Northing (km)	Initial potential (Mcfpd)
575.19	4330.10	792
575.28	4323.40	2000
577.19	4329.20	345
574.22	4323.50	2477
578.88	4333.50	119
573.70	4332.90	440
587.14	4328.30	641
575.30	4338.00	400
577.84	4331.50	1215
588.26	4325.50	1704
579.72	4333.40	1500
576.20	4327.40	1237
573.11	4334.20	226
577.88	4332.50	703
580.95	4332.70	207
579.14	4328.30	880
576.04	4333.30	641
576.60	4338.20	1500
576.67	4332.90	5180
578.77	4322.50	421
571.22	4330.60	231
587.97	4321.50	1000
573.07	4338.10	2000
577.89	4321.80	881
587.59	4333.30	1639
576.15	4332.90	16021
586.44	4322.40	539
577.61	4332.70	3500
589.56	4322.50	850
586.28	4328.10	1391
584.19	4324.10	713
588.51	4331.10	311
573.64	4334.30	778
580.21	4332.00	520
574.68	4323.00	2500
576.35	4331.00	800
577.99	4328.60	858
576.03	4324.50	2055
584.56	4329.60	1008
577.32	4321.40	2319
577.18	4332.30	2157
586.14	4321.70	1332

Easting (km)	Northing (km)	Initial potential (Mcfpd)
578.14	4325.40	440
575.04	4325.40	7000
589.28	4324.20	620
575.13	4325.80	2000
573.76	4323.50	1838
579.17	4330.70	1107
576.90	4332.00	1312
587.17	4332.60	43
576.66	4329.30	350
579.60	4323.30	610
577.08	4333.10	2100
587.67	4330.50	984
588.56	4322.00	622
579.87	4325.50	1500
575.30	4330.50	171
573.10	4332.00	272
578.27	4327.20	516
578.86	4332.80	2100
575.27	4327.00	3700
572.42	4338.10	110
576.46	4332.40	1838
587.95	4331.10	318
572.69	4334.90	713
580.28	4337.30	816
588.72	4325.30	700
572.49	4338.80	200
574.54	4325.20	517
584.54	4326.50	379
586.62	4327.60	1122
576.89	4337.40	1500
573.93	4339.10	2000
575.46	4334.00	3500
585.49	4321.50	933
587.79	4334.80	1183
579.49	4322.60	913
574.94	4330.90	1400
578.38	4327.60	5180
576.07	4336.00	5000
587.04	4322.50	1400
575.89	4329.80	382
577.44	4328.50	212
575.15	4334.20	1100

Easting (km)	Northing (km)	Initial potential (Mcfpd)
579.52	4324.30	379
579.84	4331.10	713
578.79	4329.70	1678
574.37	4323.00	2477
577.85	4328.00	2500
572.03	4336.00	492
587.53	4325.60	582
577.21	4326.80	2477
571.27	4335.70	200
588.30	4329.80	808
587.73	4325.00	320
576.57	4331.40	1007
577.41	4331.60	1299
588.44	4324.00	933
587.84	4323.60	368
578.37	4333.80	622
584.98	4328.70	762
577.79	4326.60	3156
581.77	4331.90	1020
589.60	4321.20	750
570.66	4334.40	249
570.31	4332.60	467
588.14	4327.60	750
584.88	4326.90	582
576.71	4324.50	7273
578.55	4336.80	424
576.57	4330.80	731
585.30	4321.30	1404
588.14	4327.30	600
571.75	4327.60	417
571.20	4330.20	193
589.69	4322.30	119
574.49	4325.60	1300
578.09	4330.20	730
587.99	4332.00	787
587.76	4331.60	787
578.23	4325.80	12439
574.17	4338.70	1200
578.69	4323.00	2600
574.50	4339.60	400
574.72	4326.10	1500
571.30	4334.90	492

Easting (km)	Northing (km)	Initial potential (Mcfpd)
579.78	4322.30	386
572.75	4334.40	306
583.93	4323.50	978
574.40	4326.60	141
574.93	4326.90	7773
584.34	4328.00	561
575.96	4332.40	342
588.47	4332.00	712
573.55	4335.30	46
576.06	4321.60	1948
577.32	4338.40	400
580.15	4333.10	1073
576.00	4335.80	2000
585.72	4322.10	291
580.09	4339.20	539
586.29	4329.40	678
586.67	4330.10	207
588.98	4322.70	561
586.00	4329.60	1032
588.51	4326.60	492
576.06	4334.30	1200
587.74	4332.80	600
587.27	4327.50	440
587.24	4323.50	2400
576.15	4337.60	1647
589.27	4325.20	700
578.53	4329.10	1858
578.21	4337.50	989
583.20	4335.10	1300
577.64	4325.30	2768
572.03	4336.20	1100
578.78	4331.00	1100
574.91	4331.20	124
578.36	4332.10	3816
587.48	4321.70	561
574.57	4339.10	353
587.20	4333.70	984
578.65	4337.30	438
588.96	4324.70	84
586.38	4330.50	298
573.05	4327.30	78
589.25	4331.30	696

Easting (km)	Northing (km)	Initial potential (Mcfpd)
580.48	4338.80	1055
585.31	4326.50	386
578.28	4330.70	956
574.83	4330.00	904
574.41	4338.30	400
587.37	4322.90	1500
579.38	4331.40	10000
589.79	4324.00	700
574.03	4325.00	143
574.22	4331.20	154
571.68	4330.60	87
574.76	4337.60	850
579.65	4328.20	949
584.32	4333.90	660
582.44	4328.00	1561
577.17	4321.30	1185
577.28	4330.10	1525
579.32	4330.30	300
570.93	4331.00	1917
576.11	4331.80	198
583.49	4323.70	424
571.75	4338.70	267
587.68	4333.70	1205
582.86	4322.20	762
578.46	4331.60	4012
581.58	4331.60	421
580.32	4333.50	900
588.08	4334.90	762
578.26	4323.40	2380
583.62	4334.10	852
576.40	4326.90	2316
574.87	4338.50	1000
585.28	4320.80	1080
583.04	4327.70	516
583.17	4322.20	1073
573.33	4333.60	1225
573.32	4331.70	192
575.80	4331.30	919
585.82	4330.30	467
577.50	4336.70	671
588.23	4326.10	1164
570.67	4333.30	714

Easting (km)	Northing (km)	Initial potential (Mcfpd)
572.20	4339.50	500
582.29	4328.60	211
571.41	4336.10	1000
577.56	4333.40	4000
580.64	4337.10	830
575.31	4322.20	1100
584.95	4337.80	539
572.81	4335.30	184
579.62	4326.80	2237
579.19	4337.80	978
578.01	4333.80	1205
588.42	4336.80	907
579.56	4339.30	375
588.72	4326.80	1050
577.09	4322.00	6766
580.66	4337.10	444
587.95	4329.10	1143
573.08	4339.60	1700
572.34	4329.50	2144
573.03	4332.50	492
573.91	4333.70	206
576.43	4327.90	295
589.41	4325.60	539
575.49	4333.50	5497
584.69	4330.40	2210
587.57	4327.00	933
583.72	4324.50	750
581.20	4338.30	539
574.20	4335.20	582
585.18	4330.00	1032
573.81	4325.60	189
572.41	4332.20	176
585.32	4330.50	823
580.11	4325.80	348
585.90	4323.10	450
579.89	4323.90	327
577.61	4330.90	783
576.86	4328.50	888
572.67	4337.50	7273
584.75	4325.50	390
584.61	4327.40	858

Easting (km)	Northing (km)	Initial potential (Mcfpd)
586.66	4333.30	1100
584.68	4338.30	712
575.90	4326.50	3482
580.53	4338.30	1076
585.58	4325.90	1900
571.92	4328.00	297
571.97	4335.40	149
579.14	4334.00	1100
579.17	4327.70	1255
575.81	4325.70	3700
588.26	4336.30	1283
579.76	4338.80	381
580.21	4327.90	239
574.17	4330.70	1100
582.50	4329.40	189
583.89	4333.60	1055
573.78	4339.50	1500
583.46	4335.70	363
581.09	4337.70	240
574.14	4334.30	146
574.00	4328.80	641
574.23	4326.90	31
585.83	4320.80	134
574.75	4335.30	8692
587.48	4334.40	327
579.23	4329.00	7273
586.84	4327.20	808
571.29	4338.70	131
588.10	4322.50	1350
584.50	4324.40	530
579.76	4332.00	404
580.80	4333.10	200
572.52	4329.80	87
584.33	4326.00	750
572.60	4331.50	348
579.46	4332.70	1517
578.71	4336.20	411
579.88	4333.90	1039
587.60	4336.50	1675
583.75	4335.70	1200
584.89	4327.90	321
571.49	4338.30	787

Easting (km)	Northing (km)	Initial potential (Mcfpd)
585.45	4329.10	442
589.51	4320.90	850
575.10	4324.00	1000
577.49	4326.00	7273
587.43	4323.90	1200
571.32	4332.70	492
580.15	4326.70	1107
576.26	4336.30	3750
578.05	4336.50	1050
589.12	4332.00	348
572.14	4330.20	565
575.41	4329.40	267
574.59	4339.90	88
583.09	4329.80	372
573.76	4331.20	1100
587.41	4326.10	660
579.16	4336.50	261
583.14	4321.20	490
583.04	4334.70	692
578.73	4338.10	1356
586.62	4321.00	1632
574.23	4324.20	267
576.73	4339.00	600
583.67	4329.70	122
580.84	4339.10	263
585.20	4339.00	2144
575.20	4335.90	4142
573.40	4328.70	375
587.11	4320.80	1561
570.67	4335.30	212
584.14	4337.80	289
582.90	4322.60	311
573.19	4325.80	886
587.20	4325.40	1320
571.22	4333.50	340
573.61	4324.40	150
583.32	4321.60	492
576.78	4334.40	550
589.81	4324.40	620
581.67	4332.60	1958
580.21	4327.30	492
586.79	4332.20	50

Easting (km)	Northing (km)	Initial potential (Mcfpd)
583.35	4337.40	1750
572.26	4326.80	492
575.92	4321.20	4224
586.49	4330.90	1100
581.91	4328.20	539
582.83	4339.10	1560
588.23	4328.10	800
572.48	4339.80	738
578.01	4338.60	641
574.55	4328.70	283
583.31	4338.40	2316
583.02	4337.00	412
589.29	4337.80	625
584.20	4338.70	989
584.91	4339.60	133
580.83	4322.80	957
572.99	4329.00	4760
580.54	4323.50	440
573.54	4329.40	249
570.28	4331.30	162
588.87	4337.40	527
574.13	4329.90	157
570.03	4332.00	492
585.46	4337.50	561
585.57	4327.00	412
574.57	4331.80	167
588.41	4335.60	298
573.72	4335.90	500
587.62	4335.50	1055
572.92	4325.50	152
580.09	4336.60	500
573.22	4324.90	479
576.93	4326.20	2144
573.45	4336.60	500
586.82	4331.60	900
585.53	4339.70	3714
583.81	4323.00	600
582.81	4338.10	531
588.97	4330.10	495
575.80	4328.50	481
585.60	4328.40	539
588.10	4337.20	852

Easting (km)	Northing (km)	Initial potential (Mcfpd)
582.39	4332.20	1750
588.24	4333.00	603
584.62	4337.30	1517
575.51	4336.50	37
580.10	4329.10	119
581.68	4336.70	219
581.73	4338.30	474
575.21	4332.50	7773
584.71	4333.60	1391
571.19	4328.40	1750
575.11	4328.40	260
589.92	4323.10	1517
576.28	4339.20	350
582.17	4337.50	516
584.83	4320.40	267
584.25	4320.40	984
588.43	4320.40	1762
570.72	4330.20	754
582.40	4336.70	539
589.60	4334.30	582
582.25	4329.80	298
581.22	4323.10	500
585.82	4339.10	124
582.35	4327.40	746
588.62	4329.20	146
586.47	4334.50	227
572.03	4337.00	55
582.33	4331.30	2837
589.52	4326.00	1409
580.22	4322.00	467
574.54	4333.00	130
582.96	4339.60	256
582.96	4324.40	1237
584.16	4330.50	1848
580.04	4324.90	675
583.10	4326.40	746
571.52	4329.10	285
583.60	4327.60	1164
581.13	4328.90	353
581.46	4325.50	582
587.24	4336.70	762
574.95	4321.90	1476

Easting (km)	Northing (km)	Initial potential (Mcfpd)
585.46	4337.00	492
572.34	4333.70	111
582.00	4330.70	1087
581.46	4324.70	232
578.67	4334.50	1200
582.37	4325.50	1958
580.90	4326.00	198
582.05	4339.40	1347
581.15	4336.40	1561
574.13	4327.90	348
570.85	4339.30	582
583.60	4320.30	198
583.07	4320.60	2530
582.43	4326.30	696
579.45	4321.60	1632
589.81	4334.60	381
579.03	4339.60	411
585.45	4334.00	298
581.95	4324.30	1000
584.98	4324.10	500
571.16	4337.20	350
584.21	4339.60	10646
586.17	4340.00	321
589.72	4331.50	1426
586.44	4335.20	1302
586.47	4324.00	1200
582.46	4339.90	1205
583.33	4325.40	1517
588.88	4338.60	947
584.73	4331.20	762
580.99	4330.80	492
580.01	4339.90	193
587.86	4320.30	467
579.14	4335.60	919
570.06	4333.70	1207
578.64	4321.30	2400
589.80	4337.70	440
585.26	4322.50	500
589.34	4335.40	298
581.72	4334.20	581
585.65	4335.00	30

Easting (km)	Northing (km)	Initial potential (Mcfpd)
575.38	4340.00	325
570.61	4329.10	203
577.01	4339.80	1217
581.15	4334.30	600
585.79	4320.00	1719
570.74	4327.80	2316
585.95	4325.50	1195
589.57	4336.40	1100
581.78	4321.70	500
578.14	4339.80	311
589.53	4329.70	907
586.78	4339.90	959
570.36	4338.10	207
584.39	4332.30	400
570.26	4336.40	50
589.21	4339.00	822
570.32	4339.60	444
589.41	4327.30	2000
589.68	4333.50	933
570.29	4324.80	1342

Index